POLYMER AND COVALENT FUNCTIONALIZATION OF SINGLE WALLED CARBON NANOTUBES FOR ELECTRONIC SENSOR APPLICATIONS

by
John F. Fennell Jr.
M.S. Chemistry
The Colorado School of Mines, 2008

SUBMITTED TO THE DEPARTMENT OF CHEMISTRY IN PARTIAL FULFILLMENT OF THE REQUIREMENTS FOR THE DEGREE OF

DOCTOR OF PHILOSOPHY IN CHEMISTRY

AT THE
MASSACHUSETTS INSTITUTE OF TECHNOLOGY
JUNE 2017

© 2017 Massachusetts Institute of Technology. All rights reserved.

Signature redacted

Signature of the Author..... .....
Department of Chemistry
May 16, 2017

Signature redacted

Certified by..... .....
Timothy M. Swager
John D. MacArthur Professor of Chemistry
Thesis Supervisor

Signature redacted

Accepted by..... .....
Robert W. Field
Haslam and Dewey Professor of Chemistry
Chairman, Departmental Committee of Graduate Studies

MASSACHUSETTS INSTITUTE OF TECHNOLOGY
JUL 06 2017
LIBRARIES

ARCHIVES

This doctoral thesis has been examined by a Committee of the Department of Chemistry as follows:

Signature redacted

Professor Stephen L. Buchwald..... .....
Chairman

Signature redacted

Professor Timothy M. Swager..... .....
Thesis Advisor

Signature redacted

Professor Mohammad Movassaghi..... .....
Department of Chemistry

To my wife, Caitlin

In memory of Lola,
November 15, 2006 to
February 25, 2017

POLYMER AND COVALENT FUNCTIONALIZATION OF SINGLE WALLED CARBON NANOTUBES FOR ELECTRONIC SENSOR APPLICATIONS

BY

JOHN F. FENNELL JR.

Submitted to the Department of Chemistry
In Partial Fulfillment of the Requirements for the Degree of
Doctor of Philosophy in Chemistry

ABSTRACT

In this thesis, chemiresistive devices for the detection of volatile organic compounds to include chemical warfare agents are developed. Active sensing materials were produced by crafting composites of synthetic polymers and single walled carbon nanotubes. Sensitivity to and selectivity for target analytes were augmented by the introduction of molecular recognition elements into polymer side chains or by the addition of additives into a polymer/single walled nanotube composite. Additionally, methods to create n-type single walled carbon nanotubes through covalent side wall functionalization were explored.

Chapter 1: Chemiresistive sensors are becoming increasingly important as they offer an inexpensive option to conventional analytical instrumentation, they can be readily integrated into electronic devices, and they have low power requirements. Nanowires (NWs) are a major theme in chemosensor development. High surface area, inter-wire junctions, and restricted conduction pathways give intrinsically high sensitivity and new mechanisms to transduce binding or action of analytes. This chapter details the status of NW chemosensors with selected examples from the literature. We begin by proposing a framework for understanding electrical transport and transduction mechanisms in NW sensors. Next, we offer the reader a review of device performance parameters. Then, we consider the different NW types followed by a summary of NW assembly and different device platform architectures. Subsequently, we discuss NW functionalization strategies. Finally, we propose a roadmap for future developments in NW sensing that addresses selectivity, sensor drift, sensitivity, response analysis, and emerging applications. The NW field is still in its infancy, and continuing advances present abundant opportunities.

Chapter 2: Chemical warfare agents (CWA) continue to present a threat to civilian populations and military personnel in operational areas all over the world. Reliable measurements of CWAs are critical to contamination detection, avoidance, and remediation. The current deployed systems in United States and foreign militaries, as well as those in the private sector offer accurate detection of CWAs, but are still limited by size, portability and fabrication cost. Herein,

we report a chemiresistive CWA sensor using single-walled carbon nanotubes (SWCNTs) wrapped with poly(3,4-ethylenedioxythiophene) (PEDOT) derivatives. We demonstrate that a pendant hexafluoroisopropanol group on the polymer that enhances sensitivity to a nerve agent mimic, dimethyl methylphosphonate, in both nitrogen and air environments to concentrations as low as 5 ppm and 11 ppm, respectively. Additionally, these PEDOT/SWCNT derivative sensor systems experience negligible device performance over the course of two weeks under ambient conditions.

Chapter 3: The detection of alkylating agents using carbon nanotube chemiresistive devices has confounded researchers in the sensor field for quite some time. In this work, we address this quandary by fabricating a chemiresistive device consisting of poly(4-vinylpyridine)/single walled carbon nanotube/lithium bromide composites that is able to detect gaseous ethylene oxide (EtO) and a mustard agent simulant, 2-chloroethyl ethylsulfide (CEES). Our devices were sensitive to EtO and CEES down to 1048 ppm and 33 ppm, respectively. We calculated theoretical detection limits of 212 ppm for EtO and 10 ppm for CEES. These results should encourage researchers in the field to tackle analytes once thought to be undetectable via carbon nanotube chemiresistive devices, as they offer a low cost and low power alternative to current options.

Chapter 4: The covalent functionalization and characterization of single walled carbon nanotubes (SWCNTs) by dihalocarbenes and the trifluoromethylating Togni's reagent is explored in this chapter. Covalent functionalization reactions were performed to increase the SWCNT solubility, imparting n-type semiconducting behavior while maintaining the native conductivity of the conjugated sp^2 network. Previous computational studies predicted the conservation of the electrical conductivity of SWCNTS after carbene additions, but experimental work to verify the electrical properties has not been performed. In the studies presented herein, we utilized five different covalent functionalization methods to modify SWCNTs and utilized X-ray photoelectron spectroscopy (XPS) in tandem with Resonance Raman spectroscopy to characterize our products. Though electrical characterization was not performed, we improved upon literature methods concerning the dichlorocarbene addition of $-CCl_2$ groups to pristine SWCNTs.

Thesis Supervisor: Timothy M. Swager
Title: John D. MacArthur Professor of Chemistry

TABLE OF CONTENTS

LIST OF FIGURES

LIST OF SCHEMES

LIST OF TABLES

LIST OF ABBREVIATIONS

CWA	Chemical warfare agent
CEES	2-chloroethyl ethylsulfide
DMF	*N,N*-dimethylformamide
DMMP	Dimethyl methylphosphonate
EDOT	3,4 Ethylenedioxythiophene
EtO	Ethylene oxide
FTIR-ATR	Fourier transform infrared-attenuated total reflectance
GPC	Gel permeation chromatography
HFIP	Hexafluoroisopropanol
KCTP	Kumada catalyst transfer polycondensation
MM	Mechanical milling
NBS	*N*-bromosuccninamide
NIR	Near infrared
NMR	Nuclear magnetic resonance
o-DCB	*ortho*-dichlorobenzene
m-SWCNT	Metallic single walled carbon nanotube
PEDOT	Poly(3,4 ethylenedioxythiophene)
PTFE	Poly(tetrafluoroethylene)
p-SWCNT	Pristine single walled carbon nanotube
RBM	Radial breathing mode
RH	Relative humidity
SWCNT	Single walled carbon nanotube
sc-SWCNT	Semi-conducting single walled carbon nanotube
THF	Tetrahydrofuran
TGA	Thermogravimetric analysis
VOC	Volatile organic compound
XPS	X-ray photoelectron spectroscopy

CHAPTER 1

Nanowire Chemical/Biological Sensors: Status and a Roadmap for the Future

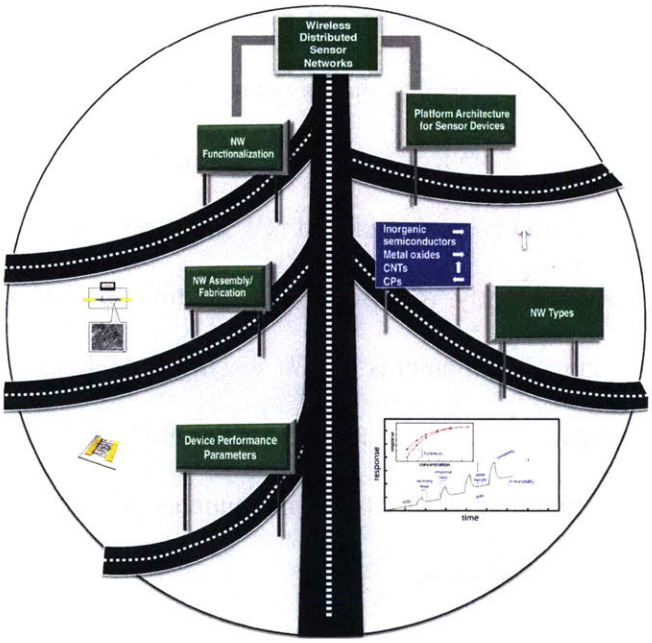

Adapted and reprinted in part with permission from:
Fennell, J. F.; Liu, S. F.; Azzarelli, J. M.; Weis, J. G.; Rochat, S.; Mirica, K. A.; Ravnsbaek, J. B.; Swager, T. M. Nanowire Chemical/Biological Sensors: Status and a Roadmap for the Future. *Angew. Chemie Int. Ed.* **2016**, *55* (4), 1266–1281

1.1 Abstract

Chemiresistive sensors are becoming increasingly important as they offer an inexpensive option to conventional analytical instrumentation, they can be readily integrated into electronic devices, and they have low power requirements. Nanowires (NWs) are a major theme in chemosensor development. High surface area, inter-wire junctions, and restricted conduction pathways give intrinsically high sensitivity and new mechanisms to transduce binding or action of analytes. This chapter details the status of NW chemosensors with selected examples from the literature. We begin by proposing a framework for understanding electrical transport and transduction mechanisms in NW sensors. Next, we offer the reader a review of device performance parameters. Then, we consider the different NW types followed by a summary of NW assembly and different device platform architectures. Subsequently, we discuss NW functionalization strategies. Finally, we propose a roadmap for future developments in NW sensing that addresses selectivity, sensor drift, sensitivity, response analysis, and emerging applications. The NW field is still in its infancy, and continuing advances present abundant opportunities.

1.2 Introduction

The omnipresence of wireless devices, cloud data, and printable electronics is an extraordinary opportunity for electronic chemical sensors. These sensors enable governments, businesses, and individuals satisfy an ever-expanding appetite to measure chemical and biological processes as well as physical quantities. Over the last decade, the electronic chemical sensor du jour contains nanowires (NWs). The assertion that NWs offer advantages in sensors is often made without justification. However, we contend that it is generally warranted. The simplest reason is their high surface area-to-volume ratios, which allows for more interactions with analytes. However, monolayers of 2-D materials such as graphene[1,2]

and MoS_2[3–7] also have high surface areas. The most important difference between 1-D NWs and 2-D materials is how they transport current.

In a NW, electrical transport is primarily along the NW axis. If the NW is small enough in diameter, high sensitivity is achieved because analytes could bind anywhere along the NW to perturb its entire conductivity. This effect is similar to what our group reported with semiconducting polymers, where we demonstrated signal gain by wiring receptors in series.[8] Although this principle was studied for exciton rather than charge transport, there was a1 correlation between carrier path length and signal amplification. Thus, long single NWs are attractive because sensitivity increases with length available for interacting with analytes. However, they are difficult to fabricate.

Alternatively, disordered NW networks can be readily deposited by solid transfer, printing, spraying, or drop-casting a dispersion. Random networks of NWs, as opposed to densely packed aligned networks, have the advantage of porosity with high surface area and limited contact between NWs to give restricted pathways that preserve 1-D character. The inter-NW contacts are critical: For NWs with high carrier mobilities, these junctions are conductivity-limiting. Various intra- and inter-NW mechanisms of transduction are illustrated for single-walled carbon nanotubes (SWCNTs) in Figure 1.1. Amongst all NWs, our group favors SWCNTs due to their excellent conductivity, exceptional aspect ratios, and numerous methods available for functionalization.

For many systems, reductions in conductivity are observed; coherence in electronic transport is destabilized by heterogeneous potentials that result from analytes. However, analytes can also enhance conductivity by facilitating charge transfer across resistive interfaces, lowering barriers, or injecting carriers through doping.

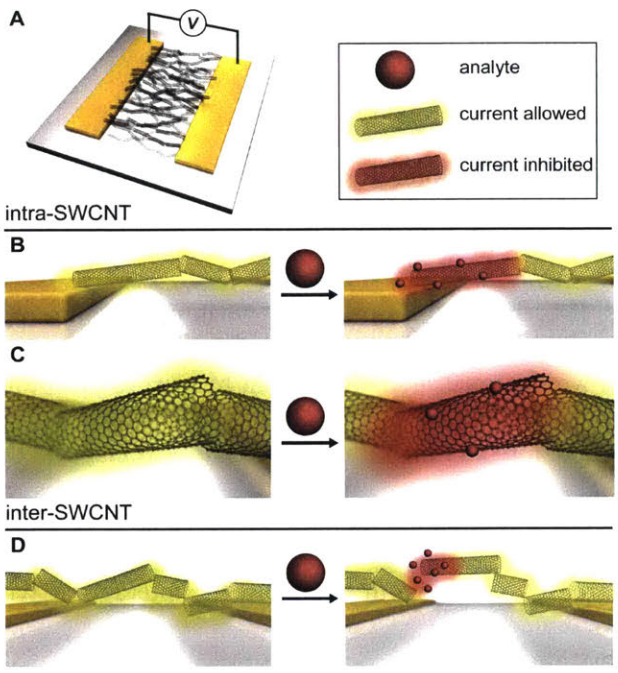

Figure 1.1 (A) A chemiresistor comprising a percolative, randomly oriented network of SWCNTs spanning two metallic electrodes has a current (yellow cloud) flowing through it when a voltage is applied. The presence of analyte (red sphere) can inhibit current flow (red cloud) via (B) Schottky barrier modulation at electrode–SWCNT junctions, (C) charge transfer between analyte and SWCNT, or (D) increasing SWCNT–SWCNT junction distance by intercalation or swelling of the SWCNT network.

That a "turn-on" response is more sensitive than "turn-off" is often stated in fluorescence; however, this assertion is only true with zero background fluorescence in the absence of analyte and emission only in presence of analyte. The analogy for NWs is an insulating device that becomes conductive upon exposure to analyte. If this activation is achieved by carrier injection, high sensitivity is obtained when the NW has very low carrier density in the absence of analyte. Alternatively, NW networks could be assembled slightly below a percolation threshold such that they are highly resistive, and analyte-triggered formation of new conduction pathways can produce a large turn-on response.

Sensitivity without selectivity, however, is simply noise. Systems should respond strongly only to desired analytes. Coupling molecular processes to conductivity changes for selectivity

often involves careful molecular constructions. Chemistry has provided decades of innovations in molecular recognition to guide development of chemical sensors. The challenge is how to produce specific electronic perturbations by analyte binding.

In this article, we survey the NW sensor landscape. First, we lay out performance parameters employed to evaluate progress. We then move on to compositions, fabrication methods, device architectures, and operational modalities. Rather than a comprehensive review, we discuss selected examples to highlight advantages of NW sensors, the status of the field, and opportunities for going forward, which we hope provides a roadmap for future innovations.

1.3 Sensory device performance parameters

The performance of a chemical sensor is a product of the physical form of the sensor material, strength of the analyte transduction event, selectivity of the response to a given analyte, and the sensor's stability. Figure 1.2 is a representative sensing trace that may assist in graphically visualizing key terms.

1.3.1 Sensitivity, dynamic range, limit of detection

The limit of detection (LOD) is the minimum amount of analyte that can be detected at a known confidence level.[9] The target LODs in sensors for environmental safety are driven by regulation. Representative values are published by the United States Environmental Protection Agency,[10] the National Institute of Occupational Safety and Health (NIOSH),[11] and the European Union Agency for Safety and Health at Work.[12]

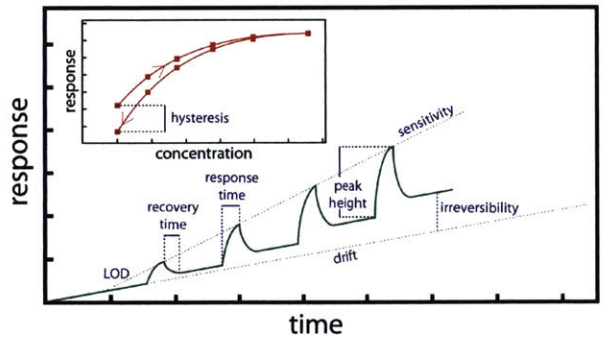

Figure 1.2 Graphical representation of selected device performance parameters in a device successively exposed to increasing concentrations of analyte.

The LOD can be influenced by receptor–analyte interactions, surface area, functionalization, and signal amplification. A low LOD is closely tied to high sensitivity (response per unit concentration). In chemiresistors[13,14] and chemicapacitors,[15] the extent to which analyte influences the electronic properties of NWs is a major factor in the LOD.

Chu et al.[16] demonstrated that alignment of receptors can be used to improve the LOD (Figure 1.3). A surface-modified Si-NW field effect transistor (FET) achieved LODs of 0.1 fM for ssDNA and 0.5 ppm for alcohols. The authors deduced that the field creates structural order to increase the efficiency of molecular reactions, strengthen the molecular dipoles, and consequently improve sensitivity. The reorganizations are likely more complicated than shown in Figure 1.3 (b, c), as APTES generally produces multilayer, polymerized coatings.

An increase in surface area offers more sites for analyte–sensor interactions and lowers LOD. Yue et al.[17] obtained high surface areas in ZnO NW devices by growing them on 3-D graphene foam, resulting in an increased surface area from 6 to 33 m^2/g and a LOD of 1 nM for uric acid and dopamine, indicators of Parkinson's disease.

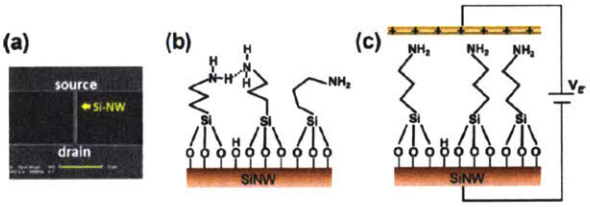

Figure 1.3 Electric field alignment of aminopropyltriethoxysilane (APTES) on SiNW FETs. (a) SEM image of a SiNW-FET. (b, c) Schematic illustrations of the possible APTES molecular structures before and after the alignment process. (Reprinted from Ref. [16] with permission. Copyright 2013 American Chemical Society.)

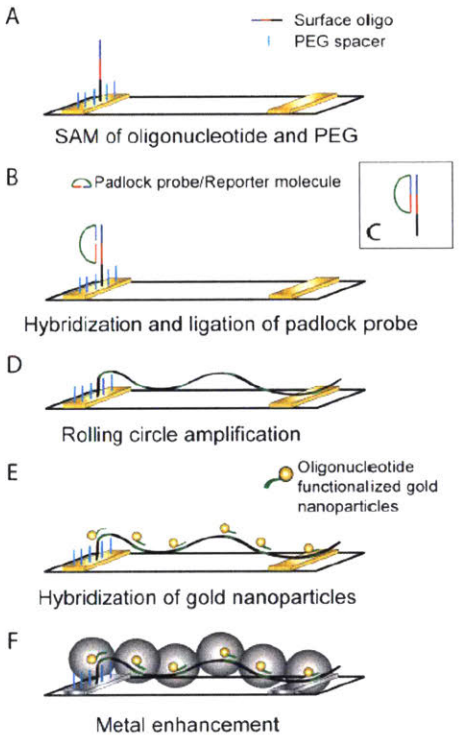

Figure 1.4 Illustration of formation of metalized wires from stretched rolling circle amplification (RCA) products to generate an electrical signal. (Reprinted from Ref. [18] with permission.) (Copyright 2014 American Chemical Society.)

Signal amplification of molecular interactions can reveal otherwise undetectable events. Russell et al.[18] employed a rolling circle amplification (RCA) technique to create DNA strands to template the formation of NWs between two electrodes (Figure 1.4). This turn-on method detected synthetic and bacterial DNA at 100 pM and 66 fM, respectively.

Bounded by the LOD and limit of linearity,[9] dynamic range is the range of analyte concentrations that can be accurately measured by a sensor. NWs can improve sensor dynamic ranges by increasing the limit of linearity (e.g., by increasing the surface area of the sensor to prevent saturation) and by lowering the LOD.

1.3.2 Selectivity

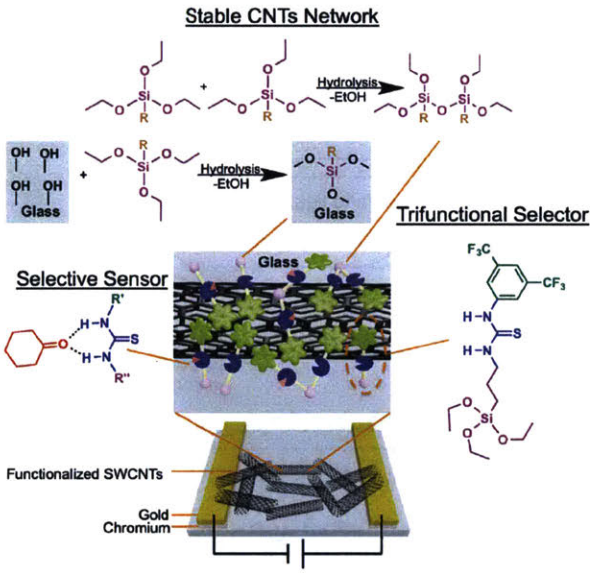

Figure 1.5 Creation of a highly stable SWCNT sensor by polymerization of functional selector around the deposited NW network (Reprinted from Ref. [23] with permission.) (Copyright 2013 American Chemical Society.)

Selectivity is measured as the ratios of sensitivity of the target analyte to that of interferents. *Specificity* should be reserved for cases of ultimate selectivity. Researchers must choose relevant interferents to effectively demonstrate selectivity.

Membrane coatings can exclude interferents based on analyte size, affinity, or permeation time.[19] The operating temperature of a sensor will also affect selectivity. Increased selectivity can also be achieved by using a separate device to bind and pre-concentrate an analyte followed by thermal desorption to the sensor.[20–22] Many sensors derive selectivity from functionalization with recognition elements that interact selectively with an analyte. In Section 6, we discuss how functionalization can impart selectivity.

1.3.3 Stability

Stability is determined by the sensor's ability to produce the same output for an identical input over time, quantified as a ratio of the aged device's response relative to a new device's response. A stable sensor should remain unchanged over the lifespan of the device.

NW functionalization has been explored to improve stability. Our group demonstrated how SWCNTs functionalized with trialkoxysilane moieties exhibit increased robustness (Figure 1.5). Hydrolytic polymerization affixes the SWCNTs in place on the glass substrate. These sensors can survive sonication in methanol.[23] Alternatively, coatings can be used to stabilize devices by functioning as a barrier to reactive chemicals or by immobilizing NWs.[23–27]

1.3.4 Drift

Drift is the stimuli-independent change of a measurable output over time. It can lead to uncertain results, false alarms, and the need for frequent recalibration or replacement of sensors. Furthermore, there is a dearth of discussion on drift in the literature. There can be both short- and long-term drift, and the difference between the two can in some cases allow one to deconvolute specific contributions.[28–30] Some potential causes include reorientation of particles and domains, segregation of mixtures, sublimation/evaporation of components, adsorption of species, doping/de-doping, and charge migration. The high surface area of NWs creates a challenge for drift, and how to mitigate these factors without passivation needs further exploration.

Drift can be addressed either by in-device recalibration[31] or algorithmically during data processing and/or workup, for instance, by using principal component analysis (PCA).[30] However, many applications cannot sustain intensive computational solutions to sensor drift. Therefore, the challenge of drift must be addressed at the device level.

1.3.5. Hysteresis

Hysteresis is the difference between outputs when an analyte concentration is approached from an increasing and decreasing range.[32] It is important to minimize as a result of the challenges it poses to reversibility and dynamic range. When this suppression is not possible, the best one can do is characterize the hysteresis of the sensor.

1.3.6. Response time, dead time, rise time

Response time is determined at 90% of its final amplitude after analyte exposure,[33] dead time is the time it takes to reach the first 10% of its final signal, and rise time is the difference.[34] Response time is critical as many applications employ sensors to activate

systems in response to changing analyte levels.[32] The factors that govern response time mirror those of reaction kinetics: surface area,[35] temperature,[33] and catalysis.[36]

1.3.7. Reversibility and recovery time

Reversibility is the extent to which signal is restored to its initial state prior to analyte exposure.[37] The recovery time is the time to decrease to 10% of the peak amplitude after removing the analyte. Although irreversibility can be exploited in dosimetry, incomplete, sluggish recovery is often undesirable.

Remedies to promote complete recovery include heating the sensor[14,38,39] or exposing the sensor to ultraviolet (UV) light.[40] However, heat and UV treatment create more complex systems with difficulties such as baseline noise and attenuated device lifetimes. Further investigations into alternate solutions for irreversibility are needed.

1.4 Nanowire types

We define a NW as a high aspect ratio nanostructure capable of charge transport. *Wire* does not imply an intrinsic metallic electronic state; most NWs in chemical sensors are in fact semiconductors. Semiconducting polymers, which can be considered molecular wires, were first recognized as affording signal amplification prior to the extensive NW sensor efforts.[41-43] However, we will restrict ourselves to a more conventional description of NWs: high aspect ratio materials that are larger than a conventional polymer chain and often polydisperse in terms of length, diameter, and composition.

1.4.1 Elemental semiconductor NWs

NWs fabricated from Si and Ge have been extensively studied in sensors, especially in FETs.[44–47] Si NWs are popular as a result of their compatibility with Si electronics and because Si doping and functionalization are mature technologies. However, they have limited stability and oxidize quickly, resulting in surface passivation. Silica NWs (SiO_2 NWs), however, have been substantially documented as an excellent material for sensing applications because of their ease of modification, functionalization, and biocompatibility.[48]

Si/Ge NW synthesis can be accomplished through methods such as thermal evaporation.[49,50] A common technique for growing various inorganic NWs is the vapor-liquid-solid (VLS) method using chemical vapor deposition (CVD) processes.[51,52] Laser ablation can be used with VLS.[53] Si/Ge NWs can also be grown from solution using a supercritical fluid-liquid-solid growth method.[54]

1.4.2. Metal chalcogenide or pnictide NWs

NWs of chalcogenides such as SnO_2, ZnO, TiO_2, In_2O_3, WO_3, V_2O_5, CuO, Cr_2O_3, Nb_2O_5 and Fe_2O_3 and pnictides such as GaN or AlGaN, have been used extensively in chemiresistive gas sensors[36,55–57] and FETs.[47,58] Their sensing often relies on redox reactions between the analyte and the surface, generating variations in carrier concentrations, or surface trapping. They are inexpensive, robust to temperature and resistant to caustic environments, easily integrated into electronic circuits, and give high sensitivity.[59] However, their use in sensing is often hampered by poor selectivity and high operating temperatures.[55,59,60] Nitrogen oxides (NO_x) have been analytes of choice to assess the performance of metal oxide-based devices.[61–64] NWs of oxides can be synthesized by methods[52] that are variations on VLS in CVD[44,57,58,65] or catalyst-free thermal oxidation.[57,66,67]

1.4.3 Carbon nanotubes (CNTs)

CNTs are excellent sensor candidates due to their mechanical and electrical properties.[68–70] Since Iijima and co-workers[71] significantly raised the profile of CNTs in 1991, there has been a widespread effort to exploit their properties. CNTs can be considered as long hollow tubes of rolled-up graphene sheets. The angles at which they are rolled (the chiral vector) and the tube diameter determine whether a CNT is semiconducting or metallic. CNTs are either single-walled (SWCNT) or multi-walled (MWCNT). MWCNTs consist of multiple concentric layers of SWCNTs. In defect-free tubes, the bonds between carbons in the sidewalls are sp^2 hybridized, and non-covalent van der Waals forces or π-stacking dominate intermolecular interactions. CNTs are synthesized via laser ablation,[72] arc discharge,[71] CVD, and combustion.[73–75] CVD is the premier method with mild conditions, high yield, simplicity, and facile mediation of physical characteristics.[76,77] Recent reviews can be found on CNTs in biotechnology and drug delivery,[69,78–80] electronics,[81] energy production and storage,[82–84] and catalysis.[85,86]

CNTs have found a special place in the sensor community because of aforementioned properties, compatibility with organic chemistry for functionalization,[87] and easy integration into electronic circuits.[88] CNTs have been used to sense biological molecules[89–95] and vapors of industrial gases and explosives.[23,96–102]

1.4.4 Transition metal NWs

Metal-based NWs such as Ni, Pt, Pd, Au, Ag, Pb, and Co have found limited applications in chemical sensing compared to their semiconducting counterparts,[55] but they excel in the use of group 10 NWs in H_2 sensing,[47,55,103] Ag NWs for NH_3 sensing,[104] Au NWs for alkanethiol sensing,[105] Ni and Cu NWs for carbohydrate sensing,[106] and organothiol-functionalized Au NWs for biosensing.[53] Metal NWs can be synthesized from chemical

etching[105] or reductive cation electrodeposition.[103,107] Metal NWs can be synthesized by bulk solution phase methods where a polyol is used as both solvent and reducing agent for metal cations.

1.4.5 Conducting Polymer NWs

Conducting (or conjugated) polymers (CPs) are a class of materials that are semiconducting upon oxidation or reduction (doping).[108] Their molecular construction allows for intimate integration of receptor units into the backbone. Sensing relies on inducing modification of band structure or structure, resulting in changes in electronic properties.[108] Many reviews exist on these materials as sensors.[109–112] We restrict this discussion to NW constructions created from CPs.

Polymers in 1-D assemblies are formed by oxidative polymerization and can have improved electrochemical capacities.[113,114] Templated synthesis relies on physical supports (hard template) to create nanostructures or on molecular self-assembly to guide growth of CP-based NWs (soft template). Template-free syntheses also exist.[115] Electrospinning of nanofibers allows control over size, alignment, morphology and surface functionalization.[116,117] Nanolithography methods allow reproduction of a pattern on a surface.[118,119] CP NW films can also be deposited by layer-by-layer (LbL), Langmuir-Blodgett (LB), inkjet printing, dip-coating and spin-coating, drop-casting, electrophoretic deposition and thermal evaporation.[120,121]

Sensors based on FETs (organic field-effect transistors, OFETs, and organic electrochemical transistors, OECTs) and chemiresistor architectures have revolutionized sensing using CPs with short response times, high sensitivity, easy device integration,[108,120] and room-temperature operation.[120] CPs can serve as a receptor layer, transducer, protective

coating, or electronic circuit.[122] Sensing with non-functionalized CPs is mostly limited to small molecules (e.g., HCl, NH_3, hydrazine, chloroform, acetone, acetonitrile, alcohols, and benzene)[123,124] and cations (e.g., Cu^{2+}[125,126], Ag^{+}[127], Pb^{2+} and Cd^{2+}[128], and K^{+} and Ca^{2+}[129]) in solution and reactive gases (e.g., H_2, N_2H_4, NH_3, H_2S, HCl).[122] CPs can be functionalized and included in formulations to improve sensor properties.[130] Long-term instability, irreversibility, and poor selectivity are the main drawbacks of CPs in sensing.[120]

1.5 NW assembly and sensor fabrication

NW devices can be classified by the number of NWs (one or many) and orientation (aligned, not aligned). Single NW devices have a NW bridging the gap between two electrodes (Figure 1.6a, 1.6b) and offer high sensitivity, fast response to changing analyte concentrations, and high spatial resolution.[131] However, single NW devices require specialized equipment to fabricate, and the low yield of functional devices increases cost. The Leiber group has used single crystalline NWs,[132] n- and p-doped Si and Ge nanowires,[133,134] in FETs[135] for detection of DNA,[136] single viruses,[137] cancer markers,[138] and small molecule-protein interactions.[139] The Nuckolls group (Figure 1.7) has shown novel NW junctions[140] where SWCNTs are cut and then reconnected by small molecules with probes to observe binding events such as methylation of DNA.[141] They also bridged SWCNT-SWCNT junctions with DNA, thus illustrating the ability of DNA-nanowire devices to serve as sensors for biochemical events.[142]

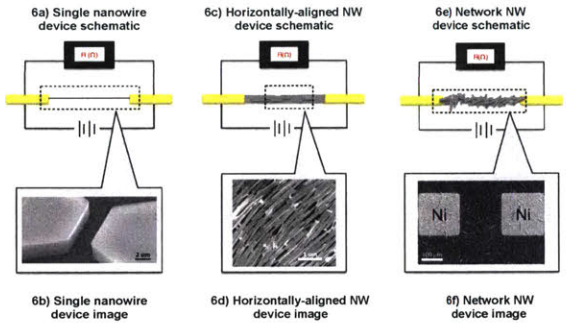

Figure 1.6 Types of NW devices (schematics and images). [Figure 1.6b provided by reference [143] with the permission of 2006 Nature Publishing Group; Figure 1.6d provided by reference [144] with the permission of American Chemical Society 2003; Figure 1.6f provided by reference [145] with the permission of the Royal Society of Chemistry 2014]

Aligned multi-NW devices (Figure 1.6c, 1.6d) have multiple NWs arranged in a single orientation. Compared to NW networks, aligned NW devices have longer mean free paths for conducting electrons and meet percolation thresholds for connectivity with fewer inter-NW contacts. Accordingly, aligned NW devices can have lower resistance and greater current density but require complicated assembly processes.

Network NW devices (Figure 1.6e, 1.6f) are those in which the orientation of NWs is random. Because of the sheer number of NWs, statistics mitigate effects of electronic heterogeneity arising from polydispersity in NW length, diameter, and structure. Network devices diminish the need for precise position or orientation of any individual NW, which lowers the difficulty of fabricating devices. On the other hand, network devices have shorter mean free paths for electrons, leading to higher resistance and lower current density. Networks contain resistive NW-NW junctions that offer prospects for innovative integration of molecular switches.

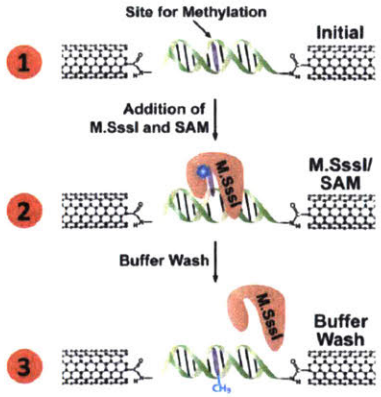

Figure 1.7 Electrical detection of methyl transferase (M.SssI) binding at a DNA-bridged CNT device. (Reprinted from Ref. [142] with permission.) (Copyright 2012 Royal Society of Chemistry.)

1.6 Platform architectures for sensor devices

The electronic properties of NWs are sensitive to changes in their chemical environment. These changes can be electrically evaluated using simple device architectures. A resistor (chemiresistor) is the simplest device with two electrodes (source and drain) on an insulating support connected by NWs (Figure 1.8A). The resistance can be measured by monitoring changes in current with a fixed voltage bias across the electrodes.

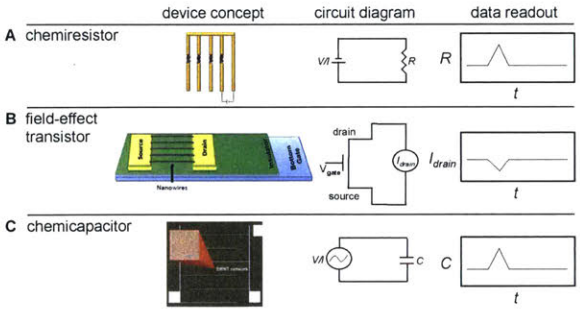

Figure 1.8 Graphical representation of chemiresistor, FET, and chemicapacitor[15] devices and corresponding circuit diagrams and data readouts.

It can be advantageous to control the carrier concentration when transduction results from charge transfer interactions between a semiconducting NW and analyte. An additional electrode (gate) underneath the support converts a resistor into a FET and introduces additional control of carrier densities through modulation of the applied gate voltage and insight into the sensory mechanism (Figure 1.8B).

Changes in capacitance can also be analyte-specific. The high surface area and prospects for polarizing interfaces are well suited to creating large capacitive signals (Figure 1.8C). The use of AC field for measurements in chemicapacitors can reduce $1/f$ noise, ensure rapid response, and avoid electrophoretic effects from an applied directional voltage, which can reduce drift and enhance reversibility. Moreover, simultaneously examining changes in conductance and capacitance can help increase specificity.

The analog nature of chemiresponsive circuit components allows for facile integration into wireless devices such as resonant circuits and radio-frequency identification (RFID) antennas. Resonant circuits are comprised of inductive, resistive, and capacitive elements, so chemiresponsive elements directly influence their resonant frequency and Q-factor. Our group leveraged these features and developed SWCNT sensors that are wirelessly powered and read by smartphones[146] (Figure 1.9). This method uses the smartphone's near field communication (NFC) by cutting the circuit of a passive sensor tag and reconnecting it with chemiresponsive SWCNTs.

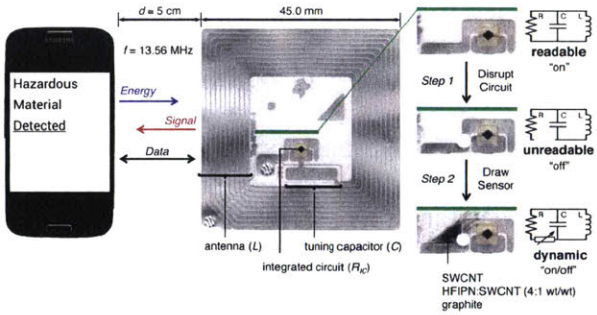

Figure 1.9 Illustration of a smartphone wirelessly powering and communicating with a passive RFID tag. (Reprinted from Ref. [146] with permission.) (Copyright 2014 Proceedings of the National Academies of Science.)

1.7 Functionalization methods for applications

NWs display useful intrinsic sensor properties, but functionalization is generally necessary to improve processability, sensitivity, selectivity, operating conditions, and stability.

1.7.1 Functionalization of inorganic semiconductor NWs

1.7.1.1 Non-covalent Functionalization of Inorganic Semiconductor NWs

Typical NW functionalization involves sputtering of metal films (Pt or Pd, typically 100 Å) on top of GaN,[147] InN,[148] or Si.[149] In the presence of catalytic Pt or Pd on NWs, H_2 binds and dissociates, modifying the carrier concentrations as evidenced by FET measurements.[150] Coating NWs with metals allows for faster, enhanced response and shortened recovery time. Au nanoparticles (AuNPs) were deposited onto GaN NWs by plasma-enhanced chemical vapor deposition (PECVD), and physisorption of gases such as N_2 and CH_4 reduced conductivity of the NW network.[151] CO_2 sensing was achieved by coating GaN NW transistors with poly(ethyleneimine) (PEI). In the presence of CO_2 and humidity, carbamic acid groups form and ionize to create new charges that affect the transport of the NWs.[152]

Specific detection of biological species is achieved by functionalization of NWs with receptors possessing high selectivity (enzymes or antibodies).[153] Glucose oxidase was immobilized in a ZnO NW matrix on top of a GaN transistor. In the presence of glucose, the enzyme catalyzes formation of gluconic acid and peroxide, which translates into a change in charge on the NWs, allowing for real-time glucose monitoring and a 0.5 nM LOD.[154] Approaches have also been reported for detection of biomarkers such as prostate-specific antigen (PSA) using In_2O_3 NWs functionalized with antibodies via phosphonic acid binding.[155] DNA sensing was achieved at 10 pM detection limit by electrostatically adsorbed complementary ssDNA onto Si NWs functionalized with amine side chains.[156]

1.7.1.. Covalent functionalization of inorganic semiconductor NWs

If an oxide layer is present, silane chemistry allows for functionalization of Si NWs with functional groups (amines, aldehydes) for further functionalization.[138] However, the passivating oxide layer lowers sensitivity,[157] so the SiO_2 is often etched away, and the exposed surface is covalently functionalized by hydrosilylation, halogenation, alkylation, thiolation, or arylation.[158]

One of the earliest reports in Si-based FET sensing described pH monitoring by APTES-functionalized NWs,[133] and the same type of NWs were found to respond to TNT in sub-fM amounts in solution and sub-ppt concentrations in air through formation of Meisenheimer complexes.[45] Si NWs modified with thiol groups showed response to Cd^{2+} and Hg^{2+}.[159] Peptides were attached to Si NWs and used in an array to detect Cu^{2+} and Pb^{2+} in low nM concentrations,[160] and Na^{+} was detected by crown ether-functionalized Si NWs.[46] Volatile organic compounds (VOCs) and small molecules (NH_3, acetone, NMe_3, acetic acid) were detected orthogonally by oligopeptides appended to Si NWs.[161] Many biosensors were

developed by appending receptors to Si NWs[162,163] such as biotin for streptavidin recognition,[164] antigens for recognition of their respective antibody,[137,165] and DNA strands for recognition of complementary oligonucleotides.[166]

1.7.2 Functionalization of metal oxide NWs

1.7.2.1 Compositional mixtures with metal oxide NWs

Metal oxides possess many desired properties, but rarely does one exhibit all desired attributes.[167] Work function and carrier density can be modulated by preparing mixed metal oxides. There has been considerable effort in the functionalization of SnO_2.[58] Gaseous analytes such as H_2S,[168] EtOH,[169–172] CO,[173] H_2[174] and formaldehyde[175–177] have been detected using mixed metal oxides. Integrating SnO_2 nanocrystals with CuO-NWs allows for detection of NH_3 at room temperature.[178] The presence of highly environment-sensitive nanosized p-n junctions was given as an explanation for the sensitivity. Copper oxide NWs have garnered attention as a non-enzymatic determination of biologically important molecules. CuO-NWs have been used as the active sensing component to determine glucose concentration in concert with a Nafion film[179] and in a Cu-CuO NW composition.[180] In both cases, the NWs electrocatalyze the oxidation of glucose; both devices display high sensitivity and linearity in the biological range of blood glucose (3-50 mM) and environmental stability. Electrochemically synthesized Cu_2O-NWs have been employed with Nafion to determine H_2O_2 concentration over a wide and relevant range (0.25 μm to 5.0 mM) and a low LOD (0.12 μm).[181]

AuNP-decorated SnO_2 NWs provide enhanced sensing performance for NO_2[182] and aromatic gases (i.e., benzene, toluene).[183] Similarly, SnO_2 NWs decorated with AgNPs displayed improved sensitivity and selectivity for ethanol over other gaseous analytes,[184] and

PtNP-decorated SnO_2 nanofibers detected acetone in sub-ppm concentrations.[185] More complex functionalization schemes exist where the (doped or mixed) metal oxide is decorated with other nanostructures. A recent example reported Mg-doped In_2O_3 NWs functionalized with metal NPs (Au, Ag, or Pt). Used in an array at room temperature, the sensors were able to discriminate vapors of CO, ethanol, and H_2 at 100 ppm, and the LOD for CO was 0.5 ppm.[186]

1.7.2.2 Covalent functionalization of metal oxide NWs

Covalent functionalization has been investigated mostly for biofunctionalization. ZnO can be modified with carboxylic acid or amine functions for further functionalization.[148] APTES was used to functionalize ZnO NWs with uricase in order to develop a FET sensor for uric acid in aqueous solution.[187] GaN NWs are also amenable to organosilane chemistry, allowing covalent functionalization to afford sensors with high stability.[188]

1.7.3. Functionalization of carbon nanotubes

CNTs offer some of the best opportunities for precise molecular assembly; however, they have considerable imprecision in structure and are mixtures with different diameters, chiralities, and lengths. They also have aperiodic functional groups (defects) that influence their properties. There is still much to learn in how to best functionalize SWCNTs in order to create optimal NW sensors.

1.7.3.1 Physical mixtures containing CNTs

Functionalization can be achieved by mixing CNTs with selectors, which often leads to composites of lower stability than covalent modification. The fabrication of metal–CNT composites is achieved through sputtering[189,190] or electrodeposition.[191] Physical mixtures of

MWCNTs and PMMA have also been used for sensing CH_2Cl_2 and $CHCl_3$, where the response was ascribed to a swelling mechanism.[192] Solution mixing was used to fabricate SWCNT mixtures with a copper(I) scorpionate for the detection of ethylene.[193] In this case, the copper(I) was modelled as binding to the CNT (Figure 1.10). Finally, physical mixtures of small molecule selectors and either MWCNTs or SWCNTs have been produced via solid-state mechanical mixing for chemiresistors.[98] This rapid prototyping method allows for screening of CNT composites as sensor materials.[98]

1.7.3.2 Non-covalent functionalization of CNTs

Non-covalent modification is less invasive than covalent functionalization as it relies on pi (π)-interactions and van der Waals interactions between molecules and CNTs. Non-covalent interactions are often integral to dispersing CNTs, achieved through solution-based mixing, in situ polymerization, or melt mixing.[194] Wei et al. showed detection of trinitrotoluene (TNT) using aminopyrene as a selector.[195] For the detection of cyclohexanone by Frazier and Swager (Figure 1.5),[23] a trifunctional molecule containing an aromatic unit (hexafluoroxylene), a selector unit (a thiourea), and an anchoring unit (a silane) gave non-covalently functionalized CNTs with superior durability and good sensitivity.

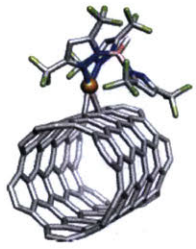

Figure 1.10 Optimized structure of copper(I) scorpionate bound to 6,5-SWCNT. (Reprinted from Ref. [193].)

A common strategy is to use polymers. The active materials are typically obtained by drop-casting,[27,196] dip-coating,[197] solution mixing[198] or in situ polymerization.[199–201] CPs are excellent for dispersion of SWCNTs.[202] Polythiophenes with receptor-based sidechains have been used in sensors to discriminate between different xylenes (Figure 1.11).[203]

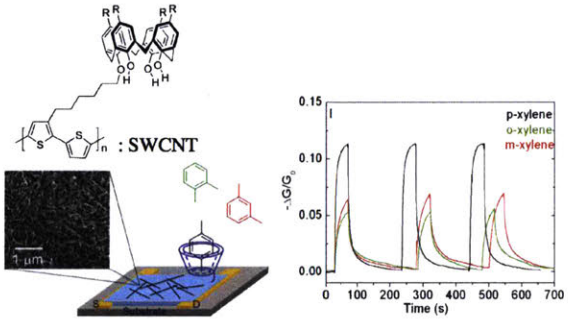

Figure 1.11 Schematic view of the SWCNT/polymer sensor that selectively adsorbs *p*-xylene. (Reprinted from Ref. [203].)

1.7.3.3 Covalent functionalization of CNTs

Covalent modification disturbs the π-electron system and adds defects but can increase the stability of dispersions. Common sidewall reactions include azomethine ylide dipolar cycloadditions and reductive reactions with diazonium ions.[194,204–206] Covalent functionalization can also be conducted at CNT termini. A common strategy relies on oxidation to produce carboxylic acid moieties at defect sites, which can be further functionalized. Weizmann et al. demonstrated exclusive regioselective functionalization SWCNT termini for the detection of single-stranded DNA (ssDNA) using a chemiresistor with detection limits of 10 fM and discrimination of single, double, and triple base pair mismatches (Figure 1.12).[207] End-of-tube oxidation followed by polymer modification has also been used to build FET sensors with ppb-level detection limits for NH_3 and NO_2.[208]

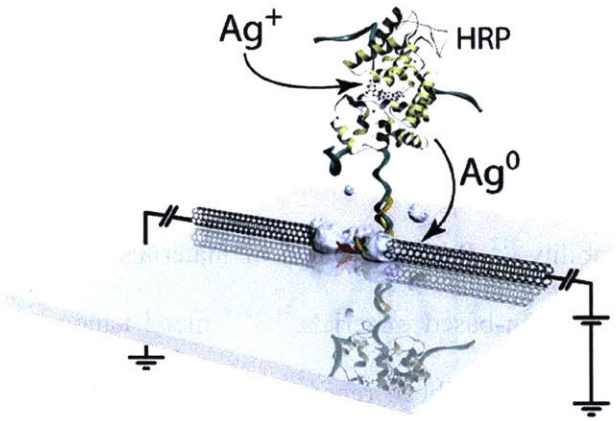

Figure 1.12. DNA–CNT NW and HRP probe hybridization for DNA junction visualization. (Reprinted from Ref. [207] with permission.) (Copyright 2011 American Chemical Society.)

Using phenyl radical addition, Vlandas et al. demonstrated covalent functionalization of SWCNT sidewalls with boronic acids for detection of glucose at 5–30 mM.[209] Huang et al. utilized a similar approach to functionalize double-walled CNTs (DWCNTs) with aromatic carboxylic acids as a selective sensor for NH_3.[210] DWCNTs allowed for higher degrees of functionalization compared to SWCNTs. Our group has demonstrated covalent functionalization of SWCNTs via thermal aziridination to introduce amino groups that were further functionalized with hydrogen bond donors for the detection of cyclohexanone and nitromethane.[96] The covalent functionalization of MWCNTs using a modular zwitterionic functionalization strategy allowed for formation of diverse densely functionalized materials. Arrays of these materials were used in detection of a number of volatile organic compounds.[211]

1.7.4 Functionalization of conducting polymer NWs

As discussed earlier, by our definition CPs are not intrinsically NWs. However, they can be used to create NWs by templated synthesis or assembled in composite structures with nanofibers or CNTs.

1.7.4.1 Physical mixtures of CP NWs

Composites with CPs can produce materials with superior properties such as high selectivity and sensitivity, enhanced resistance to humidity, low detection limits, low sensing temperatures, and enhanced stability.[212] Rational design of materials combining CPs with non-conductive polymers,[213,214] carbon-based materials,[215–218] metal nanoparticles[219,220] and oxides,[221] or biological materials[222,223] has been reported. CPs can serve as a matrix for a secondary material or can be decorated with nanostructures in an organized manner.[130,224,225]

Polyaniline (PANI) was widely investigated and combined with carbon-based materials[226] such as CNTs[215,216] or metal oxides.[221] "One-pot" procedures are used where aniline is oxidatively polymerized in the presence of CNTs.[218] For example, PANI-SWCNT composites are sensors for NH_3 and HCl.[218] Compared to chemically modified polymers, blending materials together avoids complex syntheses, and composite materials may have improved morphology, partition coefficients toward analytes, swelling behavior, mechanical or conductive properties. An additive can also help maintain properties of the polymer and increase lifetime.[120] Polymers enable the production electrospun high surface area nanofibers for gas sensors with enhanced sensitivity and reversibility over bulk films.[227]

1.7.4.2 Non-covalent functionalization of CP NWs

Non-covalent functionalization can be accomplished by deposition of NPs onto the surface of CP fibers. For example, AgNP-decorated PEDOT NWs were found to detect NH_3 with a detection limit (1 ppm) fivefold lower than that of pristine PEDOT NWs,[228] and AuNP-decorated PANI NWs show excellent response to H_2S.[229]

1.7.4.3 Covalent functionalization of CP NWs

Covalent modifications have been used to improve solubility, processability and sensing. These modifications include side-chain, co-polymer, or graft functionalization.[120] Many schemes have been developed to immobilize biocompatible receptors onto polymers in order to enhance stability under aqueous conditions.[230] Polypyrrole (PPy) is particularly amenable to covalent functionalization because the nitrogen atom can be functionalized. PPy-NTA (nitrilotriacetic acid) chelator NWs were found to detect Cu^{2+} cations at sub-ppt concentrations, and the Cu^{2+} complex could be used to detect His-tagged proteins.[231] Carboxylic acid-functionalized polypyrrole (CPPy) NWs were found to improve immobilization onto APTES-functionalized surfaces through covalent linking, with the remaining carboxylic acid moieties available for bioconjugation. FET sensors based on this scheme were developed for proteins.[232] The nitrogen position of PPy was functionalized with biomolecules, and the materials were used to detect cancer antigens (CA125),[233] bacteriophages,[234] bacterial spores,[235] or human serum albumin.[236]

1.8 Roadmap for future developments

The last two decades have produced many innovations in nanofabrication, and we are in an opportunity-rich environment for the creation of functional NW sensors. The sensor designer must continue expanding the toolbox of options in order to tackle problems of selectivity, drift, sensitivity, and stability. Improved understanding of the basis of analyte detection in NW sensors is needed to guide this development. We suggest areas of need and opportunities for the inspired sensor researcher.

1.8.1 Improving selectivity

To many critics, a fundamental limitation is that chemical/biological sensors often lack the ability to identify unambiguously an analyte.[237] It is true that high-resolution mass spectrometry can give near-perfect identification of small, readily volatilized molecules. Even so, front-end separation by gas or liquid chromatography is often necessary. There has been massive investment in creating portable spectrometers, but these systems generally sacrifice precision for portability and only offer incremental advances. In most cases, NW sensors will not provide superior identification. However, they provide useful information at a fraction of the cost by eliminating the need for expensive electronics, power supplies, and physical structures.

Broad adoption of NW chemical/biological sensors will require improvements in selectivity. Solutions will involve a combination of innovations in integration of molecular recognition as well as in increasing computational innovations and the dimensionality of sensing data.

1.8.2 Mitigating sensor drift

The effects of drift can be mitigated through data manipulation[29,30] such as baseline correction or reference device normalization but remains a fundamental limitation that hinders adoption in applications, especially for continuous monitoring and for ultra-low-cost devices without the power or computational budget to execute these techniques.

The key to minimizing thermally induced drift is developing new techniques that limit nanoscopic rearrangements of thin film sensor components. Covalent chemistries such as cross-linking that bind NWs to themselves or the substrate should continue to be developed, and matrices may also decrease drift and improve device lifetimes.

When the NW transducer and selector are distinct, drift can be minimized by strengthening the selector binding to the NW to mitigate phase segregation. Tethering can be accomplished by covalent attachment[96,211] or by increasing the number or strength of non-covalent binding moieties.[238]

Drift is also induced electrically and is dependent upon the strength of the applied field. This contribution to drift can be minimized by decreasing the voltage bias, performing a medium-to-high voltage AC pretreatment to accelerate equilibration processes, or using thermal or UV treatments to release trapped charges. Devices that operate under instantaneous applied voltage instead of a static electric field should drift less per unit time; passive RF devices are a promising platform. Less drift should lead to longer device lifetimes. It may also be possible to mitigate drift by creating dynamic fluid environments that maintain equilibrium. Indeed, mucus protects the mammalian olfactory epithelium[239], and designer fluids could selectively partition and transport analytes to sensors.

1.8.3 Improving Sensitivity

Strategies for enhanced sensitivity include the following: (1) The design of molecular recognition elements where analyte interactions are intimately coupled to carrier transport/generation/depletion. Innovations here can be made by bottom-up chemical designs employing molecular recognition, designer NWs with engineered work functions, coupling of biological recognition/catalysis, and nanostructures. (2) Developing sensors that leverage junctions between NWs and electrodes. Schottky barriers[36,103,149] and swelling-induced expansion of tunnelling barriers[113,122,216,240] have been introduced as important mechanisms. A major opportunity lies in placing responsive materials/molecules in the tunnel junction that can be chemically triggered to have resonant electronic states with the NWs. Rectifying

interfaces between p- and n-NWs can also provide opportunities for amplification in analogy to gain produced by avalanche photodiodes. (3) Complex signals can be used to minimize noise, and combinations of resistive and capacitive responses need to be understood. Advances in capacitive sensing are possible by utilizing charge polarization along the length of NWs isolated by resistive junctions. Space charge contributions to a material's dielectric constant are much larger than simple dipolar effects. Effectively harnessing space charge changes in chemical/biological sensors will involve careful positioning (orienting) of NWs, controlling the electrical transport and dielectric coupling between NWs, and choice of optimal fields and frequencies.

1.8.4 Mechanistic Analysis of Responses

Ideal designs exploiting the aforementioned mechanisms require comprehensive understanding of their contributions to NW sensor responses, which remains elusive. Deconvolution of sensor response contributors is a challenge that holds great promise for the field. In addition to informing rational design of molecular recognition and their implementation in NW sensors, the ability to extract multi-dimensional information out of a single NW sensor device is an attractive prospect. NW FETs and resonant circuits[241] hold promise as device architectures capable of accomplishing this task, but advances in multi-dimensional experimental design will be required.

1.8.5 Current and emerging applications

The first consideration when designing a NW sensor should be its environment. Common environmental problems include temperature, humidity, interferents, EM effects, and biofouling. One must also consider how data will be retrieved and how often, which leads us to consider power requirements and sensor stability. If the sensor operates for a long period

and operates passively, then a coin-cell battery and a pre-determined data logging time interval may be optimal. Conversely, if data is required on demand, a larger on-board power source may be required. Novel approaches to powering sensors include triboelectric methods,[242–245] remote photo- or thermal power harvesting, and resonant inductive coupling. The concept of coupling NWs into devices capable of wireless power transfer is relatively new, but early reports are promising.[242,246–250] One must also consider whether the sensor will be in a durable or expendable form factor.

Next, one must consider how the analytes are likely to encounter the sensing element. Point surveillance is often sufficient for object-level monitoring, while area surveillance may be necessary for situational awareness in a large 3-D space. Area surveillance requires more than one sensor, and therefore, the total cost of goods should be considered.

Selectively recognizing an analyte is perhaps the heart of sensor design. Analytes are categorized as VOCs, oxidizers and reducers, particulates, biological macromolecules, and viruses and bacteria. The ability to detect VOCs continues to improve as molecular design principles are introduced and coupled to NWs. Oxidizers and reducers are often detected by exploiting their influence on carrier concentrations and the Schottky barrier. Greater efforts are needed to detect particulates due to their vast size, shape, and charge dispersity. Biological macromolecules can be targeted by leveraging nature's biomolecular machinery, but this is not a general design approach. Viruses and bacteria interact by multivalent processes, and translating these collective processes into robust signals that are discernable from other events are needed. Robust inexpensive trace virus and bacterial detection has far-reaching implications for human health and safety.

The fidelity of information is of critical importance in chemical/biological sensing. The vast majority of chemical sensors have low specificity, and practitioners often assume that

more data from, for example, a large sensor array is better. However, Occam's razor is generally the best approach with inspired designs that produce high specificity in individual sensors. Such sensors can serve their purpose without an unnecessarily expensive or cumbersome design.

Reversible sensing is generally specified for most applications. However, for many situations where crossing a threshold is relevant, an irreversible dosimeter can be employed that conveys information about the history of the device.

New approaches to extracting more information out of a single sensor or device are beginning to emerge.[251] By combining multivariate extraction of orthogonal parameters with statistical techniques such as PCA, discrimination among analytes with an array is possible.

There is a new sensor paradigm on the horizon. The trend is moving from discrete comprehensive data collection to continuous, parsimonious data collection. Such a move will require the deployment of wireless distributed sensor networks that are linked directly to cloud storage. Chemists, material scientists, physicists, and practitioners will need to work together to develop new modalities that minimize cost per sensor and cost per sensed event. Additionally, opportunities will unfold for fusing chemical information with other inputs to derive new insights about our environment and behavior.

1.8 References

(1) Baptista, F. R.; Belhout, S. A.; Giordani, S.; Quinn, S. J. Recent developments in carbon nanomaterial sensors. *Chem. Soc. Rev.* **2015**, *44*, 4433–4453.
(2) Green, N. S.; Norton, M. L. Interactions of DNA with graphene and sensing applications of graphene field-effect transistor devices: a review. *Anal. Chim. Acta* **2015**, *853*, 127–142.
(3) Late, D. J.; Huang, Y.-K.; Liu, B.; Acharya, J.; Shirodkar, S. N.; Luo, J.; Yan, A.; Charles, D.; Waghmare, U. V; Dravid, V. P.; et al. Sensing behavior of atomically thin-layered MoS2 transistors. *ACS Nano* **2013**, *7*, 4879–4891.
(4) Rao, C. N. R.; Gopalakrishnan, K.; Maitra, U. Comparative Study of Potential Applications of Graphene, MoS 2 , and Other Two-Dimensional Materials in Energy Devices, Sensors, and Related Areas. *ACS Appl. Mater. Interfaces* **2015**, *7*, 7809–7832.
(5) Cho, B.; Hahm, M. G.; Choi, M.; Yoon, J.; Kim, A. R.; Lee, Y.-J.; Park, S.-G.; Kwon, J.-

D.; Kim, C. S.; Song, M.; et al. Charge-transfer-based gas sensing using atomic-layer MoS_2. *Sci. Rep.* **2015**, *5*, 8052.
(6) Kim, J.-S.; Yoo, H.-W.; Choi, H. O.; Jung, H.-T. Tunable volatile organic compounds sensor by using thiolated ligand conjugation on MoS2. *Nano Lett.* **2014**, *14*, 5941–5947.
(7) Perkins, F. K.; Friedman, A. L.; Cobas, E.; Campbell, P. M.; Jernigan, G. G.; Jonker, B. T. Chemical vapor sensing with monolayer MoS_2. *Nano Lett.* **2013**, *13*, 668–673.
(8) Zhou, Q.; Swager, T. M. Fluorescent Chemosensors Based on Energy Migration in Conjugated Polymers: The Molecular Wire Approach to Increased Sensitivity. *J. Am. Chem. Soc.* **1995**, *117*, 12593–12602.
(9) Harris, D. C. *Quantitative Chemical Analysis*, 7th ed.; W. H. Freeman: New York, 2006.
(10) Acute Exposure Guideline Levels (AEGLs) | OPPT | US EPA, 2012.
(11) CDC - NIOSH Regulations, 2013.
(12) Exposure to chemical agents and chemical safety. *EU Directives*, 2015.
(13) Chen, R. J.; Franklin, N. R.; Kong, J.; Cao, J.; Tombler, T. W.; Zhang, Y.; Dai, H. Molecular photodesorption from single-walled carbon nanotubes. *Appl. Phys. Lett.* **2001**, *79*, 2258.
(14) Peng, S.; Cho, K.; Qi, P.; Dai, H. Ab initio study of CNT NO2 gas sensor. *Chem. Phys. Lett.* **2004**, *387*, 271–276.
(15) Snow, E. S.; Perkins, F. K.; Houser, E. J.; Badescu, S. C.; Reinecke, T. L. Chemical detection with a single-walled carbon nanotube capacitor. *Science* **2005**, *307*, 1942–1945.
(16) Chu, C.-J.; Yeh, C.-S.; Liao, C.-K.; Tsai, L.-C.; Huang, C.-M.; Lin, H.-Y.; Shyue, J.-J.; Chen, Y.-T.; Chen, C.-D. Improving nanowire sensing capability by electrical field alignment of surface probing molecules. *Nano Lett.* **2013**, *13*, 2564–2569.
(17) Yue, H. Y.; Huang, S.; Chang, J.; Heo, C.; Yao, F.; Adhikari, S.; Gunes, F.; Liu, L. C.; Lee, T. H.; Oh, E. S.; et al. ZnO Nanowire Arrays on 3D Hierachical Graphene Foam: Biomarker Detection of Parkinson's Disease. *ACS Nano* **2014**, *8*, 1639–1646.
(18) Russell, C.; Welch, K.; Jarvius, J.; Cai, Y.; Brucas, R.; Nikolajeff, F.; Svedlindh, P.; Nilsson, M. Gold Nanowire based Electrical DNA Detection using Rolling Circle Amplification. *ACS Nano* **2014**, *8*, 1147.
(19) *Handbook of Membrane Separations: Chemical, Pharmaceutical, Food, and Biotechnological Applications*, 2nd ed.; Pabby, A. K., Rizvi, S. S. H., Sastre, A. M., Eds.; CRC Press: Boca Raton, 2009.
(20) Hobson, S. T.; Cemalovic, S.; Patel, S. V. Preconcentration and detection of chlorinated organic compounds and benzene. *Analyst* **2012**, *137*, 1284–1289.
(21) Lu, C.-J.; Zellers, E. T. A Dual-Adsorbent Preconcentrator for a Portable Indoor-VOC Microsensor System. *Anal. Chem.* **2001**, *73*, 3449–3457.
(22) Blanco, F.; Vilanova, X.; Fierro, V.; Celzard, A.; Ivanov, P.; Llobet, E.; Cañellas, N.; Ramírez, J. L.; Correig, X. Fabrication and characterisation of microporous activated carbon-based pre-concentrators for benzene vapours. *Sens. Actuators, B* **2008**, *132*, 90–98.
(23) Frazier, K. M.; Swager, T. M. Robust cyclohexanone selective chemiresistors based on single-walled carbon nanotubes. *Anal. Chem.* **2013**, *85*, 7154–7158.
(24) Nan, X.; Gu, Z.; Liu, Z. Immobilizing shortened single-walled carbon nanotubes (SWNTs) on gold using a surface condensation method. *J. Colloid Interface Sci.* **2002**, *245*, 311–318.
(25) Penza, M.; Cassano, G.; Aversa, P.; Antolini, F.; Cusano, A.; Consales, M.; Giordano, M.; Nicolais, L. Carbon nanotubes-coated multi-transducing sensors for VOCs detection. *Sens. Actuators, B* **2005**, *111*, 171–180.
(26) Liu, J.; Xie, C.; Dai, X.; Jin, L.; Zhou, W.; Lieber, C. M. Multifunctional three-

dimensional macroporous nanoelectronic networks for smart materials. *Proc. Natl. Acad. Sci. U. S. A.* **2013**, *110*, 6694–6699.
(27) Wei, C.; Dai, L.; Roy, A.; Tolle, T. B. Multifunctional chemical vapor sensors of aligned carbon nanotube and polymer composites. *J. Am. Chem. Soc.* **2006**, *128*, 1412–1413.
(28) Romain, A. C.; Nicolas, J. Long term stability of metal oxide-based gas sensors for e-nose environmental applications: An overview. *Sens. Actuators, B* **2010**, *146*, 502–506.
(29) Sisk, B. C.; Lewis, N. S. Comparison of analytical methods and calibration methods for correction of detector response drift in arrays of carbon black-polymer composite vapor detectors. *Sens. Actuators, B* **2005**, *104*, 249–268.
(30) Ziyatdinov, A.; Marco, S.; Chaudry, A.; Persaud, K.; Caminal, P.; Perera, A. Drift compensation of gas sensor array data by common principal component analysis. *Sens. Actuators, B* **2010**, *146*, 460–465.
(31) Pardo, M.; Sisk, B. C.; Sberveglieri, G.; Lewis, N. S. Comparison of Fisher's linear discriminant to multilayer perceptron networks in the classification of vapors using sensor array data. *Sens. Actuators, B* **2006**, *115*, 647–655.
(32) Bochenkov, V.; Sergeev, G. Sensitivity, Selectivity, and Stability of Gas-Sensitive Metal-Oxide Nanostructures. In *Metal Oxide Nanostructures and Their Applications*; Umar, A., Hahn, Y.-B., Eds.; American Scientific Publishers: Valencia, CA, 2010; Vol. 3, pp 31–52.
(33) Varghese, O. K.; Gong, D.; Paulose, M.; Ong, K. G.; Grimes, C. A. Hydrogen sensing using titania nanotubes. *Sens. Actuators, B* **2003**, *93*, 338–344.
(34) Calvert, J. G. Glossary of Atmospheric Chemistry Terms. *Pure & Appl. Chem.* **1990**, *62*, 2167–2219.
(35) Harris, K. D.; Huizinga, A.; Brett, M. J. High-Speed Porous Thin Film Humidity Sensors. *Electrochem. Solid-State Lett.* **2002**, *5*, H27-H29.
(36) Kolmakov, A.; Klenov, D. O.; Lilach, Y.; Stemmer, S.; Moskovits, M. Enhanced gas sensing by individual SnO_2 nanowires and nanobelts functionalized with Pd catalyst particles. *Nano Lett.* **2005**, *5*, 667–673.
(37) Saaman, A. A.; Bergveld, P. A note on the use of the word "reversible." *Sens. Actuators*, 1985, *7*, 69–71.
(38) Valentini, L.; Cantalini, C.; Armentano, I.; Kenny, J. M.; Lozzi, L.; Santucci, S. Highly sensitive and selective sensors based on carbon nanotubes thin films for molecular detection. *Diam. Relat. Mater.* **2004**, *13*, 1301–1305.
(39) Cho, W.-S.; Moon, S.-I.; Lee, Y.-L.; Lee, Y.-H.; Park, J.-H.; Ju, B. K. Multiwall carbon nanotube gas sensor fabricated using thermomechanical structure. *IEEE Electron Device Lett.* **2005**, *26*, 498–500.
(40) Li, J.; Lu, Y.; Ye, Q.; Cinke, M.; Han, J.; Meyyappan, M. Carbon Nanotube Sensors for Gas and Organic Vapor Detection. *Nano Lett.* **2003**, *3*, 929–933.
(41) Swager, T. M.; Wosnick, J. H. Self-Amplifying Semiconducting Polymers for Chemical Sensors. *MRS Bull.* **2011**, *27*, 446–450.
(42) Thomas, S. W.; Joly, G. D.; Swager, T. M. Chemical sensors based on amplifying fluorescent conjugated polymers. *Chem. Rev.* **2007**, *107*, 1339–1386.
(43) Swager, T. M. The Molecular Wire Approach to Sensory Signal Amplification. *Acc. Chem. Res.* **1998**, *31*, 201–207.
(44) Ramgir, N. S.; Yang, Y.; Zacharias, M. Nanowire-based sensors. *Small* **2010**, *6*, 1705–1722.
(45) Engel, Y.; Elnathan, R.; Pevzner, A.; Davidi, G.; Flaxer, E.; Patolsky, F. Supersensitive detection of explosives by silicon nanowire arrays. *Angew. Chem. Int. Ed.* **2010**, *49*, 6830–6835.

(46) Su, S.; Wu, W.; Gao, J.; Lu, J.; Fan, C. Nanomaterials-based sensors for applications in environmental monitoring. *J. Mater. Chem.* **2012**, *22*, 18101–18110.
(47) Chen, X.; Wong, C. K. Y.; Yuan, C. A.; Zhang, G. Nanowire-based gas sensors. *Sens. Actuators, B* **2013**, *177*, 178–195.
(48) Kaushik, A.; Kumar, R.; Huey, E.; Bhansali, S.; Nair, N.; Nair, M. Silica nanowires: Growth, integration, and sensing applications. *Microchim. Acta* **2014**, *181*, 1759–1780.
(49) Sutter, E.; Ozturk, B.; Sutter, P. Selective growth of Ge nanowires by low-temperature thermal evaporation. *Nanotechnology* **2008**, *19*, 435607.
(50) Yu, D. P.; Bai, Z. G.; Ding, Y.; Hang, Q. L.; Zhang, H. Z.; Wang, J. J.; Zou, Y. H.; Qian, W.; Xiong, G. C.; Zhou, H. T.; et al. Nanoscale silicon wires synthesized using simple physical evaporation. *Appl. Phys. Lett.* **1998**, *72*, 3458–3460.
(51) Wagner, R. S.; Ellis, W. C. Vapor-Liquid-Solid Mechanism of Single Crystal Growth. *Appl. Phys. Lett.* **1964**, *4*, 89–90.
(52) Wan, Q.; Sun, J.; Liu, H. Semiconducting Oxide Nanowires: Growth, Doping and Device applications. In *Nanowires: Implementations and Applications*; Hashim, A., Ed.; InTech: Rijeka, Croatia, 2011; pp 59–98.
(53) Wanekaya, A. K.; Chen, W.; Myung, N. V; Mulchandani, A. Nanowire-Based Electrochemical Biosensors. *Electroanalysis* **2006**, *18*, 533–550.
(54) Holmes, J. D. Control of Thickness and Orientation of Solution-Grown Silicon Nanowires. *Science.* **2000**, *287*, 1471–1473.
(55) Penner, R. M. Chemical sensing with nanowires. *Annu. Rev. Anal. Chem.* **2012**, *5*, 461–485.
(56) Shen, G.; Chen, P.-C.; Ryu, K.; Zhou, C. Devices and chemical sensing applications of metal oxide nanowires. *J. Mater. Chem.* **2009**, *19*, 828–839.
(57) Kim, I.-D.; Rothschild, A.; Tuller, H. L. Advances and new directions in gas-sensing devices. *Acta Mater.* **2013**, *61*, 974–1000.
(58) Ma, Y.; Qu, Y.; Zhou, W. Surface engineering of one-dimensional tin oxide nanostructures for chemical sensors. *Microchim. Acta* **2013**, *180*, 1181–1200.
(59) Liu, X.; Cheng, S.; Liu, H.; Hu, S.; Zhang, D.; Ning, H. A survey on gas sensing technology. *Sensors* **2012**, *12*, 9635–9665.
(60) Qin, Y.; Sun, X.; Li, X.; Hu, M. Room temperature NO2-sensing properties of Ti-added nonstoichiometric tungsten oxide nanowires. *Sens. Actuators, B* **2012**, *162*, 244–250.
(61) Afzal, A.; Cioffi, N.; Sabbatini, L.; Torsi, L. NOx sensors based on semiconducting metal oxide nanostructures: Progress and perspectives. *Sens. Actuators, B* **2012**, *171–172*, 25–42.
(62) Moon, J.; Park, J.-A.; Lee, S.-J.; Zyung, T.; Kim, I.-D. Pd-doped TiO2 nanofiber networks for gas sensor applications. *Sens. Actuators, B* **2010**, *149*, 301–305.
(63) Xu, S.; Shi, Y. Low temperature high sensor response nano gas sensor using ITO nanofibers. *Sensors Actuators B Chem.* **2009**, *143*, 71–75.
(64) Hwang, I.-S.; Kim, S.-J.; Choi, J.-K.; Choi, J.; Ji, H.; Kim, G.-T.; Cao, G.; Lee, J.-H. Synthesis and gas sensing characteristics of highly crystalline ZnO–SnO2 core–shell nanowires. *Sensors Actuators B Chem.* **2010**, *148*, 595–600.
(65) Wan, Q.; Wei, M.; Zhi, D.; MacManus-Driscoll, J. L.; Blamire, M. G. Epitaxial Growth of Vertically Aligned and Branched Single-Crystalline Tin-Doped Indium Oxide Nanowire Arrays. *Adv. Mater.* **2006**, *18*, 234–238.
(66) Choopun, S.; Hongsith, N.; Wongrat, E. Metal-Oxide Nanowires for Gas Sensors. In *Nanowires - Recent Advances*; Peng, X., Ed.; InTech: Rijeka, Croatia, 2012; pp 3–24.
(67) Wan, Q.; Lin, C. L.; Yu, X. B.; Wang, T. H. Room-temperature hydrogen storage

characteristics of ZnO nanowires. *Appl. Phys. Lett.* **2004**, *84*, 124–126.
(68) Baughman, R. H.; Zakhidov, A. A.; de Heer, W. A. Carbon nanotubes--the route toward applications. *Science.* **2002**, *297*, 787–792.
(69) De Volder, M. F. L.; Tawfick, S. H.; Baughman, R. H.; Hart, A. J. Carbon nanotubes: present and future commercial applications. *Science.* **2013**, *339*, 535–539.
(70) Liu, L.; Ma, W.; Zhang, Z. Macroscopic carbon nanotube assemblies: preparation, properties, and potential applications. *Small* **2011**, *7*, 1504–1520.
(71) Iijima, S. Helical microtubules of graphitic carbon. *Nature* **1991**, *354*, 56–58.
(72) Guo, T.; Nikolaev, P.; Thess, A.; Colbert, D. T.; Smalley, R. E. Catalytic growth of single-walled manotubes by laser vaporization. *Chem. Phys. Lett.* **1995**, *243*, 49–54.
(73) Resasco, D. E.; Alvarez, W. E.; Pompeo, F.; Balzano, L.; Herrera, J. E.; Kitiyanan, B.; Borgna, A. A Scalable Process for Production of Single-walled Carbon Nanotubes (SWNTs) by Catalytic Disproportionation of CO on a Solid Catalyst. *J. Nanoparticle Res.* **2002**, *4*, 131–136.
(74) Nikolaev, P.; Bronikowski, M. J.; Bradley, R. K.; Rohmund, F.; Colbert, D. T.; Smith, K. A.; Smalley, R. E. Gas-phase catalytic growth of single-walled carbon nanotubes from carbon monoxide. *Chem. Phys. Lett.* **1999**, *313*, 91–97.
(75) Richter, H.; Treska, M.; Howard, J. B.; Wen, J. Z.; Thomasson, S. B.; Reading, A. A.; Jardim, P. M.; Vander Sande, J. B. Large Scale Combustion Synthesis of Single-Walled Carbon Nanotubes and Their Characterization. *J. Nanosci. Nanotechnol.* **2008**, *8*, 6065–6074.
(76) Ibrahim, I.; Bachmatiuk, A.; Warner, J. H.; Büchner, B.; Cuniberti, G.; Rümmeli, M. H. CVD-grown horizontally aligned single-walled carbon nanotubes: synthesis routes and growth mechanisms. *Small* **2012**, *8*, 1973–1992.
(77) Zhang, Q.; Huang, J.-Q.; Qian, W.-Z.; Zhang, Y.-Y.; Wei, F. The road for nanomaterials industry: a review of carbon nanotube production, post-treatment, and bulk applications for composites and energy storage. *Small* **2013**, *9*, 1237–1265.
(78) Madani, S. Y.; Naderi, N.; Dissanayake, O.; Tan, A.; Seifalian, A. M. A new era of cancer treatment: carbon nanotubes as drug delivery tools. *Int. J. Nanomedicine* **2011**, *6*, 2963–2979.
(79) Kamalha, E.; Shi, X.; Mwasiagi, J. I.; Zeng, Y. Nanotechnology and carbon nanotubes; A review of potential in drug delivery. *Macromol. Res.* **2012**, *20*, 891–898.
(80) Mallick, K.; Strydom, A. M. Biophilic carbon nanotubes. *Colloids Surf., B* **2013**, *105*, 310–318.
(81) Wang, C.; Takei, K.; Takahashi, T.; Javey, A. Carbon nanotube electronics--moving forward. *Chem. Soc. Rev.* **2013**, *42*, 2592–2609.
(82) Meyyappan, M. Nanostructured materials for supercapacitors. *J. Vac. Sci. Technol. A* **2013**, *31*, 50803.
(83) Cao, Z.; Wei, B. Q. A perspective: carbon nanotube macro-films for energy storage. *Energy & Environ. Sci.* **2013**, *6*, 3183–3201.
(84) Dillon, A. C. Carbon nanotubes for photoconversion and electrical energy storage. *Chem. Rev.* **2010**, *110*, 6856–6872.
(85) *Nanomaterials in Catalysis*; Serp, P., Philippot, K., Eds.; Wiley: Weinheim, Germany, 2013.
(86) Sarkar, S.; Moser, M. L.; Tian, X.; Zhang, X.; Al-Hadeethi, Y. F.; Haddon, R. C. Metals on Graphene and Carbon Nanotube Surfaces: From Mobile Atoms to Atomtronics to Bulk Metals to Clusters and Catalysts. *Chem. Mater.* **2014**, *26*, 184–195.
(87) Karousis, N.; Tagmatarchis, N.; Tasis, D. Current progress on the chemical modification of carbon nanotubes. *Chem. Rev.* **2010**, *110*, 5366–5397.

(88) Schnorr, J. M.; Swager, T. M. Emerging Applications of Carbon Nanotubes. *Chem. Mater.* **2011**, *23*, 646–657.
(89) Liu, S.; Guo, X. Carbon nanomaterials field-effect-transistor-based biosensors. *NPG Asia Mater.* **2012**, *4*, e23.
(90) Chen, Z.; Zhang, X.; Yang, R.; Zhu, Z.; Chen, Y.; Tan, W. Single-walled carbon nanotubes as optical materials for biosensing. *Nanoscale* **2011**, *3*, 1949–1956.
(91) Yang, W.; Ratinac, K. R.; Ringer, S. P.; Thordarson, P.; Gooding, J. J.; Braet, F. Carbon nanomaterials in biosensors: should you use nanotubes or graphene? *Angew. Chem. Int. Ed.* **2010**, *49*, 2114–2138.
(92) Kruss, S.; Landry, M. P.; Vander Ende, E.; Lima, B. M. A.; Reuel, N. F.; Zhang, J.; Nelson, J.; Mu, B.; Hilmer, A.; Strano, M. Neurotransmitter detection using corona phase molecular recognition on fluorescent single-walled carbon nanotube sensors. *J. Am. Chem. Soc.* **2014**, *136*, 713–724.
(93) Jacobs, C. B.; Peairs, M. J.; Venton, B. J. Review: Carbon nanotube based electrochemical sensors for biomolecules. *Anal. Chim. Acta* **2010**, *662*, 105–127.
(94) Balasubramanian, K.; Burghard, M. Biosensors based on carbon nanotubes. *Anal. Bioanal. Chem.* **2006**, *385*, 452–468.
(95) Münzer, A. M.; Michael, Z. P.; Star, A. Carbon Nanotubes for the Label-Free Detection of Biomarkers. *ACS Nano* **2013**, *9*, 7448–7453.
(96) Schnorr, J. M.; van der Zwaag, D.; Walish, J. J.; Weizmann, Y.; Swager, T. M. Sensory Arrays of Covalently Functionalized Single-Walled Carbon Nanotubes for Explosive Detection. *Adv. Funct. Mater.* **2013**, *23*, 5285–5291.
(97) Liu, Y.; Chen, C.-L.; Zhang, Y.; Sonkusale, S. R.; Wang, M. L.; Dokmeci, M. R. SWNT Based Nanosensors for Wireless Detection of Explosives and Chemical Warfare Agents. *IEEE Sens. J.* **2013**, *13*, 202–210.
(98) Mirica, K. A.; Azzarelli, J. M.; Weis, J. G.; Schnorr, J. M.; Swager, T. M. Rapid prototyping of carbon-based chemiresistive gas sensors on paper. *Proc. Natl. Acad. Sci. U. S. A.* **2013**, *110*, E3265-70.
(99) Mirica, K. A.; Weis, J. G.; Schnorr, J. M.; Esser, B.; Swager, T. M. Mechanical Drawing of Gas Sensors on Paper. *Angew. Chemie Int. Ed.* **2012**, *51*, 10740–10745.
(100) Bondavalli, P.; Legagneux, P.; Pribat, D. Carbon nanotubes based transistors as gas sensors: State of the art and critical review. *Sensors Actuators B Chem.* **2009**, *140*, 304–318.
(101) Di Natale, C.; Ferri, G.; Llobet, E. Gas sensors using carbon nanomaterials: A review. *Sensors Actuators B Chem.* **2013**, *179*, 32–45.
(102) Kauffman, D. R.; Star, A. Carbon nanotube gas and vapor sensors. *Angew. Chem. Int. Ed. Engl.* **2008**, *47*, 6550–6570.
(103) Duan, B. K.; Zhang, J.; Bohn, P. W. Conductance-based chemical sensing in metallic nanowires and metal-semiconductor nanostructures. *Anal. Chem.* **2012**, *84*, 2–8.
(104) Murray, B. J.; Walter, E. C.; Penner, R. M. Amine Vapor Sensing with Silver Mesowires. *Nano Lett.* **2004**, *4*, 665–670.
(105) Liu, Z.; Searson, P. C. Single nanoporous gold nanowire sensors. *J. Phys. Chem. B* **2006**, *110*, 4318–4322.
(106) García, M.; García-Carmona, L.; Escarpa, A. Microfluidic system for enzymeless electrochemical determination of inulin using catalytically active metal nanowires. *Microchim. Acta* **2014**, *182*, 745–752.
(107) Favier, F.; Walter, E. C.; Zach, M. P.; Benter, T.; Penner, R. M. Hydrogen sensors and switches from electrodeposited palladium mesowire arrays. *Science* **2001**, *293*, 2227–2231.
(108) Hangarter, C. M.; Bangar, M.; Mulchandani, A.; Myung, N. V. Conducting polymer

nanowires for chemiresistive and FET-based bio/chemical sensors. *J. Mater. Chem.* **2010**, *20*, 3131–3140.
(109) Liang, J.; Li, K.; Liu, B. Visual sensing with conjugated polyelectrolytes. *Chem. Sci.* **2013**, *4*, 1377–1394.
(110) Rochat, S.; Swager, T. M. Conjugated amplifying polymers for optical sensing applications. *ACS Appl. Mater. Interfaces* **2013**, *5*, 4488–4502.
(111) Zhu, C. L.; Liu, L. B.; Yang, Q.; Lv, F. T.; Wang, S. Water-Soluble Conjugated Polymers for Imaging, Diagnosis, and Therapy. *Chem. Rev.* **2012**, *112*, 4687–4735.
(112) Lin, P.; Yan, F. Organic thin-film transistors for chemical and biological sensing. *Adv. Mater.* **2012**, *24*, 34–51.
(113) Virji, S.; Huang, J.; Kaner, R. B.; Weiller, B. H. Polyaniline Nanofiber Gas Sensors: Examination of Response Mechanisms. *Nano Lett.* **2004**, *4*, 491–496.
(114) Yan, X. B.; Han, Z. J.; Yang, Y.; Tay, B. K. NO2 gas sensing with polyaniline nanofibers synthesized by a facile aqueous/organic interfacial polymerization. *Sensors Actuators B Chem.* **2007**, *123*, 107–113.
(115) Chen, S.; Li, Y.; Li, Y. Architecture of low dimensional nanostructures based on conjugated polymers. *Polym. Chem.* **2013**, *4*, 5162–5180.
(116) Zhu, Y.; Zhang, J.; Zheng, Y.; Huang, Z.; Feng, L.; Jiang, L. Stable, superhydrophobic, and conductive polyaniline/polystyrene films for corrosive environments. *Adv. Funct. Mater.* **2006**, *16*, 568–574.
(117) Fridrikh, S. V; Yu, J. H.; Brenner, M. P.; Rutledge, G. C. Controlling the fiber diameter during electrospinning. *Phys. Rev. Lett.* **2003**, *90*, 144502.
(118) Huang, C.; Dong, B.; Lu, N.; Yang, B.; Gao, L.; Tian, L.; Qi, D.; Wu, Q.; Chi, L. A strategy for patterning conducting polymers using nanoimprint lithography and isotropic plasma etching. *Small* **2009**, *5*, 583–586.
(119) Zhang, F.; Nyberg, T.; Inganäs, O. Conducting Polymer Nanowires and Nanodots Made with Soft Lithography. *Nano Lett.* **2002**, *2*, 1373–1377.
(120) Bai, H.; Shi, G. Gas Sensors Based on Conducting Polymers. *Sensors* **2007**, *7*, 267–307.
(121) Ma, S.; Wang, Y.; Min, Z.; Zhong, L. Intrinsically conducting polymer-based fabric strain sensors. *Polym. Int.* **2013**, *62*, 983–990.
(122) Lange, U.; Roznyatovskaya, N. V; Mirsky, V. M. Conducting polymers in chemical sensors and arrays. *Anal. Chim. Acta.* **2008**, *614*, 1–26.
(123) Fratoddi, I.; Venditti, I.; Cametti, C.; Russo, M. V. Chemiresistive polyaniline-based gas sensors: A mini review. *Sensors Actuators B Chem.* **2015**, *220*, 534–548.
(124) Reemts, J.; Parisi, J.; Schlettwein, D. Electrochemical growth of gas-sensitive polyaniline thin films across an insulating gap. *Thin Solid Films* **2004**, *466*, 320–325.
(125) Saxena, V.; Shirodkar, V.; Prakash, R. Copper(II) ion-selective microelectrochemical transistor. In *Applied Biochemistry and Biotechnology - Part A Enzyme Engineering and Biotechnology*; 2001; Vol. 96, pp 63–69.
(126) Rahman, M. A.; Won, M.-S.; Shim, Y.-B. Characterization of an EDTA Bonded Conducting Polymer Modified Electrode: Its Application for the Simultaneous Determination of Heavy Metal Ions. *Anal. Chem.* **2003**, *75*, 1123–1129.
(127) Vázquez, E.; Giacalone, F.; Prato, M. Non-conventional methods and media for the activation and manipulation of carbon nanoforms. *Chem. Soc. Rev.* **2014**, *43*, 58–69.
(128) Heitzmann, M.; Bucher, C.; Moutet, J.-C.; Pereira, E.; Rivas, B. L.; Royal, G.; Saint-Aman, E. Complexation of poly(pyrrole-EDTA like) film modified electrodes: Application to metal cations electroanalysis. *Electrochim. Acta.* **2007**, *52*, 3082–3087.
(129) Yu, H.; Pullen, A. E.; Büschel, M. G.; Swager, T. M. Charge-specific interactions in

segmented conducting polymers: an approach to selective ionoresistive responses. *Angew. Chem. Int. Ed. Engl.* **2004**, *43*, 3700–3703.
(130) Hangarter, C. M.; Chartuprayoon, N.; Hernández, S. C.; Choa, Y.; Myung, N. V. Hybridized conducting polymer chemiresistive nano-sensors. *Nano Today* **2013**, *8*, 39–55.
(131) Gu, F.; Zhang, L.; Yin, X.; Tong, L. Polymer single-nanowire optical sensors. *Nano Lett.* **2008**, *8*, 2757–2761.
(132) Morales, A. M. A Laser Ablation Method for the Synthesis of Crystalline Semiconductor Nanowires. *Science.* **1998**, *279*, 208–211.
(133) Cui, Y.; Wei, Q.; Park, H.; Lieber, C. M. Nanowire nanosensors for highly sensitive and selective detection of biological and chemical species. *Science* **2001**, *293*, 1289–1292.
(134) Xu, L.; Jiang, Z.; Qing, Q.; Mai, L.; Zhang, Q.; Lieber, C. M. Design and synthesis of diverse functional kinked nanowire structures for nanoelectronic bioprobes. *Nano Lett.* **2013**, *13*, 746–751.
(135) Cui, Y.; Zhong, Z.; Wang, D.; Wang, W. U.; Lieber, C. M. High Performance Silicon Nanowire Field Effect Transistors. *Nano Lett.* **2003**, *3*, 149–152.
(136) Hahm, J.; Lieber, C. M. Direct Ultrasensitive Electrical Detection of DNA and DNA Sequence Variations Using Nanowire Nanosensors. *Nano Lett.* **2004**, *4*, 51–54.
(137) Patolsky, F.; Zheng, G.; Hayden, O.; Lakadamyali, M.; Zhuang, X.; Lieber, C. M. Electrical detection of single viruses. *Proc. Natl. Acad. Sci. U. S. A.* **2004**, *101*, 14017–14022.
(138) Zheng, G.; Patolsky, F.; Cui, Y.; Wang, W. U.; Lieber, C. M. Multiplexed electrical detection of cancer markers with nanowire sensor arrays. *Nat. Biotechnol.* **2005**, *23*, 1294–1301.
(139) Wang, W. U.; Chen, C.; Lin, K.; Fang, Y.; Lieber, C. M. Label-free detection of small-molecule-protein interactions by using nanowire nanosensors. *Proc. Natl. Acad. Sci. U. S. A.* **2005**, *102*, 3208–3212.
(140) Guo, X.; Whalley, A.; Klare, J. E.; Huang, L.; O'Brien, S.; Steigerwald, M.; Nuckolls, C. Single-molecule devices as scaffolding for multicomponent nanostructure assembly. *Nano Lett.* **2007**, *7*, 1119–1122.
(141) Wang, H.; Muren, N. B.; Ordinario, D.; Gorodetsky, A. A.; Barton, J. K.; Nuckolls, C. Transducing methyltransferase activity into electrical signals in a carbon nanotube-DNA device. *Chem. Sci.* **2012**, *3*, 62–65.
(142) Guo, X.; Gorodetsky, A. A.; Hone, J.; Barton, J. K.; Nuckolls, C. Conductivity of a single DNA duplex bridging a carbon nanotube gap. *Nat. Nanotechnol.* **2008**, *3*, 163–167.
(143) He, R.; Yang, P. Giant piezoresistance effect in silicon nanowires. *Nat. Nanotechnol.* **2006**, *1*, 42–46.
(144) Tao, A.; Kim, F.; Hess, C.; Goldberger, J.; He, R.; Sun, Y.; Xia, Y.; Yang, P. Langmuir–Blodgett Silver Nanowire Monolayers for Molecular Sensing Using Surface-Enhanced Raman Spectroscopy. *Nano Lett.* **2003**, *3*, 1229–1233.
(145) Bellew, A. T.; Bell, A. P.; McCarthy, E. K.; Fairfield, J. A.; Boland, J. J. Programmability of nanowire networks. *Nanoscale* **2014**, *6*, 9632–9639.
(146) Azzarelli, J. M.; Mirica, K. A.; Ravnsbæk, J. B.; Swager, T. M. Wireless gas detection with a smartphone via rf communication. *Proc. Natl. Acad. Sci. U. S. A.* **2014**, *111*, 18162–18166.
(147) Lim, W.; Wright, J. S.; Gila, B. P.; Johnson, J. L.; Ural, A.; Anderson, T.; Ren, F.; Pearton, S. J. Room temperature hydrogen detection using Pd-coated GaN nanowires. *Appl. Phys. Lett.* **2008**, *93*, 72109.
(148) Pearton, S.; Chang, C.; Chu, B. ZnO, GaN, and InN Functionalized Nanowires for Sensing and Photonics Applications. *IEEE J. Sel. Top. Quant. Electron.* **2011**, *17*, 1092–1101.

(149) Skucha, K.; Fan, Z.; Jeon, K.; Javey, A.; Boser, B. Palladium/silicon nanowire Schottky barrier-based hydrogen sensors. *Sensors Actuators B Chem.* **2010**, *145*, 232–238.
(150) Ren, F.; Chu, B. H.; Chen, K. H.; Chang, C. Y.; Chen, V.; Pearton, S. J. GaN-Based Sensors. In *GaN and ZnO-based Materials and Devices*; Pearton, S., Ed.; Springer Series in Materials Science; Springer: Berlin, 2012; Vol. 156, pp 165–207.
(151) Dobrokhotov, V.; McIlroy, D. N.; Norton, M. G.; Abuzir, A.; Yeh, W. J.; Stevenson, I.; Pouy, R.; Bochenek, J.; Cartwright, M.; Wang, L.; et al. Principles and mechanisms of gas sensing by GaN nanowires functionalized with gold nanoparticles. *J. Appl. Phys.* **2006**, *99*, 104302.
(152) Chang, C. Y.; Kang, B. S.; Wang, H. T.; Ren, F.; Wang, Y. L.; Pearton, S. J.; Dennis, D. M.; Johnson, J. W.; Rajagopal, P.; Roberts, J. C.; et al. CO[sub 2] detection using polyethylenimine/starch functionalized AlGaN/GaN high electron mobility transistors. *Appl. Phys. Lett.* **2008**, *92*, 232102.
(153) Ren, F.; Pearton, S. J.; Kang, B. S.; Chu, B. H. AlGaN/GaN High Electron Mobility Transistor Based Sensors for Bio-Applications. In *Biosensors for Health, Environment and Biosecurity*; Serra, P. A., Ed.; InTech: Rijeka, Croatia, 2011; pp 15–68.
(154) Kang, B. S.; Wang, H. T.; Ren, F.; Pearton, S. J.; Morey, T. E.; Dennis, D. M.; Johnson, J. W.; Rajagopal, P.; Roberts, J. C.; Piner, E. L.; et al. Enzymatic glucose detection using ZnO nanorods on the gate region of AlGaN/GaN high electron mobility transistors. *Appl. Phys. Lett.* **2007**, *91*, 252103.
(155) Li, C.; Curreli, M.; Lin, H.; Lei, B.; Ishikawa, F. N.; Datar, R.; Cote, R. J.; Thompson, M. E.; Zhou, C. Complementary detection of prostate-specific antigen using In2O3 nanowires and carbon nanotubes. *J. Am. Chem. Soc.* **2005**, *127*, 12484–12485.
(156) Bunimovich, Y. L.; Shin, Y. S.; Yeo, W.-S.; Amori, M.; Kwong, G.; Heath, J. R. Quantitative real-time measurements of DNA hybridization with alkylated nonoxidized silicon nanowires in electrolyte solution. *J. Am. Chem. Soc.* **2006**, *128*, 16323–16331.
(157) Roy, S.; Gao, Z. Nanostructure-based electrical biosensors. *Nano Today* **2009**, *4*, 318–334.
(158) Collins, G.; Holmes, J. D. Chemical functionalisation of silicon and germanium nanowires. *J. Mater. Chem.* **2011**, *21*, 11052–11069.
(159) Luo, L.; Jie, J.; Zhang, W. W.; He, Z.; Wang, J.; Yuan, G.; Wu, L. C. M.; Lee, S.-T. Silicon nanowire sensors for Hg^{2+} and Cd^{2+} ions. *Appl. Phys. Lett.* **2009**, *94*, 193101.
(160) Bi, X.; Agarwal, A.; Yang, K.-L. Oligopeptide-modified silicon nanowire arrays as multichannel metal ion sensors. *Biosens. & Bioelectron.* **2009**, *24*, 3248–3251.
(161) McAlpine, M. C.; Agnew, H. D.; Rohde, R. D.; Blanco, M.; Ahmad, H.; Stuparu, A. D.; Goddard, W. a; Heath, J. R. Peptide-nanowire hybrid materials for selective sensing of small molecules. *J. Am. Chem. Soc.* **2008**, *130*, 9583–9589.
(162) Zhang, G.-J.; Ning, Y. Silicon nanowire biosensor and its applications in disease diagnostics: a review. *Anal. Chim. Acta.* **2012**, *749*, 1–15.
(163) Chen, K.-I.; Li, B.-R.; Chen, Y.-T. Silicon nanowire field-effect transistor-based biosensors for biomedical diagnosis and cellular recording investigation. *Nano Today* **2011**, *6*, 131–154.
(164) Stern, E.; Klemic, J. F.; Routenberg, D. A.; Wyrembak, P. N.; Turner-Evans, D. B.; Hamilton, A. D.; LaVan, D. A.; Fahmy, T. M.; Reed, M. A. Label-free immunodetection with CMOS-compatible semiconducting nanowires. *Nature* **2007**, *445*, 519–522.
(165) Kim, A.; Ah, C. S.; Yu, H. Y.; Yang, J.-H.; Baek, I.-B.; Ahn, C.-G.; Park, C. W.; Jun, M. S.; Lee, S. Ultrasensitive, label-free, and real-time immunodetection using silicon field-effect transistors. *Appl. Phys. Lett.* **2007**, *91*, 103901.

(166) Zhang, G.-J.; Chua, J. H.; Chee, R.-E.; Agarwal, A.; Wong, S. M.; Buddharaju, K. D.; Balasubramanian, N. Highly sensitive measurements of PNA-DNA hybridization using oxide-etched silicon nanowire biosensors. *Biosens. & Bioelectron.* **2008**, *23*, 1701–1707.
(167) Wang, C.; Yin, L.; Zhang, L.; Xiang, D.; Gao, R. Metal oxide gas sensors: sensitivity and influencing factors. *Sensors* **2010**, *10*, 2088–2106.
(168) Dong, K.-Y.; Choi, J.-K.; Hwang, I.-S.; Lee, J.-W.; Kang, B. H.; Ham, D.-J.; Lee, J.-H.; Ju, B.-K. Enhanced H2S sensing characteristics of Pt doped SnO_2 nanofibers sensors with micro heater. *Sensors Actuators B Chem.* **2011**, *157*, 154–161.
(169) Xue, X. Y.; Chen, Y. J.; Liu, Y. G.; Shi, S. L.; Wang, Y. G.; Wang, T. H. Synthesis and ethanol sensing properties of indium-doped tin oxide nanowires. *Appl. Phys. Lett.* **2006**, *88*, 201907.
(170) Wu, J. M. A room temperature ethanol sensor made from p-type Sb-doped SnO2 nanowires. *Nanotechnology* **2010**, *21*, 235501.
(171) Wan, Q.; Wang, T. H. Single-crystalline Sb-doped SnO2 nanowires: synthesis and gas sensor application. *Chem. Commun.* **2005**, *1*, 3841–3843.
(172) Khoang, N. D.; Trung, D. D.; Van Duy, N.; Hoa, N. D.; Van Hieu, N. Design of SnO2/ZnO hierarchical nanostructures for enhanced ethanol gas-sensing performance. *Sensors Actuators B Chem.* **2012**, *174*, 594–601.
(173) Singh, N.; Yan, C.; Lee, P. S. Room temperature CO gas sensing using Zn-doped In2O3 single nanowire field effect transistors. *Sensors Actuators B Chem.* **2010**, *150*, 19–24.
(174) Yang, D.-J.; Kamienchick, I.; Youn, D. Y.; Rothschild, A.; Kim, I.-D. Ultrasensitive and Highly Selective Gas Sensors Based on Electrospun SnO2 Nanofibers Modified by Pd Loading. *Adv. Funct. Mater.* **2010**, *20*, 4258–4264.
(175) Flueckiger, J.; Ko, F. K.; Cheung, K. C. Microfabricated formaldehyde gas sensors. *Sensors* **2009**, *9*, 9196–9215.
(176) Lv, P.; Tang, Z. a.; Yu, J.; Zhang, F. T.; Wei, G. F.; Huang, Z. X.; Hu, Y. Study on a micro-gas sensor with SnO2–NiO sensitive film for indoor formaldehyde detection. *Sensors Actuators B Chem.* **2008**, *132*, 74–80.
(177) Wang, J.; Liu, L.; Cong, S.-Y.; Qi, J.-Q.; Xu, B.-K. An enrichment method to detect low concentration formaldehyde. *Sens. Actuators, B* **2008**, *134*, 1010–1015.
(178) Mashock, M.; Yu, K.; Cui, S.; Mao, S.; Lu, G.; Chen, J. Modulating gas sensing properties of CuO nanowires through creation of discrete nanosized p-n junctions on their surfaces. *ACS Appl. Mater. {&} interfaces* **2012**, *4*, 4192–4199.
(179) Zhang, P.; Zhang, L.; Zhao, G.; Feng, F. A highly sensitive nonenzymatic glucose sensor based on CuO nanowires. *Microchim. Acta* **2012**, *176*, 411–417.
(180) Wang, G.; Wei, Y.; Zhang, W.; Zhang, X.; Fang, B.; Wang, L. Enzyme-free amperometric sensing of glucose using Cu-CuO nanowire composites. *Microchim. Acta* **2010**, *168*, 87–92.
(181) Yan, Z.; Zhao, J.; Qin, L.; Mu, F.; Wang, P.; Feng, X. Non-enzymatic hydrogen peroxide sensor based on a gold electrode modified with granular cuprous oxide nanowires. *Microchim. Acta* **2012**, *180*, 145–150.
(182) Shaalan, N. M.; Yamazaki, T.; Kikuta, T. Synthesis of metal and metal oxide nanostructures and their application for gas sensing. *Mater. Chem. Phys.* **2011**, *127*, 143–150.
(183) Wang, L.; Wang, S.; Xu, M.; Hu, X.; Zhang, H.; Wang, Y.; Huang, W. A Au-functionalized ZnO nanowire gas sensor for detection of benzene and toluene. *Phys. Chem. Chem. Phys.* **2013**, *15*, 17179–17186.
(184) Hwang, I.-S.; Choi, J.-K.; Woo, H.-S.; Kim, S.-J.; Jung, S.-Y.; Seong, T.-Y.; Kim, I.-D.; Lee, J.-H. Facile control of C_2H_5OH sensing characteristics by decorating discrete Ag

nanoclusters on SnO_2 nanowire networks. *ACS Appl. Mater. & Interfaces* **2011**, *3*, 3140–3145.
(185) Shin, J.; Choi, S.-J.; Lee, I.; Youn, D.-Y.; Park, C. O.; Lee, J.-H.; Tuller, H. L.; Kim, I.-D. Thin-Wall Assembled SnO 2 Fibers Functionalized by Catalytic Pt Nanoparticles and their Superior Exhaled-Breath-Sensing Properties for the Diagnosis of Diabetes. *Adv. Funct. Mater.* **2013**, *23*, 2357–2367.
(186) Zou, X.; Wang, J.; Liu, X.; Wang, C.; Jiang, Y.; Wang, Y.; Xiao, X.; Ho, J. C.; Li, J.; Jiang, C.; et al. Rational Design of Sub-Parts per Million Specific Gas Sensors Array Based on Metal Nanoparticles Decorated Nanowire Enhancement-Mode Transistors. *Nano Lett.* **2013**, *13*, 3287–3292.
(187) Liu, X.; Lin, P.; Yan, X.; Kang, Z.; Zhao, Y.; Lei, Y.; Li, C.; Du, H.; Zhang, Y. Enzyme-coated single ZnO nanowire FET biosensor for detection of uric acid. *Sensors Actuators B Chem.* **2013**, *176*, 22–27.
(188) Chattopadhyay, S.; Ganguly, A.; Chen, K.-H.; Chen, L.-C. One-Dimensional Group III-Nitrides: Growth, Properties, and Applications in Nanosensing and Nano-Optoelectronics. *Crit. Rev. Solid State Mater. Sci.* **2009**, *34*, 224–279.
(189) Lu, Y.; Li, J.; Han, J.; Ng, H.-T.; Binder, C.; Partridge, C.; Meyyappan, M. Room temperature methane detection using palladium loaded single-walled carbon nanotube sensors. *Chem. Phys. Lett.* **2004**, *391*, 344–348.
(190) Penza, M.; Cassano, G.; Rossi, R.; Alvisi, M.; Rizzo, A.; Signore, M. a.; Dikonimos, T.; Serra, E.; Giorgi, R. Enhancement of sensitivity in gas chemiresistors based on carbon nanotube surface functionalized with noble metal (Au, Pt) nanoclusters. *Appl. Phys. Lett.* **2007**, *90*, 173123.
(191) Star, A.; Joshi, V.; Skarupo, S.; Thomas, D.; Gabriel, J.-C. P. Gas sensor array based on metal-decorated carbon nanotubes. *J. Phys. Chem. B* **2006**, *110*, 21014–21020.
(192) Abraham, J. K.; Philip, B.; Witchurch, A.; Varadan, V. K.; Reddy, C. C. A compact wireless gas sensor using a carbon nanotube/PMMA thin film chemiresistor. *Smart Mater. Struct.* **2004**, *13*, 1045–1049.
(193) Esser, B.; Schnorr, J. M.; Swager, T. M. Selective detection of ethylene gas using carbon nanotube-based devices: Utility in determination of fruit ripeness. *Angew. Chemie - Int. Ed.* **2012**, *51*, 5752–5756.
(194) Tasis, D.; Tagmatarchis, N.; Bianco, A.; Prato, M. Chemistry of carbon nanotubes. *Chem. Rev.* **2006**, *106*, 1105–1136.
(195) Wei, L.; Lu, D.; Wang, J.; Wei, H.; Zhao, J.; Geng, H.; Zhang, Y. Highly sensitive detection of trinitrotoluene in water by chemiresistive sensor based on noncovalently amino functionalized single-walled carbon nanotube. *Sensors Actuators B Chem.* **2014**, *190*, 529–534.
(196) Qi, P.; Vermesh, O.; Grecu, M.; Javey, A.; Wang, Q.; Dai, H.; Peng, S.; Cho, K. J. Toward Large Arrays of Multiplex Functionalized Carbon Nanotube Sensors for Highly Sensitive and Selective Molecular Detection. *Nano Lett.* **2003**, *3*, 347–351.
(197) Star, A.; Han, T.-R.; Joshi, V.; Gabriel, J.-C. P.; Grüner, G. Nanoelectronic Carbon Dioxide Sensors. *Adv. Mater.* **2004**, *16*, 2049–2052.
(198) Wang, F.; Gu, H.; Swager, T. M. Carbon nanotube/polythiophene chemiresistive sensors for chemical warfare agents. *J. Am. Chem. Soc.* **2008**, *130*, 5392–5393.
(199) An, K. H.; Jeong, S. Y.; Hwang, H. R.; Lee, Y. H. Enhanced Sensitivity of a Gas Sensor Incorporating Single-Walled Carbon Nanotube–Polypyrrole Nanocomposites. *Adv. Mater.* **2004**, *16*, 1005–1009.
(200) Santhanam, K. S. V; Sangoi, R.; Fuller, L. A chemical sensor for chloromethanes using

a nanocomposite of multiwalled carbon nanotubes with poly(3-methylthiophene). *Sensors Actuators B Chem.* **2005**, *106*, 766–771.
(201) Li, Y.; Wang, H.; Cao, X.; Yuan, M.; Yang, M. A composite of polyelectrolyte-grafted multi-walled carbon nanotubes and in situ polymerized polyaniline for the detection of low concentration triethylamine vapor. *Nanotechnology* **2008**, *19*, 15503.
(202) Gu, H.; Swager, T. M. Fabrication of Free-standing, Conductive, and Transparent Carbon Nanotube Films. *Adv. Mater.* **2008**, *20*, 4433–4437.
(203) Wang, F.; Yang, Y.; Swager, T. M. Molecular recognition for high selectivity in carbon nanotube/polythiophene chemiresistors. *Angew. Chem. Int. Ed. Engl.* **2008**, *47*, 8394–8396.
(204) Asuri, P.; Karajanagi, S. Water-soluble carbon nanotube-enzyme conjugates as functional biocatalytic formulations. *Biotechnol. Bioeng.* **2006**, *95*, 804–811.
(205) Georgakilas, V.; Tagmatarchis, N.; Pantarotto, D.; Bianco, A.; Mol, D. B.; Cnrs, U. P. R. Amino acid functionalisation of water soluble carbon nanotubes by organic functionalisation ; derivatisation with N-pro-. *Chem. Commun.* **2002**, 3050–3051.
(206) Li, H.; Cheng, F.; Duft, A. M.; Adronov, A. Functionalization of single-walled carbon nanotubes with well-defined polystyrene by "click" coupling. *J. Am. Chem. Soc.* **2005**, *127*, 14518–14524.
(207) Weizmann, Y.; Chenoweth, D. M.; Swager, T. M. DNA-CNT nanowire networks for DNA detection. *J. Am. Chem. Soc.* **2011**, *133*, 3238–3241.
(208) Zhang, T.; Mubeen, S.; Bekyarova, E.; Yoo, B. Y.; Haddon, R. C.; Myung, N. V; Deshusses, M. a. Poly(m-aminobenzene sulfonic acid) functionalized single-walled carbon nanotubes based gas sensor. *Nanotechnology* **2007**, *18*, 165504.
(209) Vlandas, A.; Kurkina, T.; Ahmad, A.; Kern, K.; Balasubramanian, K. Enzyme-free sugar sensing in microfluidic channels with an affinity-based single-wall carbon nanotube sensor. *Anal. Chem.* **2010**, *82*, 6090–6097.
(210) Huang, J.; Ng, A. L.; Piao, Y.; Chen, C.-F.; Green, A. a; Sun, C.-F.; Hersam, M. C.; Lee, C. S.; Wang, Y. Covalently functionalized double-walled carbon nanotubes combine high sensitivity and selectivity in the electrical detection of small molecules. *J. Am. Chem. Soc.* **2013**, *135*, 2306–2312.
(211) Wang, F.; Swager, T. M. Diverse chemiresistors based upon covalently modified multiwalled carbon nanotubes. *J. Am. Chem. Soc.* **2011**, *133*, 11181–11193.
(212) Hatchett, D. W.; Josowicz, M. Composites of intrinsically conducting polymers as sensing nanomaterials. *Chem. Rev.* **2008**, *108*, 746–769.
(213) Liu, H.; Kameoka, J.; Czaplewski, D. a.; Craighead, H. G. Polymeric Nanowire Chemical Sensor. *Nano Lett.* **2004**, *4*, 671–675.
(214) Ji, S.; Li, Y.; Yang, M. Gas sensing properties of a composite composed of electrospun poly(methyl methacrylate) nanofibers and in situ polymerized polyaniline. *Sensors Actuators B Chem.* **2008**, *133*, 644–649.
(215) Srivastava, S.; Sharma, S. S.; Agrawal, S.; Kumar, S.; Singh, M.; Vijay, Y. K. Study of chemiresistor type CNT doped polyaniline gas sensor. *Synth. Met.* **2010**, *160*, 529–534.
(216) Lobotka, P.; Kunzo, P.; Kovacova, E.; Vavra, I.; Krizanova, Z.; Smatko, V.; Stejskal, J.; Konyushenko, E. N.; Omastova, M.; Spitalsky, Z.; et al. Thin polyaniline and polyaniline/carbon nanocomposite films for gas sensing. *Thin Solid Films* **2011**, *519*, 4123–4127.
(217) Al-Mashat, L.; Shin, K.; Kalantar-zadeh, K.; Plessis, J. D.; Han, S. H.; Kojima, R. W.; Kaner, R. B.; Li, D.; Gou, X.; Ippolito, S. J.; et al. Graphene/Polyaniline Nanocomposite for Hydrogen Sensing. *J. Phys. Chem. C* **2010**, *114*, 16168–16173.
(218) Liao, Y.; Zhang, C.; Zhang, Y.; Strong, V.; Tang, J.; Li, X.-G.; Kalantar-Zadeh, K.;

Hoeck, E. M. V; Wang, K. L.; Kaner, R. B. Carbon nanotube/polyaniline composite nanofibers: Facile synthesis and chemosensors. *Nano Lett.* **2011**, *11*, 954–959.
(219) Li, Z.-F.; Blum, F. D.; Bertino, M. F.; Kim, C.-S. Amplified response and enhanced selectivity of metal-PANI fiber composite based vapor sensors. *Sensors Actuators B Chem.* **2012**, *161*, 390–395.
(220) Barkade, S. S.; Naik, J. B.; Sonawane, S. H. Ultrasound assisted miniemulsion synthesis of polyaniline/Ag nanocomposite and its application for ethanol vapor sensing. *Colloids Surfaces A Physicochem. Eng. Asp.* **2011**, *378*, 94–98.
(221) Ram, M. K.; Yavuz, O.; Aldissi, M. NO2 gas sensing based on ordered ultrathin films of conducting polymer and its nanocomposite. *Synth. Met.* **2005**, *151*, 77–84.
(222) Ramanathan, K.; Bangar, M. a; Yun, M.; Chen, W.; Myung, N. V; Mulchandani, A. Bioaffinity sensing using biologically functionalized conducting-polymer nanowire. *J. Am. Chem. Soc.* **2005**, *127*, 496–497.
(223) Arter, J. A.; Taggart, D. K.; McIntire, T. M.; Penner, R. M.; Weiss, G. A. Virus-PEDOT Nanowires for Biosensing. *Nano Lett.* **2010**, *10*, 4858–4862.
(224) Killard, A. Nanostructured Conducting Polymers for (Electro) chemical Sensors. In *Nanostructured Conductive Polymers*; 2010; pp 563–598.
(225) Itoh, T.; Matsubara, I.; Shin, W.; Izu, N.; Nishibori, M. Preparation of layered organic–inorganic nanohybrid thin films of molybdenum trioxide with polyaniline derivatives for aldehyde gases sensors of several tens ppb level. *Sens. Actuators, B* **2008**, *128*, 512–520.
(226) Ćirić-Marjanović, G. Recent advances in polyaniline composites with metals, metalloids and nonmetals. *Synth. Met.* **2013**, *170*, 31–56.
(227) Ding, B.; Wang, M.; Yu, J.; Sun, G. Gas sensors based on electrospun nanofibers. *Sensors* **2009**, *9*, 1609–1624.
(228) Park, E.; Kwon, O. S.; Park, S. J.; Lee, J. S.; You, S.; Jang, J. One-pot synthesis of silver nanoparticles decorated poly(3,4-ethylenedioxythiophene) nanotubes for chemical sensor application. *J. Mater. Chem.* **2012**, *22*, 1521–1526.
(229) Shirsat, M. D.; Bangar, M. a.; Deshusses, M. a.; Myung, N. V; Mulchandani, A. Polyaniline nanowires-gold nanoparticles hybrid network based chemiresistive hydrogen sulfide sensor. *Appl. Phys. Lett.* **2009**, *94*, 83502.
(230) Mulchandani, A.; Myung, N. V. Conducting polymer nanowires-based label-free biosensors. *Curr. Opin. Biotechnol.* **2011**, *22*, 502–508.
(231) Aravinda, C. L.; Cosnier, S.; Chen, W.; Myung, N. V; Mulchandani, A. Label-free detection of cupric ions and histidine-tagged proteins using single poly(pyrrole)-NTA chelator conducting polymer nanotube chemiresistive sensor. *Biosens. & Bioelectron.* **2009**, *24*, 1451–1455.
(232) Yoon, H.; Kim, J.-H.; Lee, N.; Kim, B.-G.; Jang, J. A novel sensor platform based on aptamer-conjugated polypyrrole nanotubes for label-free electrochemical protein detection. *ChemBioChem* **2008**, *9*, 634–641.
(233) Bangar, M. A.; Shirale, D. J.; Chen, W.; Myung, N. V; Mulchandani, A. Single conducting polymer nanowire chemiresistive label-free immunosensor for cancer biomarker. *Anal. Chem.* **2009**, *81*, 2168–2175.
(234) Shirale, D. J.; Bangar, M. a; Park, M.; Yates, M. V; Chen, W.; Myung, N. V; Mulchandani, A. Label-free chemiresistive immunosensors for viruses. *Environ. Sci. {&} Technol.* **2010**, *44*, 9030–9035.
(235) García-Aljaro, C.; Bangar, M. A.; Baldrich, E.; Muñoz, F. J.; Mulchandani, A. Conducting polymer nanowire-based chemiresistive biosensor for the detection of bacterial spores. *Biosens. {&} Bioelectron.* **2010**, *25*, 2309–2312.

(236) Tolani, S. B.; Craig, M.; DeLong, R. K.; Ghosh, K.; Wanekaya, A. K. Towards biosensors based on conducting polymer nanowires. *Anal. Bioanal. Chem.* **2009**, *393*, 1225–1231.
(237) Wolfbeis, O. S. Probes, sensors, and labels: why is real progress slow? *Angew. Chem. Int. Ed.* **2013**, *52*, 9864–9865.
(238) Mann, J. A.; Dichtel, W. R. Improving the binding characteristics of tripodal compounds on single layer graphene. *ACS Nano* **2013**, *7*, 7193–7199.
(239) Hildebrand, J. G.; Shepherd, G. M. Mechanisms of olfactory discrimination: converging evidence for common principles across phyla. *Annu. Rev. Neurosci.* **1997**, *20*, 595–631.
(240) Small, W. R.; in het Panhuis, M. Inkjet printing of transparent, electrically conducting single-walled carbon-nanotube composites. *Small* **2007**, *3*, 1500–1503.
(241) Potyrailo, R. A.; Nagraj, N.; Tang, Z.; Mondello, F. J.; Surman, C.; Morris, W. Battery-free Radio Frequency Identification (RFID) Sensors for Food Quality and Safety. *J. Agric. Food Chem.* **2012**, *60*, 8535–8543.
(242) Xu, S.; Hansen, B. J.; Wang, Z. L. Piezoelectric-nanowire-enabled power source for driving wireless microelectronics. *Nat. Commun.* **2010**, *1*, 93.
(243) Wang, Z. L. Self-powered nanosensors and nanosystems. *Adv. Mater.* **2012**, *24*, 280–285.
(244) Jie, Y.; Wang, N.; Cao, X.; Xu, Y.; Li, T.; Zhang, X.; Wang, Z. L. Self-Powered Triboelectric Nanosensor with Poly(tetrafluoroethylene) Nanoparticle Arrays for Dopamine Detection. *ACS Nano* **2015**.
(245) Wang, Z. L.; Chen, J.; Lin, L. Progress in triboelectric nanogenerators as a new energy technology and self-powered sensors. *Energy Environ. Sci.* **2015**, *8*, 2250–2282.
(246) Bogue, R. Energy harvesting and wireless sensors: a review of recent developments. *Sens. Rev.* **2009**, *29*, 194–199.
(247) Ho, J. S.; Yeh, A. J.; Neofytou, E.; Kim, S.; Tanabe, Y.; Patlolla, B.; Beygui, R. E.; Poon, A. S. Y. Wireless power transfer to deep-tissue microimplants. *Proc. Natl. Acad. Sci. U. S. A.* **2014**, *111*, 7974–7979.
(248) Xu, S.; Zhang, Y.; Jia, L.; Mathewson, K. E.; Jang, K.-I.; Kim, J.; Fu, H.; Huang, X.; Chava, P.; Wang, R.; et al. Soft microfluidic assemblies of sensors, circuits, and radios for the skin. *Science.* **2014**, *344*, 70–74.
(249) Long, Y.-Z.; Yu, M.; Sun, B.; Gu, C.-Z.; Fan, Z. Recent advances in large-scale assembly of semiconducting inorganic nanowires and nanofibers for electronics, sensors and photovoltaics. *Chem. Soc. Rev.* **2012**, *41*, 4560–4580.
(250) Mannoor, M. S.; Tao, H.; Clayton, J. D.; Sengupta, A.; Kaplan, D. L.; Naik, R. R.; Verma, N.; Omenetto, F. G.; McAlpine, M. C. Graphene-based wireless bacteria detection on tooth enamel. *Nat. Commun.* **2012**, *3*, 763.
(251) Potyrailo, R. A.; Larsen, M.; Riccobono, O. Detection of individual vapors and their mixtures using a selectivity-tunable three-dimensional network of plasmonic nanoparticles. *Angew. Chem. Int. Ed.* **2013**, *52*, 10360–10364.

CHAPTER 2

Chemiresistor Devices for Chemical Warfare Agent Detection Based on Polymer Wrapped Single-Walled Carbon Nanotubes

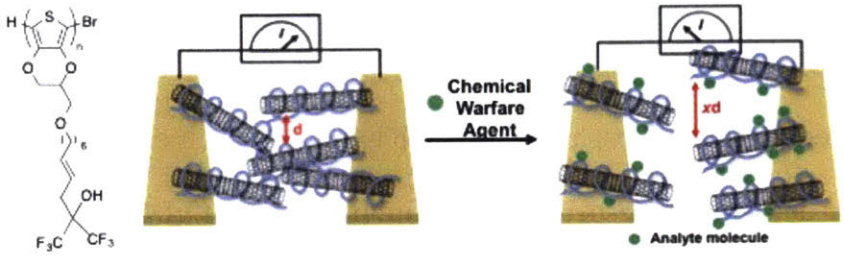

Adapted and reprinted in part with permission from:
John F. Fennell Jr.; Hitoshi Hamaguchi; Bora Yoon; Timothy M. Swager. Chemiresistor Devices for Chemical Warfare Agent Detection Based on Polymer Wrapped Single Walled Carbon Nanotubes *Sensors.* **2017**, *17* (5), 982

2.1 Abstract

Chemical warfare agents (CWA) continue to present a threat to civilian populations and military personnel in operational areas all over the world. Reliable measurements of CWAs are critical to contamination detection, avoidance, and remediation. The current deployed systems in United States and foreign militaries, as well as those in the private sector offer accurate detection of CWAs, but are still limited by size, portability and fabrication cost. In this chapter, we report a chemiresistive CWA sensor using single-walled carbon nanotubes (SWCNTs) wrapped with poly(3,4-ethylenedioxythiophene) (PEDOT) derivatives. We demonstrate that a pendant hexafluoroisopropanol group on the polymer that enhances sensitivity to a nerve agent mimic, dimethyl methylphosphonate, in both nitrogen and air environments to concentrations as low as 5 ppm and 11 ppm, respectively. Additionally, these PEDOT/SWCNT derivative sensor systems experience negligible device performance over the course of two weeks under ambient conditions.

2.2 Introduction

Intelligence surveillance and reconnaissance efforts in the military arena benefit from increasing the number of sensors on the battlefield. Placing networked chemical sensors on individual soldiers without increasing an already onerous soldier-load would exponentially surge the information density to reduce uncertainty and the "fog of war".[1] Responsive, selective, low-energy and low-cost are essential characteristics of such systems. Current military chemical warfare agent (CWA) sensors are sensitive to CWAs to the low ppb level, selective and networkable; but they are cumbersome, expensive, energy and training intensive.[2] These unfavorable characteristics may be mitigated in the future by using employing chemiresistive devices that can be deployed in large numbers, inexpensively and networked together.[3]

Chemiresistive devices utilizing single-walled carbon nanotubes (SWCNTs), with their unique mechanical and electrical properties, offer a promising platform to meet these requirements and are excellent substrates on which to build CWA sensors for use on the modern battlefield.[4–7]

There are many established ways to functionalize SWCNTs to impart selectivity for different analytes. Previous reports have used covalent-sidewall functionalization,[8–14] defect group functionalization,[15] non-covalent exohedral functionalization[16–20] (with polymer, surfactants, or composite mixtures) and endohedral functionalization.[21,22] Non-covalent exohedral functionalization with conjugated polymers was chosen for this study because the native conductivity of SWCNTs is preserved without disruption of the π-electronic states in the nanotube sidewalls. We chose to develop polymer-wrapped composites for this sensing application in lieu of a simple, physical mixture because physical mixtures containing SWCNTs phase segregate as a result of strong interactions between the nanotubes that allow them to aggregate. Favorable π-π stacking interactions between the SWCNTs and polymers disrupt this aggregation and allow for processing and the inclusion of polymer originated molecular recognition groups.[23,24]

Our group has previously demonstrated that composites of SWCNTs and polythiophenes (PTs) modified with a hexafluoroisopropanol group (HFIP) make effective chemiresistive material for a CWA simulant, dimethyl methylphosphonate (DMMP) sensing.[14] Shown in Figure 2.1a, the HFIP group exhibits a strong hydrogen bonding interaction with phosphate esters,[25] which are a common structural component of nerve agents, including sarin, soman, tabun and VX (Figure 2.1b).[26]

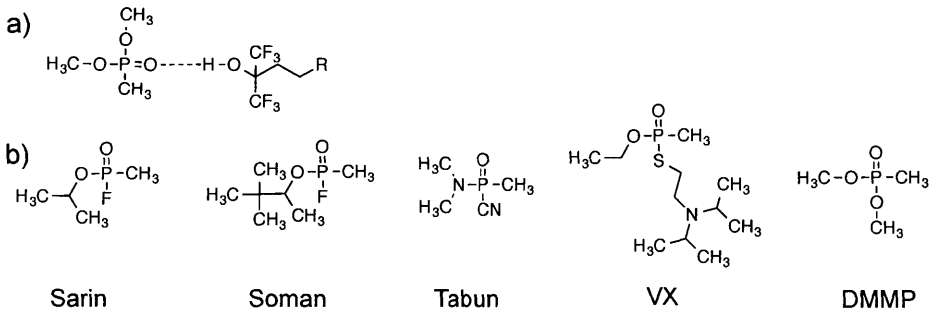

Figure 2.1 (a) Hydrogen bonding interaction between HFIP and DMMP; (b) Structures of CWAs and a CWA simulant, DMMP.

Building upon our experience, we report here a sequel to our previous method by using a derivatized poly(3,4-ethylenedioxythiophene) (PEDOT) polymer to produce a more robust CWA sensor. Though the fabricated PT/SWCNT devices proved to be selective and sensitive (sub ppm detection limit), they experienced significant performance degradation within days of fabrication, likely due to SWCNT aggregation. PEDOT, in comparison to PT, is much more polarizable and an electron-rich material, which generates stronger interactions to form a polymer-SWCNT composite with improved stability.[27,28] HFIP groups are introduced to impart selectivity for binding of DMMP and are introduced through the functionalization of terminal alkene-containing sidechain attached to the PEDOT backbone. Alkene cross metathesis reactions facilitate the attachment of molecular recognition elements to the side chains to create derivatized PEDOT polymers with desired selectivity.[29] In this chapter, we detail three PEDOT analogs, **P1**, **P2** and **P3**, to wrap SWCNTs to create CWA sensitive chemiresistive sensors (Figure 2.2a). The designed PEDOT derivatives also impart the necessary solubility to effectively de-bundle and disperse SWCNTs as shown in Figure 2.2b. In contrast to our previous work, where thin films were spin-casted upon a glass substrate, these chemiresistor devices are fabricated by drop casting of a polymer/SWCNT dispersion between two metal electrodes on a glass substrate to form random networks of polymer-wrapped SWCNTs (Figure 2.2c, top). Using

this drop-casting methodology, a very small amount of polymer/SWCNT is used to make a large number of devices.

P2 is functionalized with a pendant HFIP group on the side chain that is known to form strong hydrogen bonds with phosphonates. This interaction concentrates the selected analytes proximate to the SWCNT. The conductance is then modulated through a combination of mechanisms including directly affecting transport along a given SWCNT by charge transfer to change the doping level[30,31] or electrostatic interactions with the positive charge characters through dipolar induced pinning or scattering.[32] Inter-SWCNT transport can also be modulated by the binding of analytes to the HFIP group on the polymer sidechains and an associated swelling increases the inter-SWCNT distance to create wider tunnel junctions between SWCNTs that lower the conductivity.[4] A cartoon demonstrating the latter mechanism is drawn in Figure 2.2c. In this report we demonstrate CWA selective chemiresistors based upon a **P2**/SWCNT composition and reveal strong responses upon exposure to low concentrations (5 ppm) of the nerve agent simulant DMMP. We also demonstrate a fairly reliable performance of the **P2**/SWCNT sensor in the presence of air containing 24% relative humidity (RH). Furthermore, we explore the effects of device aging under ambient conditions. In addition, our experiments confirm that EDOT derivatives create a versatile platform polymer for the development of polymer wrapped SWCNT chemiresistors.

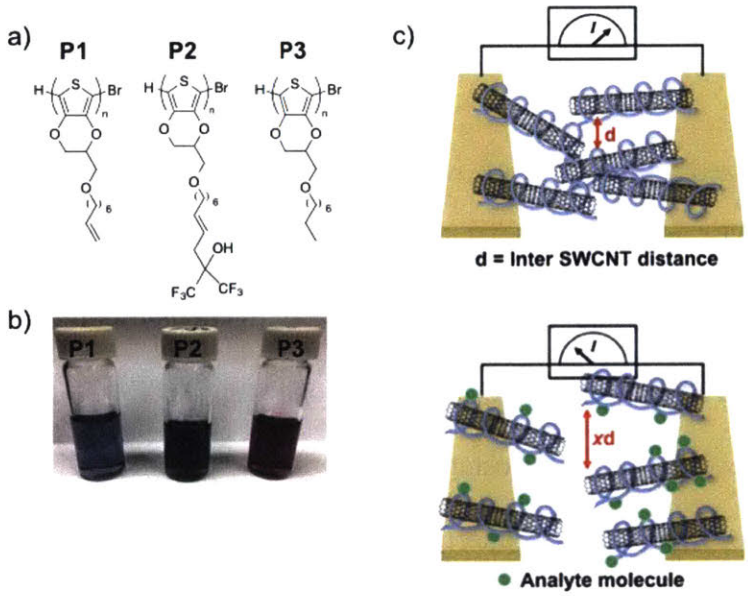

Figure 2.2 (a) Structures of derivatized PEDOTs; (b) Photograph of dispersions of **P1**–**P3**/SWCNT dispersions in THF (**P1**, **P3**) and DMF (**P2**); (c) Schematic of the swelling transduction mechanism.

2.3 Results and Discussion

2.3.1 Dispersion of SWCNTs with functionalized PEDOTs

Our goal was to create polymer/SWCNT dispersions that are resistant to re-bundling to be able to reproducibly create durable devices. Dispersed and de-bundled nanotubes have increased surface area for interaction with analytes and can create conductive pathways that can be more readily disrupted by analyte binding as is preferred for sensing applications.[17] We generated our derivatized polymer/SWCNT dispersions after experimentally determining the ratios of polymer to SWCNTs in the dispersions that produced the highest chemiresistive responses to DMMP. We identified the optimal ratio by weight of polymer/SWCNT/solvent was 2/1/1 (see Figure A.2.13).

Figure 2.3 (a-c) presents UV-vis-NIR absorbance spectra of **P1-P3** overlayed with the spectra of their respective diluted SWCNT dispersions. The absorption spectrum suggests the presence of both semiconducting and metallic nanotubes. Absorption bands in the 800 to 1600

nm as well as the 550 to 900 nm region are indicative of the E_{11} and E_{22} van Hove singularity transitions of semiconducting carbon nanotube, while the transitions of metallic nanotubes can be found in the region of 400-600 nm.[33,34] The clarity and resolution in these bands in Figure 2.3 indicate the presence of de-bundled SWCNTs in the polymer/SWCNT dispersions. All compositions have some broad absorptions in the 400-600 nm region, indicating the presence of metallic SWCNTs. The resolved absorption bands located at 880, 990, and 1120 nm are evidence of the presence of (6,5) SWCNTs.[35] It may be inferred that **P3** (Figure 3c) is more effective at dispersing SWCNTs than **P1** and **P2** from inspection of the intensity ratios of the SWCNT-based absorbances at 990 nm relative to that associated with P3 (λ_{max} =553 nm). The features at 1550 nm are attributed to a vibrational overtone from hydrazine,[36] which is used to prevent oxidation of the dispersions and stabilize de-bundled state.

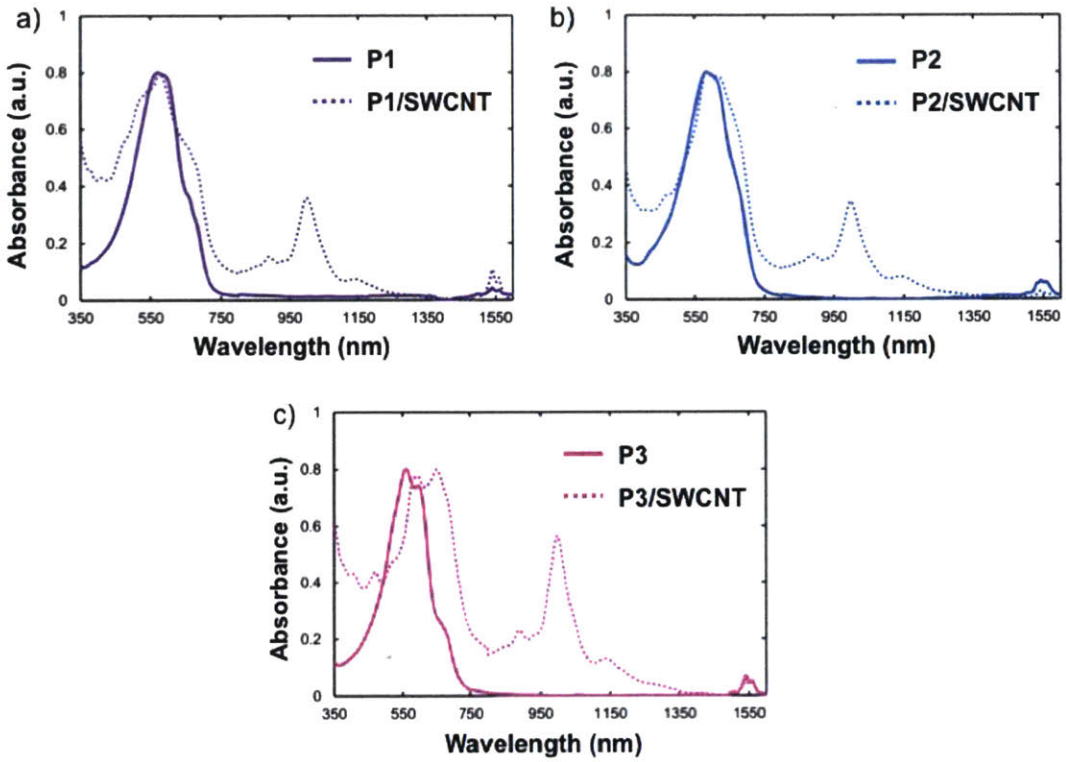

Figure 2.3 UV-vis/NIR spectra of polymer/SWCNT dispersions. (a) P1/SWCNT, (b) P2/SWCNT, (c) P3/SWCNT.

Resonance Raman spectroscopy is a useful tool in confirming the presence of SWCNTs in polymer dispersions. The full resonance Raman spectra of the composites and pure polymer are given in Figures A.2.14 and A.2.15. Thin film samples were prepared for analysis by drop casting dispersions from THF (**P1** and **P3**) or DMF (**P2**) onto a silicon wafer. A pristine SWCNT thin film was prepared by drop casting (6,5) enriched SWCNTs from a fresh dispersion in *ortho*-dichlorbenzene on to a silicon wafer. The spectra were taken using a 633 nm excitation wavelength and are normalized to the intensity of the G-band, at 1590 cm^{-1} and offset for clarity. In Figure 2.4a, Raman spectrum for the D-G band region is displayed. The D-band, located at 1290 cm^{-1}, is indicative of the disruption of the sp^2 network in conjugated nanocarbon systems.[37] The ratio of intensities of the D band (1290 cm^{-1}), to the G band (I_D/I_G) can give relative measure of disruption of the graphene π-system. After dispersion, there is a large increase in I_D/I_G from

the pristine SWCNTs to the polymer-dispersed SWCNTs. Specifically, the I_D/I_G is 0.06 in pristine SWCNTs and 0.9, 0.8, and 0.7 for the **P1**/SWCNT, **P2**/SWCNT and **P3**/SWCNT composites, respectively. This indicates an increase in the number of defects in the SWCNT sidewalls within the dispersion.[37] The source of the disruption in this case is hypothesized to be breaking of the conjugation of the SWCNT sp^2 network during the sonication step in the dispersion preparation or the result of strong associations between the graphene walls and the dispersing polymers or other molecules/molecular fragments.[38,39] The broad Raman peak located at 1422 cm^{-1} in the polymer dispersions is attributed entirely to the polymer and can be seen distinctly in Figure A.2.15. The radial breathing modes (RBM), shown in Figure 2.4b, are the signature for the presence of carbon nanotubes and are located between 100-300 cm^{-1}. The peak frequencies are inversely proportional to tube diameter. The as received pristine SWCNTs gave a peak at 252 cm^{-1} and overlapping peaks at 277 cm^{-1} and 290 cm^{-1}, whereas the polymer/SWCNT dispersions are slightly narrowed maxima and positioned at 283 cm^{-1} and 297 cm^{-1}.

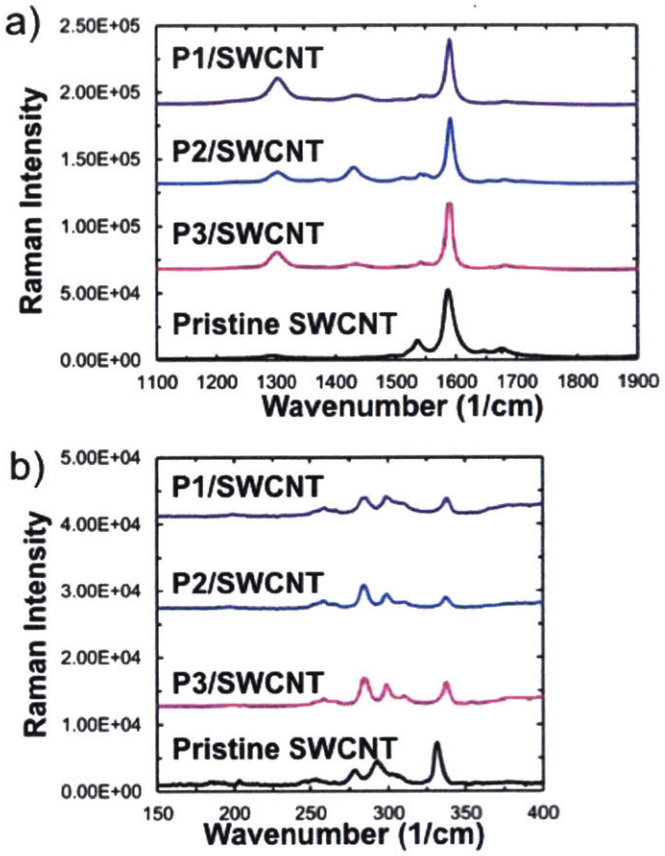

Figure 2.4 Resonance Raman spectra (truncated) of polymer/SWCNT dispersions with focus on the (a) D&G band region (1200-1700 cm^{-1}) and the (b) RBM region (100-300 cm^{-1}).

2.3.2 Polymer/SWCNT composites for DMMP detection in dry N_2 and air (24% RH)

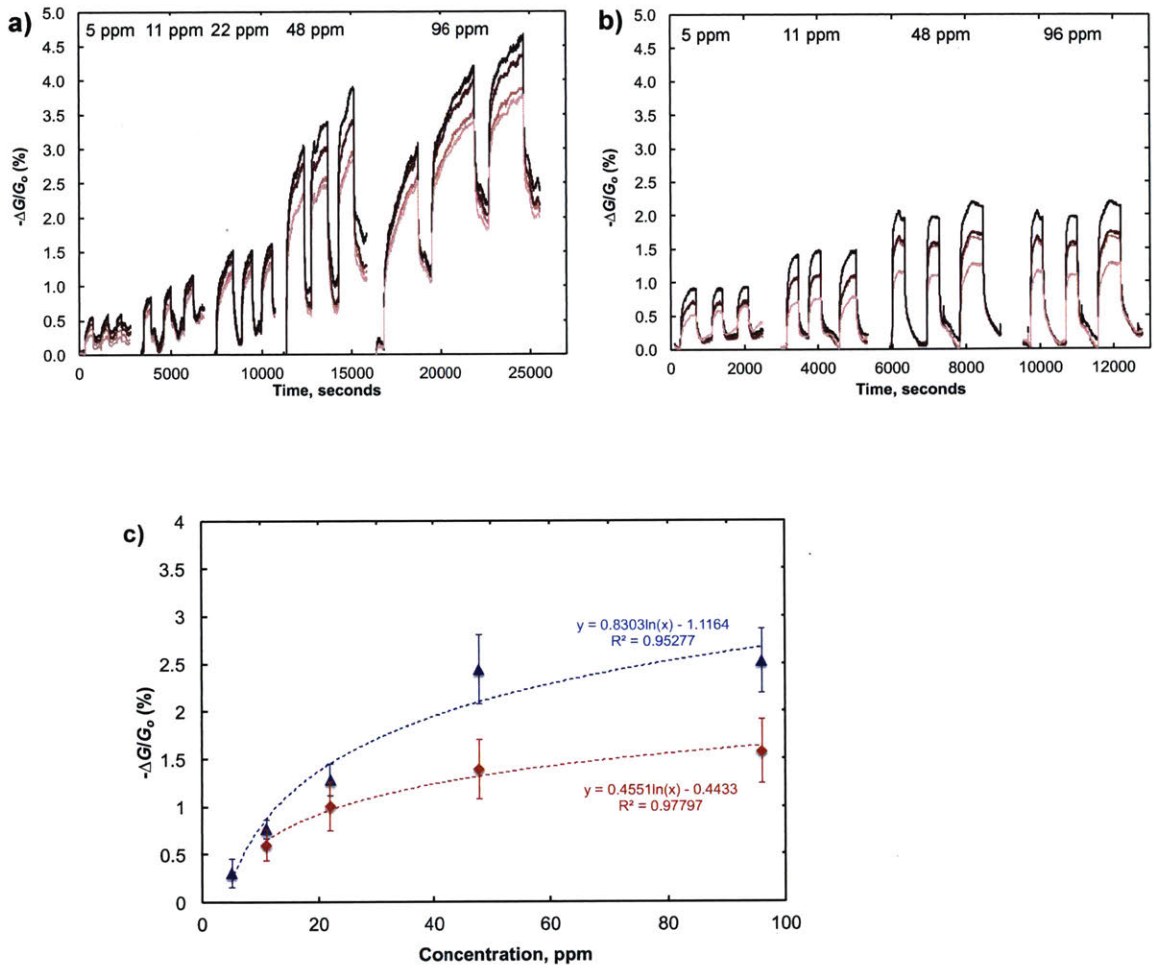

Figure 2.5 (a) Conductance traces of four **P2**/SWCNT-based chemiresistors to five concentrations of DMMP in dry N_2 at room temperature. (b) Conductance traces of four **P2**/SWCNT-based chemiresistors to four concentrations of DMMP in air (24% RH) at room temperature. c) Saturated chemiresitive responses averaged across quadruplicate trials for P2/SWCNT devices for varying amounts of DMMP in dry N_2 (blue triangles) and air (24% RH) (red diamonds) at room temperature.

With stable composites in hand, we sought to investigate the efficacy of our polymer/SWCNT composite system in detecting the nerve agent simulant, DMMP. The sensory response was investigated by measuring the change in current between two electrodes at a constant bias voltage of 0.10 V. The change in current was converted to a negative change in

conductance [$-\Delta G/G_o$ (%) = $((I_o-I)/I_o)$ x 100%], where I_o is the initial current. This normalized response allows for small differences in the resistivity that can complicate device to device comparisons. Figure 2.5a shows baseline-corrected responses of four chemiresistive devices that were tested in parallel incorporating our HFIP-PEDOT/SWCNT system (**P2**/SWCNT) that is designed to selectively detect DMMP. Figure 2.5a shows the response in dry N_2, while Figure 2.5b shows the response in air with 24% RH. Exposure times were varied to reach full saturation of the devices. In both carrier gases, the sensors show a reversible response across this concentration range. We do observe increased baseline drift in the N_2 conductance trace in contrast to the more stable baseline in the air trace. We suggest that the stability is due to the steady presence of water and oxygen at the device interface that acts to maintain consistent electronic environment in the sensor material. In Figure A.2.16, the device response becomes saturated in a shorter time period at all concentrations in air than in N2. In Figure 2.5c, we observed a linear responses range for DMMP from 5-48 ppm in dry N_2 and air. The dynamic range extends to 98 ppm, but the response curve suggests saturation behavior of the detector at or near 48 ppm. We noted a 0.30% response to DMMP at a concentration of 5 ppm with a linear response up to 48 ppm for the **P2**/SWCNT response in dry N_2. We calculated a 2.7 ppm detection limit in dry N_2 using a signal to noise ratio method[40] for **P2**/SWCNT. While we could not detect DMMP at a concentration of 5 ppm in air with 24% RH, we observed a 0.60% response to DMMP at a concentration of 11 ppm with a linear response up to 48 ppm for the P2/SWCNT. The calculated detection limit for **P2**/SWCNT in air is 6.5 ppm. Figure A.2.51 demonstrates the linear response curve for experiments in N_2 and air. The **P2**/SWCNT composite device covers an operationally relevant range for the detection of nerve agents such as sarin (GB), for which DMMP is a simulant.[41] The chemiresistive detection of DMMP by a decrease in

conductance is consistent with the notion of a transduction mechanism that relies upon a swelling of the SWCNT network or direct modulation of the SWCNT conductance by charge transfer of dipolar mechanisms. These effects are all consistent with the DMMP being concentrated in the polymer HFIP-terminated side chain as a result of hydrogen-bonding interactions with the **P2**/SWCNT composite (Figure 2.1a). Uptake of the analyte DMMP into the SWCNT network increases the resistance (reduces the current) as a result.

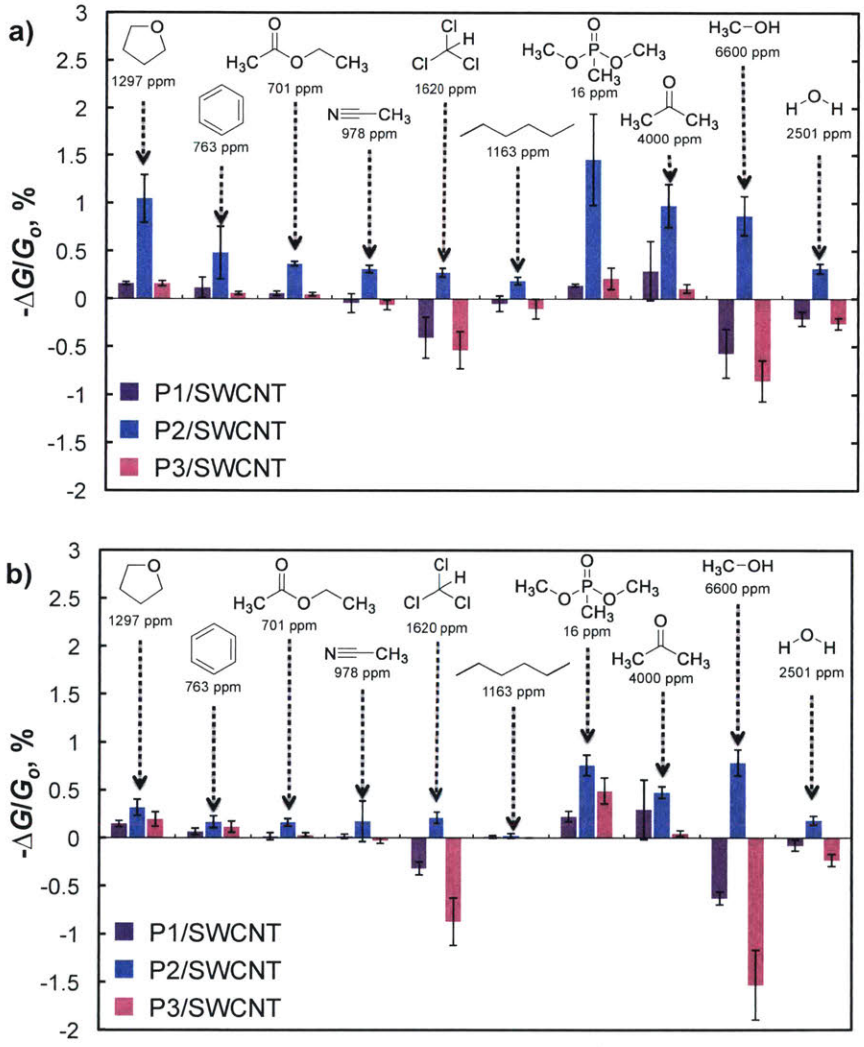

Figure 2.6 (a) Chemiresistive responses averaged across four **P1-P3**/SWCNT devices to 60 s exposures of VOCs at a flow rate of 200 ml/min in dry N_2. (b) Chemiresistive responses averaged across four **P1-P3**/SWCNT devices to 60 s exposures of VOCs at a flow rate of 200 ml/min in air (24% RH).

Detecting CWAs in a real-world environmental sample demands a strategy for detecting trace quantities in a complex background containing other vapors that may be present in higher concentrations. Figure 2.6a shows chemiresistive responses for devices **P1-P3**/SWCNTs exposed to various volatile organic chemicals (VOCs) for 60 s followed by a 140 s recovery time at a constant flow rate of 200 mL/min at room temperature in dry N_2. Figure 2.6b shows results for a similar experiment obtained by using air (24% RH). The concentrations of vapors selected to confound the sensors for this experiment were chosen to be sufficiently high to obtain a measureable response from pristine SWCNTs (Figures A.2.17, A.219 and A.2.20). In both dry N_2 and air, it is clear that the **P2**/SWCNT composite responds to polar and hydrogen bonding analytes to a much greater degree than the HFIP free reference composites (**P1**/SWCNT and **P3**/SWCNT). The enhanced response is therefore attributed to presence of the polar and proton donating HFIP group of **P2**.

The **P2**/SWCNT composite responds to all analytes in N_2 and air tested but exhibits exceptional selectivity for DMMP above all others in dry N_2. Vapor challenges of 1297 ppm THF, 4000 ppm acetone and 6600 ppm MeOH all have similar magnitude responses (around 1.0 %) to what is observed for 16 ppm DMMP in N_2. In air, the responses of all **P1-3**/SWCNT are slightly lower than in dry N_2. We hypothesize that the introduction of water at lower concentrations into the gas mixture offers competition as a hydrogen bond donor to DMMP. Therefore, the presence of water decreases the amount of DMMP that may be bound to the **P2**/SWCNT composite, thus lowering the chemiresistive response.

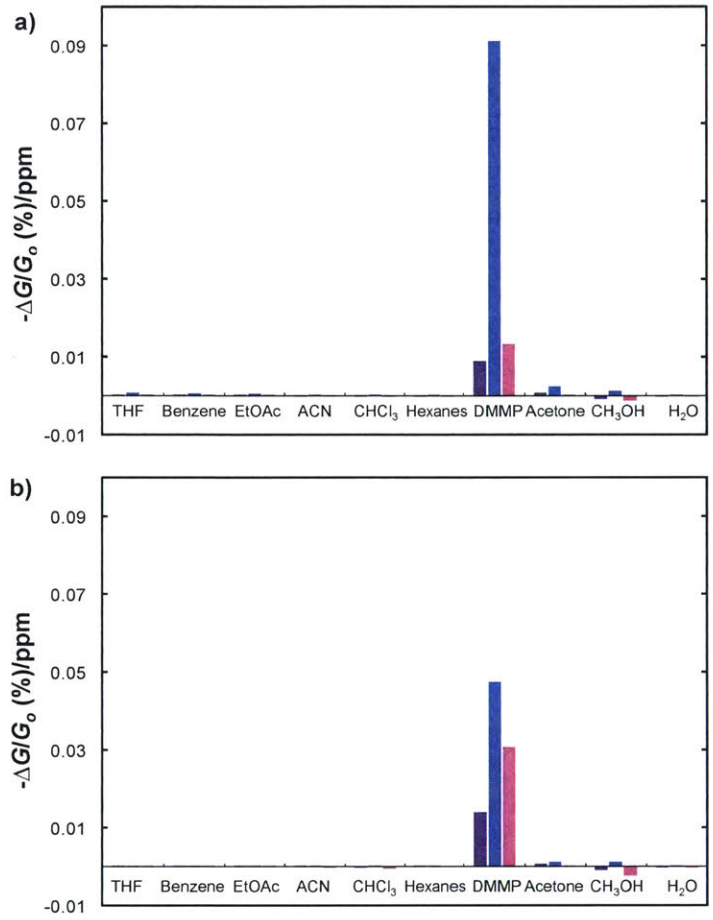

Figure 2.7 (a) Chemiresistive response ratio ($-\Delta G/G_o$ (%)/ppm) for P2/SWCNT to VOCs in N2. (b) Chemiresistive response ratio for P2/SWCNT to VOCs in air (24 % RH).

It is clear that the **P2**/SWCNT is selective as designed in N_2 and air. To put this selectivity for DMMP in perspective, we have provided a response ratio by dividing the negative change in conductance by the concentration in ppm [$(-\Delta G/G_o)$/ppm] at the given flow rate (200 ml/min). Figure 2.7b shows that the **P2**/SWCNT response ratio for DMMP in N_2 is an order of magnitude larger than that for the **P1**/SWCNT and **P3**/SWCNT composites. A similar, though smaller response ratio is shown for **P2**/SWCNT in air. The **P2**/SWCNT composite garners a nearly a two orders of magnitude larger response ratio to DMMP over the other VOCs. An interesting result

in Figures 2.6a and 2.6b show an increase in conductance for the **P1**/SWCNT and **P3**/SWCNT composites upon exposure to acetonitrile, chloroform, hexanes, methanol and water. This may be explained by a secondary doping effect.[42] Considering that the SWCNTs are naturally p-doped by molecular oxygen[43] and that the polymers are strong electron donors, the carrier levels in the SWCNTs will be reduced by strong charge transfer interactions or electron donation from the polymers to nanotubes. Some of the solvents may reduce these interactions and thereby affect an increase in carrier density. If the organic vapor molecules do not have strong interactions with the SWCNTs that pin or scatter the carriers, increased carrier levels will give rise to an increased conduction as we observe.

To establish the stability of the **P2**/SWCNT composites, we conducted a device aging study in which we measured the chemiresistive response to exposure to 11 ppm DMMP in N_2 over the course of two weeks (Figure A.1.21). These devices were stored under ambient lab conditions on the benchtop. We found no significant change in the response over that time period. However, though not recorded, we did observe that devices stored under ambient conditions over the course of a more than a month experienced significant degradation in performance. We also tested the stability of the devices in humid air (50% RH). The results in Figure A.2.22 show a slightly enhanced and reliable response at 11 ppm to this level of humidity with a response of 0.95 %. As mentioned before, the response in air (24% RH) was 0.60%. While the presence of water at lower RH served to compete with the **P2**/SWCNT composite for hydrogen bonding with DMMP, at higher RH, there likely is water available in the gas mixture to compensate hole carriers in the p-type SWCNTs, thus reducing conductance. This observation of decreasing conductance of SWCNTs with increasing humidity has been reported

previously[44,45] and is linear until high RH (> 65 % are reached). It will continue be important in future SWCNT-based device design to take into account the effect of humidity.

2.4 Conclusions

In summary, we developed a chemiresistive sensor for the detection of nerve agent simulant DMMP. This sensor was fabricated using a derivatized PEDOT/SWCNT composite and with strong responses to 5 ppm DMMP and a calculated detection limit of 2.7 ppm in N_2. The same devices in a "real world" environment (air with 24% RH), experienced a strong response at 11 ppm and a detection limit of 6.5 ppm. We explored the effects on the devices of aging in an ambient environment and higher humidity (50% RH). Additionally, we propose that the transduction mechanism responsible for the decrease in conductance in the device upon the introduction of DMMP is a hydrogen bonding interaction between the DMMP and an HFIP moiety incorporated in the derivatized PEDOT sidechain. Finally, we demonstrated that our polymer/SWCNT composites maintain stable, debundled dispersions in solution via resonance Raman and UV–vis–NIR spectroscopy.

2.5 Experimental

2.5.1 Materials

All chemicals and reagents were purchased from Sigma-Aldrich and used without additional purification, except that tetrahydrofuran was distilled from sodium metal and benzophenone. SWCNTs (6,5 chirality, carbon (95%), with 93% as SWCNTs) were acquired from Sigma Aldrich, Inc. (Saint Louis, MO, USA). 3,4-dimethoxythiophene (95%) and 2-(allyl)hexafluoroisopropanol (99%) were purchased from Matrix Scientific (Columbia, SC, USA). 1,3-bis(diphenylphosphino)propane nickel (II) (99%) was purchased from Strem

Chemicals (Newburyport, MA, USA). Deuterated solvents for NMR were obtained from Cambridge Isotope Laboratories (Tewksbury, MA, USA).

2.5.2 Instrumentation

^{1}H, ^{13}C and ^{19}F NMR spectra were recorded at 400 MHz (100 MHz) or 500 MHz (125 MHz) using either Bruker AVANCE-400 or JEOL JNM-ECZR-500 NMR spectrometers, respectively. Chemical shifts are reported in ppm and referenced to residual NMR solvent peaks (^{1}H NMR: δ 3.62 ppm for THF, δ 7.26 ppm for $CDCl_3$; ^{13}C NMR: δ 77.2 ppm for $CDCl_3$). High-resolution mass spectra were determined with a Bruker Daltonics APEXIV 4.7 Tesla FT–ICR–MS using ESI or DART ionization. The MALDI-MS spectra were acquired in linear and reflection modes in the Koch Institute at MIT using a Bruker Microflex MALDI-MS spectrometer. UV–Vis absorption spectra were measured using an Agilent Cary 4000 Series UV–Vis spectrophotometer. Gel permeation chromatography (GPC) measurements were performed in tetrahydrofuran using an Agilent 1260 Infinity system and calibrated with a polystyrene standard. ATR–FTIR spectra were acquired using a Thermo Scientific Nicolet 6700 FT–IR with either a Ge or ZnSE crystal for ATR and subjected to the 'atmospheric suppression' correction in OMNIC™ Spectra software. Raman spectra were collected with excitation at 633 nm laser using a Horiba LabRAM HR800 Raman spectrometer.

2.5.3 Synthesis of monomers and polymers

Detailed procedures for the synthesis of all compounds can be found in the supplementary information. Briefly, brominated EDOT monomers can be polymerized using Kumada catalyst transfer polycondensation (KCTP) [33–38].[46–51] The monomer synthesis begins by O-alkylation of the inexpensive reagent solketal (**1**) to yield compounds **3a** and **3b** in moderate yields (Scheme 2.1). Intermediates **4a** and **4b** were next obtained by acid-catalyzed deprotection in a

mixture of 1.0 M HCl (aq) and THF. Monomer precursors **6a** and **6b** were formed by an acid-catalyzed substitution of the methoxy groups of compound **5** by diols **4a** and **4b**. Products **6a** and **6b** were then brominated with *N*-bromosuccinnamide (NBS) in THF to provide KCTP monomers **7a** and **7b**.

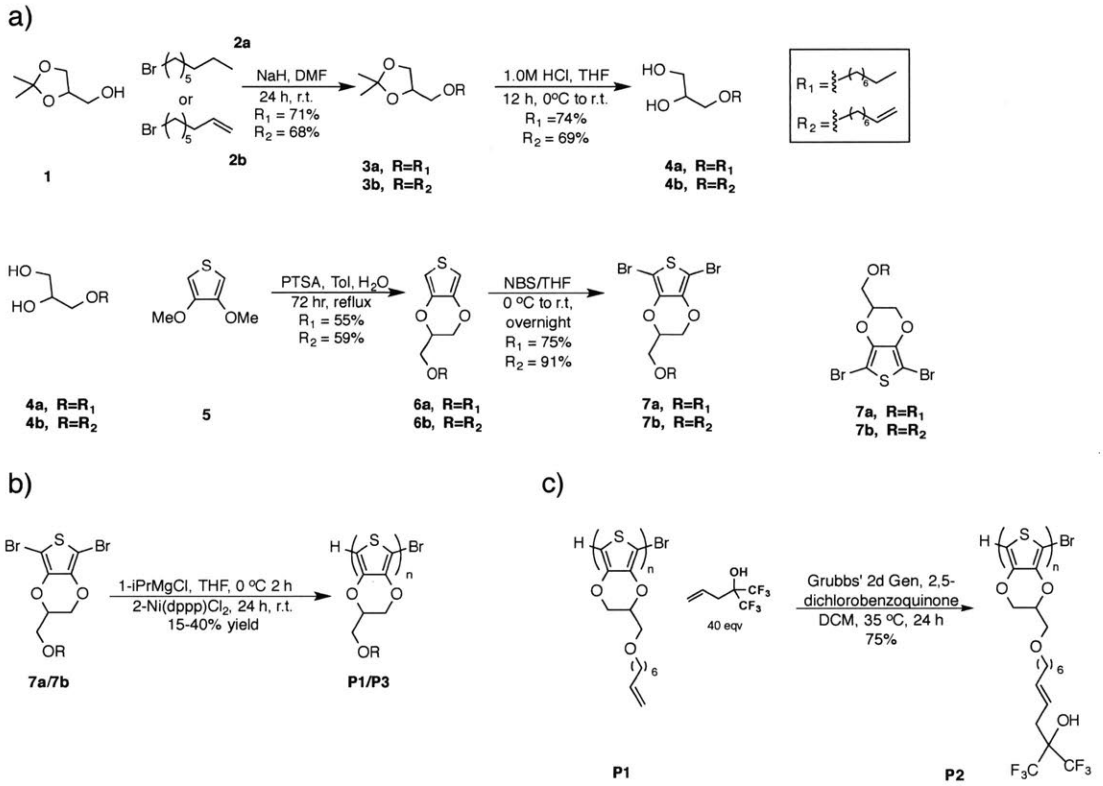

Scheme 2.1 (a) Synthesis of derivatized EDOT monomers for (b) Kumada catalyst transfer polycondensation (c) Post-polymerization modification via alkene cross-metathesis of **P1** and allyl-HFIP to form **P2**.

KCTP was chosen as the polymerization method to generate our derivatized PEDOT derivatives over electrochemical polymerization[52,53] and $FeCl_3$-catalyzed oxidative polymerization.[54] Though oxidative polymerizations do not often yield cross-linked polymer products in the preparation of polythiophenes, in this case, both of these methods yielded insoluble products that appeared to be highly cross-linked. We hypothesize that the terminal

alkene on the side chain of **P1** reacts with the radical cation intermediates generated under oxidizing conditions to give cross-linked products.

P1 is, in principle, a platform polymer upon which we can incorporate a number of desired recognition elements. **P2** contains a HFIP moiety that was attached via a cross metathesis reaction.[29,55–57] As a result of its unique hydrogen bonding characteristics, HFIP is a known selector for DMMP (Figure 2.1). **P3** was studied as a control polymer. **P1** and **P3** were synthesized using KCTP, which were then solvent fractionated to isolate the highly soluble material. Such soluble fractions were produced in acceptable yields (15–40%) (Scheme 2.1b), with M_n values of 2700 to 2900 g/mol and polydispersities of 1.2–1.3 (Figure A.2.1). Although higher molecular weight fractions with masses up to 6100 g/mol were identified using MALDI-MS for **P1** (Figure A.2.2), higher molecular weight samples were found to be only slightly soluble in organic solvents and unable to form composites with SWCNTs. For **P1–P3**, we observed that molecular weights determined by MALDI MS were smaller than that of GPC.[58] Additionally, molecular weights determined by end group analysis with ^{1}H NMR are higher than GPC or MALDI MS results (Table A.2.3 and Figures A.2.2, A.2.4-A.2.6). The lower molecular weights obtained by MALDI MS analysis as compared to GPC is consistent with previous work that demonstrated GPC tends to overestimate molecular weights of rod-like conjugated systems [44]. It is possible that MALDI-MS analysis provides smaller molecular weights than ^{1}H NMR end group analysis because the higher laser power required to volatize higher molecular weight fractions leads to chain fragmentation.[59]

P2 was synthesized via a post-polymerization modification of **P1** using an alkene cross metathesis reaction (Scheme 2.1c). This transformation was successful, as evidenced by an increase in molecular weight from 2900 to 3900 g/mol. The conversion of a terminal alkene in

P1 to an internal alkene in **P2** was confirmed by analysis of the ^{1}H NMR spectrum. The disappearance of a doublet at δ 5.78 ppm and multiplet centered at δ 4.96 ppm in **P1** (Figure A.2.7) to yield a doublet at δ 5.40 ppm in **P2** indicates full conversion of the terminal alkene to an internal olefin (Figure A.2.8). The intensity of both peaks in this doublet suggests an approximately equal proportion of both *cis* and *trans* stereoisomers are present in **P2**. In Figure A.2.9, ^{19}F NMR confirms the presence of a HFIP group in **P2** with a resonance at δ 76.7 ppm.

2.5.4 Preparation of polymer/SWCNT dispersions

To a solution of **P1(P3)** (M_n = 2900 g/mol, 10 mg) in dry tetrahydrofuran (THF, 5 mL) or **P2** in dry dimethyl formamide (DMF, 5 mL), 5 mg of SWCNT was added and followed by 10 μL hydrazine (a reducing/de-doping agent). Then the resulting mixture was sonicated for 1 h in an ultrasonic bath (Branson, 3510) chilled with ice and then allowed to reach room temperature. Subsequently, the suspension was centrifuged for 30 min at 9500 g. The supernatant was decanted and centrifuged again for an additional 30 min at 9500 g and allowed to stand overnight undisturbed. The isolated supernatant was directly used for the device fabrication via dropcasting unless otherwise indicated. For UV–vis–NIR absorption spectroscopy, the isolated supernatant was diluted to 1:2 in THF or DMF, further sonicated for 5 min, and recorded in a 1 cm optical path quartz cuvette.

2.5.5 Preparation of gold electrodes on glass microscope slides

Glass substrates deposited with chromium adhesion layers (10 nm) and gold electrodes (100 nm) were prepared according to a literature procedure.[18] Briefly, glass slides (VWR Microscope Slides) were cleaned by sonication in acetone for 5 min followed by UV-ozone treatment using a UVO cleaner (Jelight Company Inc., Model 42, Irvine, CA, USA, for 20 min. A 15 nm layer of

chromium (99.99%, R.D. Mathis) and a subsequent 150 nm layer of gold (99.99%, R.D. Mathis) were deposited through a custom stainless steel mask using a thermal evaporator (Angstrom Engineering, Kitchener, Ontario, Canada), which resulted in three sets of four channel electrode patterns on a single glass slide, which was cut into three individual devices. Each device contains a gold pattern of four isolated working electrodes with one shared reference-counter electrode on the glass substrate. The gap between one pair of gold electrodes is 1 mm.

2.5.6 Fabrication of a polymer-SWCNT chemiresistor platform

The desired amount of polymer-SWCNT dispersion in THF or DMF was dropcasted with a 20 μL syringe between four gold electrode pairs on the glass substrate. Typically, between 4–20 μL of the dispersion was required to reach the target electrode resistance of 10–50 kΩ.

2.5.7 Volatile organic compound (VOC) gas detection measurement

For VOC gas detection measurement, the fabricated array device was placed into a custom-built PTFE enclosure with a small gas inlet and outlet, the gold electrodes of the device were connected to a PalmSens EmStat potentiostat with a MUX16 multiplexer. A KIN-TEK gas generator system calibrated for each VOC was used to deliver to the device's enclosure a known concentration of a given VOC analyte diluted in N_2 gas at a fixed gas flow rate (200 mL/min) to minimize drift in the baseline resistance. For calibration, emission rate of each VOC by monitoring the decrease in mass of each liquid for an hour at a 200 mL/min flow rate and a designated temperature (40 °C–70 °C). Three trials for each VOC were performed. The potentiostat applied a constant potential of 0.1 V across the electrodes, and the current for each channel of the device was recorded using PS Trace software (v. 4.7) during 60 s of VOC vapor exposures. After a linear baseline correction, the change in current resulting from exposure to the

analyte was converted to the negative change in conductance ($-\Delta G/G_0$ (%) = $(I_0 - I)/I_0) \times 100$), where I_0 is initial current), which was taken as the device's response. Schematics and photographs of the experimental setup can be found in the Chapter 2.7 Appendix, Figure A.2.11 (Schematic/cartoon for sensing experimental set up), Figure A.2.12 (Photograph of sensing experimental set up) and Figure A.2.13 (Schematic/cartoon for sensing experimental set up in humid air).

2.6 References

(1) Arampatzis, T.; Lygeros, J.; Manesis, S. A Survey of Applications of Wireless Sensors and Wireless Sensor Networks. *Proc. IEEE Int. Symp. on, Mediterrean Conf. Control Autom. Intell. Control* **2005**, No. August 2016, 719–724.
(2) Sferopoulos, R. A Review of Chemical Warfare Agent (CWA) Detector Technologies and Commercial-Off-The-Shelf Items. *Aust. Gov. Dep. Def.* **2009**, 98.
(3) Azzarelli, J. M.; Mirica, K. A.; Ravnsbæk, J. B.; Swager, T. M. Wireless gas detection with a smartphone via rf communication. *Proc. Natl. Acad. Sci. U. S. A.* **2014**, *111*, 18162–18166.
(4) Fennell, J. F.; Liu, S. F.; Azzarelli, J. M.; Weis, J. G.; Rochat, S.; Mirica, K. A.; Ravnsbaek, J. B.; Swager, T. M. Nanowire Chemical/Biological Sensors: Status and a Roadmap for the Future. *Angew. Chemie Int. Ed.* **2016**, *55*, 1266–1281.
(5) Kauffman, D. R.; Star, A. Carbon nanotube gas and vapor sensors. *Angew. Chem. Int. Ed. Engl.* **2008**, *47*, 6550–6570.
(6) Potyrailo, R. A.; Surman, C.; Nagraj, N.; Burns, A. Materials and Transducers Toward Selective Wireless Gas Sensing. *Chem. Rev.* **2011**, *111*, 7315–7354.
(7) Schnorr, J. M.; Swager, T. M. Emerging Applications of Carbon Nanotubes. *Chem. Mater.* **2011**, *23*, 646–657.
(8) Hirsch, A. Functionalization of Single-Walled Carbon Nanotubes. *Angew. Chemie Int. Ed.* **2002**, *41*, 1853.
(9) Svensson, J.; Campbell, E. E. B. Schottky barriers in carbon nanotube-metal contacts. *J. Appl. Phys.* **2011**, *110*.
(10) Bahr, J. L.; Yang, J.; Kosynkin, D. V; Bronikowski, M. J.; Smalley, R. E.; Tour, J. M. Functionalization of carbon nanotubes by electrochemical reduction of aryl diazonium salts: A Bucky Paper Electrode. *J. Am. Chem. Soc.* **2001**, *123*, 6536–6542.
(11) Bahr, J. L.; Tour, J. M.; Yu, M.-F.; Files, B. S.; Arepalli, S.; Ruoff, R. S.; O'Connell, M. J.; Boul, P. J.; Ericson, L. M.; Huffman, C. B.; et al. Covalent chemistry of single-wall carbon nanotubes. *J. Mater. Chem.* **2002**, *12*, 1952–1958.
(12) Weis, J. G.; Ravnsbæk, J. B.; Mirica, K. A.; Swager, T. M. Employing Halogen Bonding Interactions in Chemiresistive Gas Sensors. *ACS Sensors* **2016**, *1*, 115–119.
(13) Schnorr, J. M.; van der Zwaag, D.; Walish, J. J.; Weizmann, Y.; Swager, T. M. Sensory Arrays of Covalently Functionalized Single-Walled Carbon Nanotubes for Explosive Detection. *Adv. Funct. Mater.* **2013**, *23*, 5285–5291.
(14) Wang, F.; Gu, H.; Swager, T. M. Carbon nanotube/polythiophene chemiresistive sensors for chemical warfare agents. *J. Am. Chem. Soc.* **2008**, *130*, 5392–5393.

(15) Ya-Ping Sun; Kefu Fu; Yi Lin, A.; Huang, W. Functionalized Carbon Nanotubes: Properties and Applications. **2002.**
(16) Liu, S. F.; Petty, A. R.; Sazama, G. T.; Swager, T. M. Single-walled carbon nanotube/metalloporphyrin composites for the chemiresistive detection of amines and meat spoilage. *Angew. Chem. Int. Ed. Engl.* **2015**, *54*, 6554–6557.
(17) Yoon, B.; Liu, S. F.; Swager, T. M. Surface-Anchored Poly(4-vinylpyridine)–Single-Walled Carbon Nanotube–Metal Composites for Gas Detection. *Chem. Mater.* **2016**, *28*, 5916–5924.
(18) Frazier, K. M.; Swager, T. M. Robust cyclohexanone selective chemiresistors based on single-walled carbon nanotubes. *Anal. Chem.* **2013**, *85*, 7154–7158.
(19) Mirica, K. A.; Weis, J. G.; Schnorr, J. M.; Esser, B.; Swager, T. M. Mechanical Drawing of Gas Sensors on Paper. *Angew. Chemie Int. Ed.* **2012**, *51*, 10740–10745.
(20) Mirica, K. A.; Azzarelli, J. M.; Weis, J. G.; Schnorr, J. M.; Swager, T. M. Rapid prototyping of carbon-based chemiresistive gas sensors on paper. *Proc. Natl. Acad. Sci. U. S. A.* **2013**, *110*, E3265-70.
(21) Bracamonte, M. V.; Melchionna, M.; Stopin, A.; Giulani, A.; Tavagnacco, C.; Garcia, Y.; Fornasiero, P.; Bonifazi, D.; Prato, M. Carboxylated, Fe-Filled Multiwalled Carbon Nanotubes as Versatile Catalysts for O_2 Reduction and H_2 Evolution Reactions at Physiological pH. *Chem. - A Eur. J.* **2015**, *21*, 12769–12777.
(22) Stopin, A.; Pineux, F.; Marega, R.; Bonifazi, D. Magnetically Active Carbon Nanotubes at Work. *Chem. - A Eur. J.* **2015**, *21*, 9288–9301.
(23) Star, A.; Stoddart, J. F.; Steuerman, D.; Diehl, M.; Boukai, A.; Wong, E. W.; Yang, X.; Chung, S.-W.; Choi, H.; Heath, J. R. Wrapped single-walled carbon nanotubes. *Angew. Chemie Int. Ed.* **2001**, *40*, 1721–1725.
(24) Samanta, S. K.; Fritsch, M.; Scherf, U.; Gomulya, W.; Bisri, S. Z.; Loi, M. A. Conjugated polymer-assisted dispersion of single-wall carbon nanotubes: The power of polymer wrapping. *Acc. Chem. Res.* **2014**, *47*, 2446–2456.
(25) Grate, J. W. Hydrogen-bond acidic polymers for chemical vapor sensing. *Chemical Reviews*, 2008, *108*, 726–745.
(26) Geoghegan, J.; Tong, J. L. Chemical warfare agents. *Contin. Educ. Anaesthesia, Crit. Care Pain* **2006**, *6*, 230–234.
(27) Groenendaal, L.; Jonas, F.; Freitag, D.; Pielartzik, H.; Reynolds, J. R. Poly(3,4-ethylenedioxythiophene) and Its Derivatives: Past, Present, and Future. *Adv. Mater.* **2000**, *12*, 481–494.
(28) Kim, E. G.; Brédas, J. L. Electronic evolution of poly(3,4-ethylenedioxythiophene) (PEDOT): From the isolated chain to the pristine and heavily doped crystals. *J. Am. Chem. Soc.* **2008**, *130*, 16880–16889.
(29) Trnka, T. M.; Grubbs, R. H. The Development of L 2 X 2 RuCHR Olefin Metathesis Catalysts: An Organometallic Success Story. *Acc. Chem. Res.* **2001**, *34*, 18–29.
(30) Kong, J. Nanotube Molecular Wires as Chemical Sensors. *Science.* **2000**, *287*, 622–625.
(31) Star, A.; Gabriel, J.-C. P.; Bradley, K.; Grüner, G. Electronic Detection of Specific Protein Binding Using Nanotube FET Devices. *Nano Lett.* **2003**, *4*, 459–463.
(32) Star, A.; Han, T. R.; Joshi, V.; Gabriel, J. C. P.; Grüner, G. Nanoelectronic carbon dioxide sensors. *Adv. Mater.* **2004**, *16*, 2049–2052.
(33) O'Connell, M. J.; Bachilo, S. M.; Huffman, C. B.; Moore, V. C.; Strano, M. S.; Haroz, E. H.; Rialon, K. L.; Boul, P. J.; Noon, W. H.; Kittrell, C.; et al. Band Gap Fluorescence from Individual Single-Walled Carbon Nanotubes. *Science.*. **2002**, *297*, 593-596.

(34) Naumov, A. V; Ghosh, S.; Tsyboulski, D. A.; Bachilo, S. M.; Weisman, R. B. Analyzing absorption backgrounds in single-walled carbon nanotube spectra. *ACS Nano* **2011**, *5*, 1639–1648.
(35) Tu, X.; Manohar, S.; Jagota, A.; Zheng, M. DNA sequence motifs for structure-specific recognition and separation of carbon nanotubes. *Nature* **2009**, *460*, 250–253.
(36) Murray, M.; Kurtz, J. Near-infrared absorptions of monomethylhydrazine. *J. Quant. Spectrosc. Radiat. Transf.* **1993**, *50*, 585–590.
(37) Jorio, A.; Saito, R.; Dresselhaus, G.; Dresselhaus, M. S. *Raman Spectroscopy in Graphene Related Systems*; Wiley-VCH Verlag GmbH & Co. KGaA: Weinheim, Germany, 2011.
(38) Jorio, A.; Pimenta, M. A.; Souza Filho, A. G.; Saito, R.; Dresselhaus, G.; Dresselhaus, M. S. Characterizing carbon nanotube samples with resonance Raman scattering. *New J. Phys.* **2003**, *5*, 139–139.
(39) Bergin, S. D.; Sun, Z.; Streich, P.; Hamilton, J.; Coleman, J. N. New solvents for nanotubes: Approaching the dispersibility of surfactants. *J. Phys. Chem. C.* **2010**, *114*, 231–237.
(40) Ammu, S.; Dua, V.; Agnihotra, S. R.; Surwade, S. P.; Phulgirkar, A.; Patel, S.; Manohar, S. K. Flexible, all-organic chemiresistor for detecting chemically aggressive vapors. *J. Am. Chem. Soc.* **2012**, *134*, 4553–4556.
(41) Lillie, S. H.; Hanlon, E. J.; Kelly, J. M.; Rayburn, B. B. *Potential Military Chemical / Biological Agents and Compounds*; 2005.
(42) MacDiarmid, A. G.; Epstein, A. J. Secondary doping in polyaniline. *Synth. Met.* **1995**, *69*, 85–92.
(43) Derycke, V.; Martel, R.; Appenzeller, J.; Avouris, P. Controlling doping and carrier injection in carbon nanotube transistors. *Appl. Phys. Lett.* **2002**, *80*, 2773–2775.
(44) Na, P. S.; Kim, H.; So, H.-M.; Kong, K.-J.; Chang, H.; Ryu, B. H.; Choi, Y.; Lee, J.-O.; Kim, B.-K.; Kim, J.-J.; et al. Investigation of the humidity effect on the electrical properties of single-walled carbon nanotube transistors. *Appl. Phys. Lett.* **2005**, *87*, 93101.
(45) Han, J. W.; Kim, B.; Li, J.; Meyyappan, M. Carbon nanotube based humidity sensor on cellulose paper. *J. Phys. Chem. C* **2012**, *116*, 22094–22097.
(46) Yokozawa, T.; Yokoyama, A. Chain-growth condensation polymerization for the synthesis of well-defined condensation polymers and pi-conjugated polymers. *Chem. Rev.* **2009**, *109*, 5595–5619.
(47) Yokoyama, A.; Miyakoshi, R.; Yokozawa, T. Chain-Growth Polymerization for Poly(3-hexylthiophene) with a Defined Molecular Weight and a Low Polydispersity. *Macromolecules* **2004**, *37*, 1169–1171.
(48) Sheina, E. E.; Liu, J.; Lovu, M. C.; Laird, D. W.; McCullough, R. D. Chain growth mechanism for regioregular nickel-initiated cross-coupling polymerizations. *Macromolecules* **2004**, *37*, 3526–3528.
(49) Jeffries-El, M.; Sauvé, G.; McCullough, R. D. Facile Synthesis of End-Functionalized Regioregular Poly(3-alkylthiophene)s via Modified Grignard Metathesis Reaction. *Macromolecules* **2005**, *38*, 10346–10352.
(50) Loewe, R. S.; McCullough, R. D. Effects of Structural Regularity on the Properties of Poly(3-alkylthienylenevinylenes). *Chem. Mater.* **2000**, *12*, 3214–3221.
(51) Kiriy, A.; Senkovskyy, V.; Sommer, M. Kumada catalyst-transfer polycondensation: Mechanism, opportunities, and challenges. *Macromol. Rapid Commun.* **2011**, *32*, 1503–1517.
(52) Sotzing, G. A.; Reynolds, J. R. Poly[trans-bis(3,4-ethylenedioxythiophene)vinylene]: a low band-gap polymer with rapid redox switching capabilities between conducting transmissive and

insulating absorptive states. *J. Chem. Soc. Chem. Commun.* **1995**, No. 6, 703.
(53) Sotzing, G. A.; Reynolds, J. R.; Steel, P. J. Electrochromic conducting polymer via electrochemical polymerization of bis(2-(3,4-ethylenedioxy)thienyl) monomers. *Chem. Mater.* **1996**, *8*, 882–889.
(54) Hirai, T.; Sato, M.; Kido, M.; Nagae, Y.; Kaetsu, K.; Kiyoshima, Y.; Fujii, S.; Ohishi, T.; White, K. L.; Higaki, Y.; et al. X-ray absorption fine structure study on the role of solvent on polymerization of 3-hexylthiophene with solid FeCl 3 particles. *J. Polym. Sci. Part A Polym. Chem.* **2015**, *53*, 2075–2078.
(55) Sanford, M. S.; Love, J. A.; Grubbs, R. H. Mechanism and Activity of Ruthenium Olefin Metathesis Catalysts. *J. Am. Chem. Soc.* **2001**, *123*, 6543–6554.
(56) Chatterjee, A. K.; Choi, T.-L.; Sanders, D. P.; Grubbs, R. H. A general model for selectivity in olefin cross metathesis. *J. Am. Chem. Soc.* **2003**, *125*, 11360–11370.
(57) Wang, F.; Swager, T. M. Diverse chemiresistors based upon covalently modified multiwalled carbon nanotubes. *J. Am. Chem. Soc.* **2011**, *133*, 11181–11193.
(58) Liu, J.; Loewe, R. S.; McCullough, R. D. . Employing MALDI-MS on Poly(alkylthiophenes): Analysis of Molecular Weights, Molecular Weight Distributions, End-Group Structures, and End-Group Modifications. **1999**.
(59) Martin, K.; Spickermann, J.; Rader, H. J.; Mullen, K. Why does matrix-assisted laser desorption/ionization time-of-flight mass spectrometry give incorrect results for broad polymer distributions? *Rapid Commun. Mass Spectrom.* **1996**, *10*, 1471–1474.

2.7 Appendix

Chapter 2: Chemiresistor Devices for Chemical Warfare Agent Detection Based on Polymer Wrapped Single-Walled Carbon Nanotubes

Figure A.2.1 Gel Permeation Chromatogram (GPC) of **P1-P3** (THF fractions)

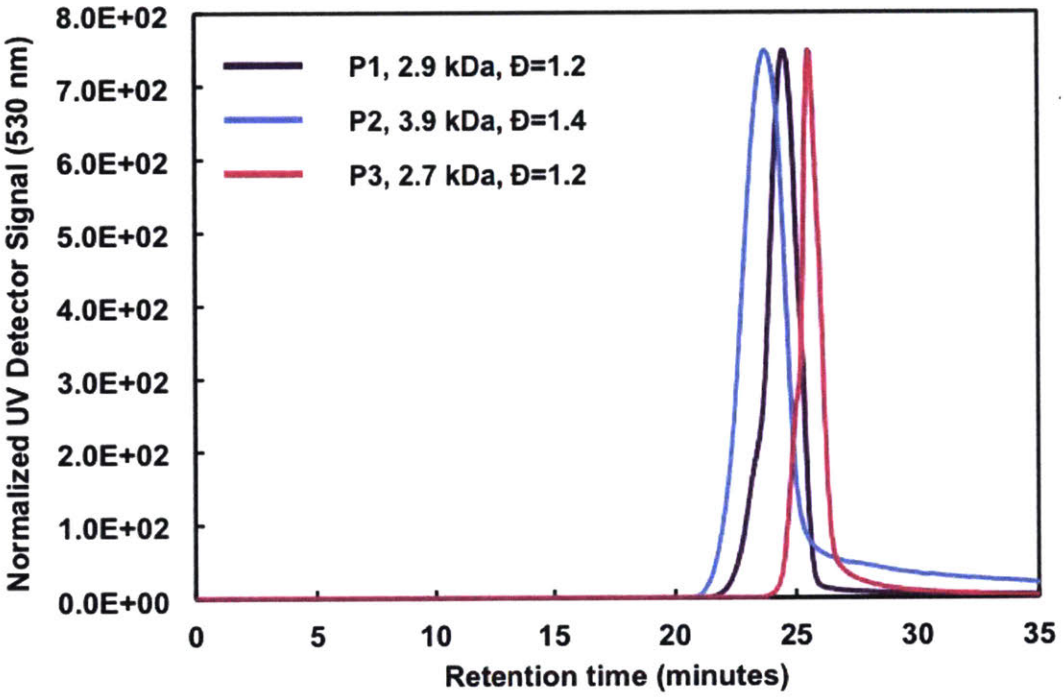

Figure A.2.2 MALDI-TOF MS of Compound **P1**- poly(octenylEDOT), high molecular weight, sparingly soluble fraction

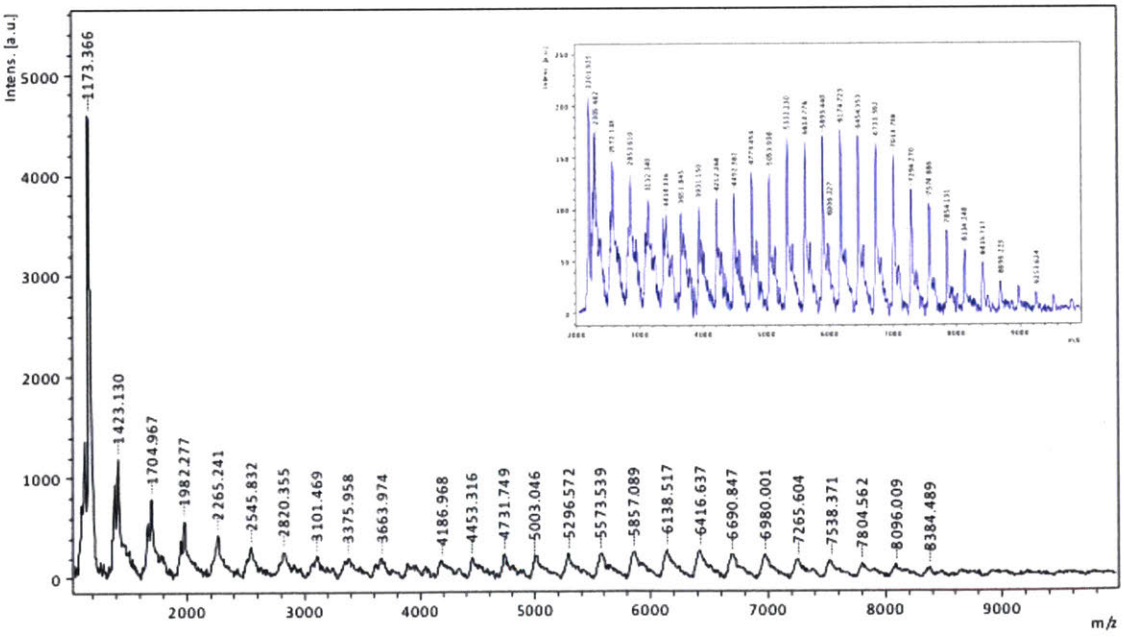

Table A.2.3 Molecular Weight Analysis

Analytical Technique	P1 MW (repeat units)	P2 MW (repeat units)	P3 MW (repeat units)
GPC	2,900 g/mol Đ=1.2 (10)	3,900 g/mol Đ=1.2 (8)	2,700 g/mol Đ=1.2 (9)
^{1}H NMR (end group analysis)	5,800 g/mol (20)	6,600 g/mol (13)	9,300 g/mol (33)
MALDI-TOF MS	2,245 g/mol (8)	1322 g/mol (3)	3,395 g/mol (12)

Figure A.2.4 MALDI-TOF MS of Compound **P1**- poly(octenylEDOT)

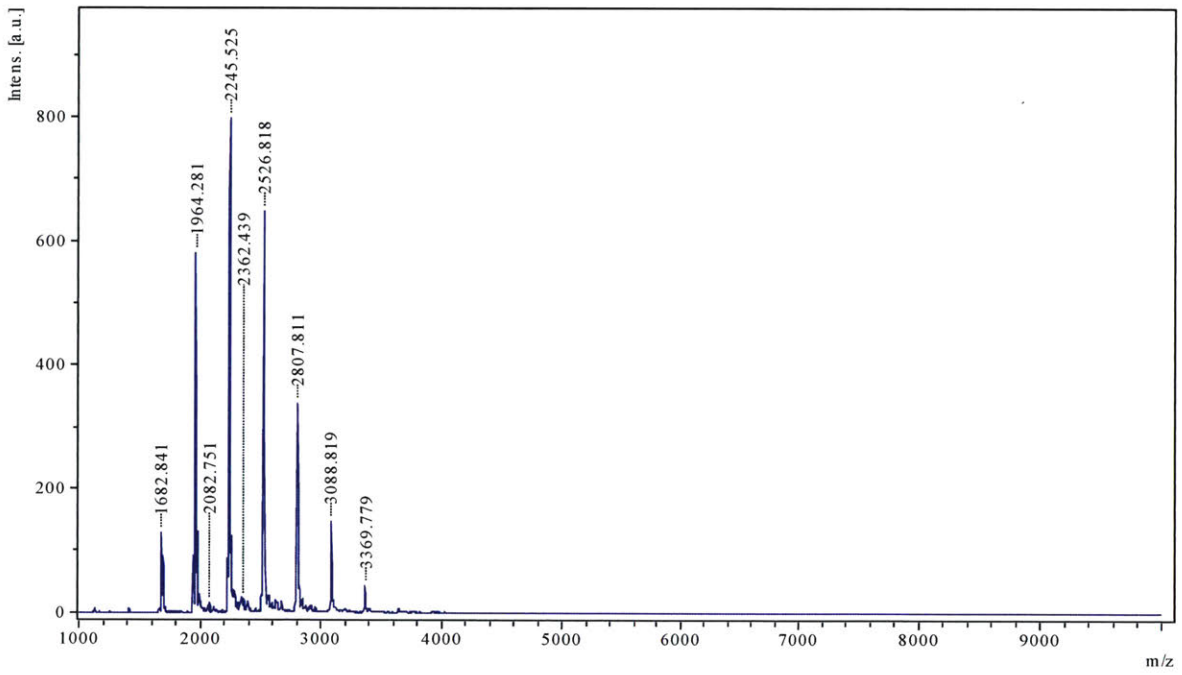

Figure A.2.5 MALDI-TOF MS Compound **P2**- Poly(octenyl-HFIP-PEDOT)

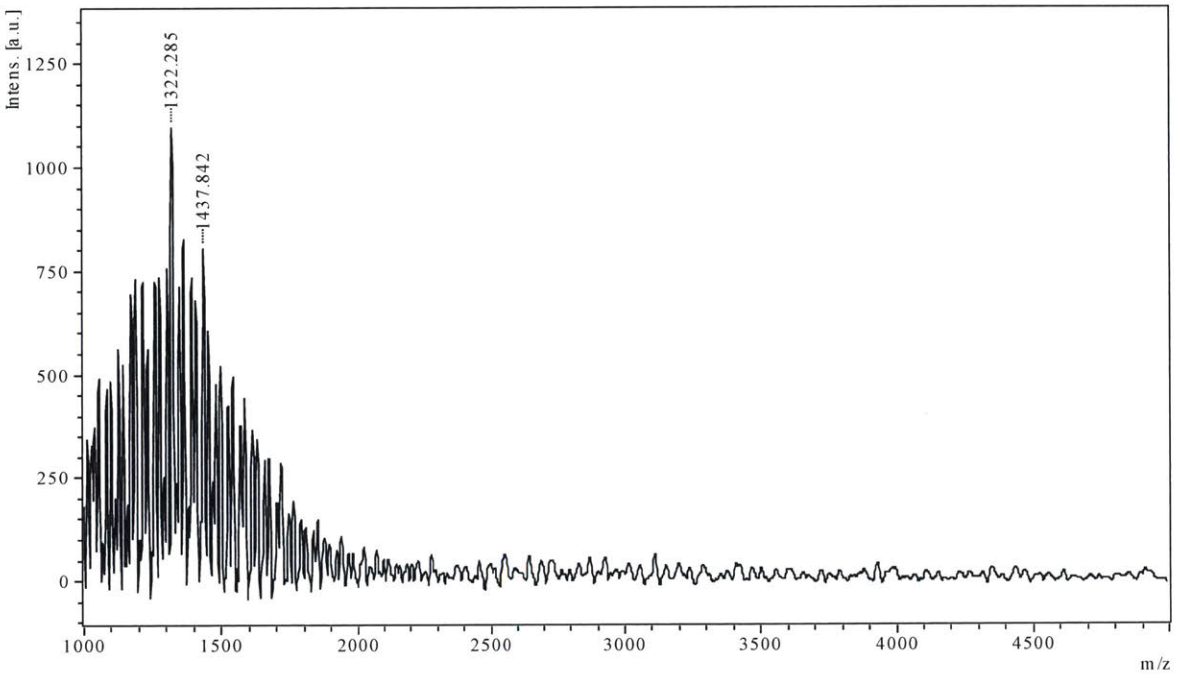

Figure A.2.6 MALDI-TOF MS Compound **P3**- poly(octylPEDOT)

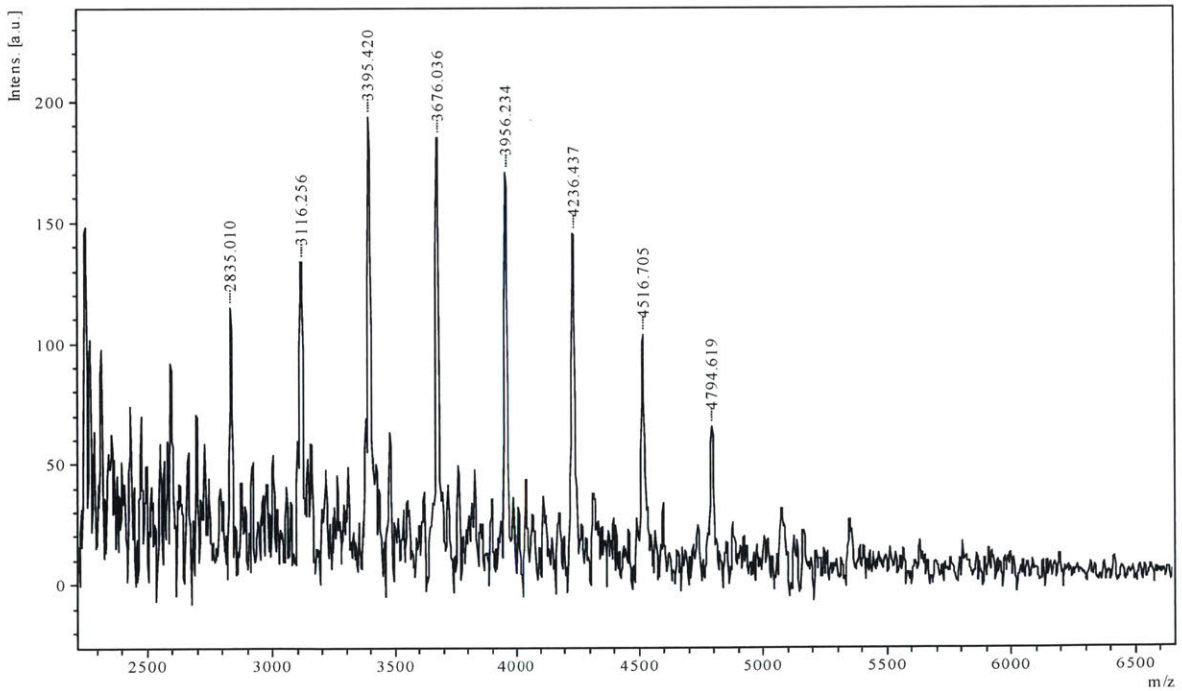

Figure A.2.7 ^{1}H NMR of Compound **P1**- poly(octenylEDOT)

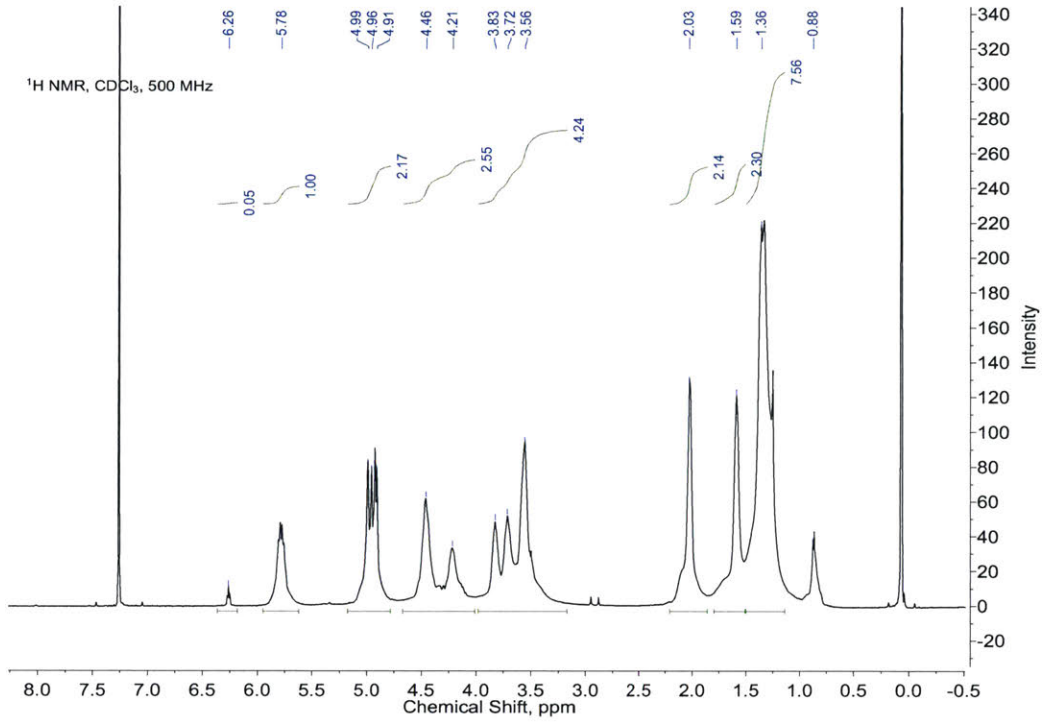

Figure A.2.8 ^{1}H NMR of Compound **P2**- Poly(octenyl-HFIP-PEDOT)

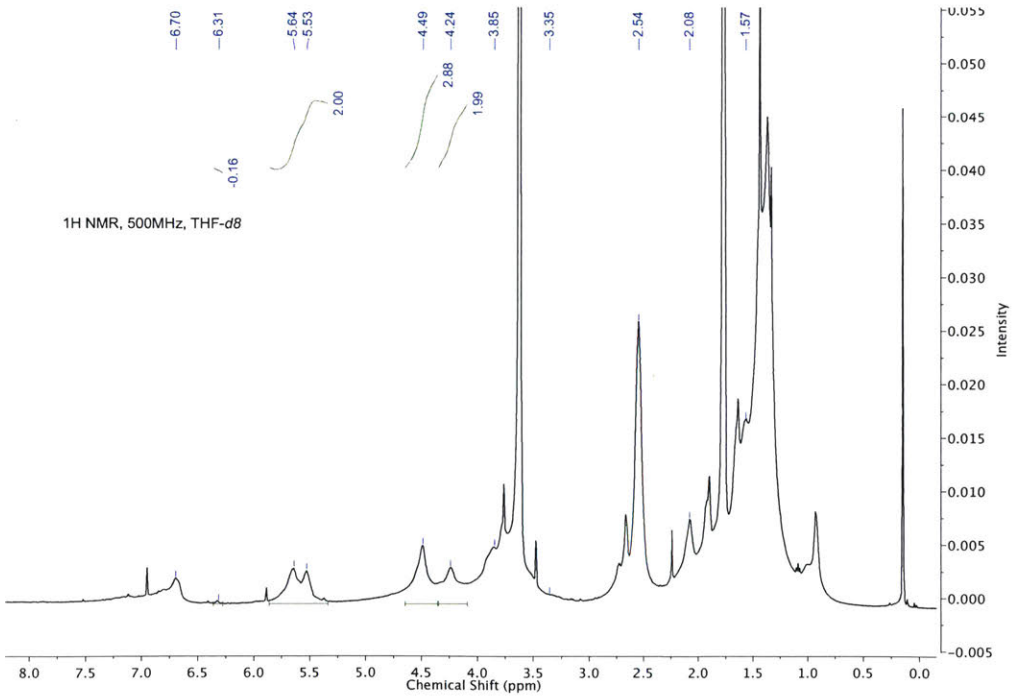

Figure A.2.9 ^{19}F NMR of Compound **P2**- Poly(octenyl-HFIP-PEDOT)

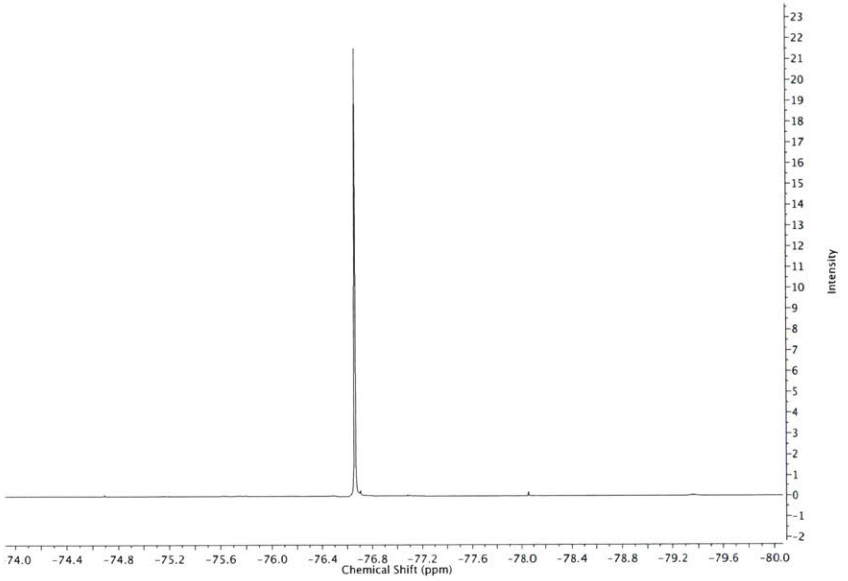

Figure A.2.10 Schematic/cartoon of sensing experimental set up

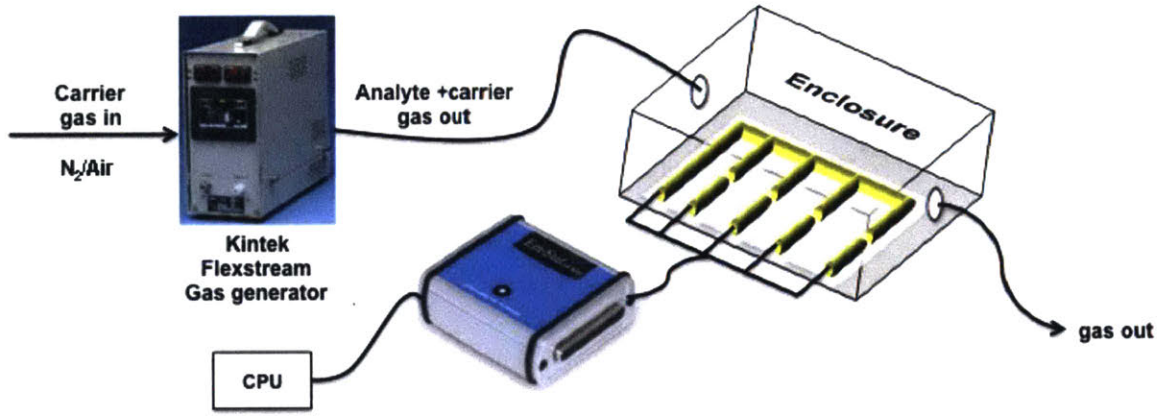

Figure A.2.11 Photograph of sensing experimental set up

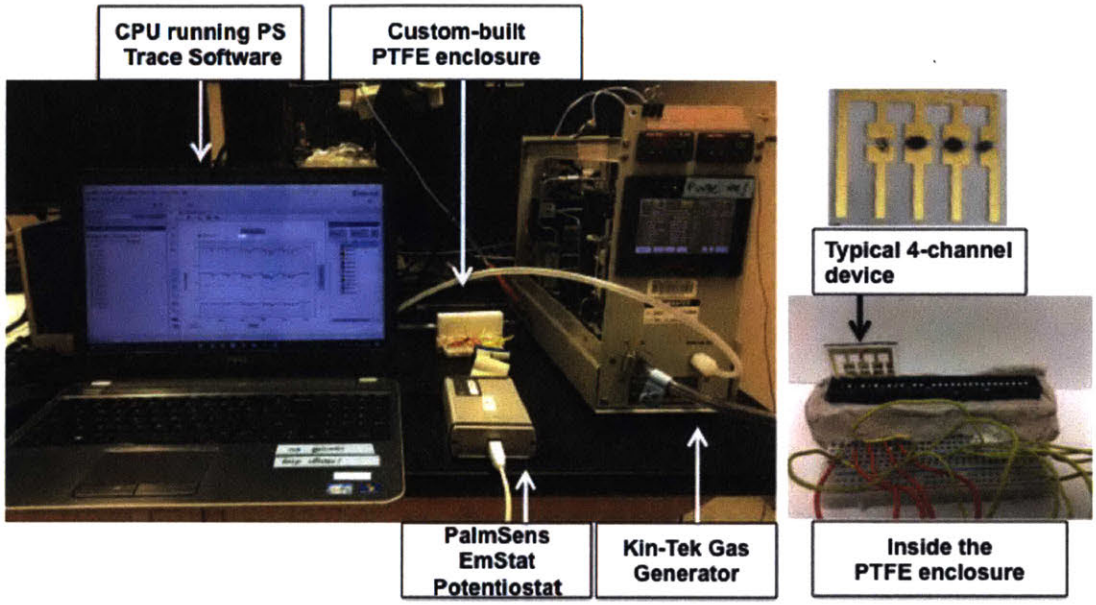

Figure A.2.12 Schematic/cartoon of sensing experimental set up for sensing in humidified carrier gas (air)

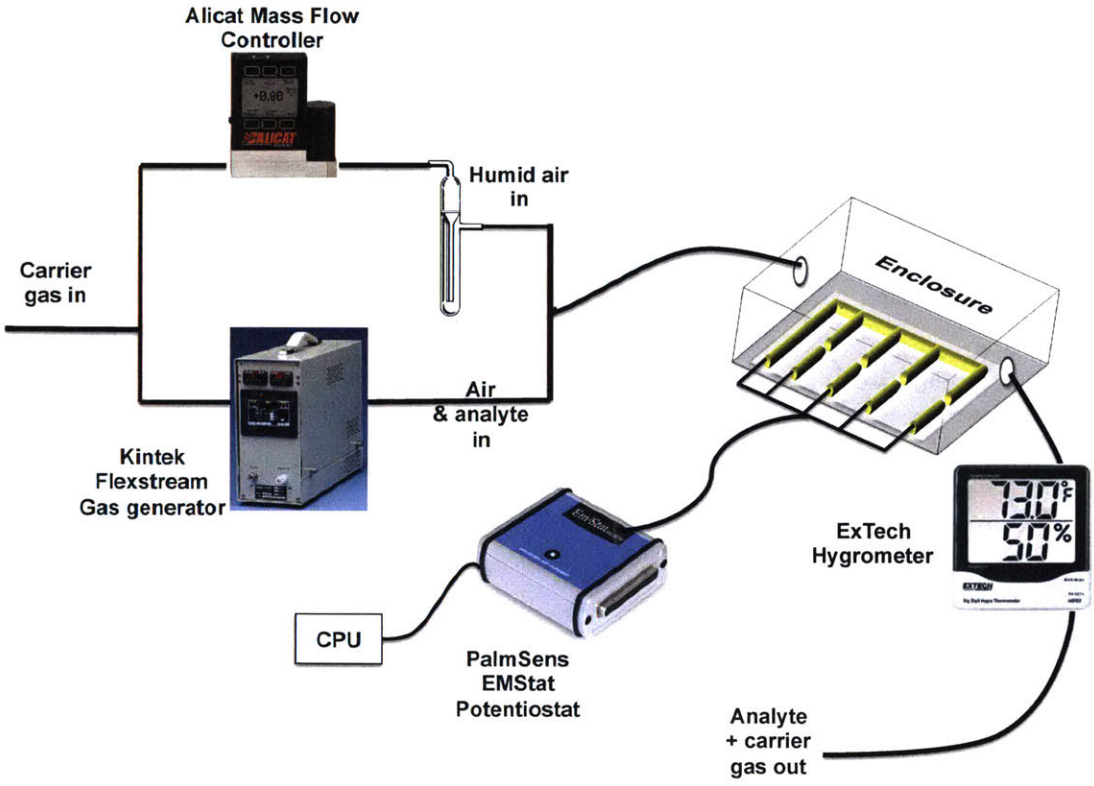

Figure A.2.13 Response of three devices with three ratios of P2/SWCNT to 2.0 ppm DMMP for a 60 second exposure with N_2 as a diluent gas.

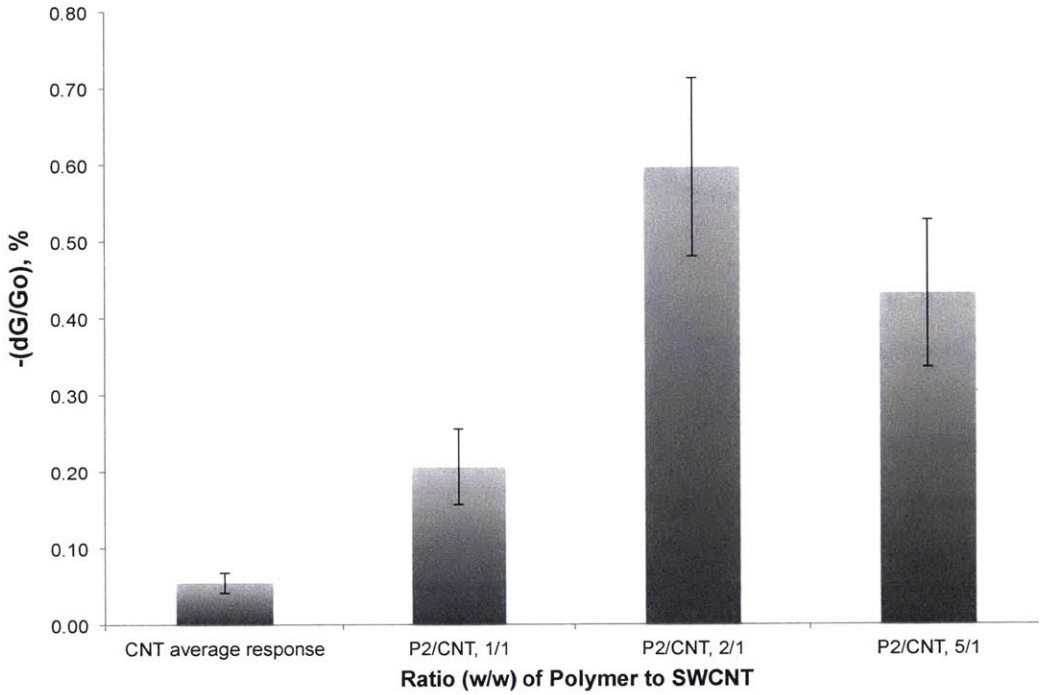

Figure A.2.14 Full Raman Spectra of pristine SWCNT, P1/SWCNT, P2/SWCNT, P3/SWCNT taken at an excitation wavelength of 633 nm

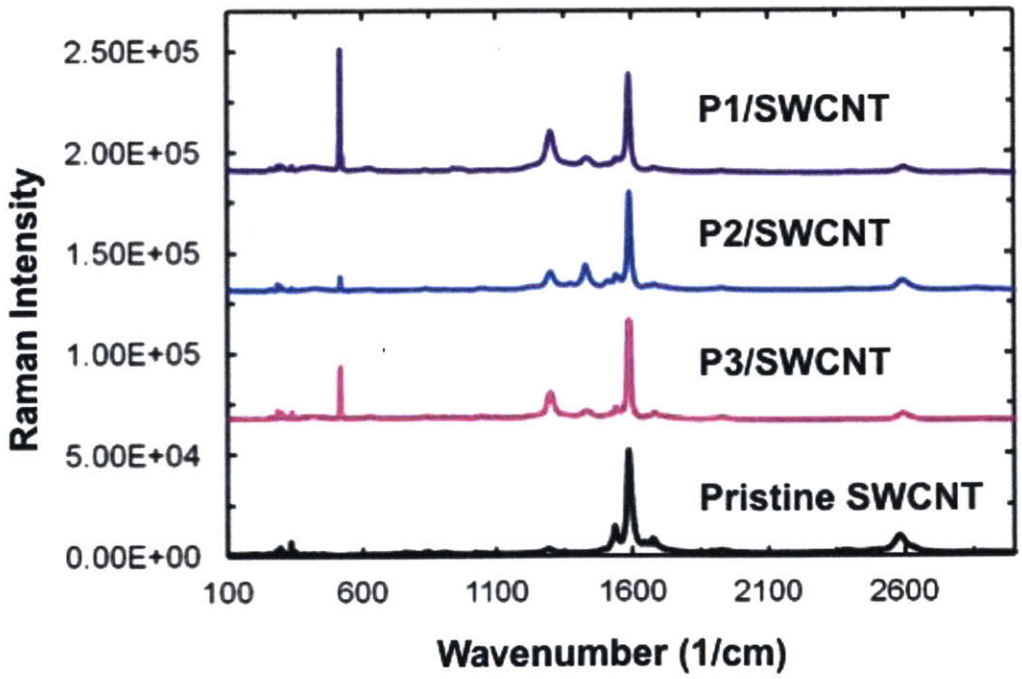

Figure A.2.15 Full Raman Spectra of **P1-P3** and Pristine SWCNTs taken at an excitation wavelength of 633 nm

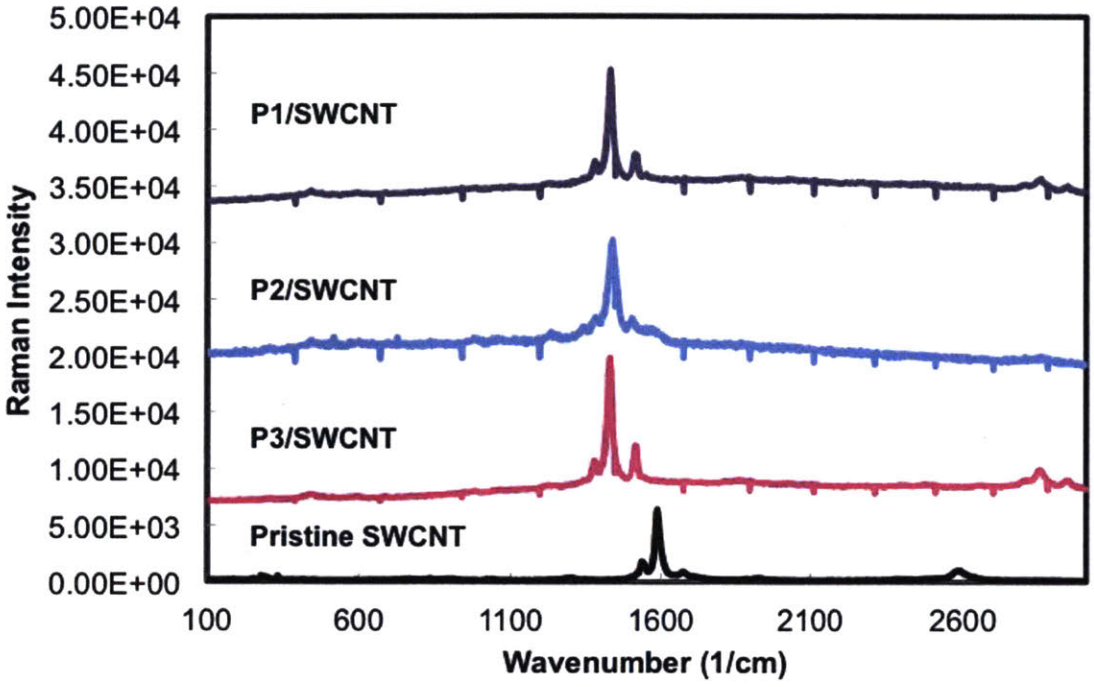

Figure A.2.16 Chemiresistive response saturation times for **P2**/SWCNT in N_2 (blue triangles) and air (24% RH) (red diamonds) to increasing concentrations of DMMP(The legend for air data here is a square not a diamond)

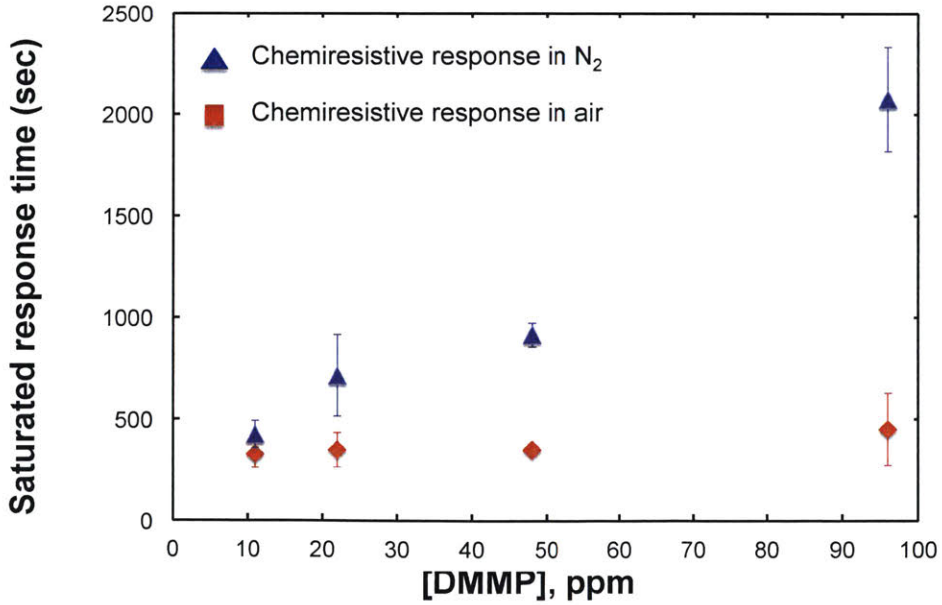

Figure A.2.17 Combined sensing traces of a pristine SWCNT device (black trace) and P2/SWCNT (blue trace) and P3/SWCNT devices (pink trace) to 60 s exposures followed by of VOCs at a flow rate of 200 mL/min. The traces are offset for clarity.

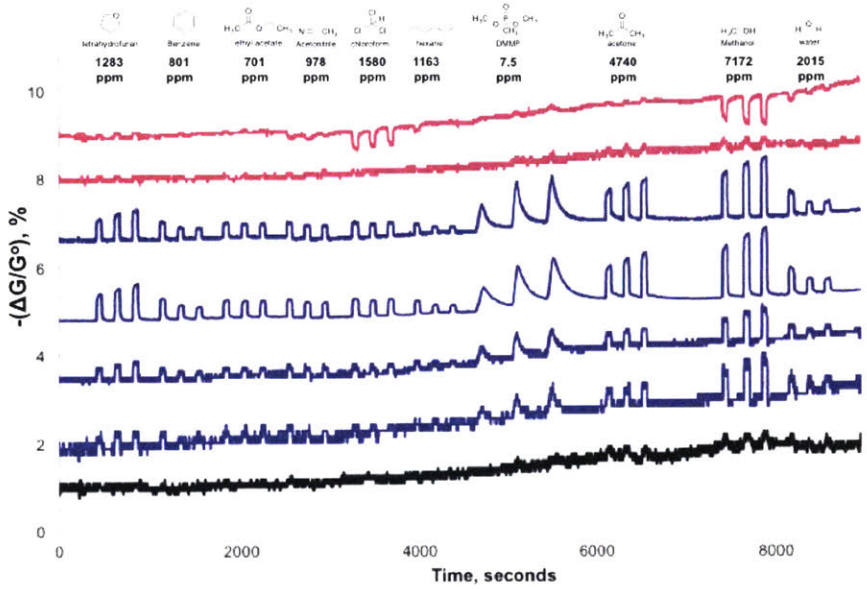

Figure A.2.18 Sensing trace of a pristine SWCNT device resulting from 60 s exposures followed by of VOCs at a flow rate of 200 mL/min.

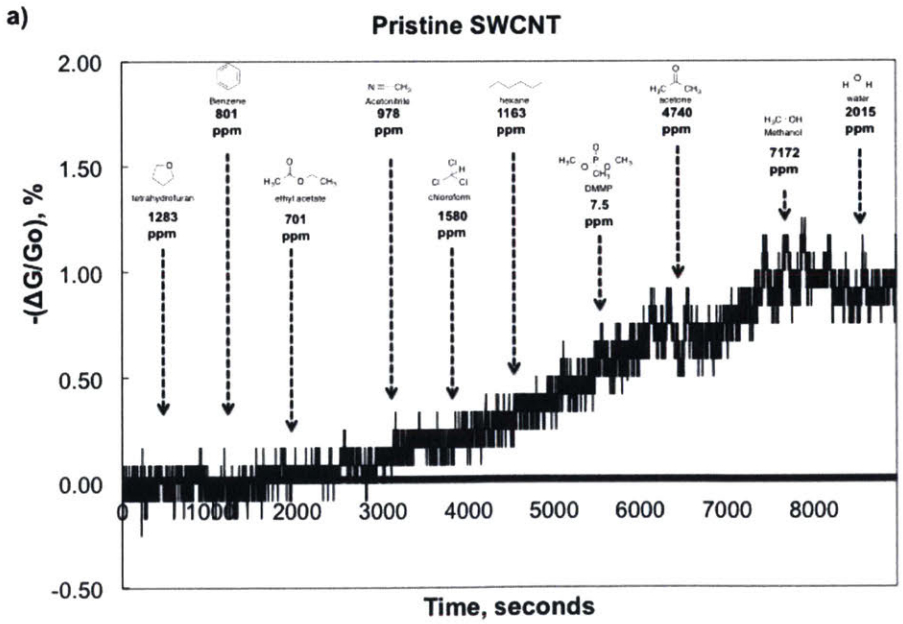

Figure A.2.19 Sensing trace of a P2/SWCNT device resulting from 60 s exposures followed by of VOCs at a flow rate of 200 mL/min.

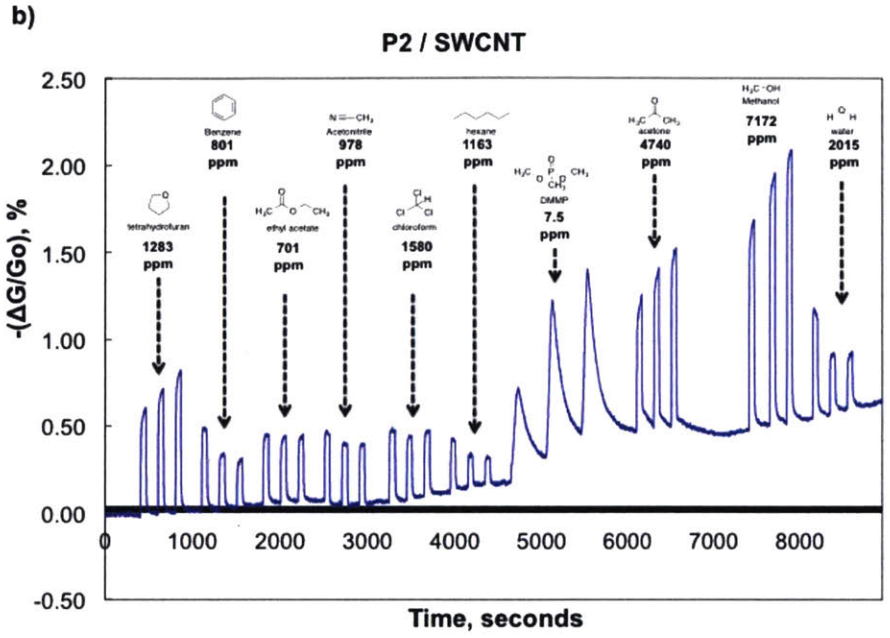

Figure A.2.20 Sensing trace of a P3 / SWCNT device resulting from 60 s exposures followed by of VOCs at a flow rate of 200 mL/min.

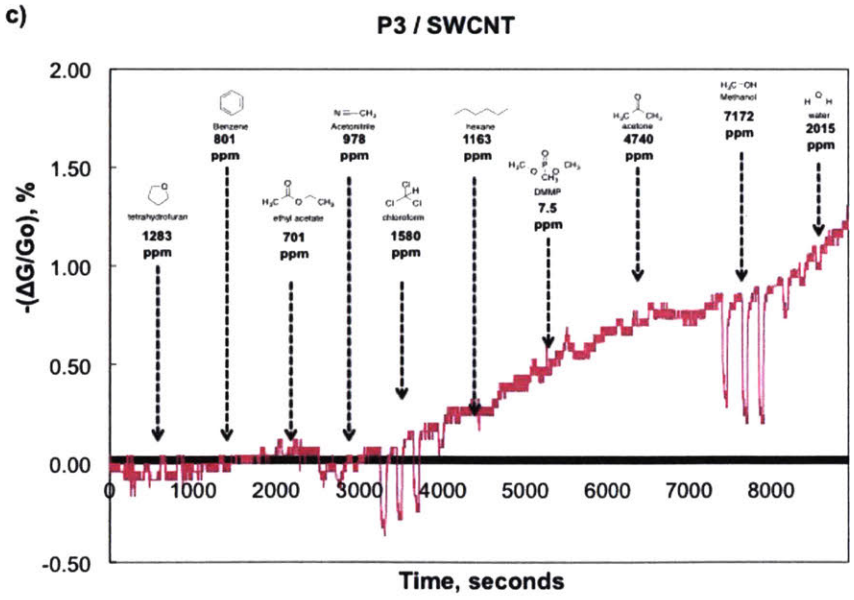

Figure A.2.21 Chemiresistive response versus **P2**/SWCNT device age, in days. Devices were exposed to 11 ppm DMMP diluted with N_2 until saturation was reached, then stored under ambient conditions.

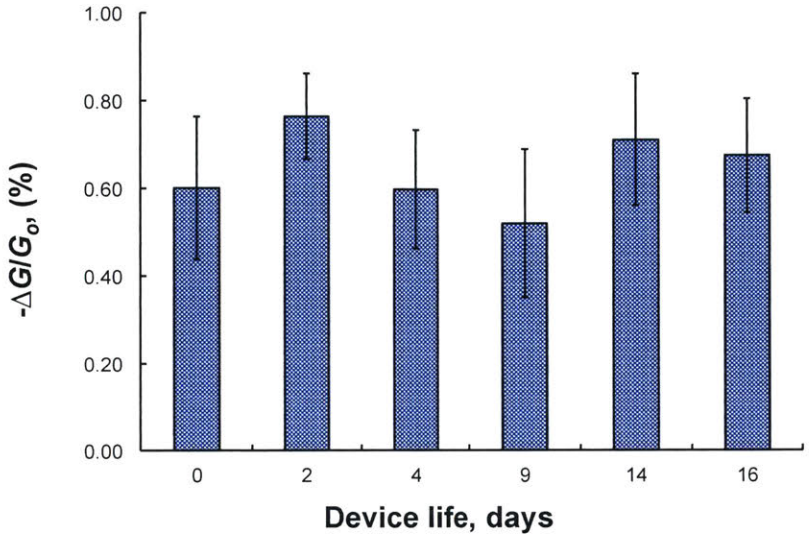

Figure A.2.22 Conductance traces of three **P2**/SWCNT chemiresistors to 11 ppm DMMP in humid air (50% RH)

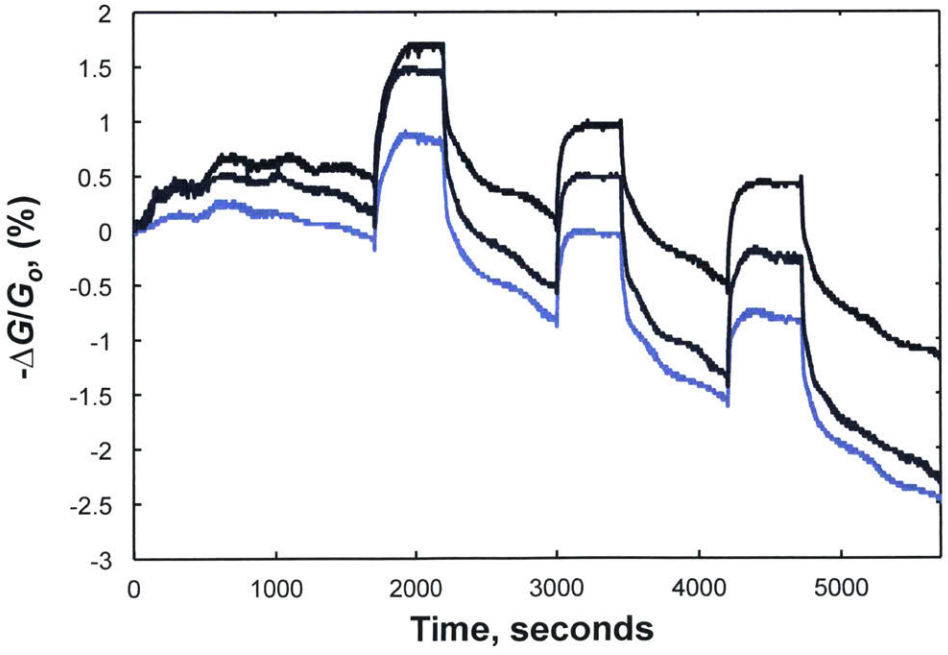

Figure A.2.23 ^{1}H NMR of Compound **P3-** poly(octylEDOT)

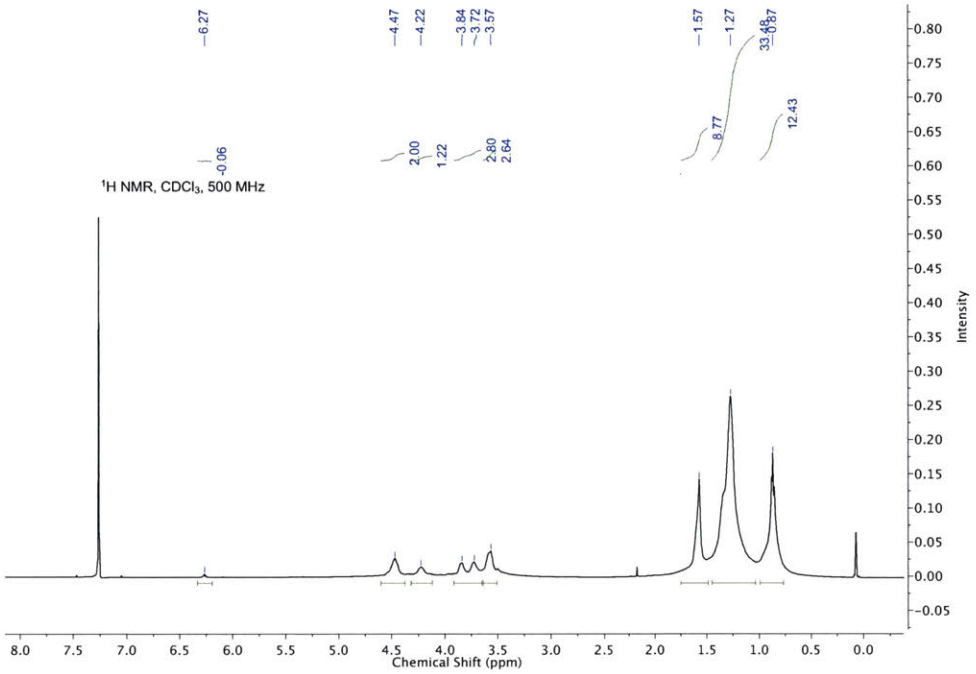

Figure A.2.24 ^{1}H NMR of Compound **3a -** 2,2-dimethyl-4-((octyloxy)methyl)-1,3-dioxolane

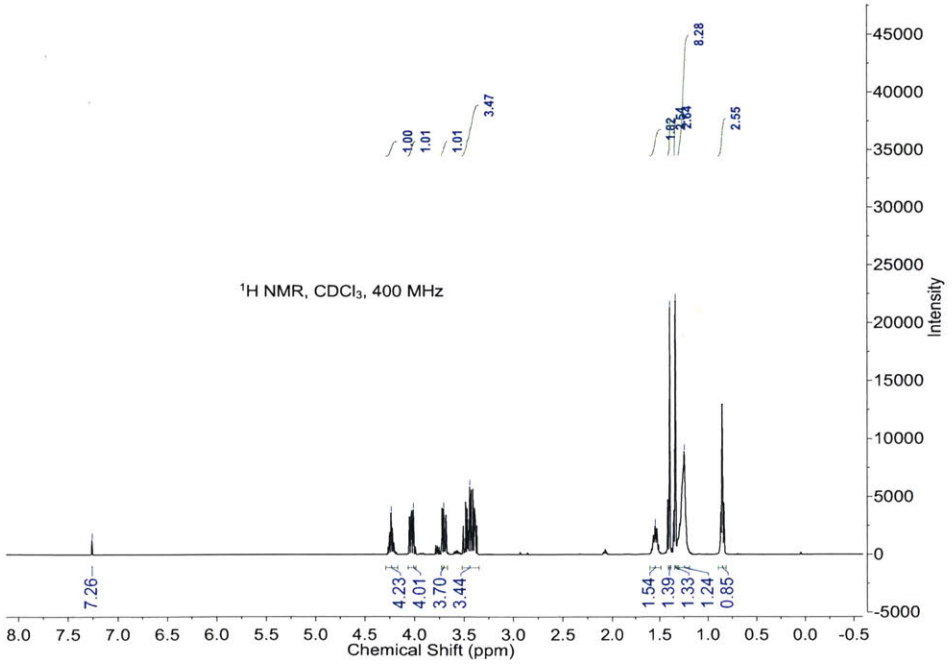

Figure A.2.25 ^{13}C NMR of Compound **3a** - 2,2-dimethyl-4-((octyloxy)methyl)-1,3-dioxolane

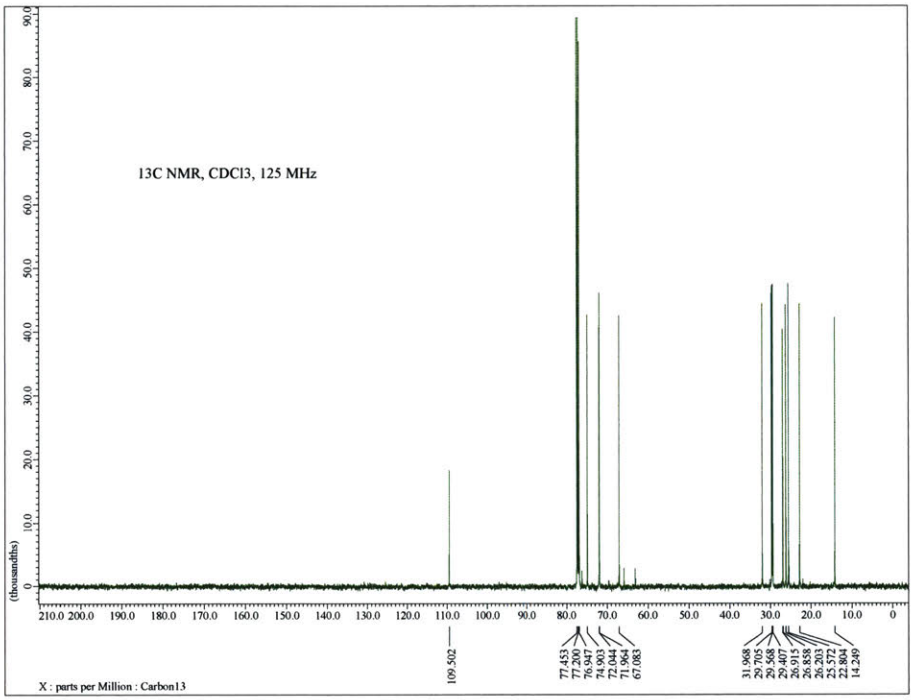

Figure A.2.26 ^{1}H NMR of Compound **3b** - 2,2-dimethyl-4-((oct-7-en-1-yloxy)methyl)-1,3-dioxolane

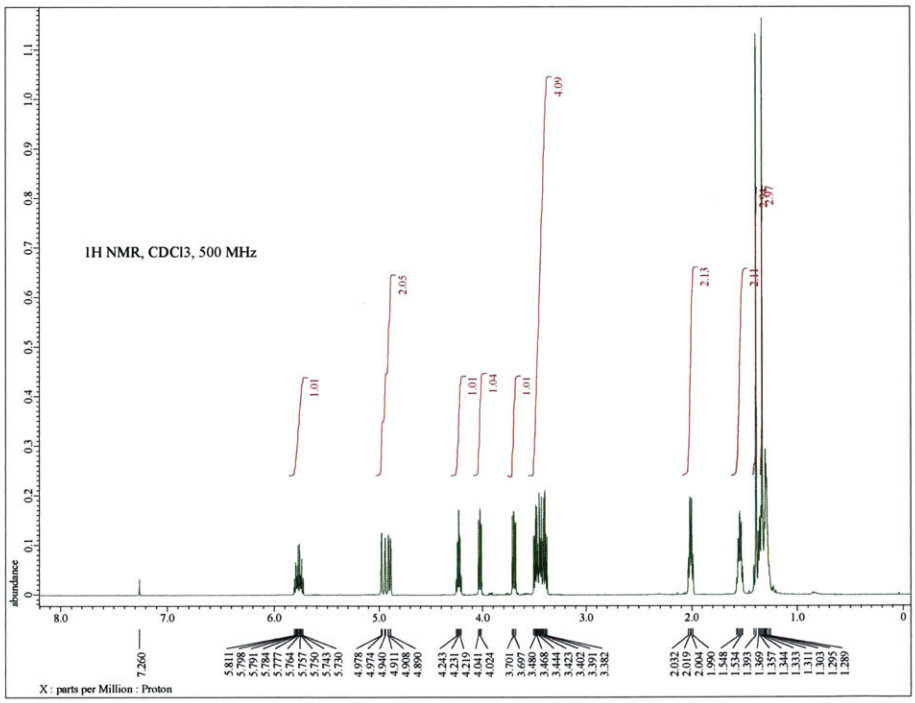

Figure A.2.27 ^{13}C NMR of Compound **3b** - 2,2-dimethyl-4-((oct-7-en-1-yloxy)methyl)-1,3-dioxolane

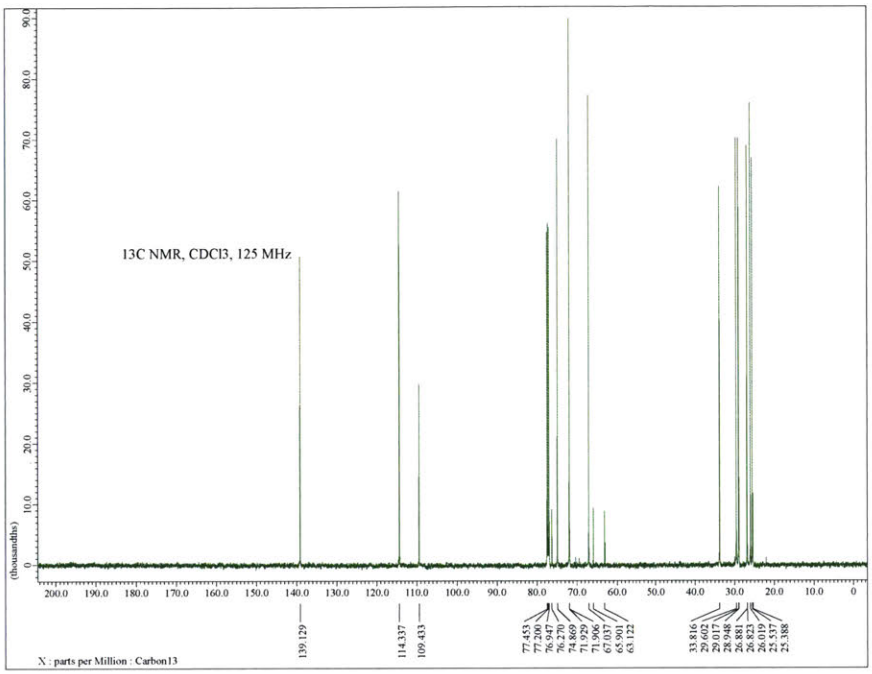

Figure A.2.28 ^{1}H NMR of Compound **4a** 3-(octyloxy)propane-1,2-diol

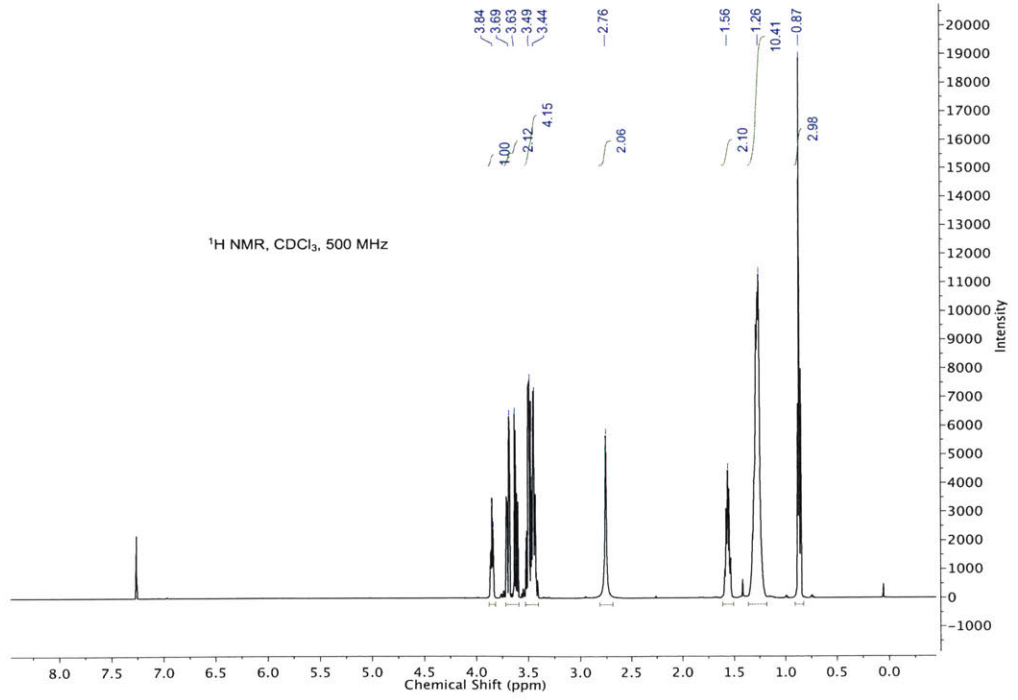

Figure A.2.29 ^{13}C NMR of Compound **4a** 3-(octyloxy)propane-1,2-diol

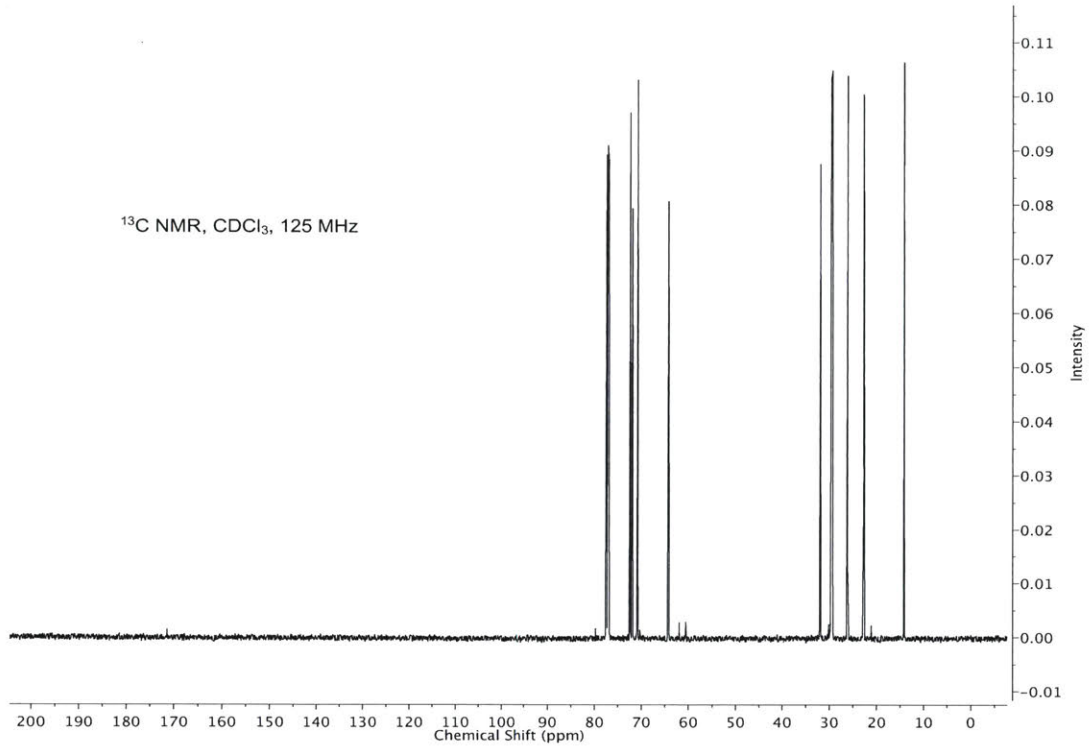

Figure A.2.30 ^{1}H NMR of Compound **4b** - 3-(oct-7-en-1-yloxy)propane-1,2-diol

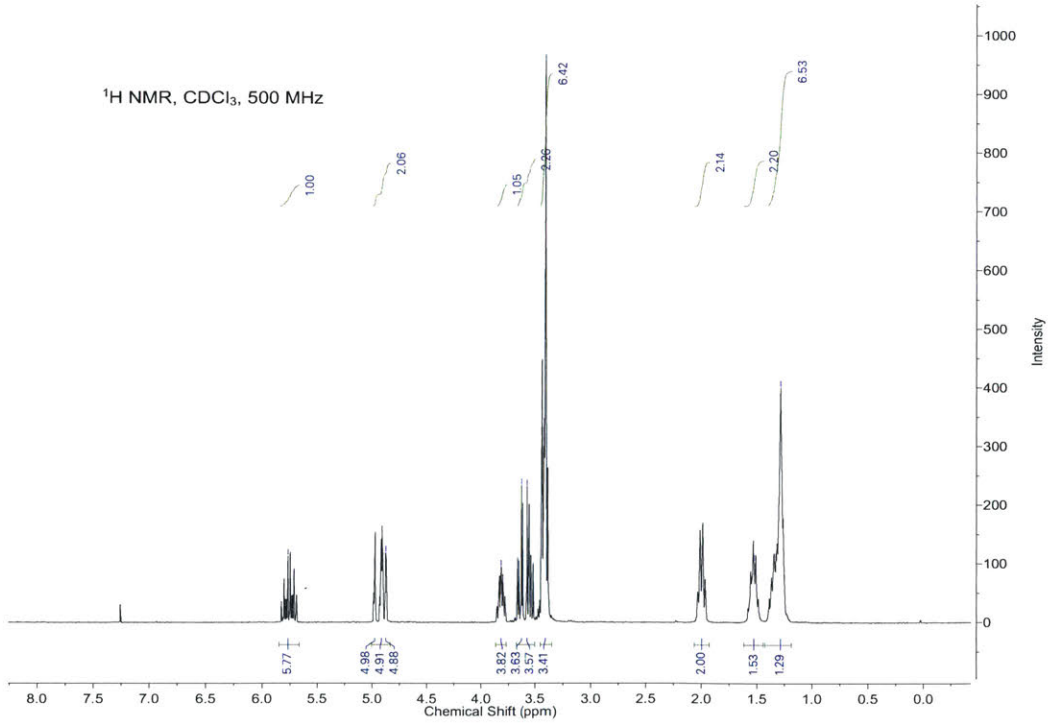

Figure A.2.31 ^{13}C NMR of Compound **4b** - 3-(oct-7-en-1-yloxy)propane-1,2-diol

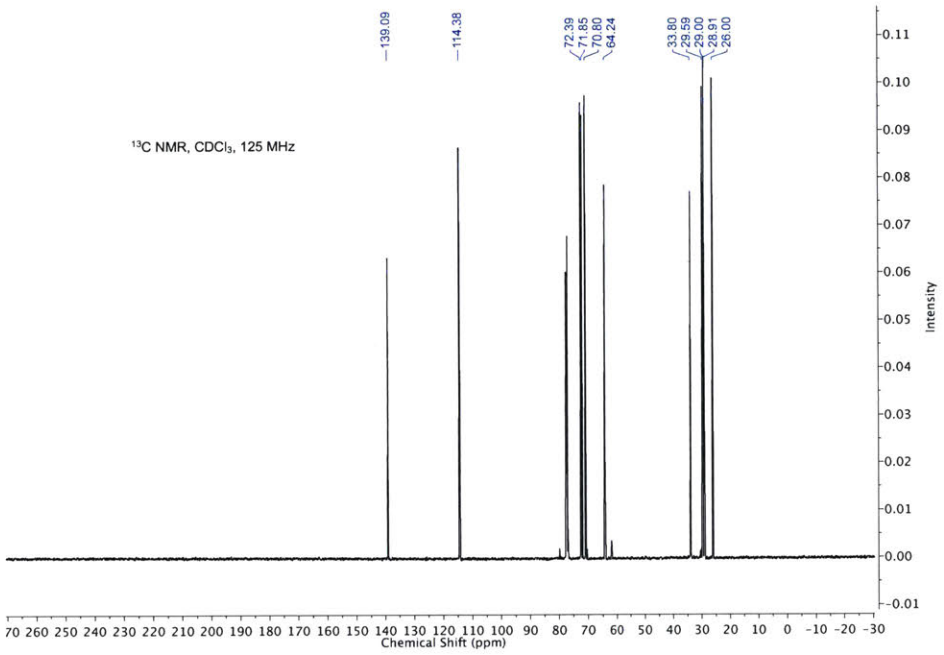

Figure A.2.32 ^{1}H NMR of Compound **6a** - 2-((octyloxy)methyl)-2,3-dihydrothieno[3,4-*b*][1,4]dioxine

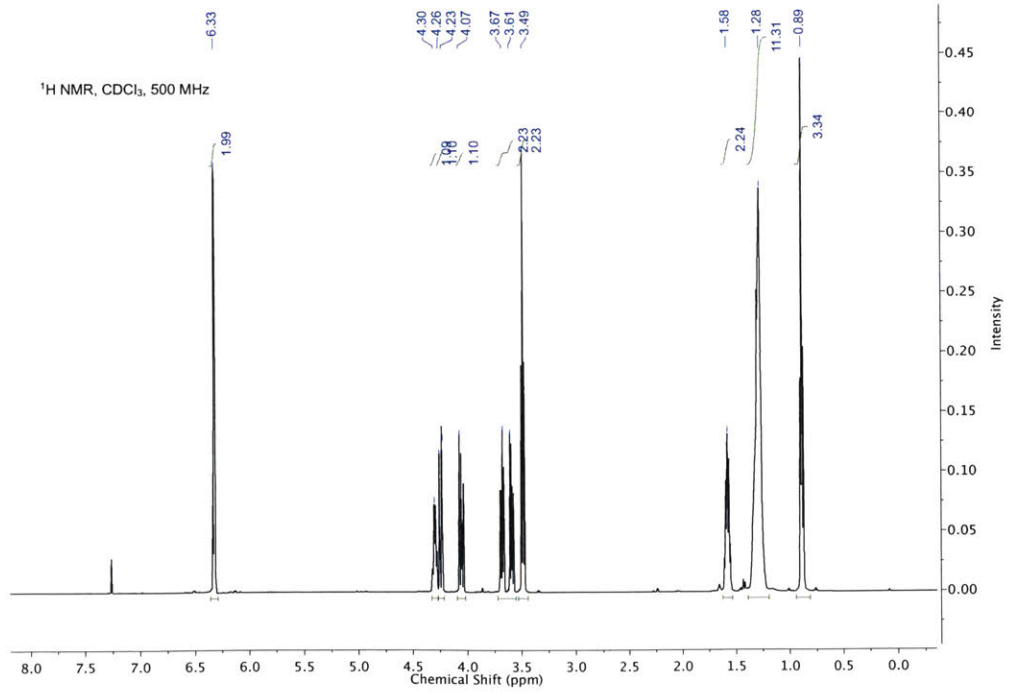

Figure A.2.33 ^{13}C NMR of Compound **6a** - 2-((octyloxy)methyl)-2,3-dihydrothieno[3,4-*b*][1,4]dioxine

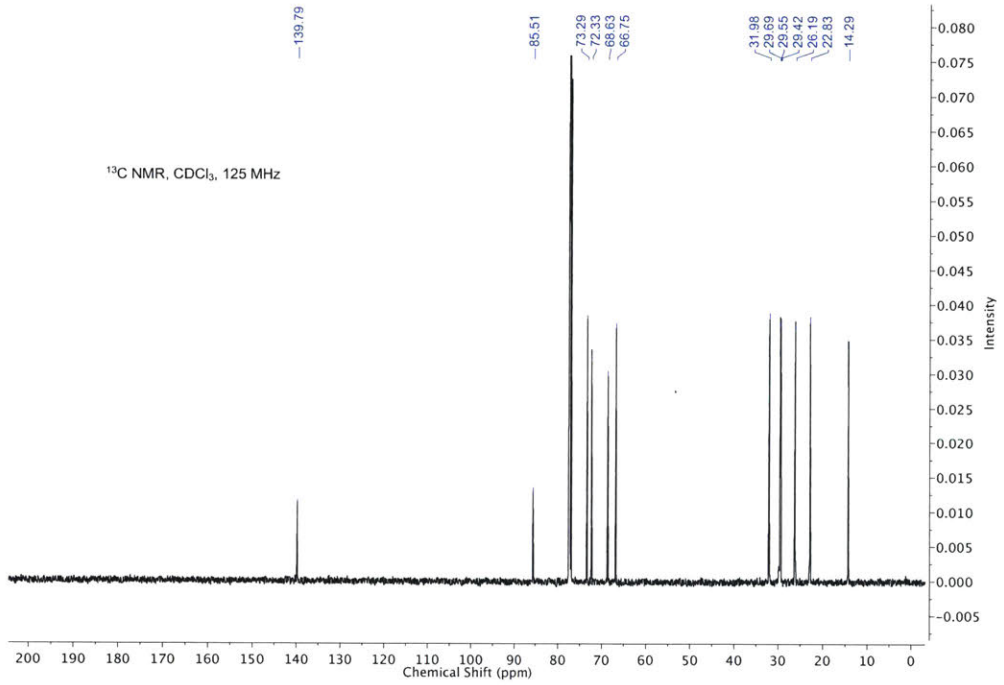

Figure A.2.34 ^{1}H NMR of Compound **6b** - 2-((oct-7-en-1-yloxy)methyl)-2,3-dihydrothieno[3,4-*b*][1,4]dioxine

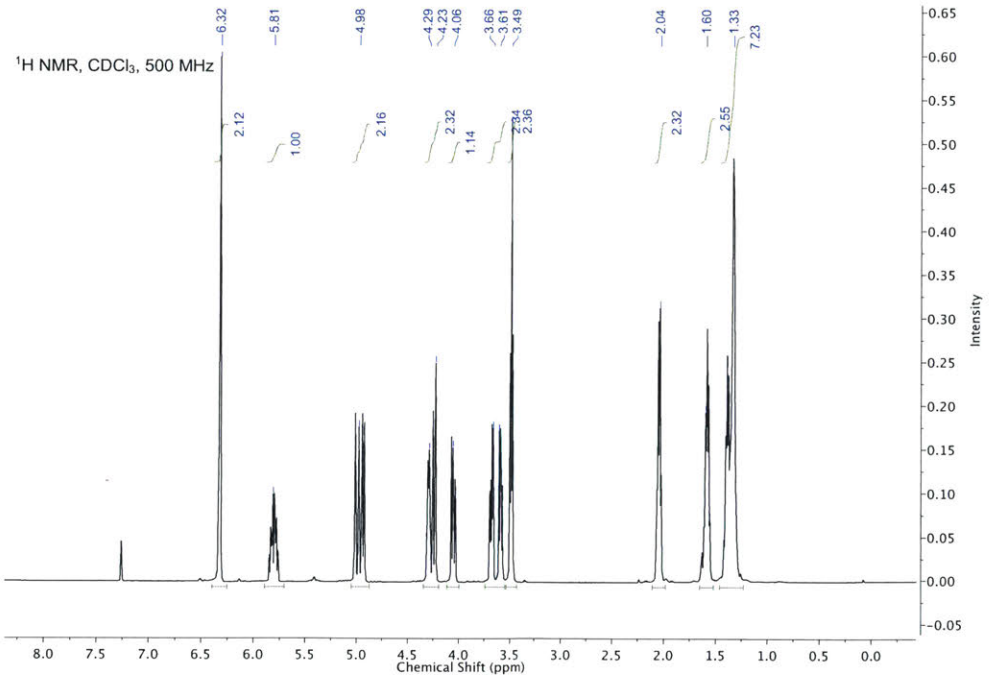

Figure A.2.35 ^{13}C NMR of Compound **6b** - 2-((oct-7-en-1-yloxy)methyl)-2,3-dihydrothieno[3,4-*b*][1,4]dioxine

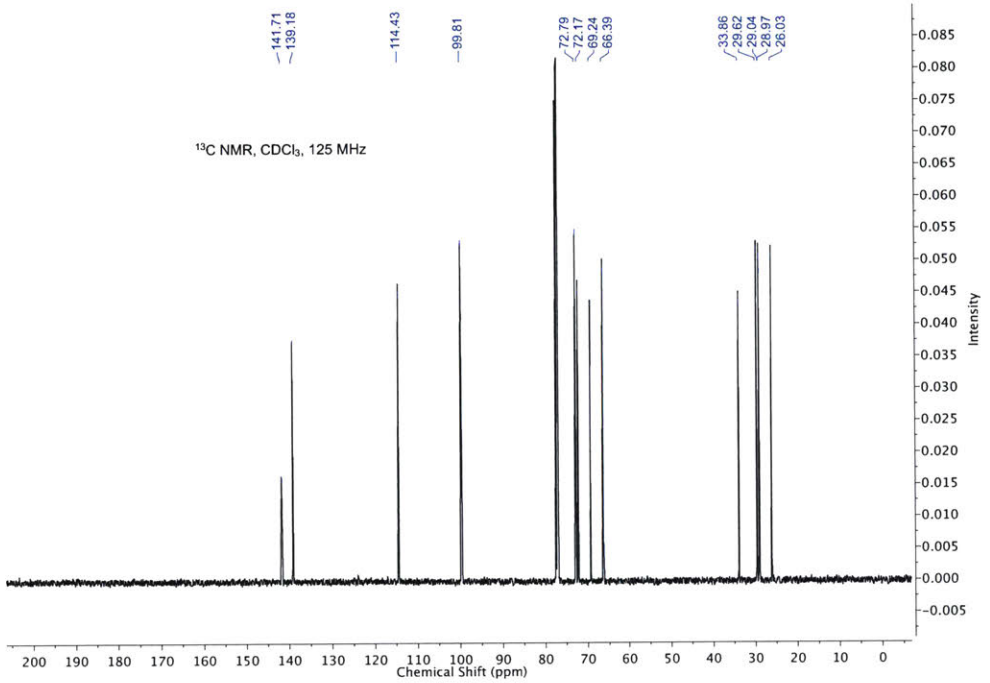

Figure A.2.36 ^{1}H of Compound **7a** - 5,7-dibromo-2-((octyloxy)methyl)-2,3-dihydrothieno[3,4-*b*][1,4]dioxine

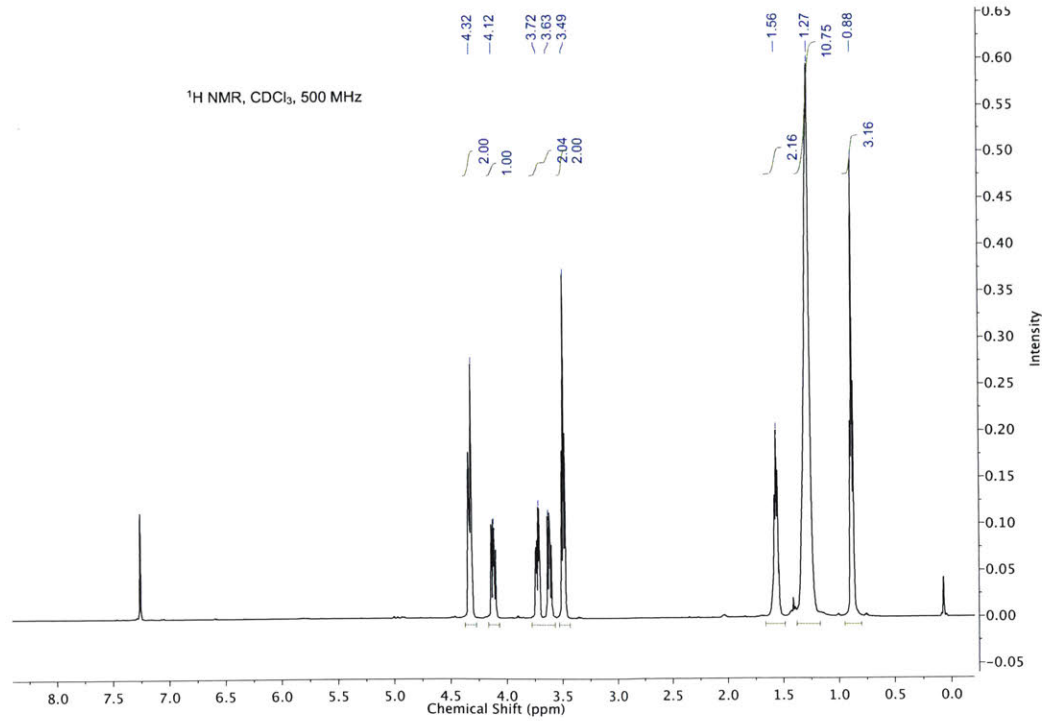

Figure A.2.37 ^{13}C NMR of Compound **7a** - 5,7-dibromo-2-((octyloxy)methyl)-2,3-dihydrothieno[3,4-*b*][1,4]dioxine

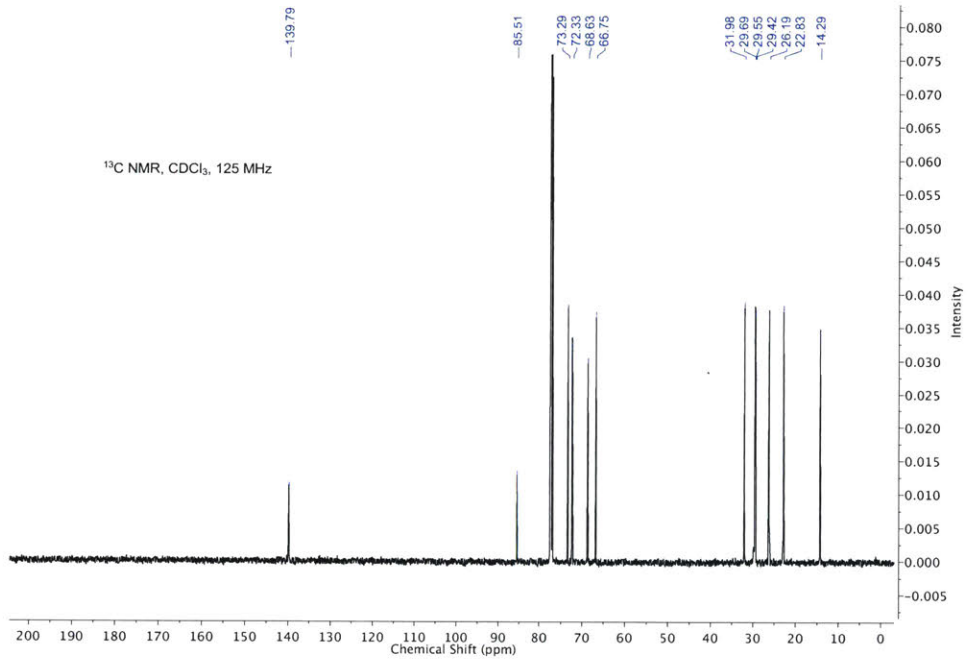

Figure A.2.38 ^{1}H NMR of Compound **7b** - 5,7-dibromo-2-((oct-7-en-1-yloxy)methyl)-2,3-dihydrothieno[3,4-*b*][1,4]dioxine

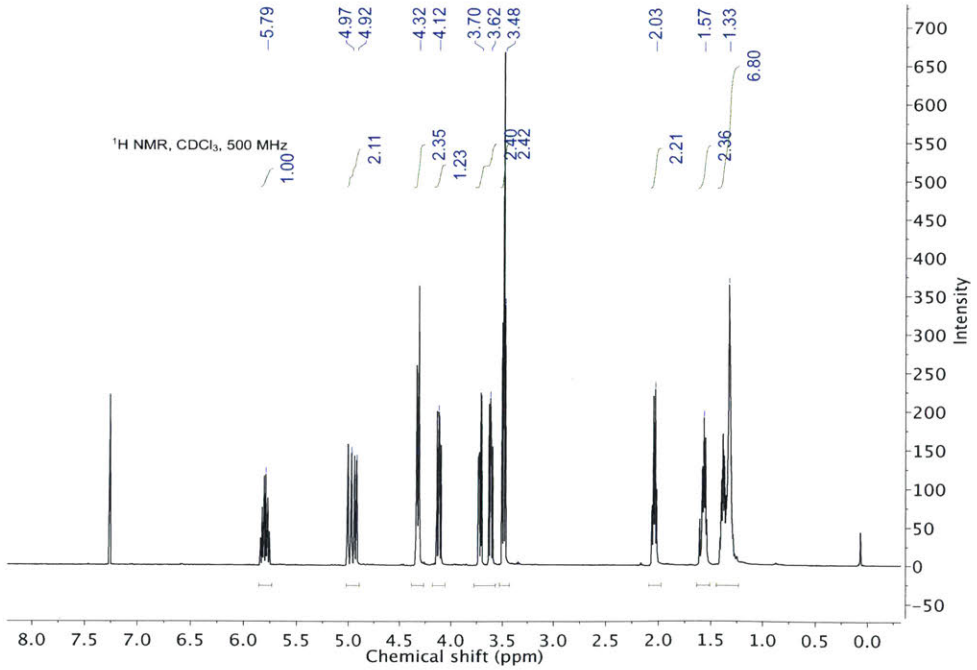

Figure A.2.39 ^{13}C NMR of Compound **7b** - 5,7-dibromo-2-((oct-7-en-1-yloxy)methyl)-2,3-dihydrothieno[3,4-*b*][1,4]dioxine

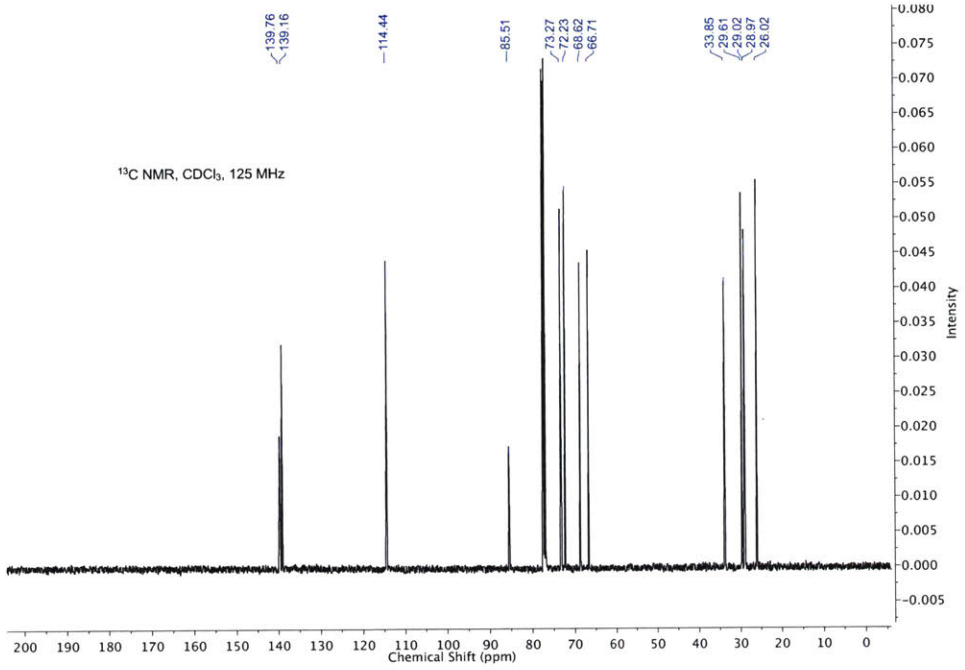

Figure A.2.40 FTIR-ATR of Compound **3a** - 2,2-dimethyl-4-((octyloxy)methyl)-1,3-dioxolane

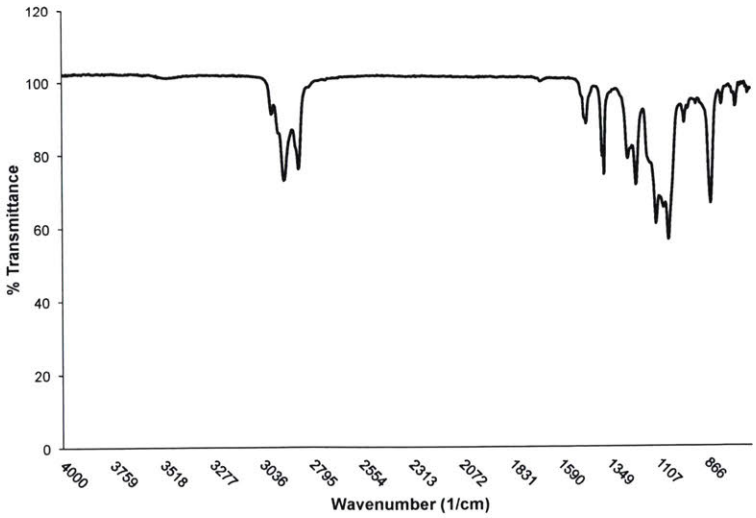

Figure A.2.41 FTIR-ATR of Compound **3b** - 2,2-dimethyl-4-((oct-7-en-1-yloxy)methyl)-1,3-dioxolane

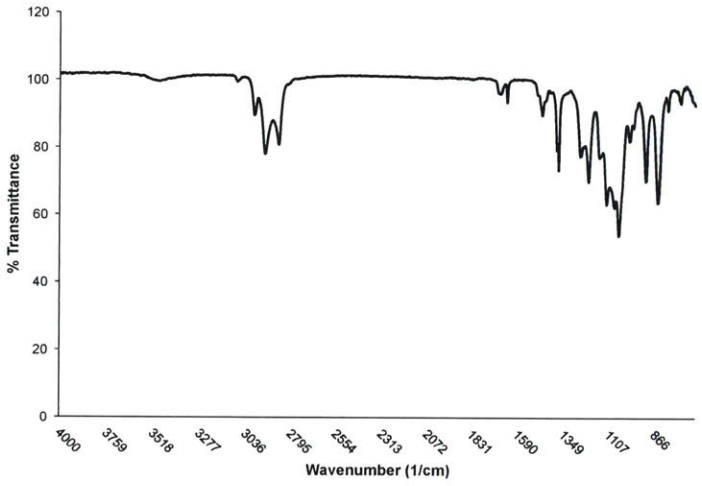

Figure A.2.42 FTIR-ATR of Compound **4a** 3-(octyloxy)propane-1,2-diol

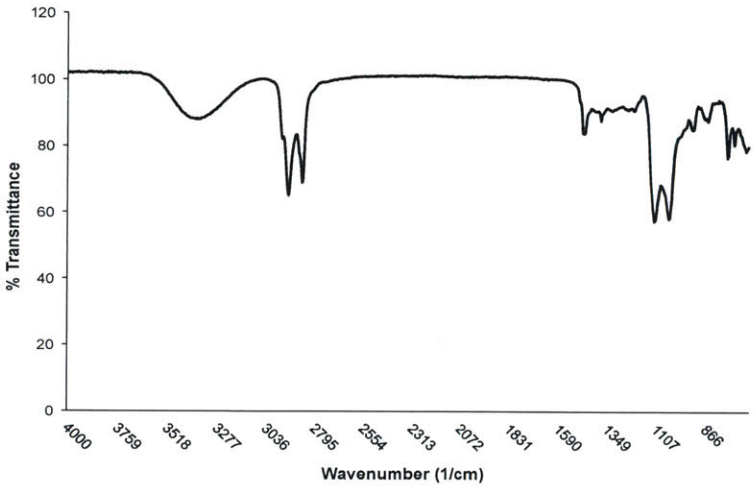

Figure A.2.43 FTIR-ATR of Compound **4b** - 3-(oct-7-en-1-yloxy)propane-1,2-diol

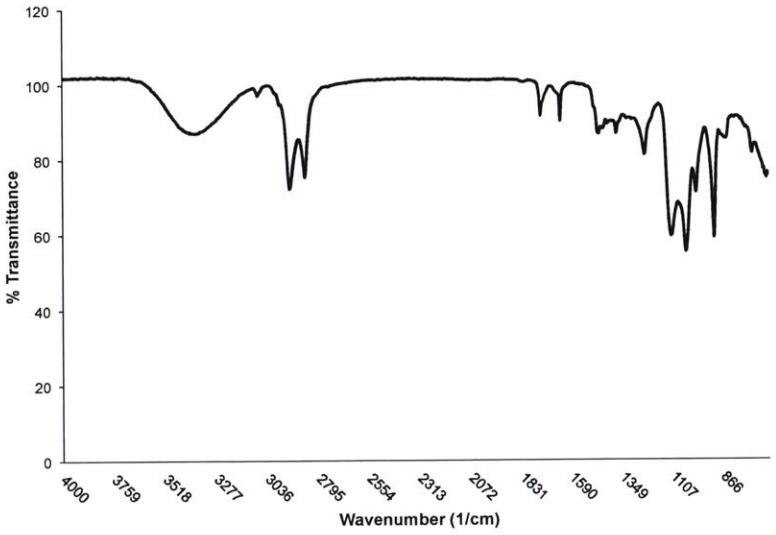

Figure A.2.44 FTIR-ATR of Compound **6a** - 2-((octyloxy)methyl)-2,3-dihydrothieno[3,4-*b*][1,4]dioxine

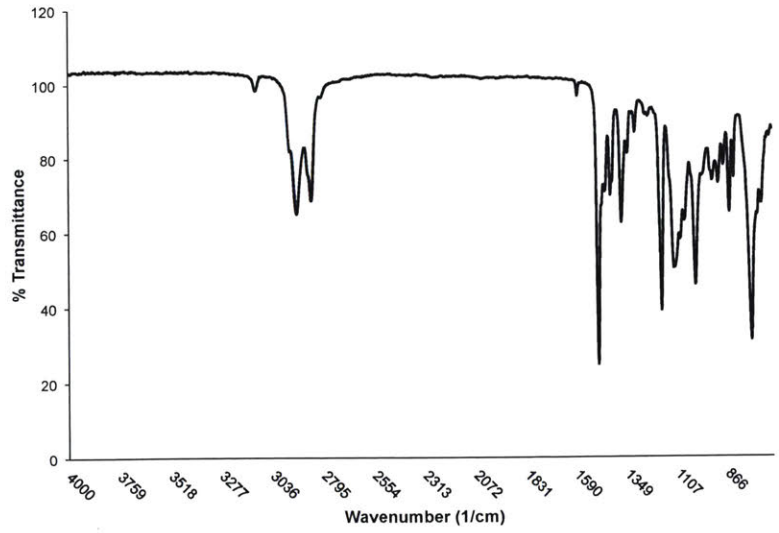

Figure A.2.45 FTIR-ATR of Compound **6b** - 2-((oct-7-en-1-yloxy)methyl)-2,3-dihydrothieno[3,4-*b*][1,4]dioxine

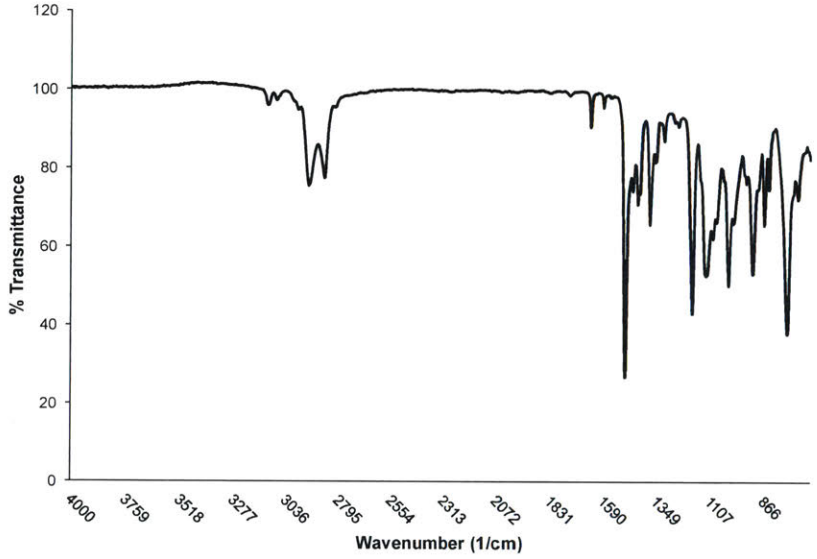

Figure A.2.46 FTIR-ATR of Compound **7a** - 5,7-dibromo-2-((octyloxy)methyl)-2,3-dihydrothieno[3,4-*b*][1,4]dioxine

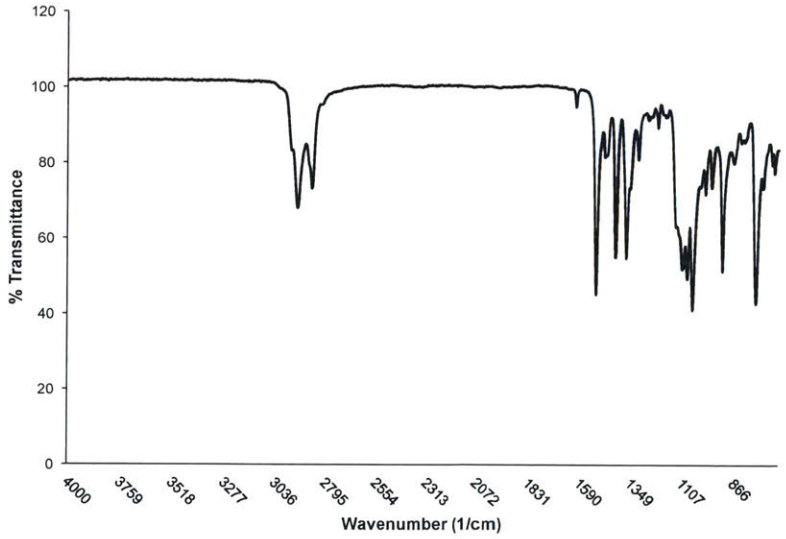

Figure A.2.47 FTIR-ATR of Compound **7b** - 5,7-dibromo-2-((oct-7-en-1-yloxy)methyl)-2,3-dihydrothieno[3,4-*b*][1,4]dioxine

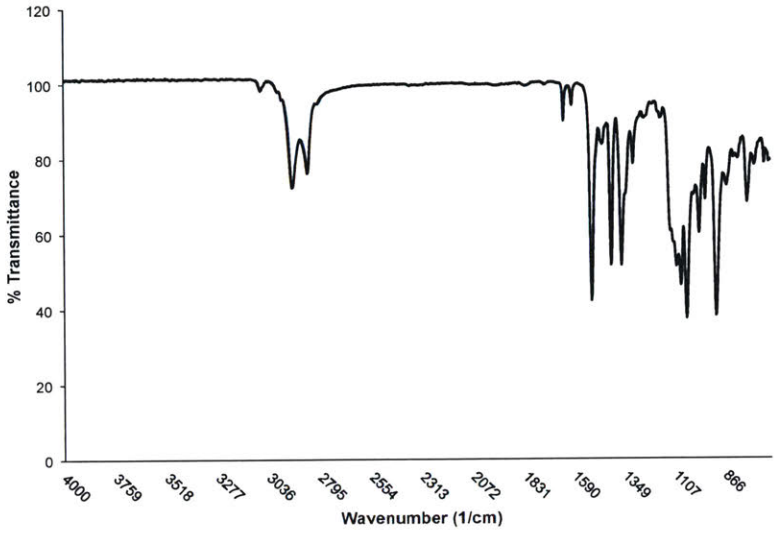

Figure A.2.48 FTIR-ATR of Compound **P1**- poly(octenylEDOT)

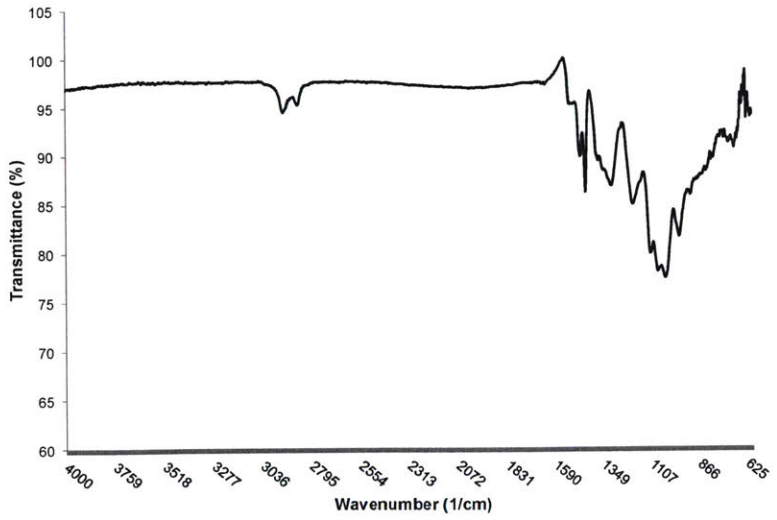

Figure A.2.49 FTIR-ATR of Compound **P2**- Poly(octenyl-HFIP-PEDOT)

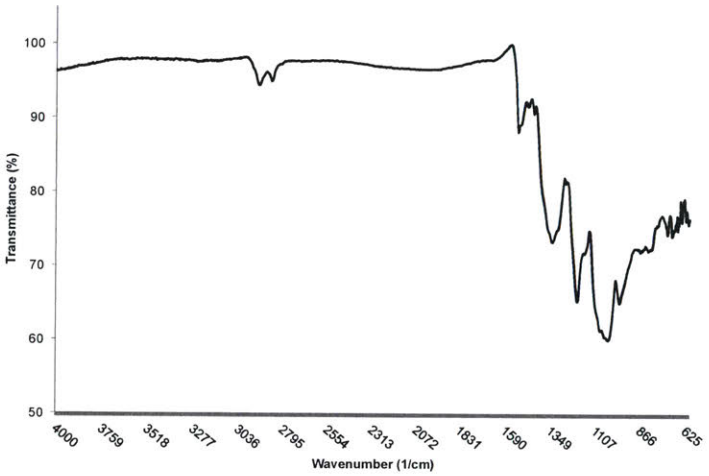

Figure A.2.50 FTIR-ATR of Compound **P3**- poly(octyl-PEDOT)

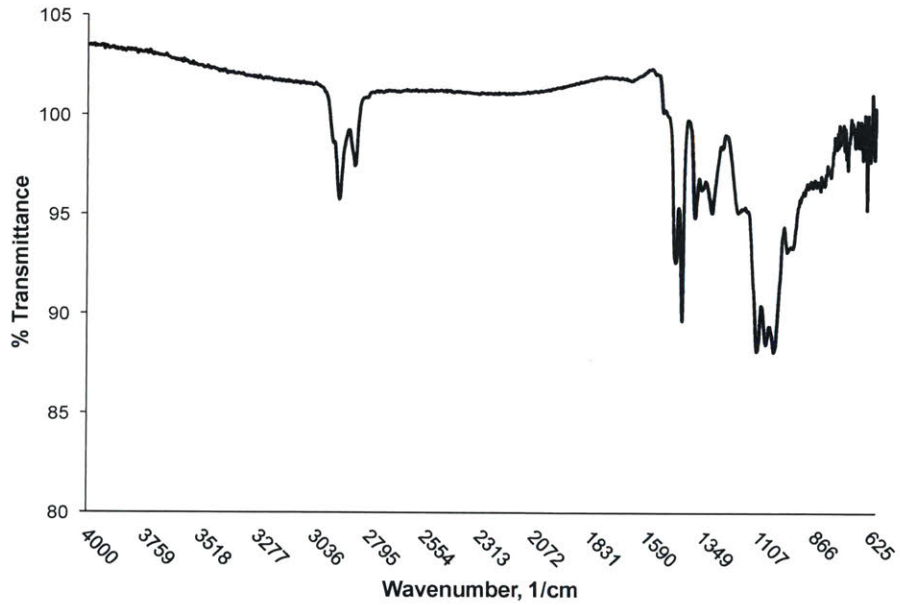

Figure A.2.51 Linear response curves for **P2**/SWCNT in N_2 (blue triangles) and air (24% RH) (red diamonds) to increasing concentrations of DMMP

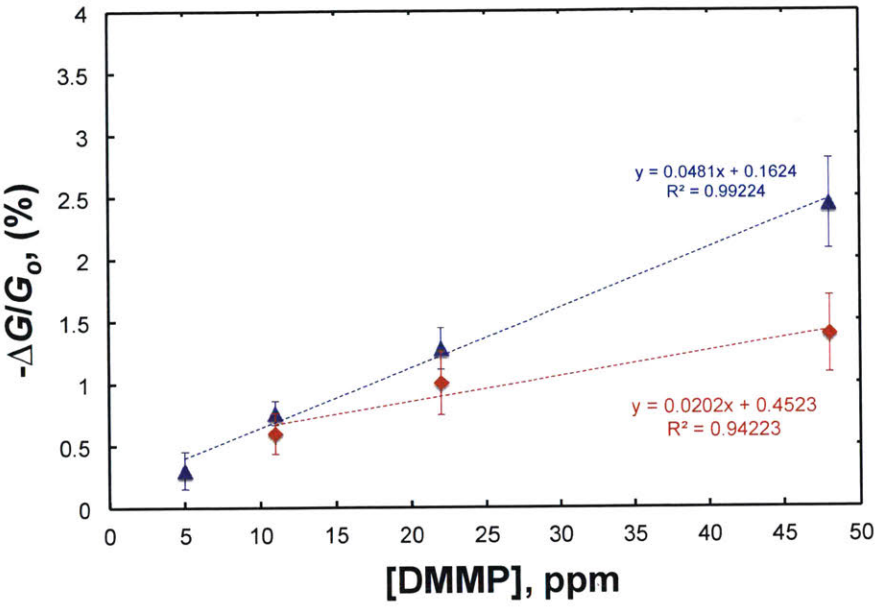

CHAPTER 3

Chemiresistive Detection of Ethylene Oxide and Mustard Gas:

Poly(vinylpyridine)/Single Walled Carbon Nanotube Composites

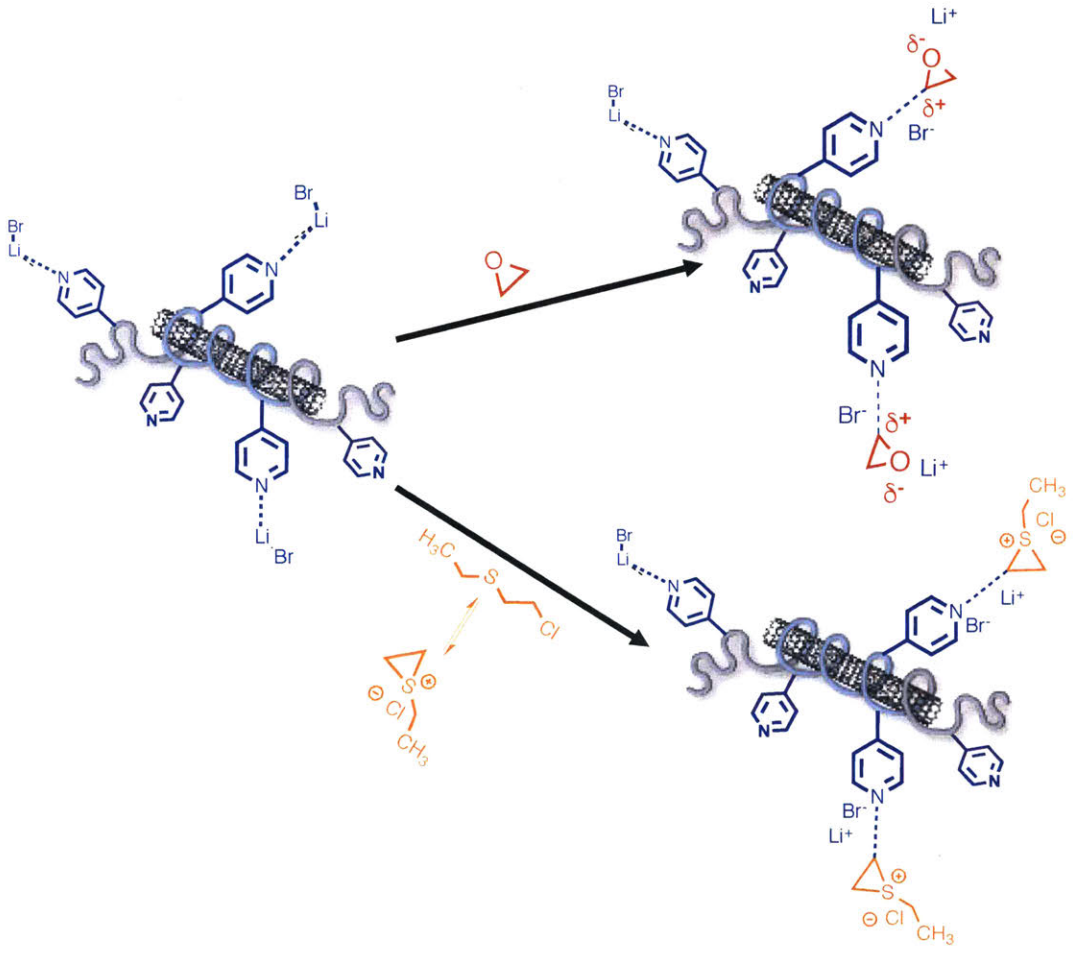

This work was supported in part by the U. S. Army Research Laboratory and the U. S. Army Research Office through the Institute for Soldier Nanotechnologies, under contract number W911NF-13-D-0001.

3.1 Abstract

The selective robust detection of alkylating agents using carbon nanotube chemiresistive devices has confounded researchers in the sensor field for quite some time. In this work, we address this quandary by fabricating a chemiresistive device consisting of poly(4-vinylpyridine)/single walled carbon nanotube/lithium bromide composites that is able to detect gaseous ethylene oxide (EO) and a mustard agent simulant, 2-chloroethyl ethylsulfide (CEES). Our devices were sensitive to EO and CEES down to 1048 ppm and 33 ppm, respectively. We achieve calculated theoretical detection limits of 212 ppm for EO and 10 ppm for CEES. These results should encourage researchers in the field to tackle analytes once thought to be undetectable via carbon nanotube chemiresistive devices, as they offer a low cost and low power alternative to current options.

3.2 Introduction

Carbon nanotubes continue to offer promise as the active sensor material in both chemiresistive[1] and field effect transistor devices.[2,3] To date, the unique electrical, thermal and mechanical properties of carbon nanotubes[4] have been used to detect industrial and agriculturally important gases,[5,6] explosive compound precursors,[7] biological molecules and chemical warfare agents (CWAs), amongst others.[8–11] Although they are promising materials for sensing, single walled carbon nanotubes (SWCNTs) often lack selectivity for target analytes that do not have a high affinity for the hydrophobic graphitic surface of nanotubes. To address this limitation, researchers have developed three main approaches to impart selectivity to their carbon nanotube-based systems: physical mixtures and covalent and non-covalent functionalization of SWCNTs.[12] Each method has its inherent advantages and disadvantages. Physical mixtures allow for rapid prototyping of SWCNT composites for sensing materials, but they often lack stability

and phase segregate over a short time frame. Covalent modifications disrupt the π-electron system and generate defects on the nanotube surface, but produces soluble nanotubes that can be solution processed. Non-covalent functionalization does not disrupt the π-electron system, but favorable van der Waals and π-interactions between the SWCNTs and the polymer are necessary for durable composites to be produced.

A common tactic for non-covalent functionalization is polymer wrapping.[13–16] With this approach, interactions between the polymer, SWCNTs, and the target analyte(s) can be tuned by rational selection of the polymer backbone and side chains. Recently, our group has developed a surface-anchored, poly(4-vinylpyridine)/SWCNT system.[17] This method involved the surface immobilization of a P4VP/SWCNT composite via a quaternization reaction between surface-bound bromopropylsilane and the pyridyl units of P4VP. Unreacted pyridyl units in this quaternization reaction are free to coordinate metal nanoparticles or ions chosen to grant selectivity and sensitivity to target gas analytes.

We sought to extend the use of this P4VP/SWCNT platform by focusing on the nucleophilic nature of the pyridine moiety in P4VP.[18] We hypothesized that the pyridyl nitrogens can react or strongly interact with electrophilic analytes and result in a chemiresistive response. To increase this response, we proposed that the addition of a metal salt (MX) could act to stabilize a forming intermediate or have favorable activating associations with the selected electrophilic analyte.[19,20] We selected ethylene oxide (EO) and 2-chloroethyl ethylsulfide (CEES), a CWA simulant for sulfur mustard (SM), because of their high reactivity as electrophilic analytes to detect chemiresistively with a P4VP/SWCNT composite. After some initial assays with a variety of metal salts and additives (Figure A.3.7) for CEES detection, we selected LiBr due to its chemiresistive response when incorporated into a P4VP/SWCNT

composite.

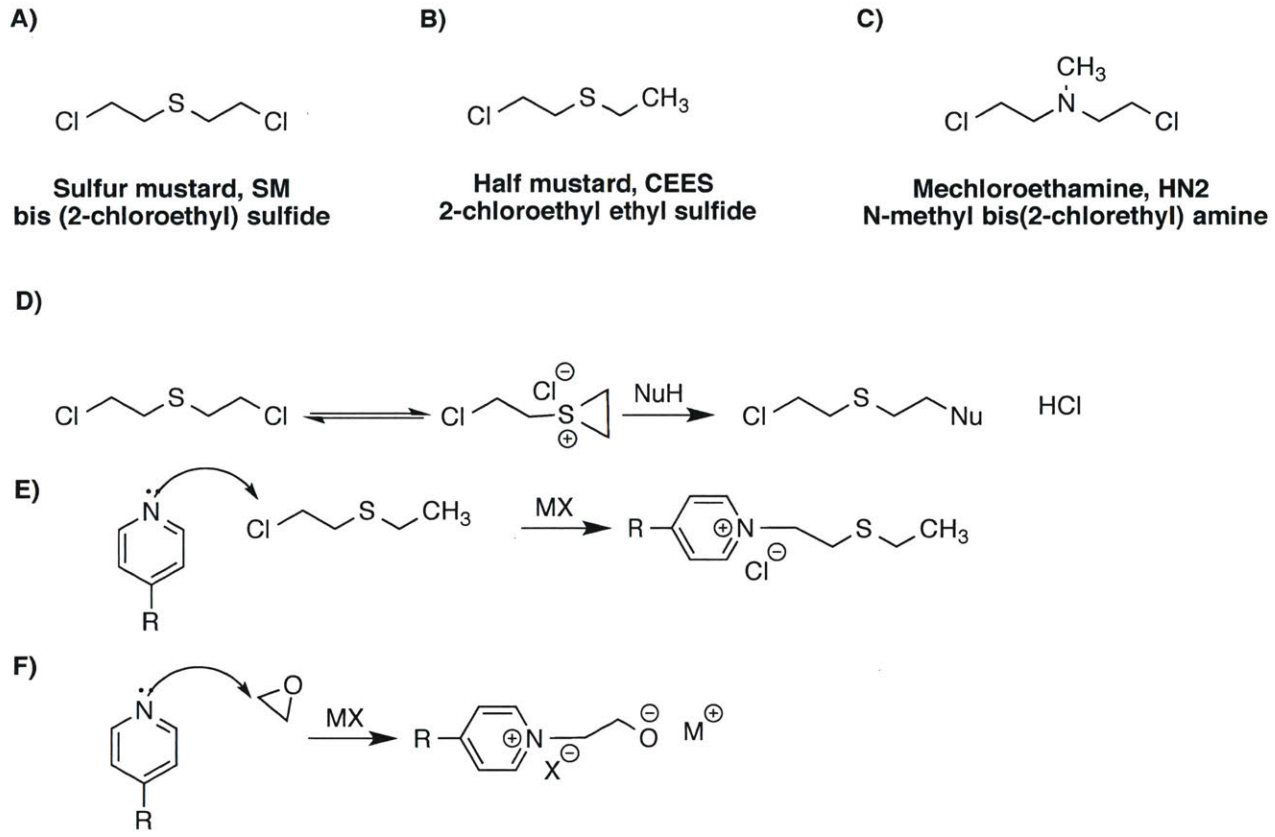

Figure 3.1 (a) Structure of sulfur mustard (SM); (b) structure of 2-chloroethyl ethylsulfide (CEES); (c) structure of mechloroethamine (HN-2); (d) formation of cyclic sulfonium cation and ring opening by a nucleophile; (e) quaterniztion of pyridine by CEES; (f) ring opening of EO by pyridine

EO is a highly reactive gas, the simplest cyclic ether. It is used as a raw material in the production of ethylene glycols, surfactants and ethanolamines.[21] Interestingly, EO is also used as a fumigant[22,23] and a sterilizing agent for medical equipment.[24] Despite its broad utility, EO is known to be mutagenic[25] and carnicogenic[26] in addition to being extremely flammable and explosive. EO is very reactive because its highly strained three membered ring can be opened easily by a variety of nucleophiles (Figure 3.1a).

CEES, SM, and nitrogen mustard derivative (HN-2) share the common characteristic of forming cyclic, three membered ring intermediates *in situ* (Figure 3.1b,c).[27] These cyclic cationic

sulfonium intermediates are formed via an intramolecular nucleophilic attack of sulfur (nitrogen for HN-2) on a primary carbon attached to a halogen, such as chlorine. The formation of the cyclic intermediate in CEES is the origin of it high instability, reactivity and toxic health effects. Sulfur mustard is a strong vesicant which causes severe skin/eye blistering and lung lesions upon exposure and may lead to death.[28] Furthermore, mustard agents have been demonstrated to be carcinogenic and mutagenic.[29,30] SM differentiates itself from the other classes of CWAs by persistence in the environment, latency of biological activity, and debilitating effects that incapacitate its victims and cause a burdensome response on evacuation medical care systems. In effect, both EO and CEES are electrophilic alkylating agents susceptible to nucleophilic attack and subsequent ring opening by a variety of nucleophiles to include water, alcohols, amines and biomolecules under the favorable conditions.

Herein, we fabricate and characterize chemiresistive devices consisting of P4VP/SWCNT and P4VP/SWCNT/LiBr as the active sensing material. We demonstrate that the P4VP/SWCNT/LiBr composite gives a chemiresistive response to EO and CEES. Additionally, the response to CEES is selective in comparison to other volatile organic compounds (VOC). We show that the presence of LiBr in the P4VP/SWCNT composite increases the chemiresistive response over P4VP/SWCNT composites.

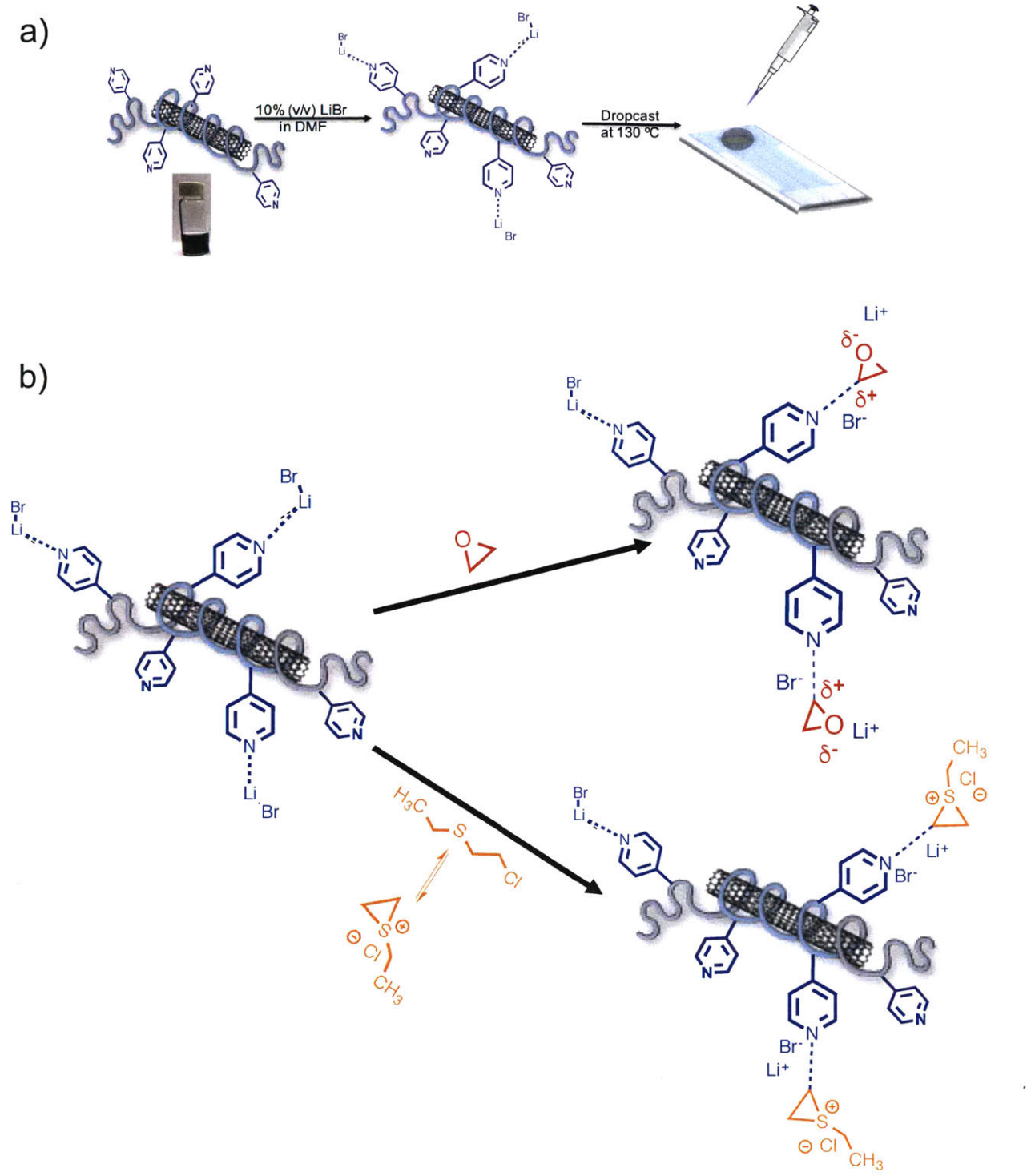

Figure 3.2 (a)Schematic of fabrication of a P4VP/SWCNT-based chemiresistive sensor dropcasted on an interdigitated electrode and photograph of the P4VP/SWCNT dispersion in DMF. (b) Proposed interaction between the P4VP/SWCNT/LiBr composite and target analytes EO (top) an CEES (bottom).

3.3 Results and Discussion

3.3.1 Dispersion of SWCNTs with P4VP

To quickly assay our hypothesis of using the P4VP-SWCNT dispersion in the presence of LiBr for the chemiresistive detection of EO and CEES, we fabricated devices as shown in Figure 3.2a. After the synthesis of P4VP via free radical polymerization (yield = 20%, M_n= 57.8 kDa, Đ=3.1), dispersions with P4VP/SWCNT in *N*,*N*-dimethylformamide (DMF) were generated using established procedures.[9,17] LiBr (4 mg/mL in DMF) was incorporated into the dispersion at a concentration of 10% (v/v). Next, the dispersions were dropcasted via micropipette onto interdigitated electrodes (CC1.W1, BVT Technologies) on a hot plated heated to 130 °C to rapidly remove solvent. Next, the IDEs were placed under vacuum at 50 °C until for a minuimum of two hours.

3.3.2 Spectroscopic characterization of P4VP-SWCNT composites

A necessary characteristic of durable polymer/SWCNT dispersions for chemiresistive devices is to ensure that the dispersions are resistant to re-bundling and phase segregation. Sensing applications demand percolative pathways that can be easily disrupted by analyte binding. These pathways are achieved by dispersing and de-bundling the nanotubes by polymer wrapping, which leads to higher surface area for interaction amongst the analyte and polymer/nanotube composite.

We determined the ratio of P4VP/SWCNT/DMF to be 10 mg/1 mg/2 mL based our previous work with P4VP/SWCNT system. Figure 3.3 presents UV–Vis–NIR absorbance spectra of P4VP, P4VP/SWCNT, and P4VP/SWCNT/LiBr dispersions in DMF. It is clear that P4VP has no significant absorption in this region of the spectrum and we can attribute all absorptions to the presence of SWCNTs and the LiBr additive. The absorption spectra of P4VP/SWCNT suggests the presence of both semiconducting and metallic nanotubes.

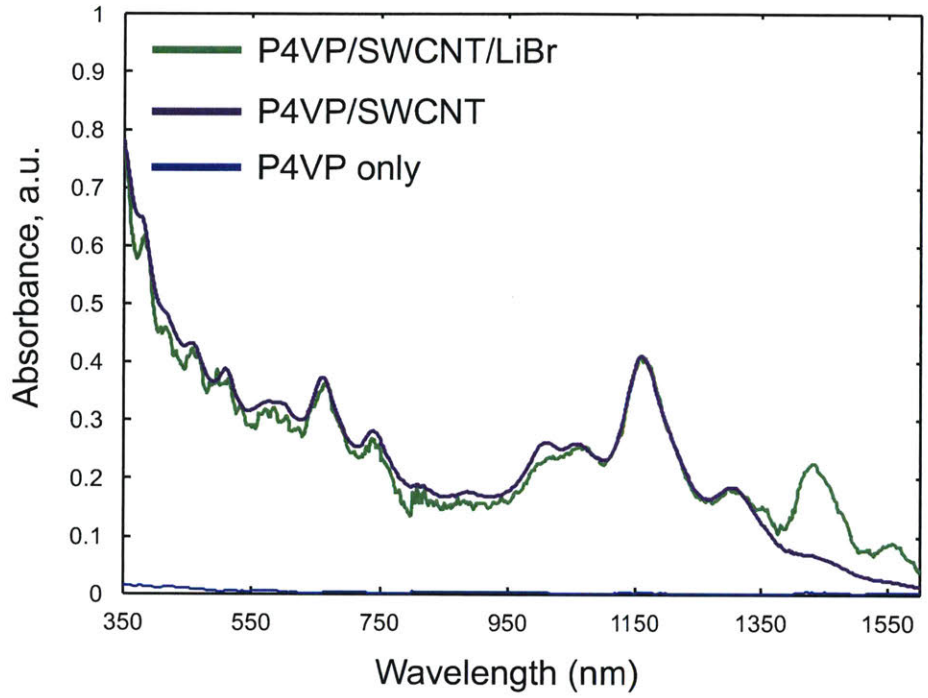

Figure 3.3 UV–vis/NIR spectra of polymer/SWCNT dispersions in DMF. P4VP only (blue); P4VP/SWCNT (purple); P4VP/SWCNT/LiBr (green).

Absorption bands in the 800 to 1600 nm region as well as the 550 to 900 nm region are indicative of the E11 and E22 van Hove singularity transitions of semiconducting carbon nanotubes, respectively, while the transitions of metallic nanotubes can be found in the region of 400–600 nm.[31,32] The clarity and resolution in these bands in Figure 3.3 indicate the presence of de-bundled SWCNTs in the P4VP/SWCNT dispersions. All compositions have some broad absorptions in the 400–600 nm region, indicating the presence of metallic SWCNTs. The P4VP/SWCNT/LiBr spectra is differentiated from the P4VP/SWCNT spectra by the relatively large absorbance at 1400 nm.[33,34] We attribute the feature to vibrational overtones from water absorbed by LiBr, which is known to be extremely hygroscopic and is often used as a dessicant.[21] The resolved absorption bands located at 650 and 1159 nm are evidence of the presence of (7,6) SWCNTs.[35]

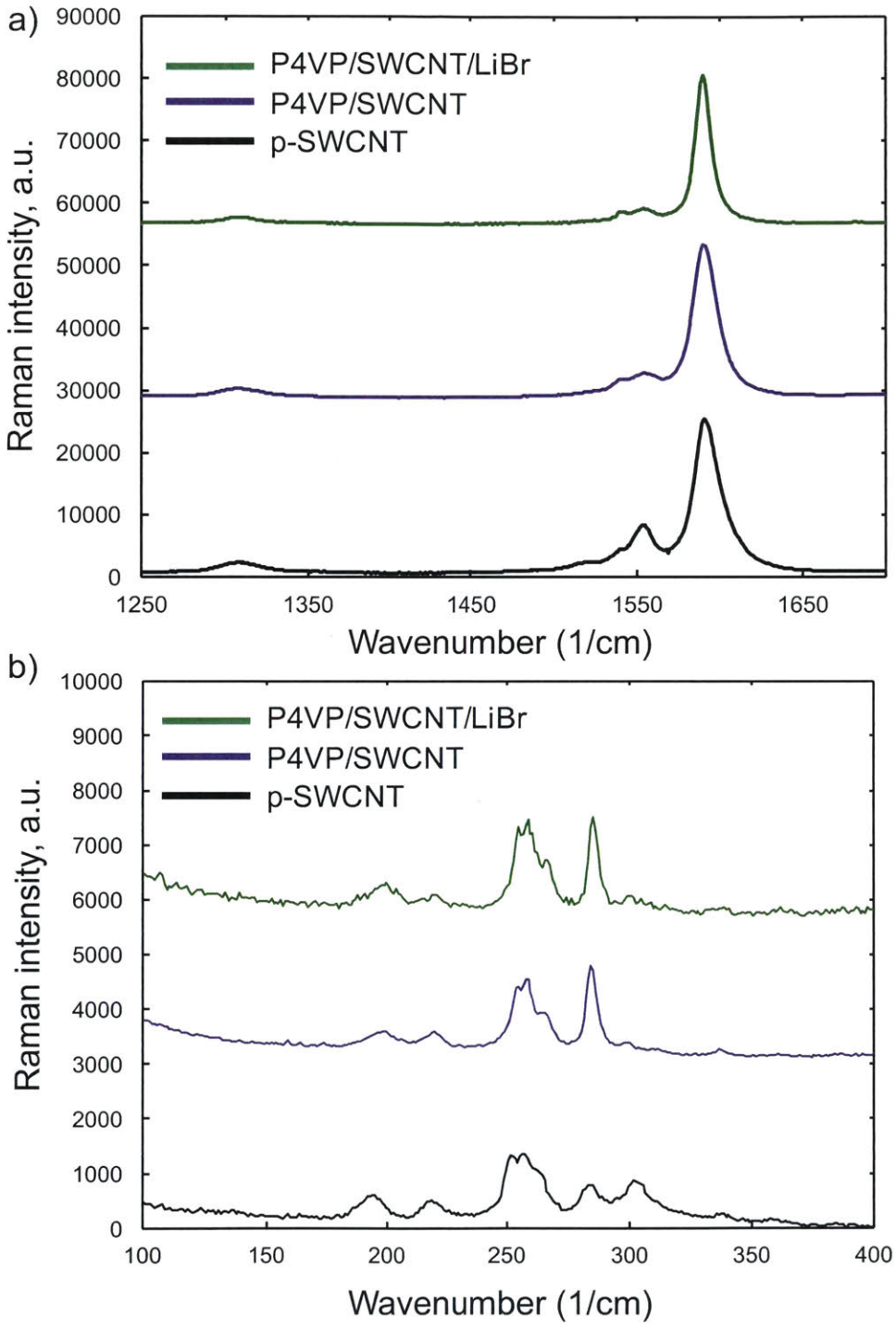

Figure 3.4 (a) Resonance Raman spectra of p-SWCNT only (black); P4VP/SWCNT (purple); P4VP/SWCNT/LiBr (green), and (b) those in the RBM region.

Resonance Raman spectroscopy can confirm the presence of SWCNTs in polymer dispersions. The full resonance Raman spectra of the composites and pure polymer are shown in Figure A3.5. Thin film samples were prepared for analysis by drop casting dispersions from DMF onto a silicon wafer. A pristine SWCNT thin film was prepared by drop casting enriched SWCNTs from a fresh dispersion in *ortho*-dichlorbenzene onto a silicon wafer. The spectra were taken using a 633 nm excitation wavelength and are normalized to the intensity of the G-band, at 1590 cm^{-1} and offset for clarity. In Figure 3.4a, Raman spectrum for the D-G band region is displayed. The D-band, located at 1290 cm^{-1} is diagnostic of the disruption of the sp^2 network in conjugated nanocarbon systems.[36] The ratio of intensities of the D band (1290 cm^{-1}) to the G band (I_D /I_G) can give relative measure of disruption of the graphene system. After dispersion, there is an increase in I_D /I_G from the pristine SWCNTs to the P4VP-dispersed SWCNTs. Specifically, the I_D /I_G is 0.09 in pristine SWCNTs and 0.59 and 0.65 for the P4VP/SWCNT and P4VP/SWCNT/LiBr composites, respectively. An increase in the I_D /I_G indicates an growth in the number of defects or strong chemisorption to the carbon atoms in the SWCNT sidewalls within the dispersion.[36] The source of the disruption in this case is posited to be due to interruptions of the conjugation of the SWCNT sp^2 network during the sonication step in the dispersion preparation or the outcome of strong interactions between the nanotube graphitic walls and the dispersing polymers or other molecules/molecular fragments.[17,37] The radial breathing modes (RBMs) are located between 100–300 cm^{-1} and are shown in Figure 3.4b. They are the signature for the presence of single walled carbon nanotubes. At the 633 nm excitation wavelength, peaks below 250 cm^{-1} represent larger diameter metallic SWCNTs, while peaks above 250 cm^{-1} represent smaller diameter semi-conducting SWCNTs.[38] We observe that

all SWCNTs used in this work are slightly enriched in semi-conducting SWCNTs based upon the relative intensity of the peaks above and below 250 cm^{-1}.

FTIR-ATR was used to confirm the incorporation of LiBr into the P4VP-SWCNT composite (Figure 3.5). The shift of the absorbance of the pyridine ring stretches (C-N str) to higher wavenumbers in the P4VP/SWCNT/LiBr dispersion from 1595 cm^{-1} to 1640 cm^{-1} can be attributed to increased coordination of pyridine to Li^+.[39,40] The lack of any residual absorbance at 1595 cm^{-1} suggest that all pyridines have been coordinated to Li^+. Additionally, the full FTIR-ATR spectra (Figure A.3.9) of P4VP/SWCNT/LiBr shows a broad, strong absorption at 3450 cm^{-1} that is not observed in the other dispersions: this is further evidence that the P4VP/SWCNT/LiBr contains water.

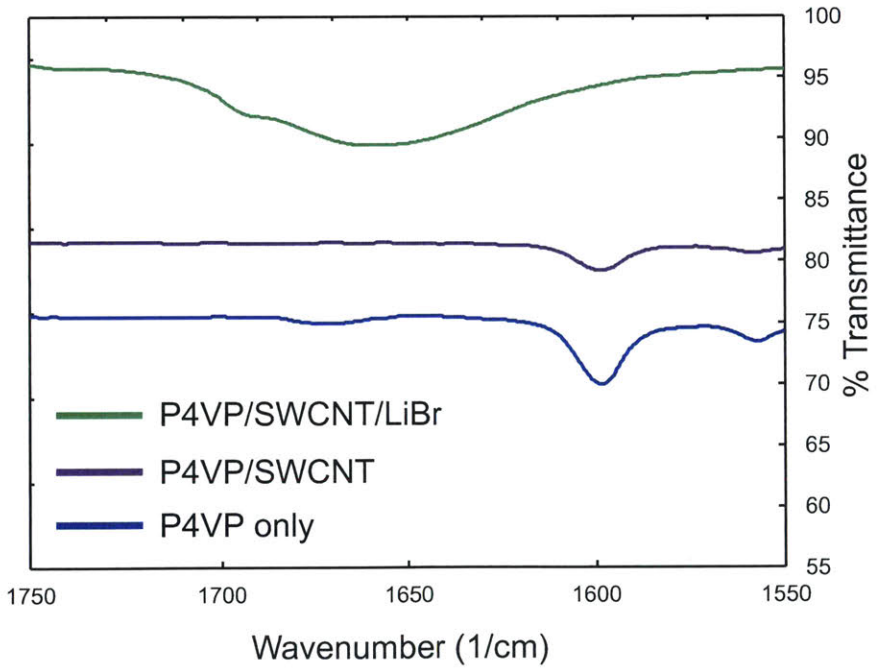

Figure 3.5 Offset FITR-ATR spectra of polymer/SWCNT dispersions focused on the pyridine ring stretch region (1550-1670 cm^{-1}). P4VP only (blue); P4VP/SWCNT (purple); P4VP/SWCNT/LiBr (purple).

3.3.3 P4VP/SWCNT/LiBr composite for the detection of ethylene oxide (EO) and 2-chloroethyl ethylsulfide (CEES)

Having developed stable composites and successfully characterizing them, we set out to study the efficacy of our P4VP/SWCNT composite system in detecting ethylene oxide (EO). Chemiresistive sensors were prepared by drop casting 2-3 μL of the P4VP/SWCNT dispersions onto interdigitated Au electrodes (0.2 mm gaps) until a

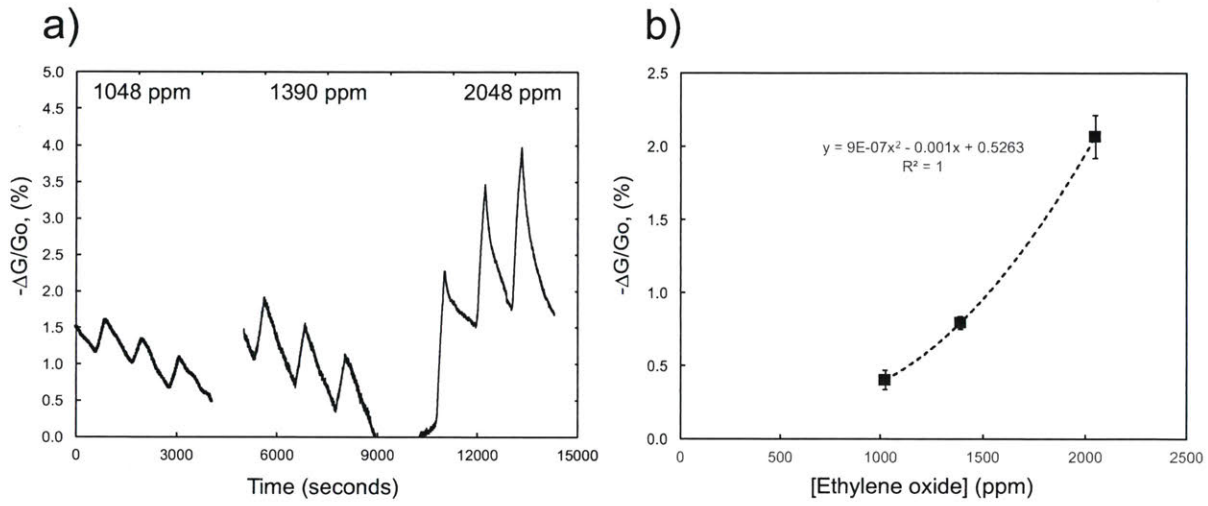

Figure 3.6 (a) Representative conductance traces of a P4VP/SWCNT/LiBr-based chemiresistor to three concentrations of EO in N_2 at room temperature. (b) Chemiresistive responses to varying amounts of EO for P4VP/SWCNT/LiBr-based devices in N_2 (black squares) at room temperature.

resistance of 20-50 kΩ was reached. The variation in the conductivity upon exposure to various types of analyte vapors, including EO and CEES, was measured by detecting the current with an applied bias voltage of 0.1 V. The change in current was converted to a negative change in conductance [$-\Delta G/G_o$ (%) = $((I_o-I)/I_o)$ *x 100%*], where I_o is the initial current. This normalized response allows for small differences in the resistivity that can complicate device to device comparisons. Figure 3.6a shows representative baseline-corrected response of a chemiresistive

device incorporating a P4VP/SWCNT/LiBr that was designed to detect EO and CEES. Exposure times were limited to 300 seconds followed by a 900 second recovery time. The sensors show a reversible response across this concentration range under N_2 atmosphere, from 1048-2048 ppm. In Figure 3.6b, we observed a 0.40% response to EO at a concentration of 1048 ppm with an increasing, slightly exponential response up to 2048 ppm. We calculated a theoretical detection limit of 212 ppm.[41] This is an operationally relevant range for the detection of EO, since the concentration of EO which is of immediate danger to life and health (IDLH) is 800 ppm.[42] The chemiresistive detection of EO by a decrease in conductance is consistent with the notion of a transduction mechanism that relies upon a swelling of the SWCNT network or direct modulation of the SWCNT conductance by charge transfer or dipolar mechanisms. These effects are all consistent with oxygen of the EO being coordinated to the lithium ions or H-bond with water molecules associated with the polymer salt wrapper (Figure 3.2b). In the case of a reaction with the EO, these same interactions can stabilize the oxyanion produced. As mentioned above, water is present in the P4VP/SWCNT/LiBr composite. Water may act as a concentrator for EO at the device surface and increase the effective concentration of EO through hydrogen bonding. These effects all contribute to the swelling of the polymer/SWCNT network which acts to increase the resistance (reduces the current) as a result.[9] It is important to note that the sensing traces in Figure 3.6a appear to be reversible. This provides evidence for interaction of the pyridine:LiBr complex to the EO rather than covalent bond formation between pyridine and EO via quaternization.

Having successfully detected EO, we turned our attention to CEES sensing. The signal transduction mechanism is likely similar to that of EO, as the most stable conformation of CEES is that of a cyclic sulfonium ion (Figure 3.1c) and also may be attacked by a nucleophilic

pyridine group. Figure 3.7a shows representative baseline-corrected response of a chemiresistive device incorporating P4VP/SWCNT/LiBr that was designed to detect CEES (and EO). Exposure and recovery times were identical as those used with EO. The sensors show a reversible response across a 33-72 ppm concentration range under N_2. In Figure 3.7b, we observed a 0.30% response to CEES at a concentration of 33 ppm with an exponential response up to 72 ppm. We calculated a theoretical detection limit of 10 ppm. Though this is not an operationally relevant range for the detection of CEES (IDLH of sulfur mustard is 140 ppb), it is a step toward a sulfur mustard detector using chemiresistive, carbon nanotube based device.[43] Since there is a

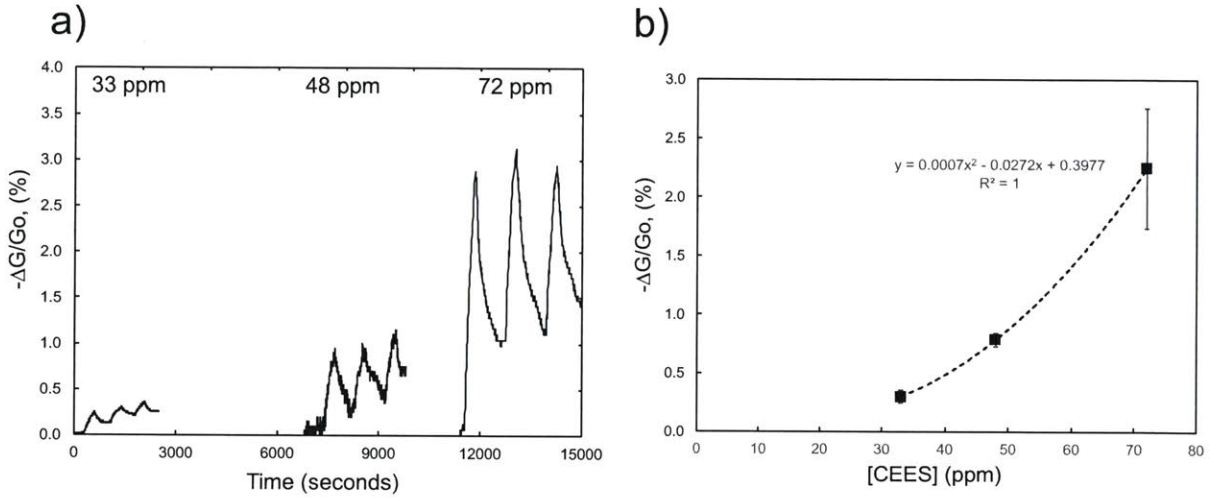

Figure 3.7 (a) Representative conductance traces of a P4VP/SWCNT/LiBr-based chemiresistor to three concentrations of CEES in N_2 at room temperature; (b) Chemiresistive responses to varying amounts CEES for P4VP/SWCNT/LiBr-based devices for varying amounts in N_2 (black squares) at room temperature.

decrease in conductance upon CEES exposure, and structural similarities between EO and CEES, we propose a swelling mechanism to explain the chemiresistive response of P4VP/SWCNT/LiBr towards CEES. Moreover, we propose the greater strength of the chemiresistive response to CEES (0.40% at 33 ppm) over EO (0.40% at 1048 ppm) is ascribed to the more reactive nature of the sulfonium ion towards coordination with pyridine. Interestingly, we would expect the

increased reactivity of CEES would lead to an alkylation reaction with pendant pyridines. Evidence for this case would be an irreversible or dosimetric sensing response. In contrast, we observed a dominately reversible response which indicates that the alkylation of the pyridyl groups is not occurring with CEES. We have hypothesized that equipping our polymer wrapping system with a group more nucleophilic than pyridine would lead to alkylation of CEES and a dosimetric chemisresistive response. To this end, our group has made efforts into include vinyl imidazole in a copolymer with vinylpyridine for this purpose. However, the polymer failed to provide high stability dispersions with SWCNTs.

To assess the relative degree of selectivity of the P4VP/SWCNT/LiBr composite, Figure 3.8a demonstrates the device's chemiresistive response to various volatile chemicals for 60 seconds exposure followed by a 140 second recovery time at a constant flow rate of 200 mL/min at room temperature in N_2. The concentrations of these vapors were chosen to be sufficiently high enough to obtain a measurable response to the P4VP/SWCNT composite, a control device. The P4VP/SWCNT and P4VP/SWCNT/LiBr devices respond to all of these VOCs in addition to EO and CEES. However, it is clear that the presence of LiBr in the P4VP/SWCNT composite amplifies the response across the panel. Furthermore, when we utilize

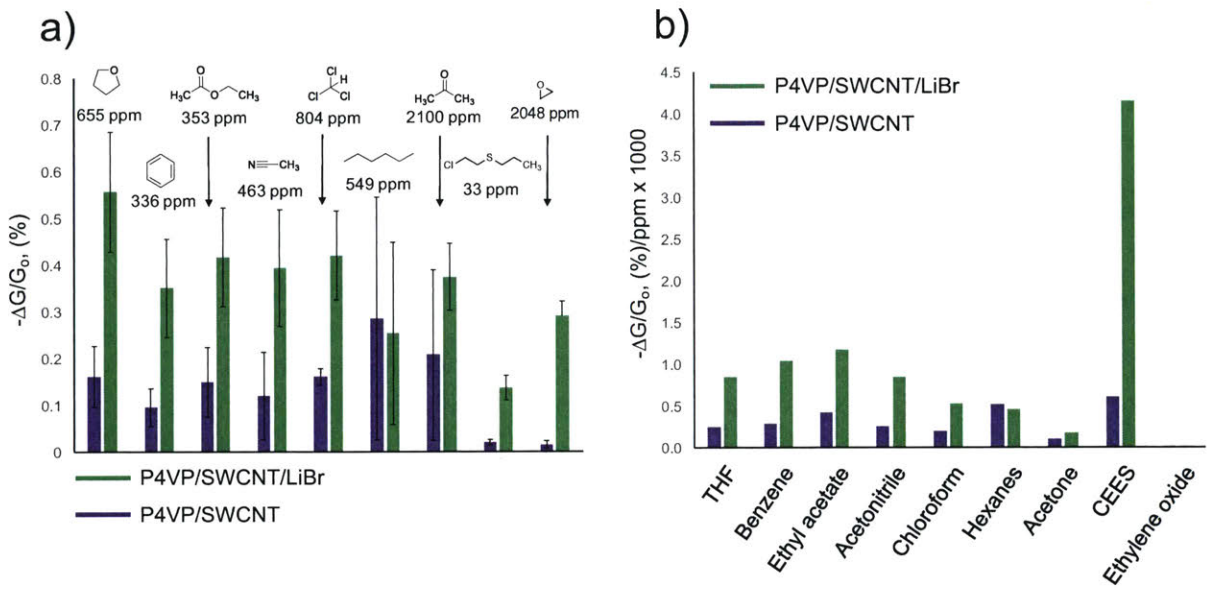

Figure 3.8 (a) Chemiresistive responses for P4VP/SWCNT (purple) and P4VP/SWCNT/LiBr (green) averaged across three devices to 60 s exposures of VOCs at a flow rate of 200 mL/min in N_2; (b) Chemiresistive response ratio ($-\Delta G/G_0$ (%)/ppm) for P4VP/SWCNT (purple) and P4VP/SWCNT/LiBr (green) to VOCs in N_2.

a response ratio,[9] as shown in Figure 3.8 (b), we see that CEES provides the greatest response per ppm of analyte by a factor of more than four. In contrast, EO barely registers a response for this metric (see Table 3.A.1). This analysis reinforces the lower reactivity of EO in comparison to CEES toward our P4VP/SWCNT-based chemiresistor.

3.3.4 Related work: Poly(4-vinylpyridine) copolymers with vinyl ferrocene (P4VP-*co*-VFc) and ferrocenylmethylmethacrylate (P4VP-*co*-FcMMA)

The ability to surface anchor the P4VP/SWCNT composite system (not performed in this work) to glass and other surfaces brings to mind a myriad of applications outside of gas sensing. We propose that we can use this method to anchor P4VP/SWCNT composites to an electrode surface for electrochemical detection of anions in aqueous environments.[44–46] To this end, we developed two copolymers that include electroactive ferrocene-based repeat units into the P4VP main chain. We accomplished this via free radical polymerization and set the loading of the

ferrocene-containing units at 9-10% to retain enough pyridine units to quaternize to a surface and coordinate to metal centers for sensing applications.[47–50] The resulting random copolymers, vinyl pyridine with vinyl ferrocene (P4VP-*co*-VFc) and with ferrocenylmethylmethacrylate (P4VP-*co*-FcMMA) were synthesized in good yields and their composites with SWCNTs were characterized via ^{1}H NMR (Figures A.3.2-3), FTIR-ATR (Figures A.3.8-10), gel permeation chromatography (GPC) (Figure A.3.4) and thermogravimetric analysis (TGA) (Figures A.3.11-13).

3.3.4.1 Spectroscopic characterization of P4VP, P4VP-*co*-VFc and P4VP-*co*-FcMMA composites with SWCNTs

A key requirement for any application in which either P4VP-*co*-VFc and P4VP-*co*-FcMMA are to be used in a composite with SWCNT is that they must form stable dispersions that resist aggregation and re-bundling in solution with SWCNTs. We used UV-vis/NIR (Figure 3.9a) and Resonance Raman spectroscopy (Figure 3.9b) to confirm that the dispersions with

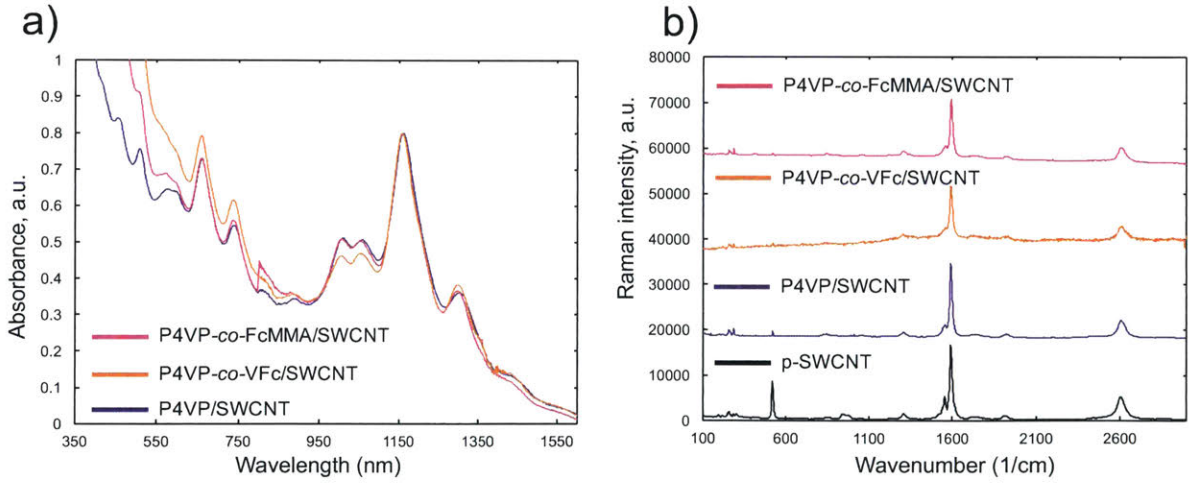

Figure 3.9 (a) UV–vis/NIR spectra of polymer/SWCNT dispersions in DMF. P4VP/SWCNT only (purple); P4VP-*co*-VFc/SWCNT (orange); P4VP-*co*-FcMMA /SWCNT/ (pink). (b) Resonance Raman spectra of pristine-SWCNT (black); a P4VP-SWCNT composite (purple); P4VP-*co*-VFC/composite (orange); a P4VP-*co*-FcMMA/SWCNT composite (pink).

vinyl pyridine based copolymers were stable. The UV-vis/NIR and Raman spectra very closely resemble the P4VP/SWCNT spectra that were discussed in Figures 3.3 and 3.4, respectively.

3.3.4.2 Electrochemical characterization of P4VP, P4VP-*co*-VFc and P4VP-*co*-FcMMA composites with SWCNTs via cyclic voltammetry.

With stable composites in hand, we set out to conduct cyclic voltammetry (CV) to determine baseline behavior of these composites in aqueous environments in preparation for aqueous anion sensing. We deposited 20 μL of each polymer/SWCNT dispersion in DMF on a glassy carbon electrode (GCE) and evaporated residual solvent to form films on the GCE. The reference electrode was Ag/AgCl and the counter electrode was platinum. We conducted the CV experiments in a 0.10 M $KCl_{(aq)}$ electrolyte solution and scanned from -1.0 to 1.0 V. Voltammograms in which we varied the scan rate were informative with respect to reversibility of the electron transfer in the copolymer films. The CVs at scan rates of 50, 100, and 500 mV/s for the P4VP/SWCNT film (Figure A.3.15) were featureless because it lacks an electroactive center. An Fc/Fc^+ wave couple appears in the ferrocene-containing copolymer/SWCNT films, P4VP-*co*-VFc/SWCNT (Figure A.3.16) and P4VP-*co*-FcMMA (Figure A.3.17) films. We observed different electron transfer rates and peak potentials for each scan rate for the Fc/Fc^+ wave couple. These observations are characteristic of electrochemically irreversible (slow electron transfer) processes likely are due to the limited amount of the electroactive ferrocene repeat units (recall the copolymers contain only 9-10% ferrocene repeat units). Moreover, the copolymer/SWCNT composite film likely changes conformation in the aqueous media as it swells in solution and adjusts to a changing electronic environment.

3.3.4.3 Electrochemical detection of HSO_4^- and $H_2PO_4^-$ with a P4VP-*co*-VFc film

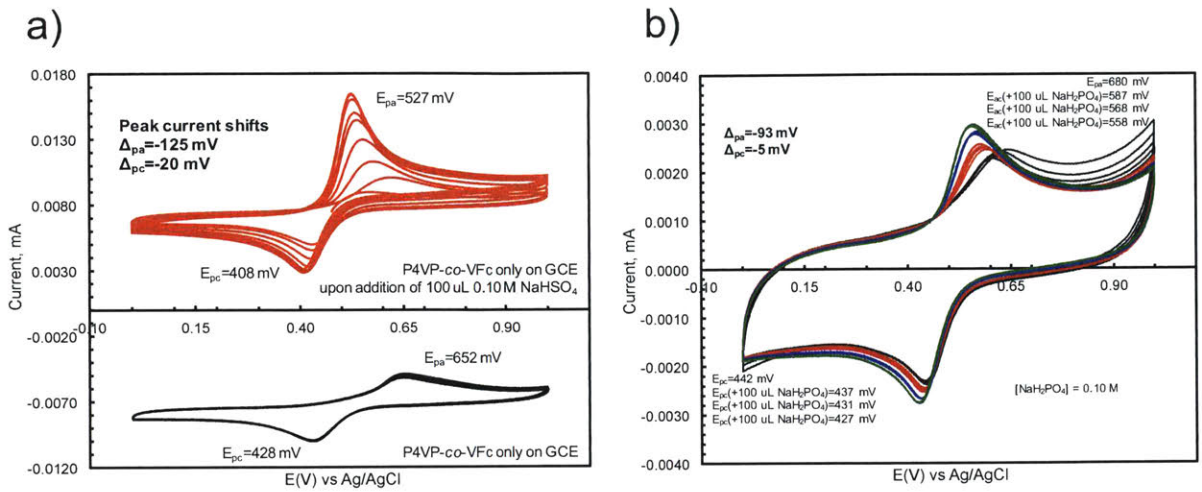

Figure 3.10 (a) Electrochemical detection via CV of HSO_4^- anion with P4VP-*co*-VFc film under aqueous conditions. Bottom (black), P4VP-*co*-VFc film on a GCE. Top (red), P4VP-co-VFc film exposed to 100 µL of 0.10 M $NaHSO_4$ and a scan rate of 100 mV/s in a 0.10 M KCl. (b) Electrochemical detection of $H_2PO_4^-$ anion with P4VP-*co*-VFc film under aqueous conditions. The black trace represents the film prior to exposure to NaH_2PO_4 at a scan rate of 100 mV/s in 0.10 M KCl. The red, blue and green traces represent the CV after delivering successive 100 µL aliquots of 0.10 M NaH_2PO_4 to the electrochemical cell.

A first step towards aqueous anion sensing using polymer/SWCNT sensing was ensuring that our copolymers alone could indeed give a detectable electrical response to anions. To analyze this response, we observed the changes to the CV trace as we added sodium salts of the analytes HSO_4^- and $H_2PO_4^-$ to an electrochemical cell equipped as above with a P4VP-*co*-VFc film on a GCE. In Figure 3.10a, the Fc/Fc^+ wave couple experiences an anodic peak shift of -125 mV and cathodic peak shift of -20 mV upon delivery of 100 µL of 0.10 M HSO_4^-. In Figure 3.10b, we added successive aliquots of 100 µL of 0.10 M $H_2PO_4^-$ and the Fc/Fc^+ wave couple undergoes an anodic peak shift of -93 mV and cathodic peak shift of -5 mV. The larger shift in anodic potential for HSO_4^- indicates an affinity of the Fc^+ moiety for that anion. These initial experiments with P4VP-*co*-VFc were promising and warrant further exploration in compositions with SWCNTs.

3.4 Conclusions

We demonstrated an extended utility of the P4VP/SWCNT composite chemiresistive system with the introduction of the metal salt, LiBr. The infusion of LiBr into the P4VP/SWCNT composite produced a sensor material that enabled our devices to detect the industrial gas EO and the CWA stimulant CEES. The calculated detection limits for EO and CEES were 10 ppm and 212 ppm, respectively. Moreover, we demonstrated that P4VP/SWCNT/LiBr composite based device is four times as selective for CEES as it is for other VOCs tested. The device is not selective for EO, and we attribute this low selectivity to the significantly lower reactivity of EO to nucleophiles when compared to CEES. Additionally, we identified that water was present in our P4VP/SWCNT/LiBr composite and posit that it could play a role in device performance by increasing adsorption of analytes in/on the composite. Though at present, the chemiresistive detection of EO and CEES is not competitive with commercial or military sensors, this does represent a step towards chemiresistive devices that may be a low cost, low power, simple alternative to complicated, expensive and energy intensive sensors that are currently in field use. Finally, we synthesized two new copolymers, P4VP-*co*-VFc and P4VP-*co*-FcMMA with the intent of utilizing them for anionic sensing in aqueous media. We conducted initial electrochemical experiments and successfully detected HSO_4^- and $H_2PO_4^-$ in 0.10 M KCl.

3.5 Experimental

3.5.1 Materials

All chemicals and reagents were purchased from Sigma-Aldrich and used without additional purification, except that tetrahydrofuran was distilled from sodium metal and

benzophenone. Purified SWCNTs (UPT 200, Batch 1167-24) were acquired from Nano-C, (Westwood, MA) or Sigma Aldrich, Inc. (Saint Louis, MO, USA) (6,5 chirality, carbon (95%), with 93% as SWCNTs). 3-Bromopropyltrichlorosilane was purchased from Gelest (Morrisville, PA, USA). 2-(2-hydroxy-1,1,1,3,3,3-hexfluoroisoproyl)-1-napthol was purchased from Synquest Laboratories (Alachua, FL, USA). 1,3-bis[3,5-bis(trifluoromethyl)-phenyl]thiourea was purchased from TCI America (Portland, OR, USA).

3.5.2 Instrumentation

^{1}H NMR spectra were recorded 500 MHz using a JEOL JNM-ECZR-500 NMR spectrometer. Chemical shifts are reported in ppm and referenced to residual NMR solvent peaks (^{1}H NMR: δ 7.26 ppm for $CDCl_3$). UV–vis/NIR absorption spectra were measured using an Agilent Cary 4000 Series UV–Vis spectrophotometer. ATR–FTIR spectra were acquired using a Thermo Scientific Nicolet 6700 FT–IR with either a Ge or ZnSE crystal for ATR and subjected to the 'atmospheric suppression' correction in OMNIC™ Spectra software. Raman spectra were collected with excitation at 633 nm laser using a Horiba LabRAM HR800 Raman spectrometer. Gel Permeation Chromatography (GPC) was performed on an Agilent 1260 LC stack equipped with an Agilent multiwavelength UV/vis detector, Wyatt TrEX refractive index detector, Wyatt DAWN EOS 18-angle light scattering detector, and two Shodex KD-806M GPC columns. The GPC system was set to 60 °C with a 1 mL/min flow rate with 0.025M LiBr in DMF. 8W SANKYO DENKI Black light lamps emitting near ultraviolet rays (315 nm – 400 nm) with peak emission at 352 nm, were used as the UV radiation source. Interdigitated microelectrode (CC1.W1) with electrode gap of 200 μm was purchased from BVT Technologies for some sensing experiments. Cyclic voltammetry experiments were performed on a BioLogic VSP work station.

3.5.3 Synthesis

3.5.3.1 Synthesis of poly(4-vinylpyridine) (P4VP).

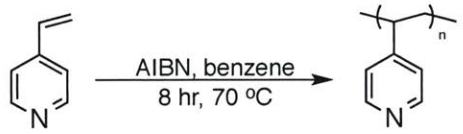

Yield=49%
M_n=57.8 kDa
M_n/M_w=3.1

To a flame dried 25 mL round-bottomed Schlenck flask, 15.23 mg of azobisisobutyronitrile (AIBN) was added then evacuated and refilled three times with argon. Then, 10 mL of dry benzene and 975 mg 4-vinylpyridine was added via syringe. The reaction mixture was subjected to three freeze-pump-though cycles. After eight hours of stirring at 70 °C, the reaction mixture was precipitated into cold diethyl ether and filtered. The resulting white solid powder was precipitated and filtered again and then placed in a vacuum oven overnight at 60 °C. The reaction yielded 611 mg (49%) of a white, fluffy powder.

3.5.3.2 Synthesis of poly(4-vinylpyridine-co-vinylferrocene) (P4VP-co-VFc).

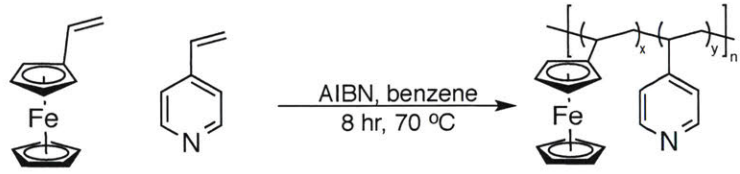

Yield=20%
M_n=60.5 kDa
M_n/M_w= 3.84

To a flame dried 25 mL round-bottomed Schlenck flask, 15.23 mg of azobisisobutyronitrile (AIBN) and 196 mg of vinylferrocene was added then evacuated and refilled three times with argon. Then, 10 mL of dry benzene and 975 mg 4-vinylpyridine was added via syringe. The reaction mixture was subjected to three freeze-pump-though cycles. After eight hours of stirring at 70 °C, the reaction mixture was precipitated into cold diethyl ether and filtered. The resulting yellowish white solid powder was precipitated and filtered again and then placed in a vacuum oven overnight at 70 °C. The reaction yielded 634 mg (20%) of a white, fluffy powder.

3.5.3.3 Synthesis of poly(4-vinylpyridine-co-ferrocenylmethylmethacrylate) (P4VP-co-FcMMA)

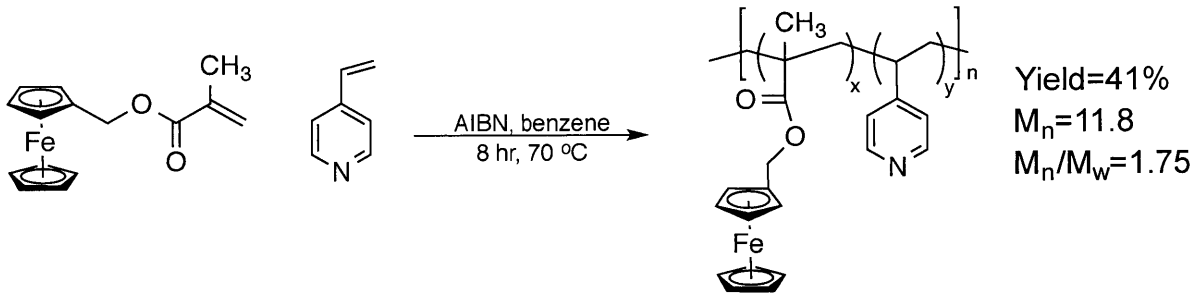

To a flame dried 25 mL round-bottomed Schlenck flask, 15.62 mg of azobisisobutyronitrile (AIBN) and 270.22 mg of ferrocenylmethylmethacrylate (FcMMA) was added then evacuated and refilled three times with argon. Then, 10 mL of dry benzene and 1.00 mg 4-vinylpyridine was added via syringe. The reaction mixture was subjected to three freeze-pump-though cycles. After eight hours of stirring at 70 °C, the reaction mixture was precipitated into cold diethyl ether and filtered. The resulting yellowish white solid powder was precipitated and filtered again and then placed in a vacuum oven overnight at 70 °C. The reaction yielded 523 mg (41%) of an off white, fluffy powder.

3.5.4 Chemiresistor and gas sensing experiments

3.5.4.1 Dispersion of SWCNT and device fabrication

To a solution of 50 mg P4VP in DMF, 5 mg of SWCNT was added. The resulting mixture was sonicated for 1 h in an ultrasonic bath (Branson, 3510) chilled with ice and then allowed to reach room temperature. Subsequently,the suspension was centrifuged for 30 min at 9500 g. The supernatant was decanted and centrifugedagain for an additional 30 min at 9500 g and allowed to stand overnight undisturbed. The isolated supernatant was directly used for the device fabrication via dropcasting unless otherwise indicated. To fabricate chemiresistive

devices, 2-3 μL of the P4VP/SWCNT or P4VP/SWCNT/LiBr dispersions were dropcasted onto an interdigitated microelectrode (CC1.W1 from BVT Technologies, Czechoslovakia) to reach the target electrode resistance of 20-40 kΩ. For UV–vis/NIR absorption spectroscopy, the isolated supernatant was diluted to 1:2 in DMF and further sonicated for 5 min, and recorded in a 1 cm optical path quartz cuvette.

3.5.4.2 Ethylene oxide (EO) Gas Detection Measurement

For EO detection measurement, the fabricated array device was placed into a custom-built PTFE enclosure with a small gas inlet and outlet, the gold electrodes of the device were connected to a PalmSens EmStat potentiostat with a MUX16 multiplexer. The inlet port was connected to a gas delivery system (Sierra's Smart-Trak Series 100). Delivery of controlled concentration of gases to devices. To obtain concentrations of EO between 834 ppm – 2000 ppm, a 4% mixture of EO in N_2 was supplied from a gas cylinder (Airgas) was diluted further N_2 using the gas mixing system at total flow rate supplied to devices ranging between 200 – 700 mL/min. Controlled delivery of gas to devices was accomplished by encasing a device within a custom-built teflon chamber equipped with an inlet and an outlet for gas flow. The potentiostat applied a constant potential of 0.1 V across the electrodes, and the current for each channel of the device was recorded using PS Trace software (v. 4.8) during 60 s or 300 s of EO vapor exposures. After a linear baseline correction, the change in current resulting from exposure to the analyte was converted to the negative change in conductance ($-\Delta G/G_o\ (\%) = (I_o - I)/I_o) \times 100$), where I_o is initial current), which was taken as the device's response.

3.5.4.3 VOC gas detection measurement

The fabricated array device was placed into a custom-built PTFE enclosure with a small gas inlet and outlet, the interdigitated microelectrodes of the devices were connected to a PalmSens EmStat potentiostat with a MUX16 multiplexer. A KIN-TEK gas generator system calibrated for each VOC was used to deliver to the device's enclosure a known concentration of a given VOC analyte diluted in N_2 gas at a fixed gas flow rate (200 mL/min) to minimize drift in the baseline resistance. For calibration, emission rate of each VOC by monitoring the decrease in mass of each liquid for an hour at a 500 mL/min flow rate and a designated temperature (40 °C–70 °C). Three trials for each VOC were performed. The potentiostat applied a constant potential of 0.1 V across the electrodes, and the current for each channel of the device was recorded using PS Trace software (v. 4.8) during 60 s of VOC vapor exposures. After a linear baseline correction, the change in current resulting from exposure to the analyte was converted to the negative change in conductance ($-\Delta G/G_0$ (%) = $(I_0 - I)/I_0) \times 100$), where I_0 is initial current), which was taken as the device's response.

3.6 References

(1) Tang, R.; Shi, Y.; Hou, Z.; Wei, L. Carbon Nanotube-Based Chemiresistive Sensors. *Sensors* **2017**, *17*, 882.
(2) Star, A.; Gabriel, J.-C. P.; Bradley, K.; Grüner, G. Electronic Detection of Specific Protein Binding Using Nanotube FET Devices. *Nano Lett.* **2003**, *4*, 459–463.
(3) Shim, M.; Javey, A.; Kam, N. W. S.; Dai, H. Polymer functionalization for air-stable n-type carbon nanotube field-effect transistors. *J. Am. Chem. Soc.* **2001**, *123*, 11512–11513.
(4) Schnorr, J. M.; Swager, T. M. Emerging Applications of Carbon Nanotubes. *Chem. Mater.* **2011**, *23*, 646–657.
(5) Esser, B.; Schnorr, J. M.; Swager, T. M. Selective detection of ethylene gas using carbon nanotube-based devices: Utility in determination of fruit ripeness. *Angew. Chemie - Int. Ed.* **2012**, *51*, 5752–5756.
(6) Mirica, K. A.; Weis, J. G.; Schnorr, J. M.; Esser, B.; Swager, T. M. Mechanical Drawing of Gas Sensors on Paper. *Angew. Chemie Int. Ed.* **2012**, *51*, 10740–10745.
(7) Frazier, K. M.; Swager, T. M. Robust cyclohexanone selective chemiresistors based on

single-walled carbon nanotubes. *Anal. Chem.* **2013**, *85*, 7154–7158.
(8) Wang, F.; Yang, Y.; Swager, T. M. Molecular recognition for high selectivity in carbon nanotube/polythiophene chemiresistors. *Angew. Chem. Int. Ed. Engl.* **2008**, *47*, 8394–8396.
(9) Fennell, J.; Hamaguchi, H.; Yoon, B.; Swager, T. Chemiresistor Devices for Chemical Warfare Agent Detection Based on Polymer Wrapped Single-Walled Carbon Nanotubes. *Sensors 2017, Vol. 17,* **2017**, *17*, 982.
(10) Ding, M.; Star, A. Selecting fruits with carbon nanotube sensors. *Angew. Chem. Int. Ed. Engl.* **2012**, *51*, 7637–7638.
(11) Liu, S. F.; Petty, A. R.; Sazama, G. T.; Swager, T. M. Single-walled carbon nanotube/metalloporphyrin composites for the chemiresistive detection of amines and meat spoilage. *Angew. Chem. Int. Ed. Engl.* **2015**, *54*, 6554–6557.
(12) Fennell, J. F.; Liu, S. F.; Azzarelli, J. M.; Weis, J. G.; Rochat, S.; Mirica, K. A.; Ravnsbaek, J. B.; Swager, T. M. Nanowire Chemical/Biological Sensors: Status and a Roadmap for the Future. *Angew. Chemie Int. Ed.* **2016**, *55*, 1266–1281.
(13) Samanta, S. K.; Fritsch, M.; Scherf, U.; Gomulya, W.; Bisri, S. Z.; Loi, M. A. Conjugated polymer-Assisted dispersion of single-wall carbon nanotubes: The power of polymer wrapping. *Acc. Chem. Res.* **2014**, *47*, 2446–2456.
(14) Ishihara, S.; Azzarelli, J. M.; Krikorian, M.; Swager, T. M. Ultratrace Detection of Toxic Chemicals: Triggered Disassembly of Supramolecular Nanotube Wrappers. *J. Am. Chem. Soc.* **2016**, *138*, 8221–8227.
(15) Rice, N. A.; Adronov, A. Supramolecular Interactions of High Molecular Weight Poly(2,7-carbazole)s with Single-Walled Carbon Nanotubes. *Macromolecules* **2013**, *46*, 3850–3860.
(16) Imin, P.; Imit, M.; Adronov, A. Supramolecular Functionalization of Single-Walled Carbon Nanotubes (SWNTs) with Dithieno[3,2- b :2′,3′- d]pyrrole (DTP) Containing Conjugated Polymers. *Macromolecules* **2011**, *44*, 9138–9145.
(17) Yoon, B.; Liu, S. F.; Swager, T. M. Surface-Anchored Poly(4-vinylpyridine)–Single-Walled Carbon Nanotube–Metal Composites for Gas Detection. *Chem. Mater.* **2016**, *28*, 5916–5924.
(18) Fréchet, J. M. J.; de Meftahi, M. V. Poly(vinyl pyridine)s: Simple reactive polymers with multiple applications. *Br. Polym. J.* **1984**, *16*, 193–198.
(19) Mirica, K. A.; Azzarelli, J. M.; Weis, J. G.; Schnorr, J. M.; Swager, T. M. Rapid prototyping of carbon-based chemiresistive gas sensors on paper. *Proc. Natl. Acad. Sci. U. S. A.* **2013**, *110*, 3265-70.
(20) Frazier, K. M.; Mirica, K. A.; Walish, J. J.; Swager, T. M. Fully-drawn carbon-based chemical sensors on organic and inorganic surfaces. *Lab Chip.* **2014**, *14*, 4059–4066.
(21) Wietelmann, U.; Steinbild, M. *Ullmann's Encyclopedia of Industrial Chemistry*; Wiley-VCH Verlag GmbH & Co. KGaA: Weinheim, Germany, 2000.
(22) Fowles, J.; Mitchell, J.; McGrath, H. Assessment of cancer risk from ethylene oxide residues in spices imported into New Zealand. *Food Chem. Toxicol.* **2001**, *39*, 1055–1062.
(23) Wesley, F.; Rourke, B.; Darbshire, O. The Formation of Persistent Toxic Chlorohydrins in Foodstuffs by Fumigation with Ethylene Oxide and with Propylene Oxide. *J. Food Sci.* **1965**, *30*, 1037–1042.
(24) Mendes, G. C. C.; Brandão, T. R. S.; Silva, C. L. M. Ethylene oxide sterilization of medical devices: A review. *American Journal of Infection Control*, 2007, *35*, 574–581.
(25) Ethrenberg, L.; Hiesche, K. D.; Osterman-Golkar, S.; Wennberg, I. Evaluation of genetic risks of alkylating agents: Tissue doses in the mouse from air contaminated with ethylene oxide. *Mutat. Res. - Fundam. Mol. Mech. Mutagen.* **1974**, *24*, 83–103.

(26) Thier, R.; Bolt, H. M. Carcinogenicity and genotoxicity of ethylene oxide: new aspects and recent advances. *Crit. Rev. Toxicol.* **2000**, *30*, 595–608.
(27) Wang, Q.-Q.; Begum, R. A.; Day, V. W.; Bowman-James, K. Sulfur, oxygen, and nitrogen mustards: stability and reactivity. *Org. Biomol. Chem.* **2012**, *10*, 8786.
(28) Shakarjian, M. P.; Heck, D. E.; Gray, J. P.; Sinko, P. J.; Gordon, M. K.; Casillas, R. P.; Heindel, N. D.; Gerecke, D. R.; Laskin, D. L.; Laskin, J. D. Mechanisms mediating the vesicant actions of sulfur mustard after cutaneous exposure. *Toxicol. Sci.* **2010**, *114*, 5–19.
(29) Hosseini-khalili, A.; Haines, D. D.; Modirian, E.; Soroush, M.; Khateri, S.; Joshi, R.; Zendehdel, K.; Ghanei, M.; Giardina, C. Mustard gas exposure and carcinogenesis of lung. *Mutat. Res. - Genet. Toxicol. Environ. Mutagen.* **2009**, *678*, 1–6.
(30) Aasted, A.; Darre, E.; Wulf, H. C. Mustard gas: clinical, toxicological, and mutagenic aspects based on modern experience. *Ann. Plast. Surg.* **1987**, *19*, 330–333.
(31) O'Connell, M. J.; Bachilo, S. M.; Huffman, C. B.; Moore, V. C.; Strano, M. S.; Haroz, E. H.; Rialon, K. L.; Boul, P. J.; Noon, W. H.; Kittrell, C.; et al. Band Gap Fluorescence from Individual Single-Walled Carbon Nanotubes. *Science.*. **2002**, *297*, 593-596.
(32) Naumov, A. V; Ghosh, S.; Tsyboulski, D. A.; Bachilo, S. M.; Weisman, R. B. Analyzing absorption backgrounds in single-walled carbon nanotube spectra. *ACS Nano* **2011**, *5*, 1639–1648.
(33) Viscarra Rossel, R. A.; Walvoort, D. J. J.; McBratney, A. B.; Janik, L. J.; Skjemstad, J. O. Visible, near infrared, mid infrared or combined diffuse reflectance spectroscopy for simultaneous assessment of various soil properties. *Geoderma* **2006**, *131*, 59–75.
(34) Büning-Pfaue, H. Analysis of water in food by near infrared spectroscopy. In *Food Chemistry*; 2003; Vol. 82, pp 107–115.
(35) Tu, X.; Manohar, S.; Jagota, A.; Zheng, M. DNA sequence motifs for structure-specific recognition and separation of carbon nanotubes. *Nature* **2009**, *460*, 250–253.
(36) Jorio, A.; Saito, R.; Dresselhaus, G.; Dresselhaus, M. S. *Raman Spectroscopy in Graphene Related Systems*; Wiley-VCH Verlag GmbH & Co. KGaA: Weinheim, Germany, 2011.
(37) Bergin, S. D.; Sun, Z.; Streich, P.; Hamilton, J.; Coleman, J. N. New solvents for nanotubes: Approaching the dispersibility of surfactants. *J. Phys. Chem. C* **2010**, *114*, 231–237.
(38) Fong, D.; Bodnaryk, W. J.; Rice, N. A.; Saem, S.; Moran-Mirabal, J. M.; Adronov, A. Influence of Polymer Electronics on Selective Dispersion of Single-Walled Carbon Nanotubes. *Chem. - A Eur. J.* **2016**, *22*, 14560–14566.
(39) Belfiore, L. A.; Pires, A. T. N.; Wang, Y.; Graham, H.; Ueda, E. Transition-metal coordination in polymer blends and model systems. *Macromolecules* **1992**, *25*, 1411–1419.
(40) Handy, P. R.; Popov, A. I. Spectroscopic studies of ionic solvation-XII. Ionic solvation in pyridine and substituted pyridine solutions. *Spectrochim. Acta Part A Mol. Spectrosc.* **1972**, *28*, 1545–1553.
(41) Ammu, S.; Dua, V.; Agnihotra, S. R.; Surwade, S. P.; Phulgirkar, A.; Patel, S.; Manohar, S. K. Flexible, all-organic chemiresistor for detecting chemically aggressive vapors. *J. Am. Chem. Soc.* **2012**, *134*, 4553–4556.
(42) National Institute for Occupational Safety and Health. CDC - NIOSH Pocket Guide to Chemical Hazards - Ethylene oxide https://www.cdc.gov/niosh/npg/npgd0275.html (accessed May 9, 2017).
(43) National Institute for Occupational Safety and Health. CDC - The Emergency Response Safety and Health Database: Blister Agent: Sulfur Mustard - NIOSH https://www.cdc.gov/niosh/ershdb/emergencyresponsecard_29750008.html (accessed May 9,

2017).
(44) Beer, P. D.; Gale, P. A. Anion recognition and sensing: the state of the art and future perspectives. *Angew. Chemie, Int. Ed.* **2001**, *40*, 486–516.
(45) Langton, M. J.; Serpell, C. J.; Beer, P. D. Anion recognition in water: Recent advances from a supramolecular and macromolecular perspective. *Angewandte Chemie - International Edition*, 2016, *55*, 1974–1987.
(46) Beer, P. D.; Gale, P. A.; Chen, G. Z. Mechanisms of electrochemical recognition of cations, anions and neutral guest species by redox-active receptor molecules. *Coord. Chem. Rev.* **1999**, *185–186*, 3–36.
(47) Hudson, R. D. A. Ferrocene polymers: current architectures, syntheses and utility. *J. Organomet. Chem.* **2001**, *637*, 47–69.
(48) Mao, X.; Rutledge, G. C.; Hatton, T. A. Polyvinylferrocene for noncovalent dispersion and redox-controlled precipitation of carbon nanotubes in nonaqueous media. *Langmuir* **2013**, *29*, 9626–9634.
(49) George, M. H.; Hayes, G. F. Free-radical polymerization of vinylferrocene. I. Kinetics. *J. Polym. Sci. Polym. Chem. Ed.* **1975**, *13*, 1049–1070.
(50) Wiles, A. A.; Zhang, X.; Fitzpatrick, B.; Long, D.-L.; Macgregor, S. A.; Cooke, G.; Balzani, V.; Becher, J.; Credi, A.; Nielsen, M. B. Redox-mediated reactions of vinylferrocene: toward redox auxiliaries. *Dalt. Trans.* **2016**, *45*, 7220–7225.

3.7 Appendix

Chapter 3: Chemiresistive Detection of Ethylene Oxide and Mustard Gas: Poly(vinylpyridine)/Single Walled Carbon Nanotube Composites

Figure A.3.1 1H-NMR of poly(4-vinylpyridine) taken in $CDCl_3$ on a JEOL 502MHz NMR.

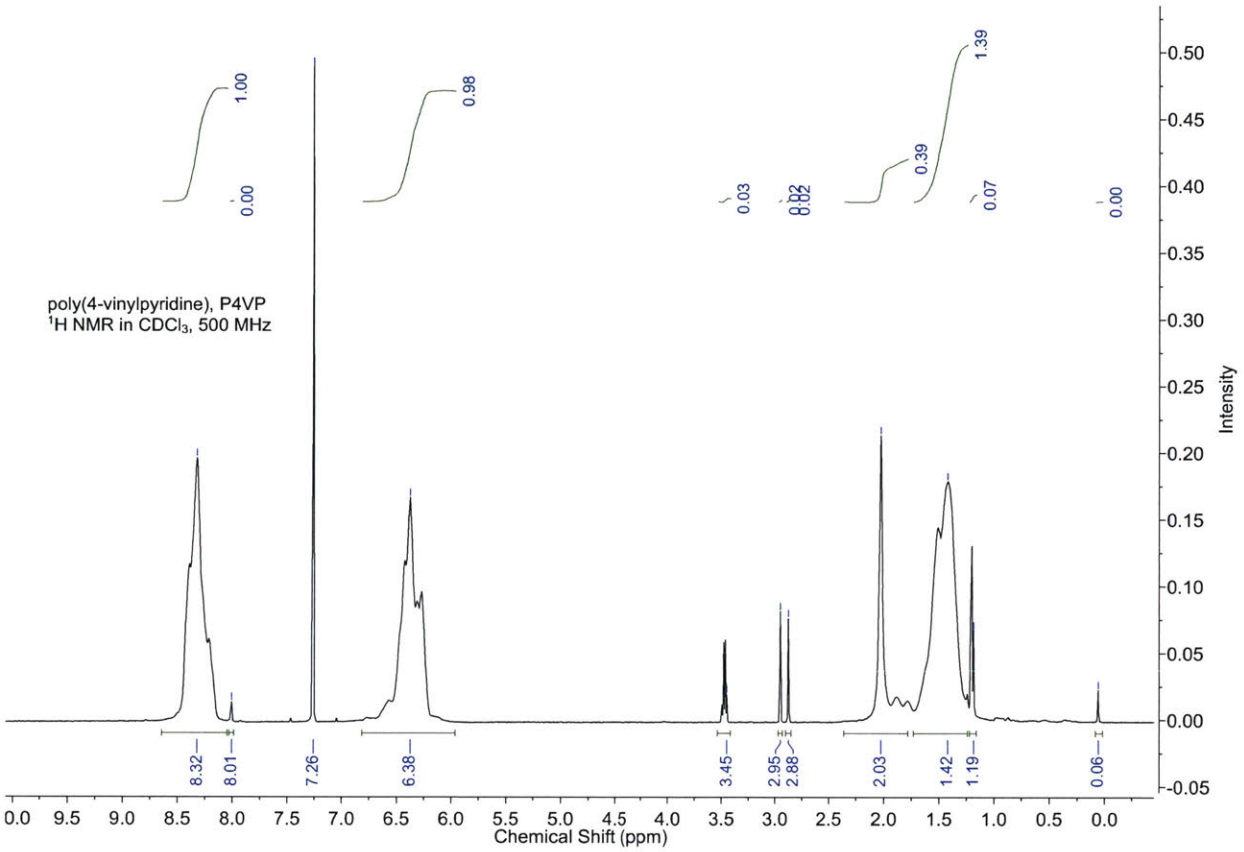

Figure A.3.2 1H-NMR of poly(4-vinylpyridine-*co*-vinylferrocene) taken in $CDCl_3$ on a JEOL 502MHz NMR. 9% mole percent loading of vinyl ferrocene into the free radical polymerization.

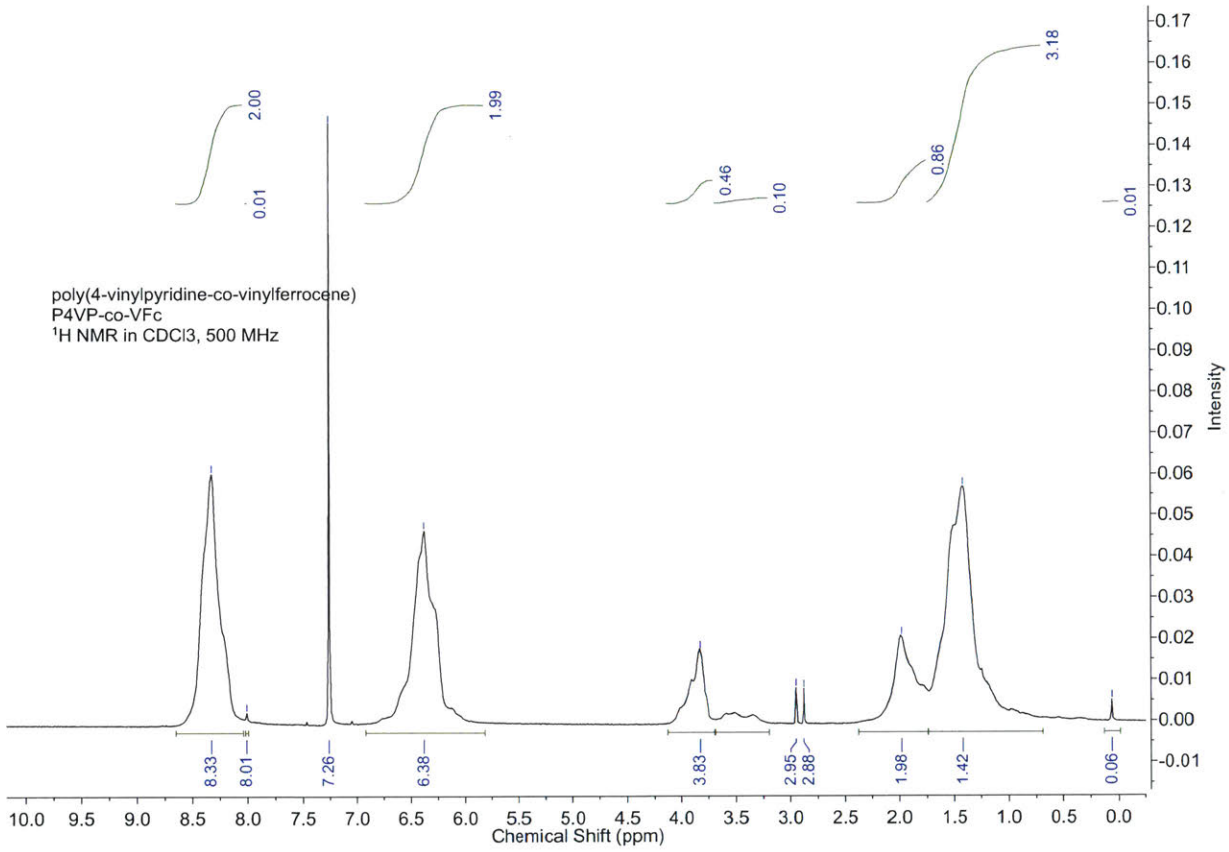

Figure A.3.3 1H-NMR of poly(4-vinylpyridine-*co*-ferrocenylmethylmethacrylate) taken in $CDCl_3$ on a JEOL 502MHz NMR. 9% mole percent loading of vinyl ferrocene into the free radical polymerization.

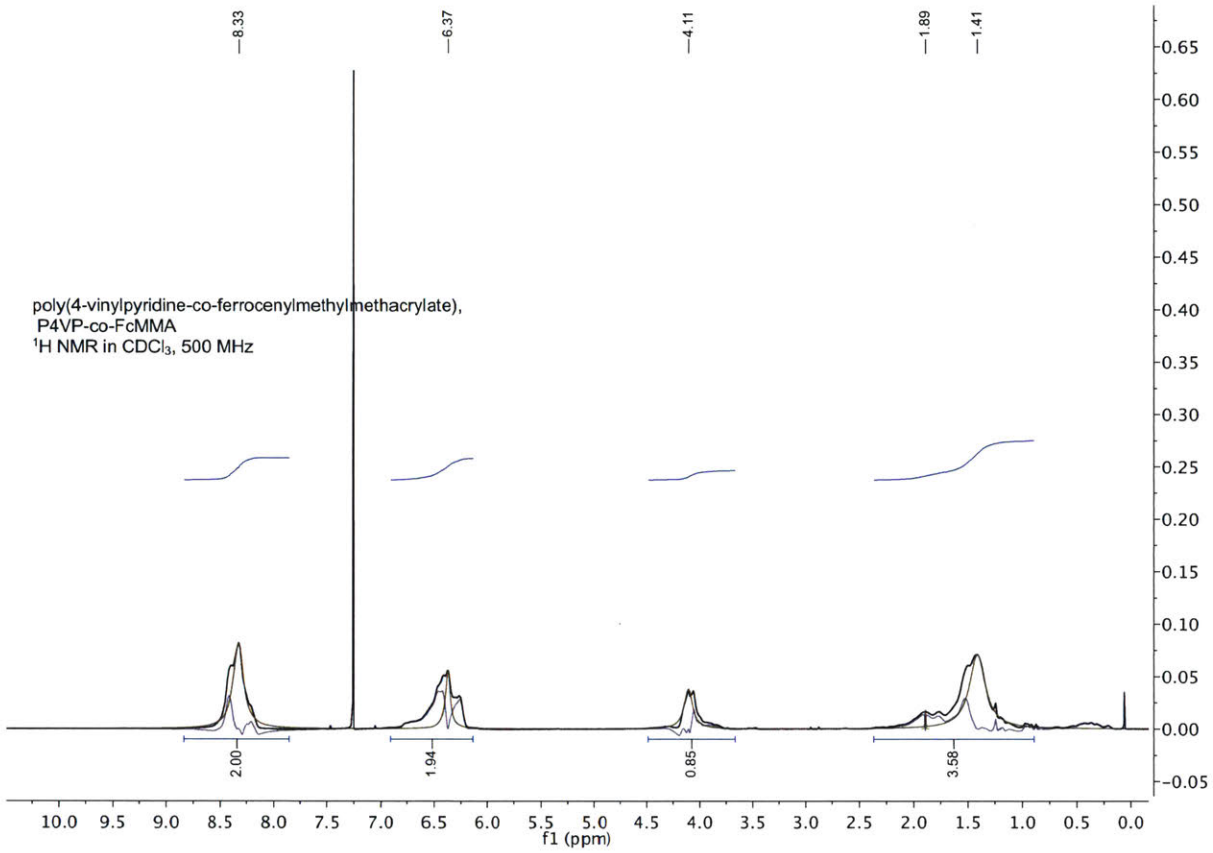

Figure A.3.4 Gel permeation chromatogram of P4VP (M_n = 57.8 kDa ; M Đ=3.1); P4VP-*co*-VFC (M_n = 60.5 kDa ; M Đ=3.84); P4VP-*co*-FcMMA (M_n = 11.8 kDa ; M Đ=1.75).

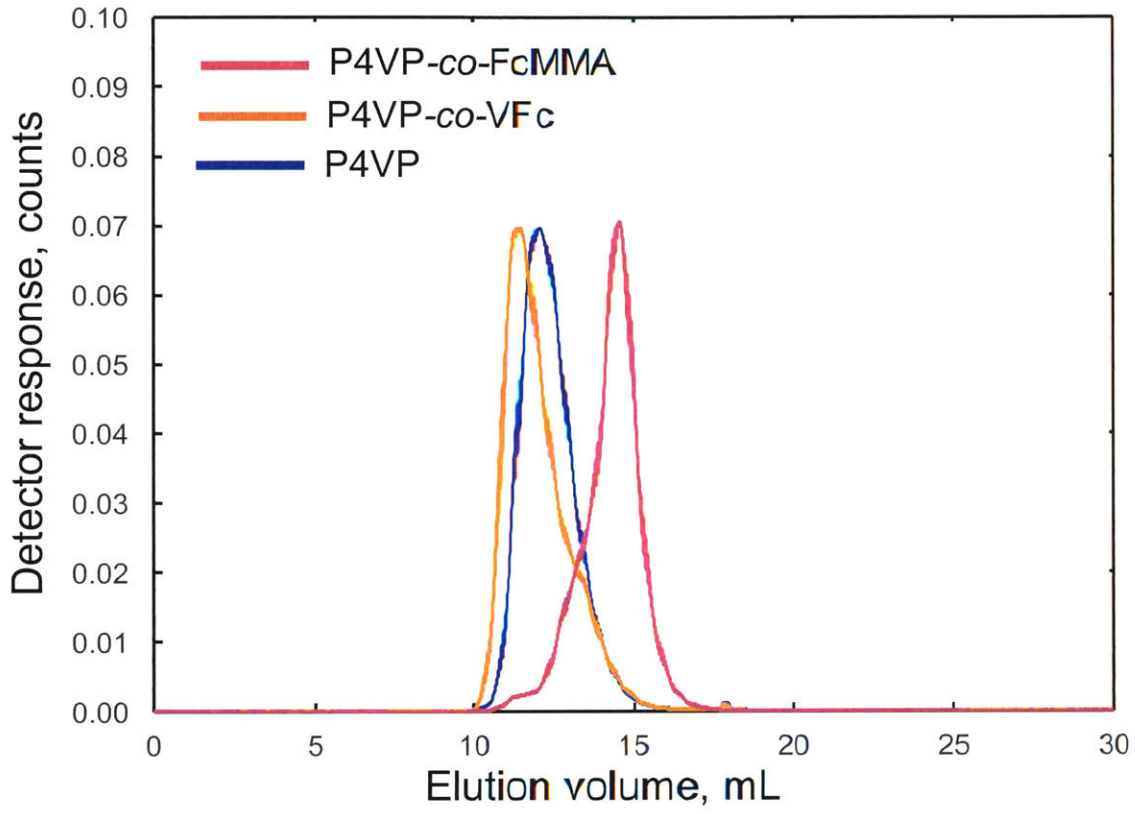

Figure A.3.5 Resonance Raman spectra of pristine-SWCNT (black); a P4VP-SWCNT composite (purple); a P4VP/SWCNT/LiBr composite (green). Measurements were taken at a 633 nm excitation wavelength. Samples were drop casted on a Si wafer with a 120 nm SiO_2.

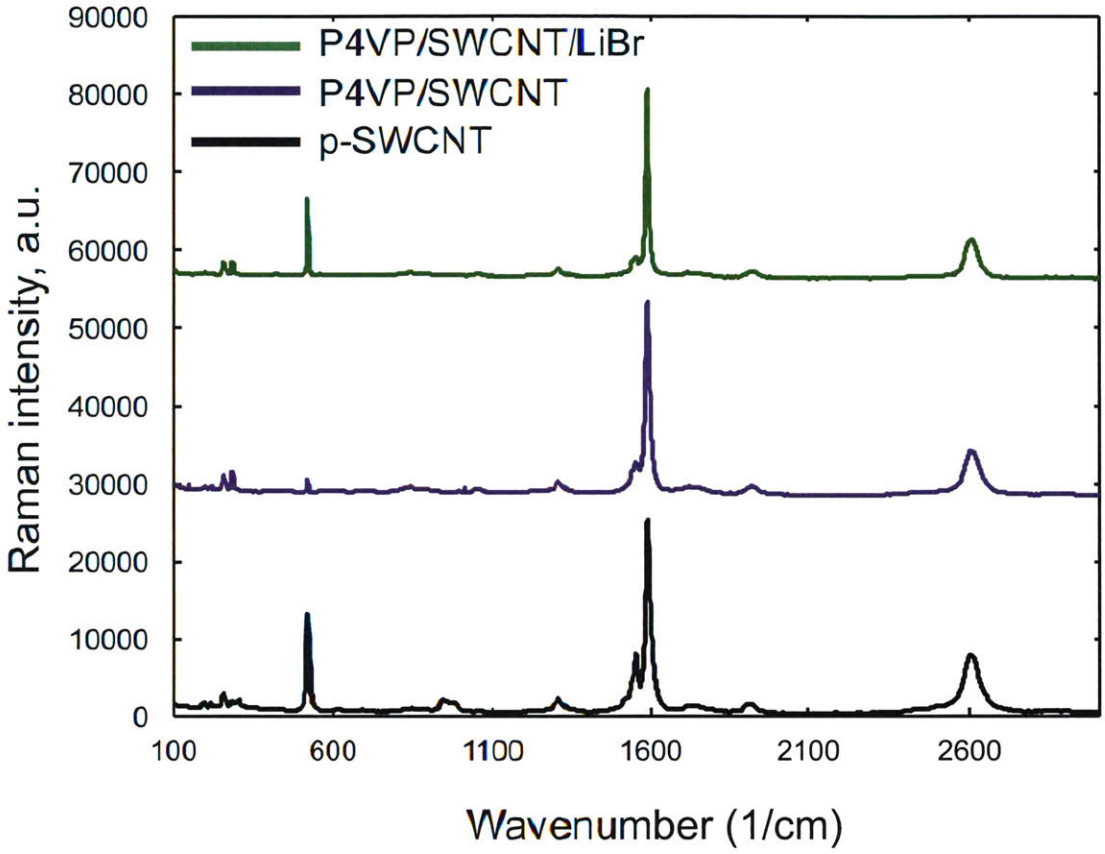

Figure A.3.6 Chemiresistive traces of the responses of various additives (10 v/v % additive) in P4VP/SWCNT dispersion in DMF. Concentration of additives was 4 mg/mL in DMF.

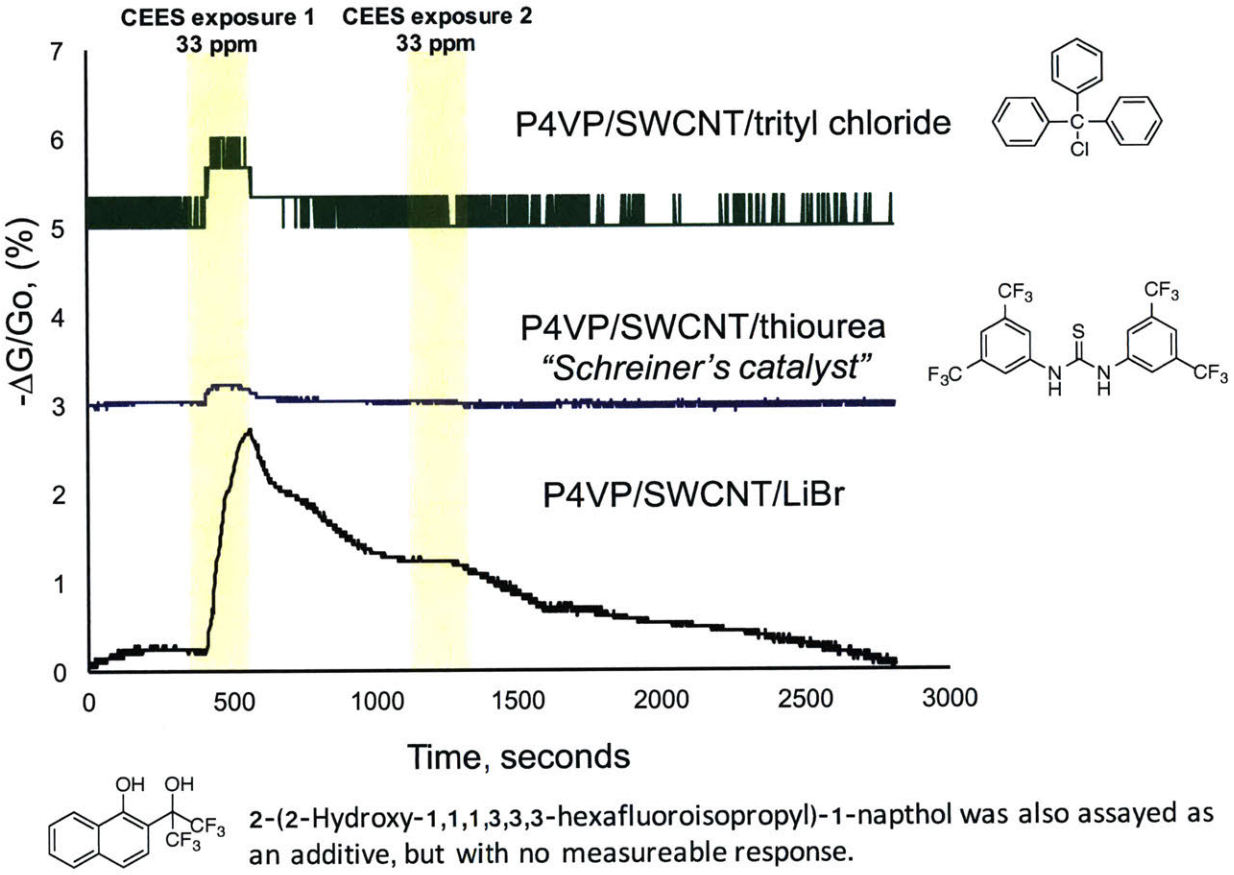

2-(2-Hydroxy-1,1,1,3,3,3-hexafluoroisopropyl)-1-napthol was also assayed as an additive, but with no measureable response.

Figure A.3.7 FTIR-ATR spectra of P4VP only (blue); a P4VP-SWCNT composite (purple); a P4VP/SWCNT/LiBr composite (green).

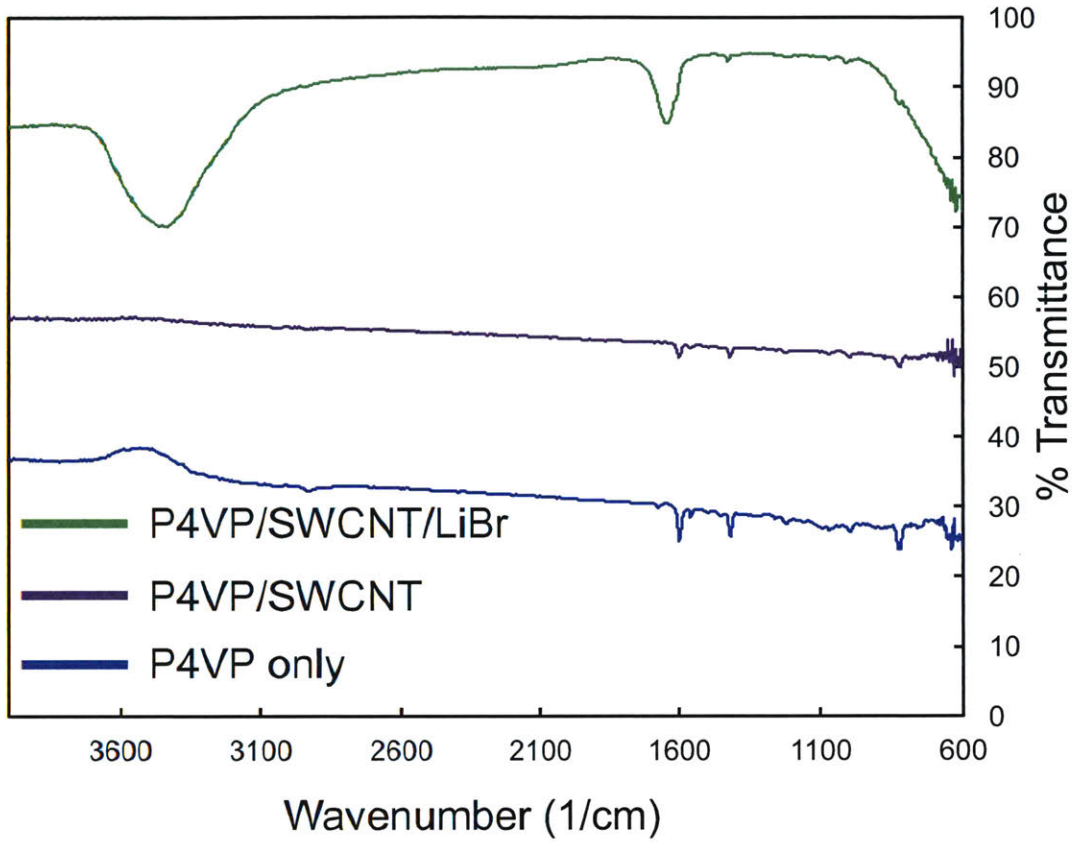

Figure A.3.8 FTIR-ATR spectra of P4VP.

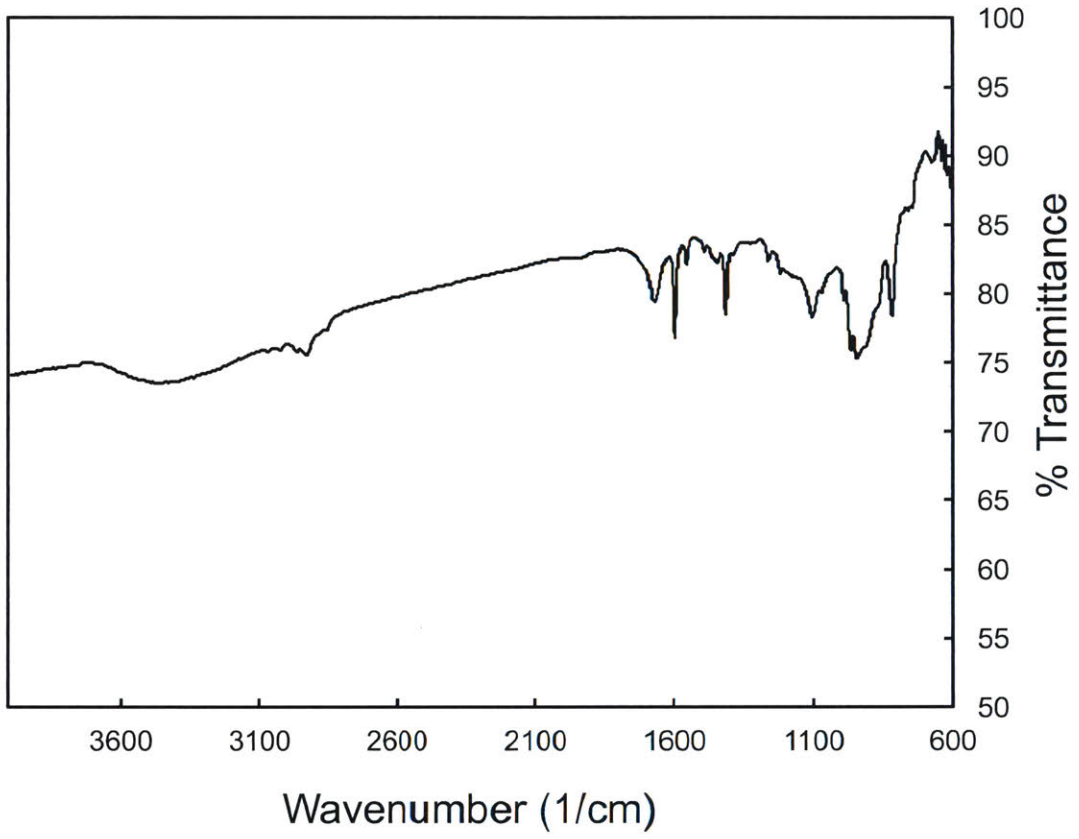

Figure A.3.9 FTIR-ATR spectra of P4VP-*co*-VFc.

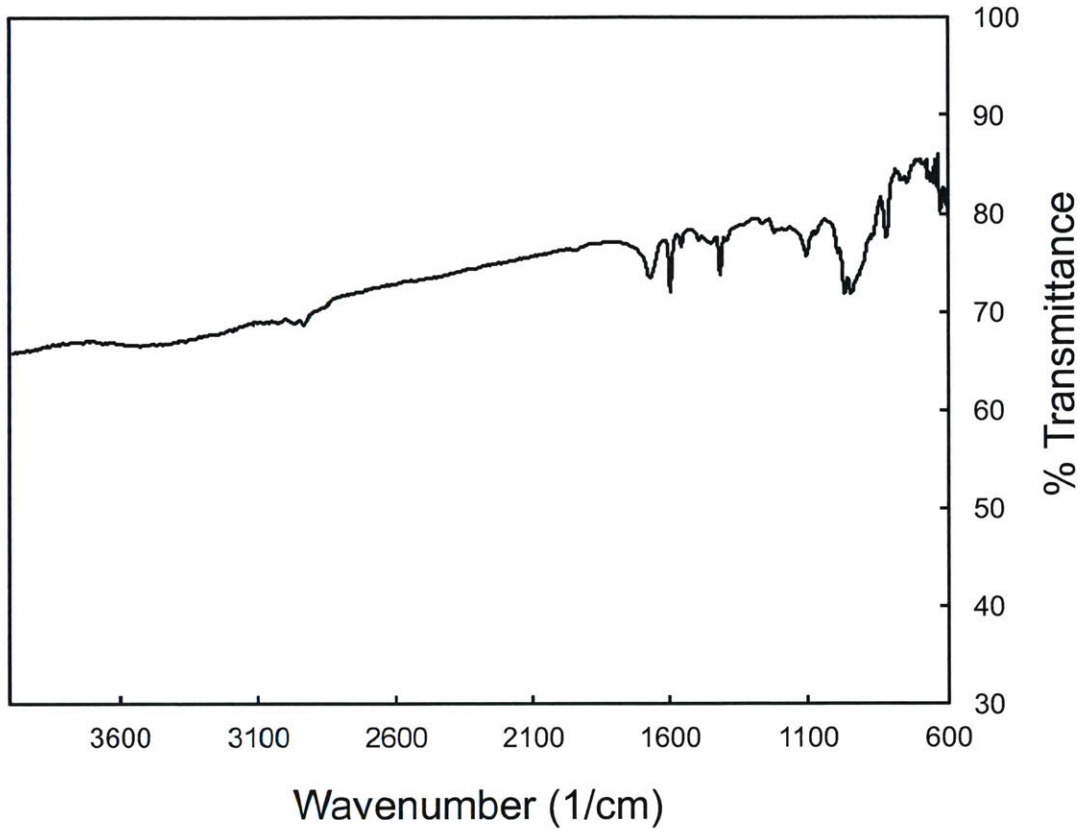

Figure A.3.10 FTIR-ATR spectra of P4VP-*co*-FcMMMA.

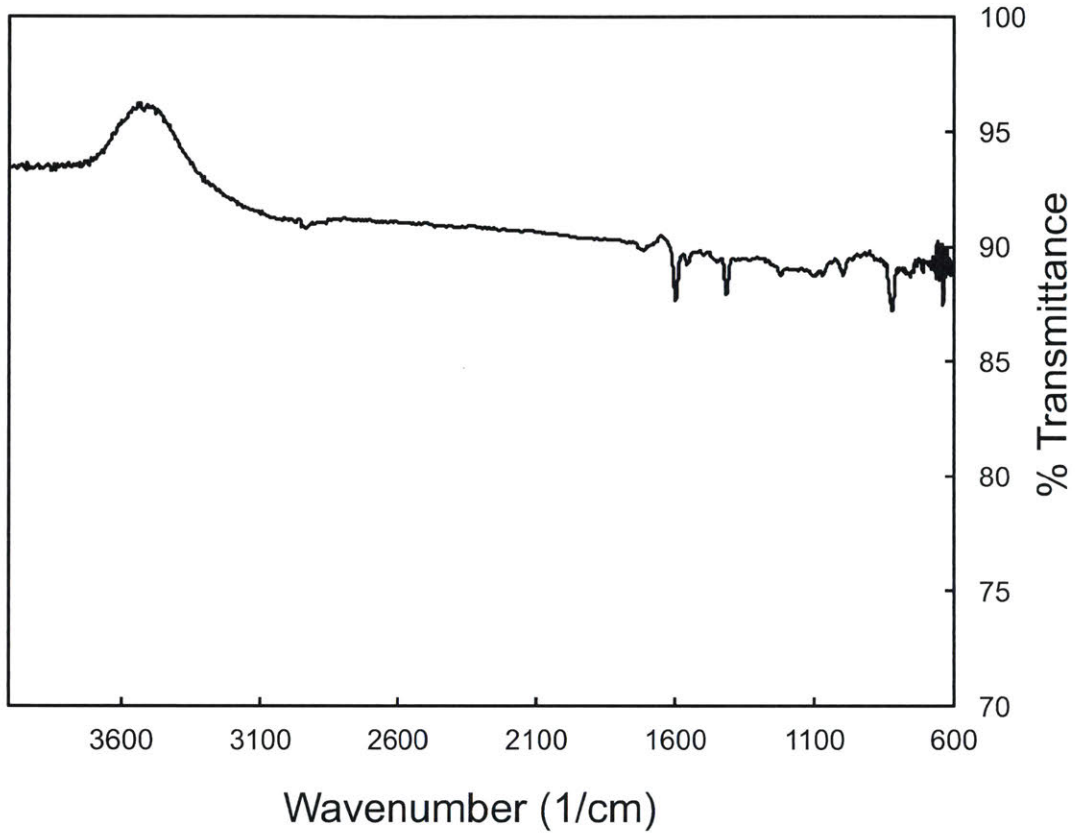

Figure A.3.11 Thermogravimetric analysis of P4VP.

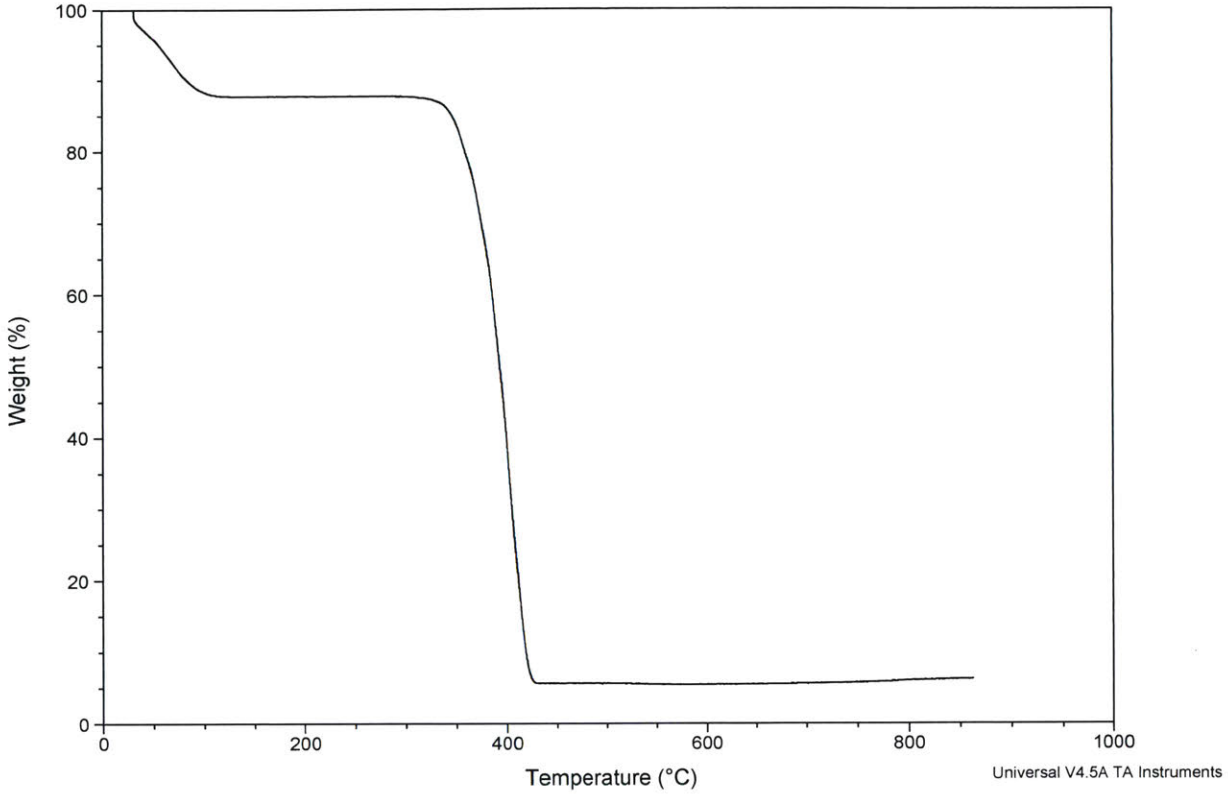

Figure A.3.12 Thermogravimetric analysis of P4VP-*co*-VFC.

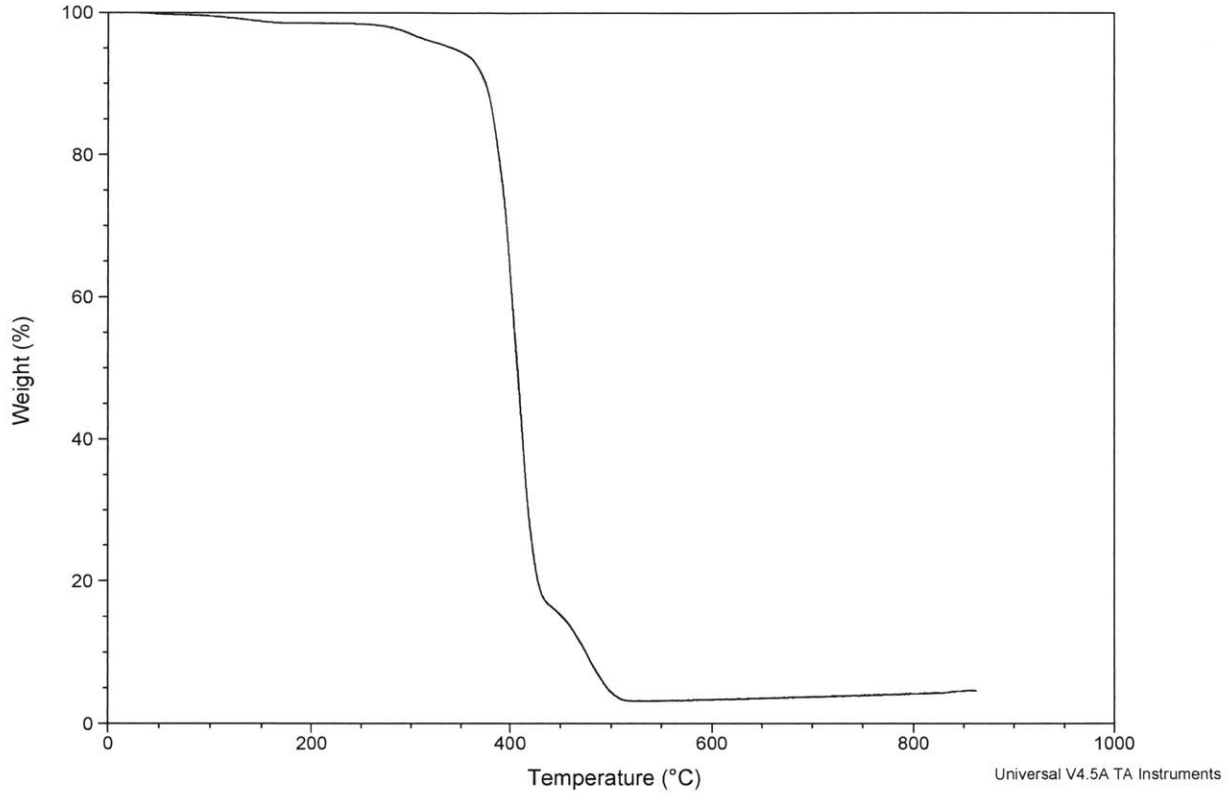

Figure A.3.13 Thermogravimetric analysis of P4VP-*co*-FcMMA

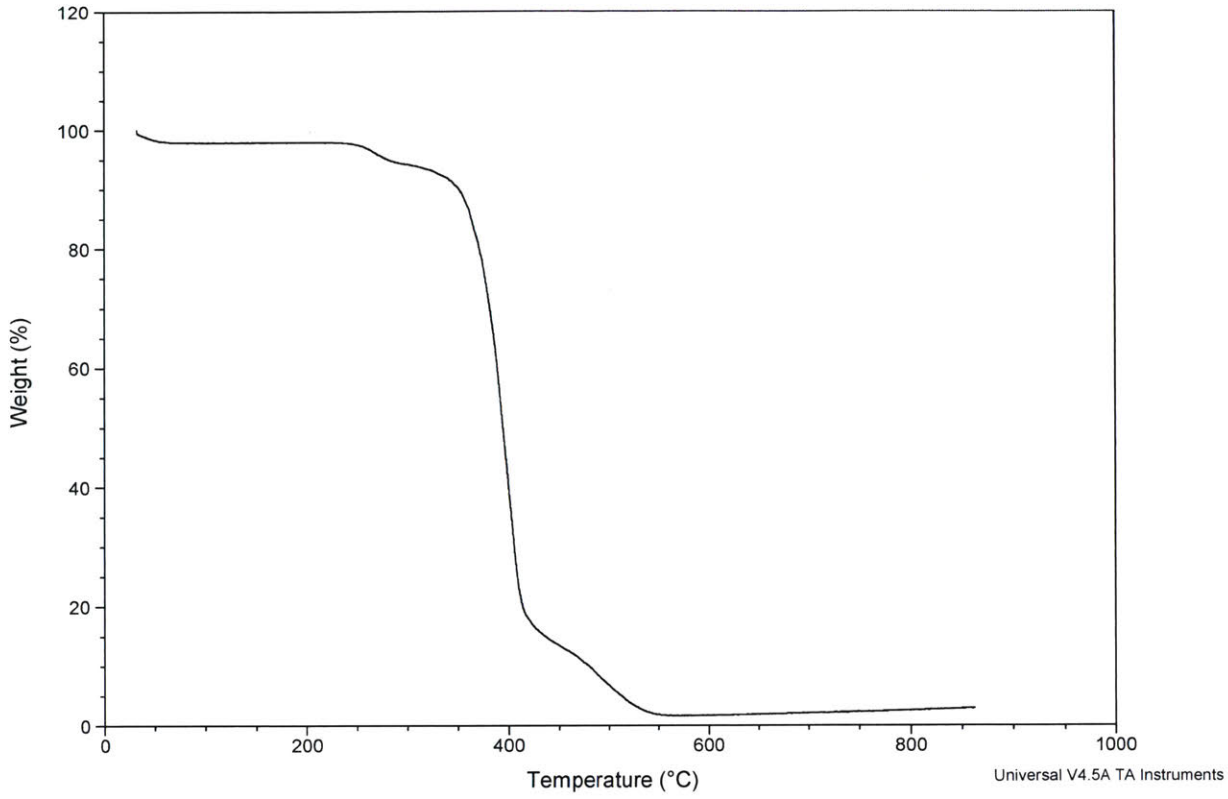

Table A.3.1 Table listing the average chemiresistive responses, their standard deviations and response ratio. This data is charted in Figure 3.8 (a, b).

Average Response	THF	Benzene	EtOAc	Acetonitrile	CHCl3	Hexanes	Acetone	CEES	Ethylene oxide
P4VP/SWCNT	0.161	0.095333333	0.149333333	0.1194	0.160667	0.285	0.206667	0.02	0.015
P4VP/SWCNT/LiBr	0.556667	0.35	0.416666667	0.393333333	0.42	0.253333333	0.373667	0.137	0.2904
Response Standard Deviation	THF	Benzene	Ethyl acetate	Acetonitrile	Chloroform	Hexanes	Acetone	CEES	Ethylene oxide
P4VP/SWCNT	0.064954	0.040375686	0.074224884	0.093654044	0.017673	0.259751805	0.182155	0.006	0.007998
P4VP/SWCNT/LiBr	0.128582	0.105356538	0.105987421	0.125033329	0.095394	0.195021366	0.071347	0.026153394	0.03124
Response ratio	THF	Benzene	Ethyl acetate	Acetonitrile	Chloroform	Hexanes	Acetone	CEES	Ethylene Oxide
Exposure concentration, ppm	655	336	353	463	804	549	2100	33	2048
P4VP/SWCNT	0.25	0.28	0.42	0.26	0.20	0.52	0.10	0.606060606	0.007324219
P4VP/SWCNT/LiBr	0.85	1.04	1.18	0.85	0.52	0.46	0.18	4.15	0.141796875

Figure A.3.14 Cyclic voltammogram of SWCNT deposited on a glassy carbon working electrode from *o*-dichlorobenzene (*o*-DCB). Residual *o*-DCB was removed under reduced pressure. The film was subjected to various scan rates in a 0.10 M solution of KCl. The counter and reference electrodes were platinum Ag/AgCl, respectively.

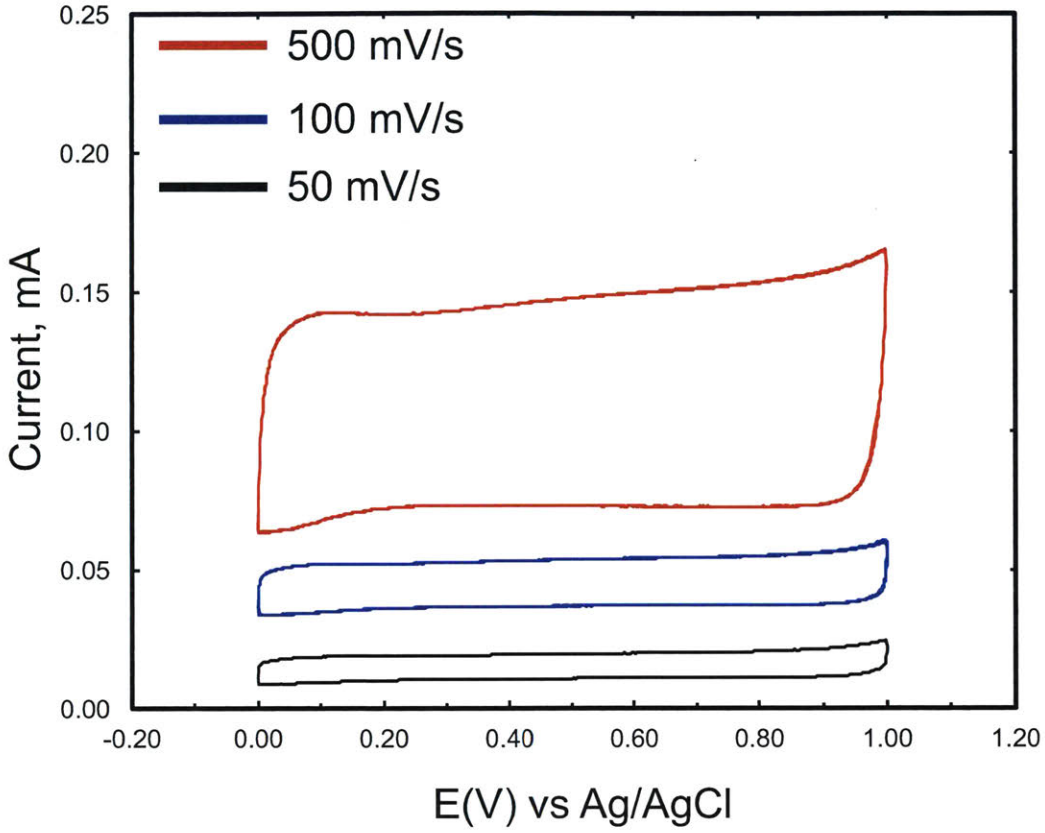

Figure A.3.15 Cyclic voltammogram of P4VP/SWCNT dispersion dropcasted from DMF on a glassy carbon working electrode. Residual DMF was removed via reduced pressure. The film was subjected to various scan rates in a 0.10 M solution of KCl. The counter and reference electrodes were platinum Ag/AgCl, respectively.

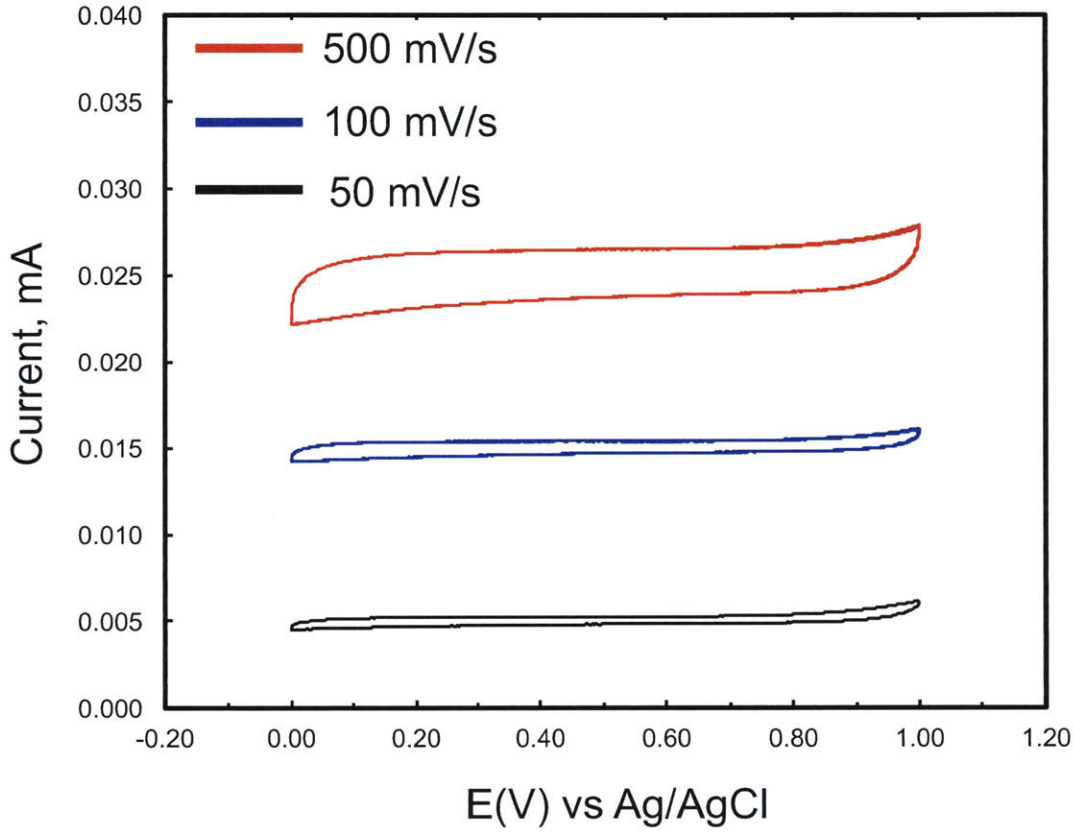

Figure A.3.16 Cyclic voltammogram of P4VP-*co*-VFc/SWCNT dispersion dropcasted from DMF on a glassy carbon working electrode. Residual DMF was removed via reduced pressure. The film was subjected to various scan rates in a 0.10 M solution of KCl. The counter and reference electrodes were platinum Ag/AgCl, respectively.

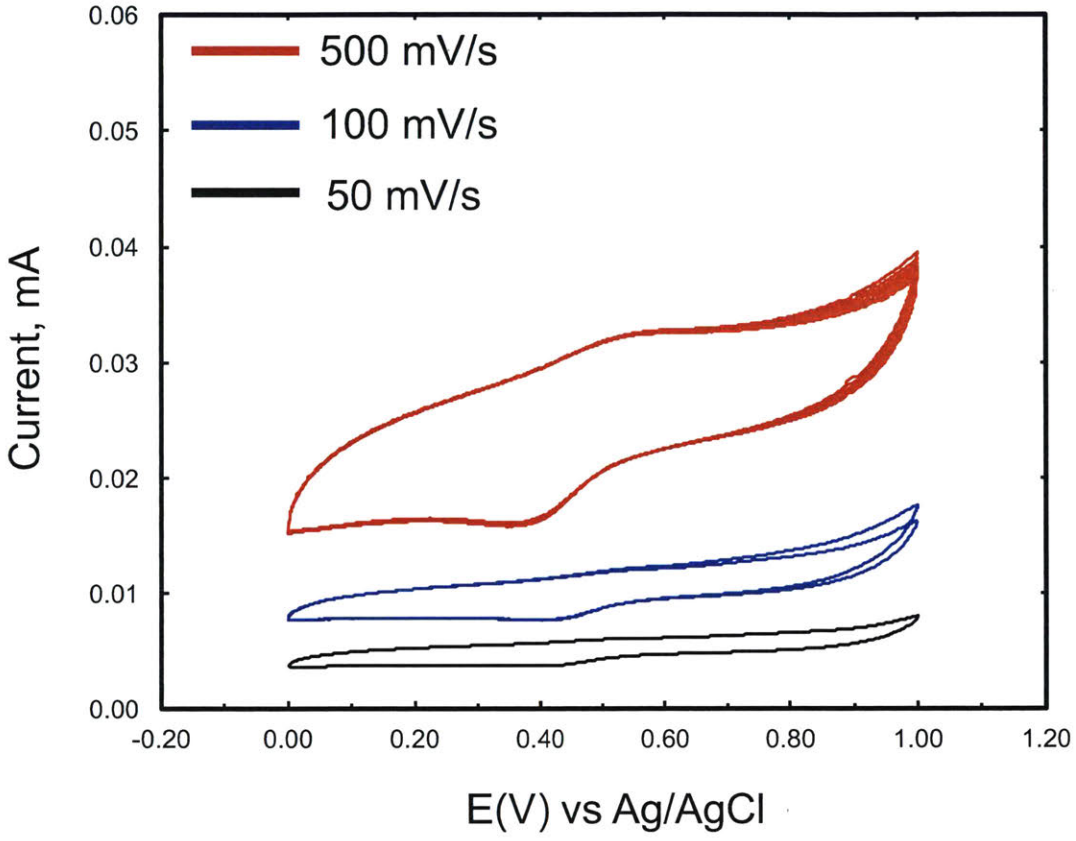

Figure A.3.17 Cyclic voltammogram of P4VP-*co*-FcMMA/SWCNT dispersion dropcasted from DMF on a glassy carbon working electrode. Residual DMF was removed via reduced pressure. The film was subjected to various scan rates in a 0.10 M solution of KCl. The counter and reference electrodes were platinum Ag/AgCl, respectively.

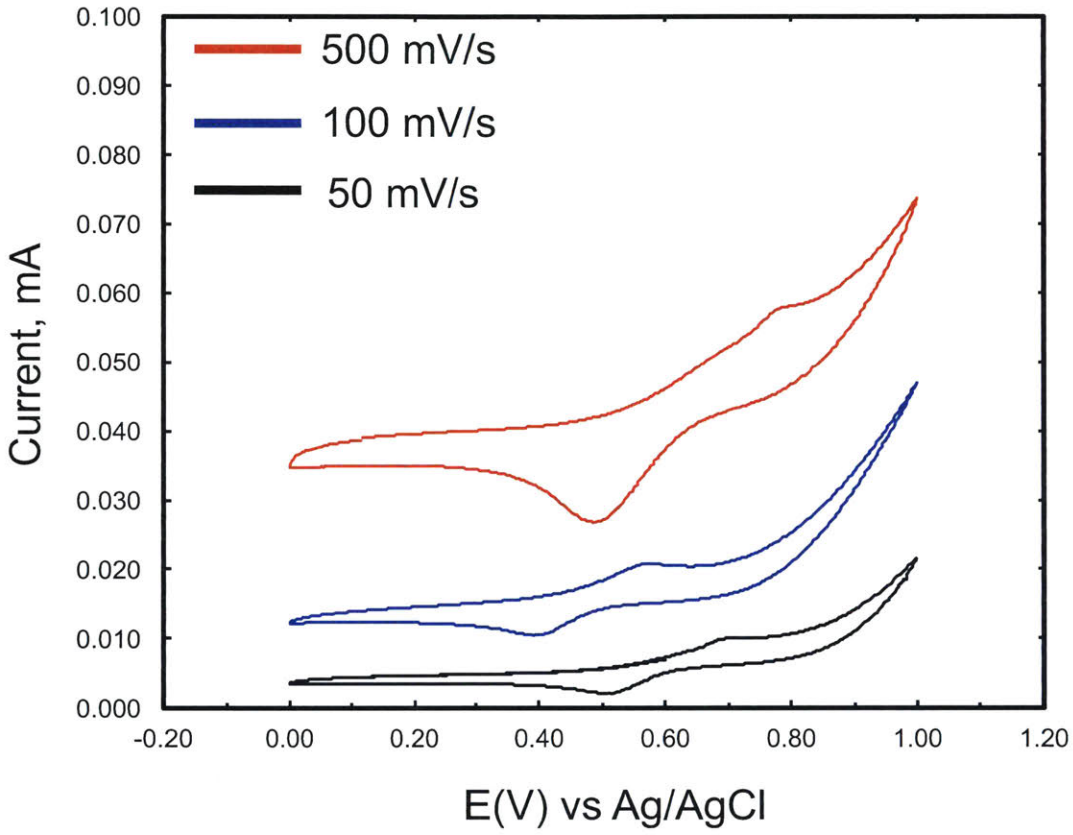

Figure A.3.18 Cyclic voltammogram of P4VP dropcasted from chloroform on a glassy carbon working electrode. Residual chloroform was removed via reduced pressure.
The film was subjected to a 100mV/s scan rate in a 0.10 M solution of KCl. The counter and reference electrodes were platinum Ag/AgCl, respectively.

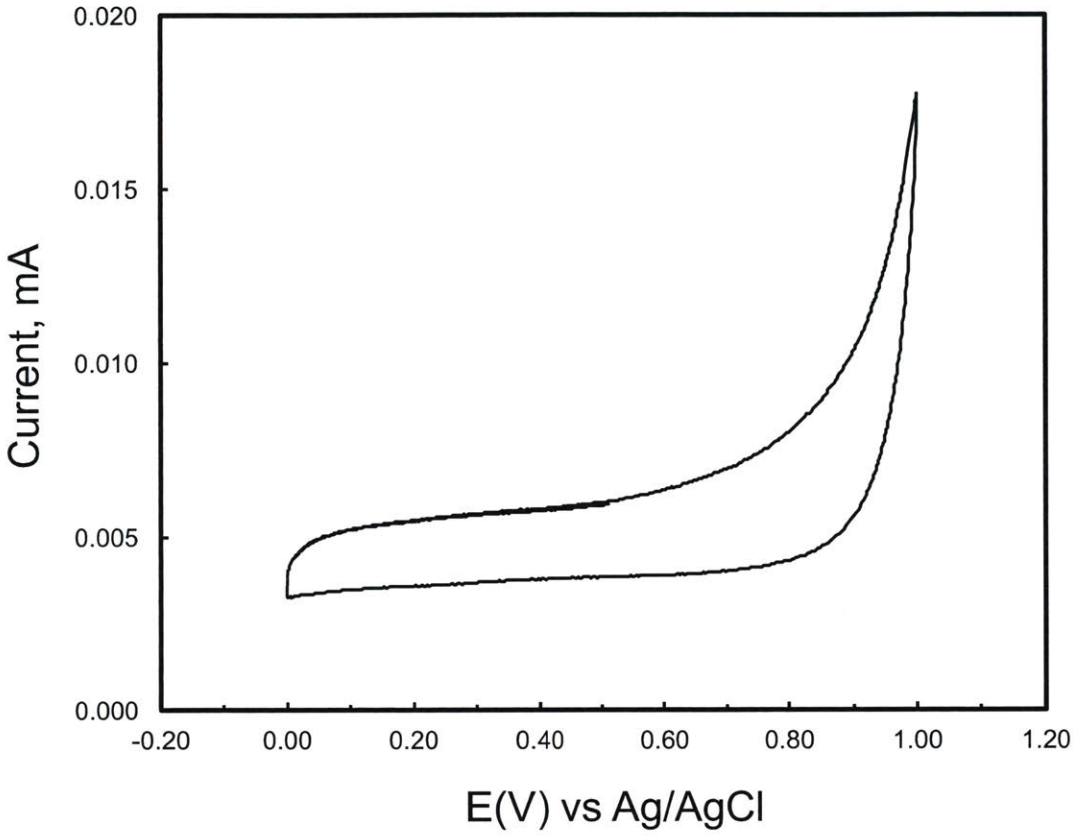

Figure A.3.19 Cyclic voltammogram of P4VP-*co*-VFc dropcasted from chloroform on a glassy carbon working electrode. Residual chloroform was removed via reduced pressure. The film was subjected to a 100mV/s scan ratein a 0.10 M solution of KCl. The counter and reference electrodes were platinum Ag/AgCl, respectively.

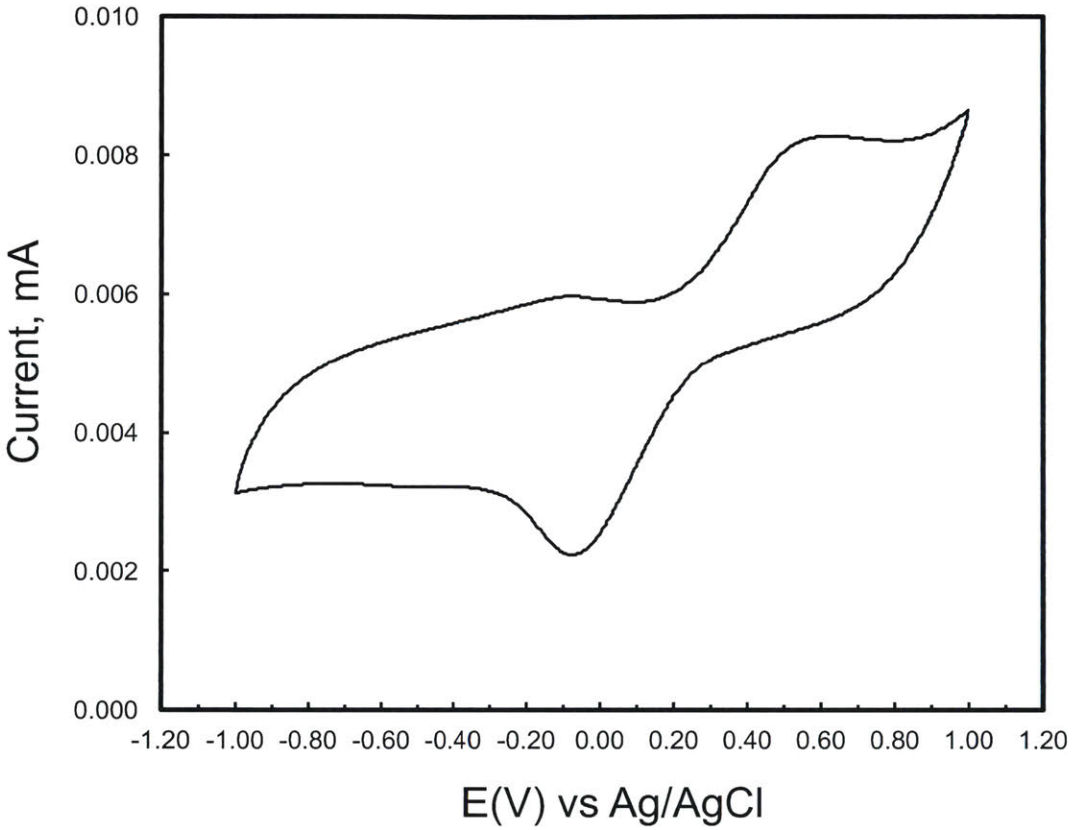

Figure A.3.20 Cyclic voltammogram of P4VP-*co*-FcMMA dropcasted from chloroform on a glassy carbon working electrode. Residual chloroform was removed via reduced pressure. The film was subjected to a 100mV/s scan rate in a 0.10 M solution of KCl. The counter and reference electrodes were platinum Ag/AgCl, respectively.

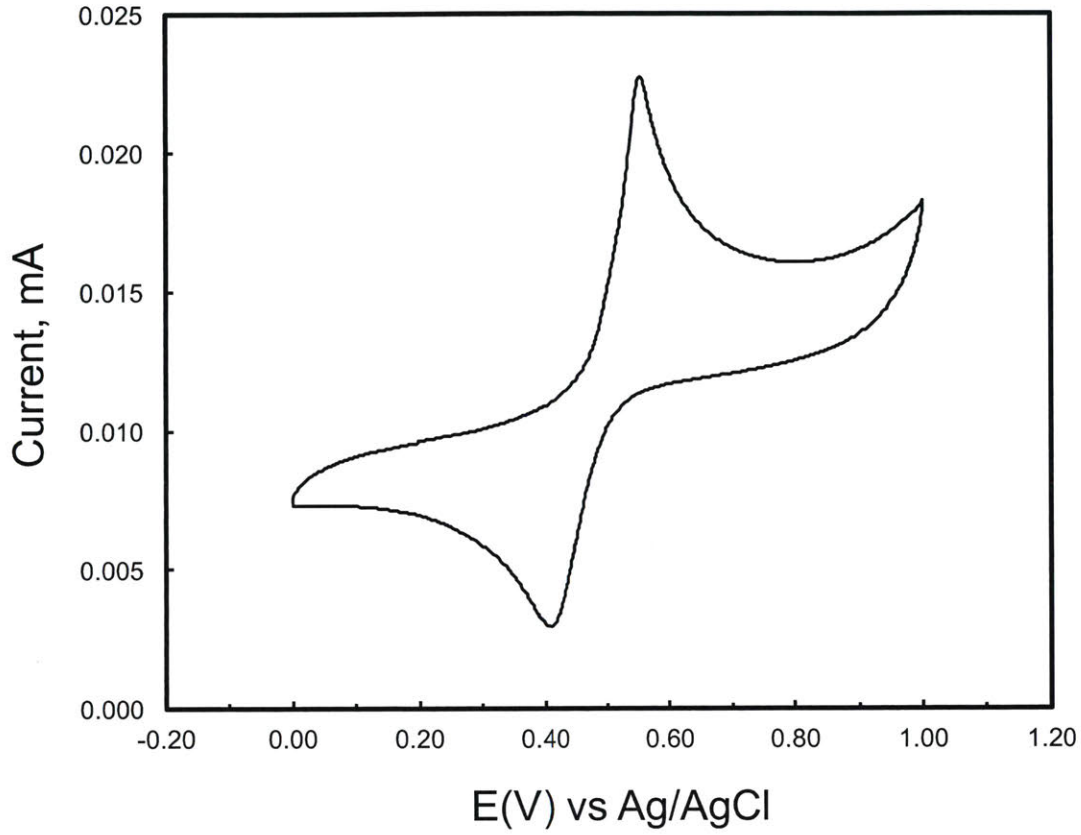

Figure A.3.21 Cyclic voltammogram of P4VP-*co*-VFc dropcasted from chloroform on a glassy carbon working electrode. Residual chloroform was removed via reduced pressure. The film was subjected to a 50 and 100mV/s scan rate in a 0.10 M solution of KCl. The counter and reference electrodes were platinum Ag/AgCl, respectively.

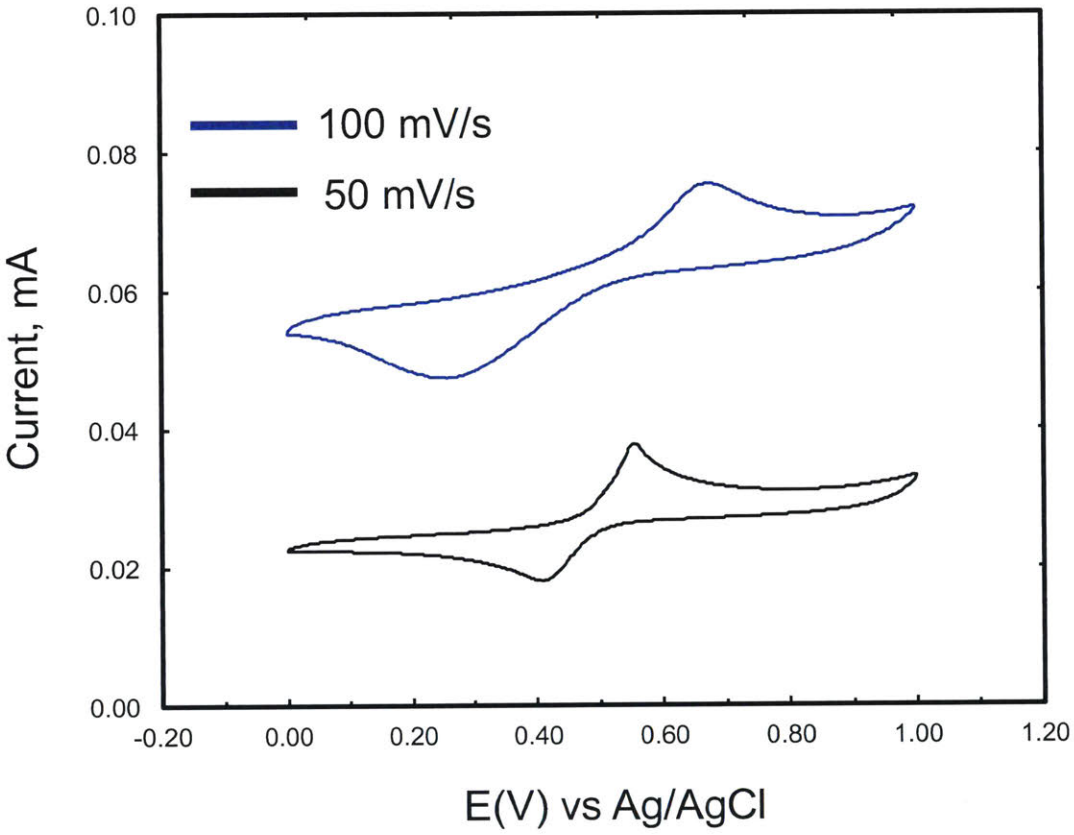

Figure A.3.22 Cyclic voltammogram of P4VP-*co*-FcMMA dropcasted from chloroform on a glassy carbon working electrode. Residual chloroform was removed via reduced pressure. The film was subjected to a 50 and 100mV/s scan rate in a 0.10 M solution of KCl. The counter and reference electrodes were platinum Ag/AgCl, respectively.

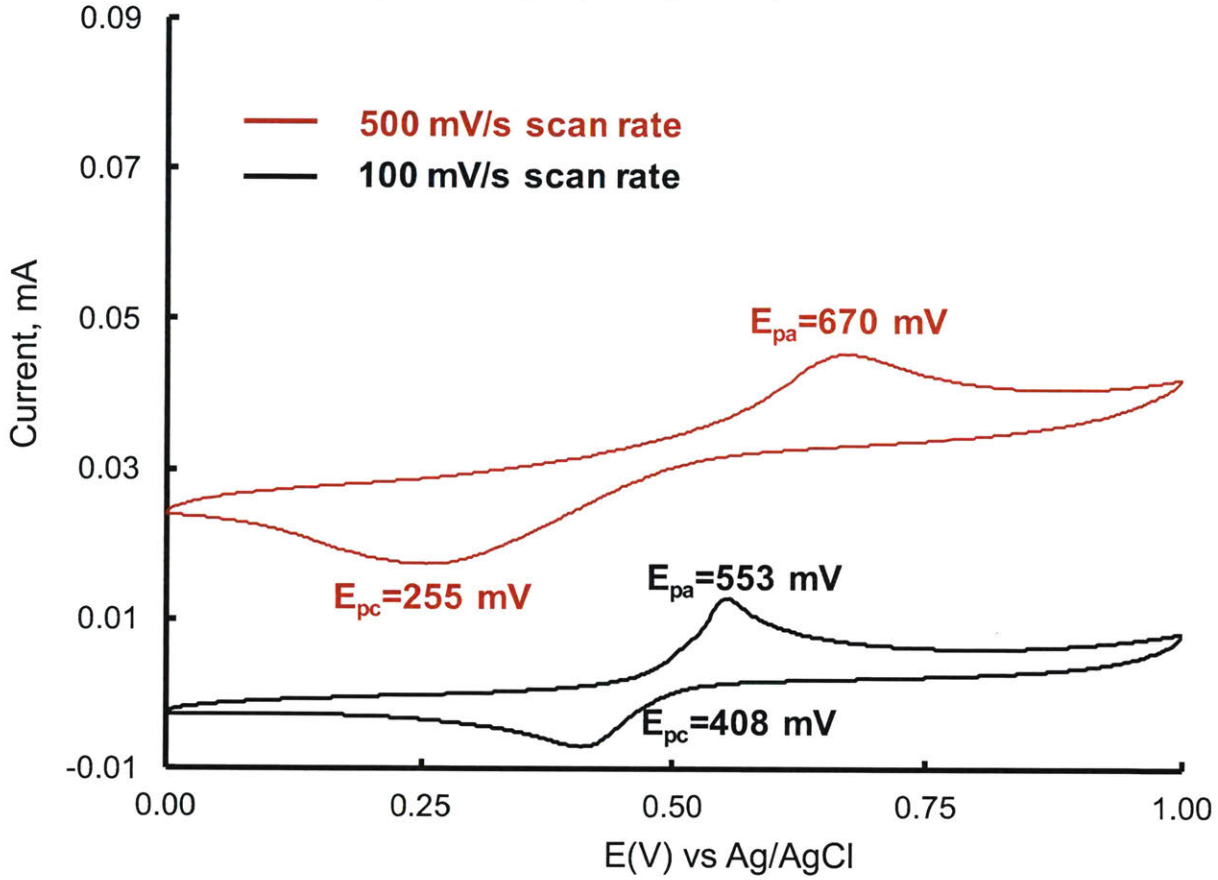

CHAPTER 4

Covalent Functionalization of Single Walled Carbon Nanotubes via [2+1] Cycloaddition and Trifluoromethylation Reactions

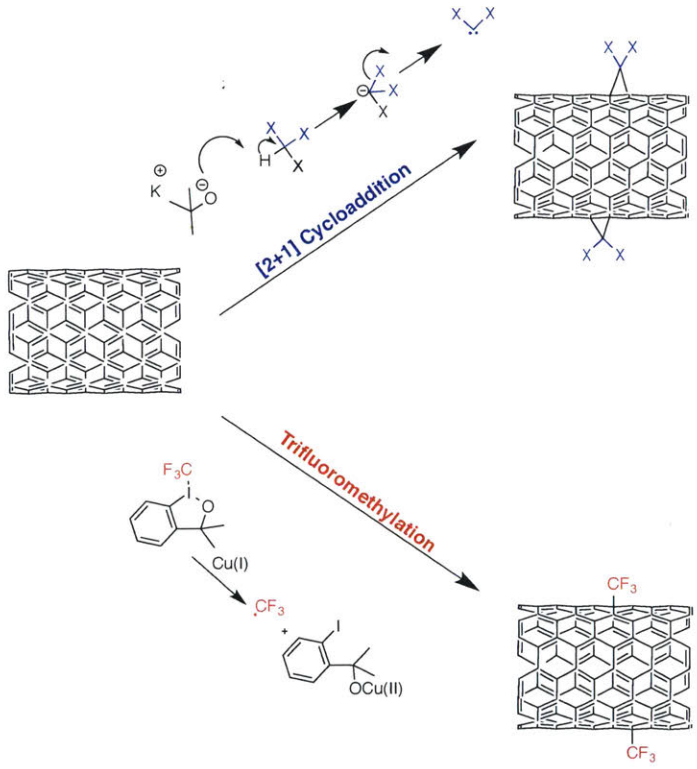

This work was supported in part by the U. S. Army Research Laboratory and the U. S. Army Research Office through the Institute for Soldier Nanotechnologies, under contract number W911NF-13-D-0001.

4.1 Abstract

The covalent functionalization and characterization of single walled carbon nanotubes (SWCNTs) by dihalocarbenes and the trifluoromethylating Togni's reagent is explored in this chapter. Covalent functionalization reactions were performed to increase the SWCNT solubility, imparting n-type semiconducting behavior while maintaining the native conductivity of the conjugated sp^2 network. Previous computational studies predicted the conservation of the electrical conductivity of SWCNTS after carbene additions, but experimental work to verify the electrical properties has not been performed. In the studies presented herein, we utilized five different covalent functionalization methods to modify SWCNTs and utilized X-ray photoelectron spectroscopy (XPS) in tandem with Resonance Raman spectroscopy to characterize our products. Though electrical characterization was not performed, we improved upon literature methods concerning the dichlorocarbene addition of $-CCl_2$ groups to pristine SWCNTs.

4.2 Introduction

Carbon nanotubes continue to offer significant promise as a material that will be useful in a variety of technological areas.[1,2] The inimitable electrical, thermal, optical and mechanical properties of semiconducting single walled carbon nanotubes (SWCNTs) have found utility as key materials in sensors, capacitors, catalysis filters, and membranes.[3–6] However, SWCNTs have a major drawback in the form of limited solubility in both aqueous and organic solvents because of the strong π-π interactions between SWCNTs that leads to aggregation. Covalent functionalization of the SWCNTs offer a way to increase the solubility and the environmental stability of these materials.

In recent years, a manifold of methodologies has been developed in the carbon nanotube covalent functionalization arena which has been documented in a variety of reviews.[7–9] The research objective or commercial application determines the target properties, and it follows that the desired characteristics are governed by the type of covalent modification. In this work, we wish to increase the solubility of SWCNTs and impart n-type semiconducting behavior by targeting the preparation of SWCNT-CCl_2, SWCNT-CF_2 and SWCNT-CF_3 adducts.

To generate SWCNT-CCl_2 and SWCNT-CF_2 adducts, we chose to employ dihalocarbenes as a reactive intermediate. Carbene [2+1] cycloadditions with other moieties have been demonstrated to increase the solubility of SWCNTs in organic solvents.[10–12] Furthermore, it was expected that halocarbenes would convey increased electron affinity to their SWCNT adducts, making them electron-accepting materials and conducive to the reduction by additing electrons; the key characteristic of n-type semi-conductors.[13,14] Additionally, computational experiments have shown that the SWCNT-CX_n adducts maintain a significant portion of their conductivity after covalent functionalization.[15]

To produce SWCNT-CF_3 adduct, we employed a trifluoromethylation tactic using a hypervalent iodine compound, Togni's reagent.[16,17] In principle, a pendant -CF_3 group covalently bound to the surface of a SWCNT would create an electron-acceptor material with very high electron affinity as well as with increased solubility and thereby be classified as an acceptor material. An n-type SWCNT and a p-type polymer (such as polythiophene or PEDOT) could be excellent partners in a charge transfer type interaction that may be an advantageous characteristic for the polymer wrapping of SWCNTs for sensor applications.

Dihalocarbenes can be formed in a variety of ways. One of which involves the deprotonation of a haloform such as chloroform or bromoform and subsequent α-elimination of

the halogen (**Scheme 4.1a**). Another way to access the dihalocarbene species is the decarboxylation and α-elimination of a halogen from the sodium salts of trichloroacetate and difluorochloroacetate (**Scheme 4.1b-c**). In reactions using trichloroacetate, we chose to mechanically mill (MM) the reaction rather than using a solvent. Both of these methods produce dihalocarbenes that are known to generate singlet carbenes,[10,18,19] which can undergo a [2+1] cycloaddition with a double bond on the SWCNT (**Scheme 4.1d**). In keeping with our goal on creating n-type SWNTs, we were inspired by the work of Buchwald and co-workers concerning the copper-catalyzed trifluoromethylation of unactivated alkenes.[20,21] A reaction between SWCNTs and the Togni's reagent is demonstrated in Scheme **4.1e**. This electrophilic trifluoromethylating reagent is employed in concert with a copper catalyst to generate SWNT–CF_3.

We examined the efficacy of the chemical transformations to SWCNT adducts using two analytical techniques. First, we used X-ray photoelectron spectroscopy (XPS) to verify the atomic composition of SWCNT adducts. Using XPS atomic composition data, we estimated the degree of SWNT functionalization according to a calculation reported by Hu and co-workers:[11]

$$C_{wall}\% = (C\% - C_{adduct}\%) \approx (C\% - \tfrac{1}{2}\, Cl\%)$$

The degree of functionalization is given by (C_{wall}/CCX_n)

Next, we used Resonance Raman spectroscopy to corroborate the XPS results.[22] Specifically, the ratio of intensities of the Raman D (1290 cm^{-1}) and G bands (1590 cm^{-1}) (I_D/I_G) is used to evaluate the disruption of the sp^2 network in conjugated nanocarbon systems [22]. An increase in I_D/I_G from the pristine SWCNTs (p-SWCNT) to the SWCNT adducts has been used

as an indicator of the increase in the number of defects in the SWCNT sidewalls within the dispersion [22] or the disruption of the sp^2 network of p-SWCNTs, likely due to the chemical functionalization. The radial breathing modes (RBM) are also a signature for the presence of carbon nanotubes and are located between 100-300 cm^{-1}.

Herein we survey here five methodologies to covalently modify the sidewalls of SWCNTs with $-CCl_2$, $-CBr_2$, $-CF_2$, and $-CF_3$ groups. We used dihalocarbenes to create the first four SWCNT adducts and electrophilic trifluoromethylations employing Togni's reagent to construct SWCNT-CF_3. We characterize the SWCNT adducts using XPS and Resonance Raman spectroscopy.

a) Formation of dihalocarbene from a haloform

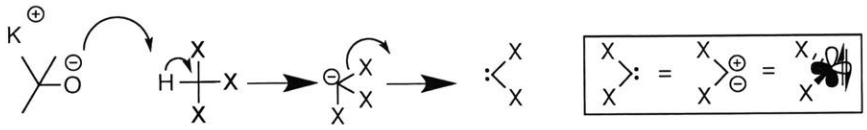

b) Formation of dichlorocarbene from sodium trichloroacetate

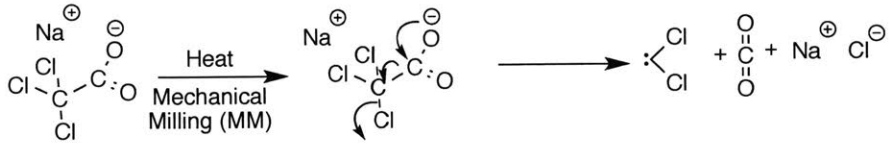

c) Formation of difluorocarbene from sodium difluorochloroacetate

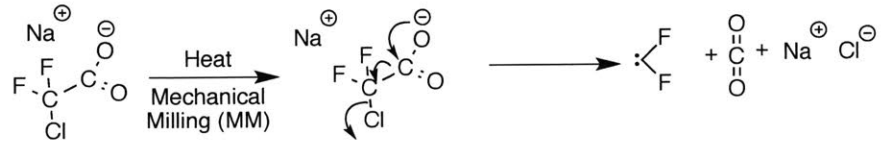

d) Synthesis of SWCNT-CX_2 Adducts

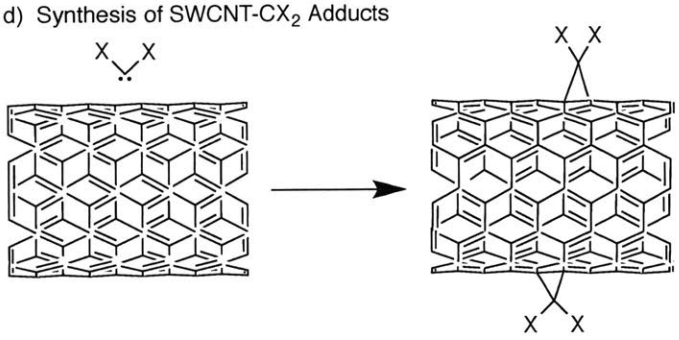

e) Synthesis of SWCNT-CF_3 adducts via Togni's reagent

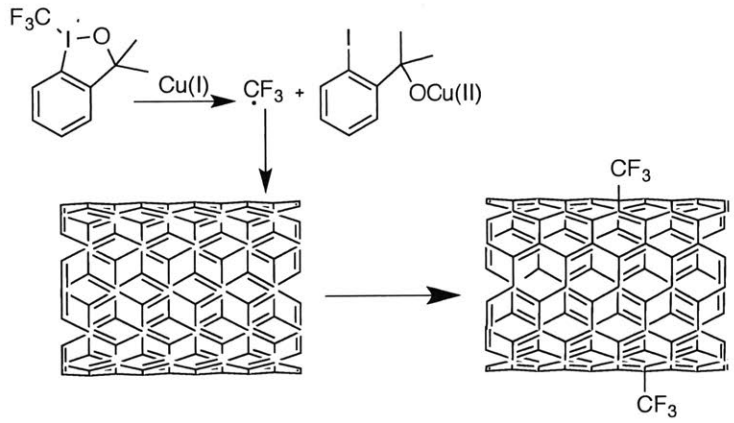

Scheme 4.1 Formation of dihalocarbenes and synthesis of SWCNT-CX_2 and SWCNT-CF_3 adducts. (a-c) Formation of dihalocarbenes, (d) Synthesis of SWCNT-CX_2 adducts, (e) Synthesis of SWCNT-CF_3 from Togni's reagent

4.3 Results and Discussion

Entry	Reactants/ carbene source	Conditions	% Cl (Br)	C_{wall}/CCl_2 (CBr_2)
1	$CHCl_3$	THF, tert-BuOK, DOWEX (1x2), 22 °C, 10 min	0.64±0.18	143±38
2	$CHCl_3$	THF, tert-BuOK, DOWEX (1x2), 22 °C, 10 min	2.27±0.41	35±8
3	$CHCl_3$	THF, tert-BuOK, DOWEX (1x2), -78 °C, 10 min	0.77±0.06	122±10
4	$CHCl_3$	THF, tert-BuOK, DOWEX (1x2), 40 °C, 10 min	0.79±0.16	113±12
5	$CHCl_3$	THF, tert-BuOK, DOWEX (1x2), 60 °C, 10 min	0.84±0.02	109±12
6	$CHCl_3$	THF, tert-BuOK, 22 °C, DOWEX (1x2), 10 min	0.47±0.03	200±13
7	$CHCl_3$	THF, 22 °C, DOWEX (1x2), 10 min	0.22±0.05	444±23
8	$CHCl_3$	o-DCB, tert-BuOK, DOWEX (1x2), 60 °C, 600 min	2.98±0.08	30±1
9	$CHCl_3$	o-DCB, tert-BuOK, DOWEX (1x2), 22 °C, 600 min	2.01±0.42	48±11
10	$CHCl_3$	o-DCB, tert-BuOK, DOWEX (1x2), 22 °C, 10 min	0.75±0.08	127±11
11*	$CHCl_3$	o-DCB, tert-BuOK, DOWEX (1x2), DOWEX (1x2), 75 °C, 10 min	1.86±0.22	48±7
12*	$CHBr_3$	o-DCB, tert-BuOK, DOWEX (1x2), 60 °C, 600 min	8.33±1.90	7±3

Table 4.1 Reaction conditions for the formation of SWCNT-CCl_2 (1-11) and SWCNT-CBr_2 (12*). (*) indicates the use of Sigma-Aldrich (6,5) enriched SWCNTs. % Cl (Br) and C_{wall}/CCl_2 (CBr_2) determined using XPS analysis.

4.3.1 Functionalization of SWCNT via [2+1] cycloaddition using chloroform with potassium tert-butoxide or sodium trichloroacetate to form SWCNT-CCl_2

With an established literature procedure in hand for the dichlorocarbene [2+1] cycloaddition to p-SWCNTs,[10] we set out to produce the SWCNT-CCl_2 adduct. Unfortunately, we were not able to achieve reproducible results with acceptable chlorine incorporation into the

SWCNTs as deterimined by XPS (**Table 4.1**, entries 1-6). However, we did note that a control experiment showed that running the reaction without a base markedly decreased in the % Cl by XPS analysis (**Table 4.1**, entry 7). The presence of residual chlorine in the control reaction not subjected to potassium *tert*-butoxide treatment may indicate incomplete removal of chloroform during washing of the SWCNT-CCl_2.

After attempting four different temperature regimes using THF as the reaction solvent, we changed the solvent to *ortho*-dichlorobenzene, (*o*-DCB)[23] to increase the sparing solubility of SWCNTs. We observed better than a two-fold increase in the degree of functionalization of the SWCNTs using *o*-DCB with higher temperatures and longer reaction times (**Table 4.1**, entries 8,9,11). Our results with this dichlorocarbene addition method are on the same order of magnitude of those using similar carbene additions with $CHCl_3$.[24]

Figure 4.1a-c shows two reactions to form SWCNT-CCl_2. The reaction on the left shows optimized conditions for the chloroform-derived dichlorocarbene. XPS and Raman results are tabulated in **Figure 4.1b**, while XPS and Raman spectra are shown in **Figure 4.1c-d**, respectively. XPS results show clearly the presence of chlorine at 200 eV (2.98±0.08 %) in the SWCNT that is not present in the p-SWCNT. A calculated C_{wall}/Cl_{atoms} of 48 indicates that there is one dichlorocarbene group per five hexagonal units on the SWCNT sidewall surface. The I_D/I_G from the Raman spectra shows an increase from 0.076 in the p-SWCNT to 0.56 in the SWCNT-Cl_2 adduct indicating disruption of the sp^2 network and successful functionalization via dichlorocarbene.

a)

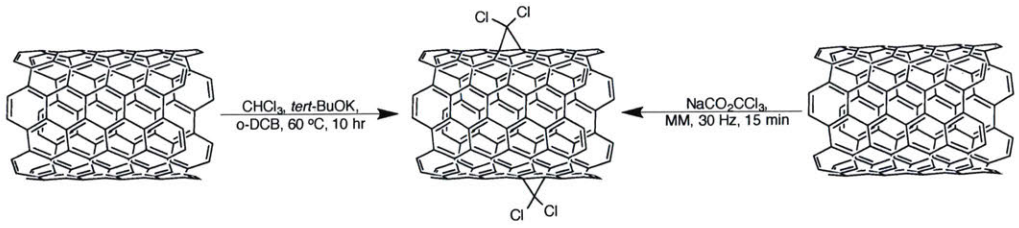

b)

Material	Raman I_D/I_G	XPS % C1s	XPS % O1s	XPS % Cl2p	#C_{wall}/ -CCl_2
p-SWCNT	0.076	91.49±2.01	5.17±1.99	0.23±0.16	461
SWCNT-Cl_2 ($CHCl_3$)	0.56	91.65±1.04	2.59±0.42	2.98±0.08	48
SWCNT-Cl_2($NaCO_2CCl_3$)	.053	93.97±0.39	4.48±0.34	0.77±0.08	121

c)

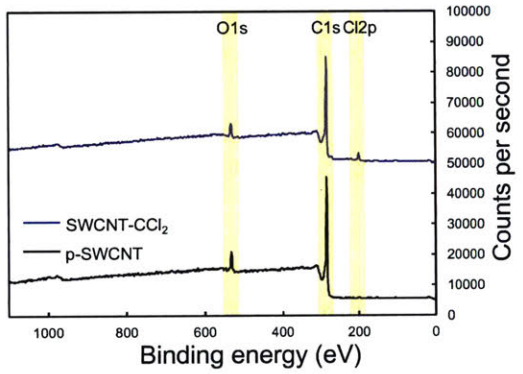

d)

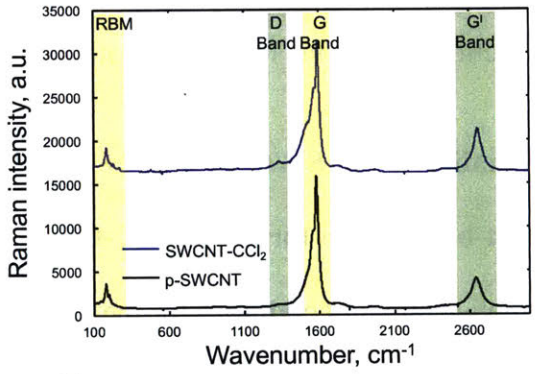

e)

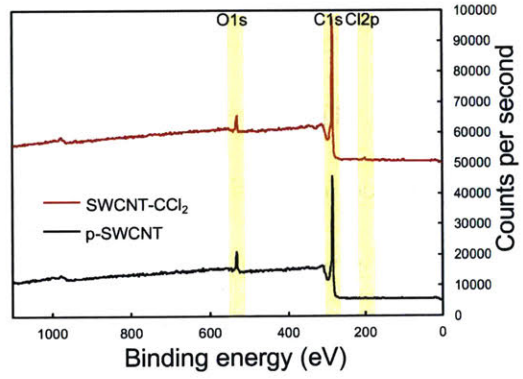

f)

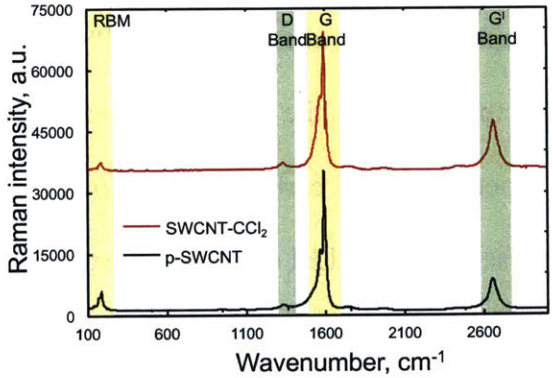

Figure 4.1 (a) Reactions of SWCNT to form SWCNT-CCl_2 adduct via chloroform and organic base (left) and MM with sodium trichloroacetate (right). (b) Table showing Raman I_D/I_G ratio, atomic composition (%), and calculated carbon atoms per chlorine atom. (c) XPS survey spectrum of chloroform-derived SWCNT-CCl_2 and p-SWCNT. (d) Resonance Raman spectrum of chloroform-derived SWCNT-CCl_2 and p-SWCNT. (e) XPS survey spectrum of sodium trichloroacetate-derived SWCNT-CCl_2 and p-SWCNT. f) Resonance Raman spectrum of sodium trichloroacetate-derived SWCNT-CCl_2 and p-SWCNT.

Entries 1-3 in **Table 4.2** show our attempts at the solvent-free preparation of SWCNT-CCl_2 via MM with sodium trichloroacetate. The extrusion of CO_2 and the formation of NaCl(s) drives the formation of the dichlorocarbene species. Using this method, we earned much less degree of functionalization. XPS analysis gave only 0.77±0.08 % Cl and a C_{wall}/CCl_2 of 121. The Raman I_D/I_G gave a ratio of 0.053, which shows no significant difference with that of p-SWCNT.

Entry	Reactants/ carbene source	Conditions	% Cl	C_{wall}/CCl_2
1	30 eq $NaCO_2CCl_3$, 1 eq SWCNT	MM, 15 min, 30 Hz	0.77±0.08	121±13
2	60 eq $NaCO_2CCl_3$, 1 eq SWCNT	MM, 15 min, 30 Hz	0.65±0.14	147±34
3	15 eq $NaCO_2CCl_3$, 1 eq SWCNT	MM, 15 min, 30 Hz	0.70±0.03	130±9

Table 4.2 Reaction conditions for the formation of SWCNT-Cl_2 from the MM of $NaCO_2Cl_3$.

4.3.2 Functionalization of SWCNT via [2+1] cycloaddition using bromoform with potassium tert-butoxide to form SWCNT-CBr_2

We applied similar conditions for the sidewall functionalization of SWCNTs with bromoform as we did with chloroform (**Table 4.1**, entry 12). XPS and Raman data are reported in Figure are reported in **Figure 4.2 (a-c)**. XPS analysis shows the presence of bromine (8.33±1.90 %) that indicates the successful cycloaddition of $-CBr_2$. This gives a calculated one $-CBr_2$ groups per 7 sidewall carbon atoms. However, the occurrence of chlorine (3.95±0.59 %) implies the presence of residual o-DCB that was not removed during washing procedures. The Raman analyses substantiates the XPS evidence and shows a and I_D/I_G of 0.61 in the bromoform-derived SWCNT-CBr_2, an increase from 0.076 in the p-SWCNTs.

a)

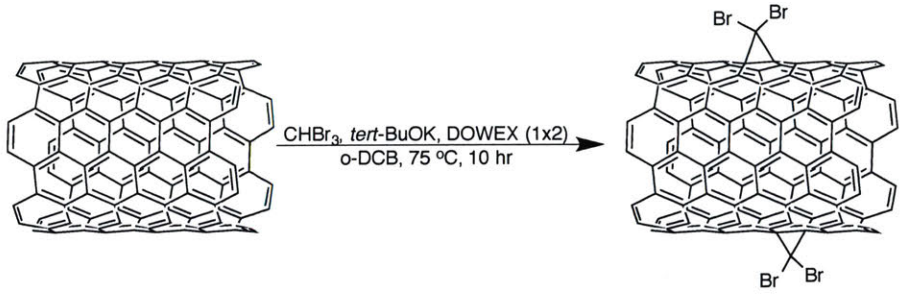

b)

Material	Raman I_D/I_G	XPS % C1s	XPS % O1s	XPS % Cl2p	XPS % Br3d	$\#C_{wall}$ / CBr_2
p-SWCNT	0.076	91.49±2.01	5.17±1.99	0.23±0.16	0.00±0.00	N/A
SWCNT-CBr_2	0.61	69.61±5.53	8.91±1.89	3.95±0.59	8.33±1.90	7±3

c)

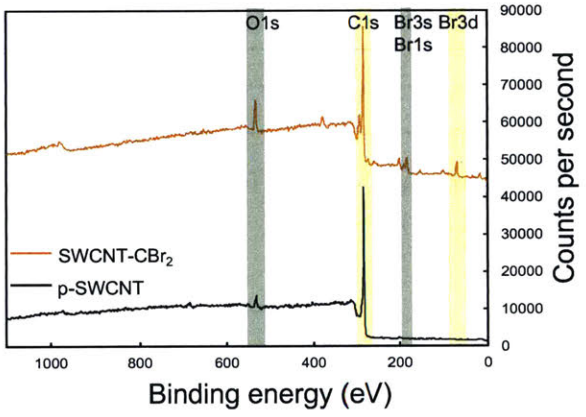

d)

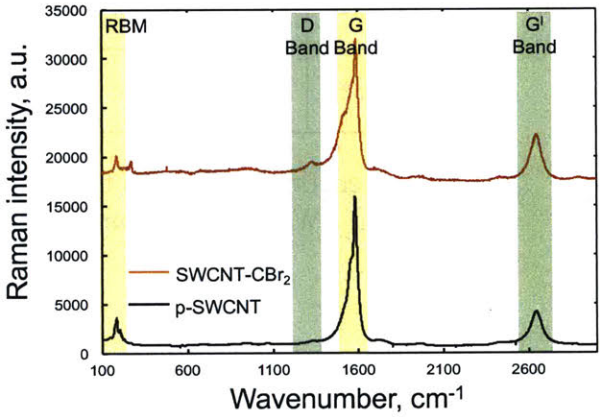

Figure 4.2 (a) Reaction of SWCNT to form SWCNT-CBr_2 adduct via bromoform and organic base. (b) Table showing Raman I_D/I_G ratio, atomic composition (%), and calculated carbon atoms per $-CBr_2$ group. (c) XPS survey spectrum of SWCNT-CBr_2 and p-SWCNT. (d) Resonance Raman spectrum of SWCNT-CBr_2 and p-SWCNT.

4.3.3 Functionalization of SWCNT via [2+1] cycloaddition using sodium difluorchloroacetate to form SWCNT-CF_2.

Given our limited success with the solvent-free preparation of SWCNT-Cl_2 with sodium trichloroacetate, we attempted to perform the difluorcarbene addition to SWCNTs under solvent conditions using difluorochloroacetate. Under the conditions in entry 1, **Table 4.3**, we achieved similar results for the $-CF_2$ cycloaddition to SWCNTs as we did for the solvent free preparation of the SWCNT-Cl_2. As reported in **Figure 4.3**, we observed a modest amount of fluorine functionalization of the SWCNTs (0.96±0.16 %) with a calculated one $-CF_2$ groups per 110 sidewall carbon atoms.

Entry	Reactants/ carbene source	Conditions	% F	$C_{wall}/CF_2(CF_3)$
1	$NaCO_2ClF_2$,	DMF, diglyme, 90 °C, 720 min	0.96±0.16	110±2
2*	Togni's Reagent	SWCNT/Tognis/Cu(I)=1/5/0.1	0.69±0.01	138±1
3*	Togni's Reagent	SWCNT/Tognis/Cu(I)=1/15/0.3	0.91±0.17	106±19
4*	Togni's Reagent	SWCNT/Tognis/Cu(I)=1/6.7/0.15	1.21±0.11	78±8
5*	Togni's Reagent	SWCNT/Tognis/Cu(I)=1/15/0.3	1.00±0.37	102±42

Table 4.3 Reaction conditions for the formation of SWCNT-CF_2 from $NaCO_2ClF_3$ (1) and the formation of SWCNT-CF_3 from Togni's reagent (2-5)

a)

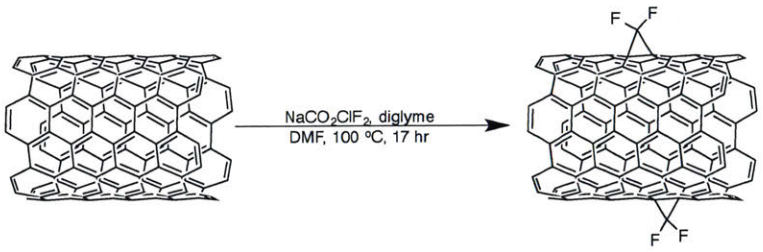

b)

Material	XPS % C1s	XPS % O1s	XPS % F1s	#C atoms per F atom
p-SWCNT	0.076	91.49±2.01	5.17±1.99	0.23±0.16
SWCNT-CF_2	94.42 ±1.88	4.04±1.30	0.96±0.16	110±2

c)

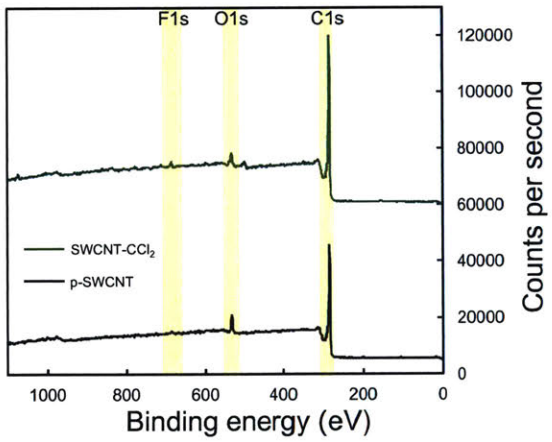

Figure 4.3 (a) Reaction of SWCNT to form SWCNT-CF_2 adduct via MM of SWCNT and sodium difluorochloroacetate. (b) Table showing atomic composition (%), and calculated carbon atoms per fluorine atom. (c) XPS survey spectrum of SWCNT-CF_2 and p-SWCNT

4.3.4 Functionalization of SWCNT via trifluoromethylation using Togni's reagent to form SWCNT-CF_3

After experimenting with different ratios of SWCNT/Togni's reagent/Cu (I) catalyst, we settled on the conditions in entry 4 of **Table 4.3**. Our best result, reported in **Figure 4.4**, afforded 1.21±0.11 % fluorine via XPS. This gave a calculated on $-CF_3$ group per 78 sidewall carbon atoms. The I_D/I_G from Raman analysis is 0.11. This result is very modest in comparison to our Raman analysis of SWCNT-CCl_2 functionalization efforts. This low level of functionalization may be attributed to a wide variety of sources: dimerization of the trifluoromethyl radical, recombination of the radical with its parent molecule (Togni's reagent), or just an insufficient amount of $-CF_3$ radical formation under the conditions selected. Regardless of the reason, more experiments could be performed to improve upon this preliminary data set.

a)

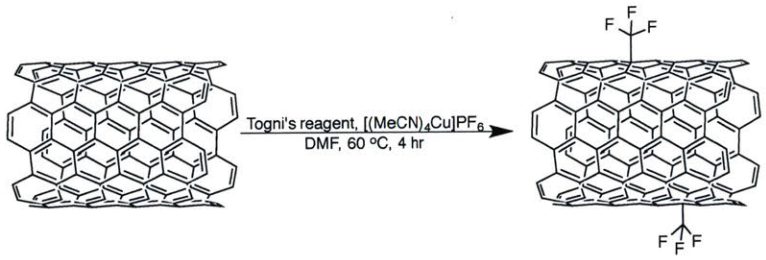

b)

Material	Raman I_D/I_G	XPS % C1s	XPS % O1s	XPS % F1s	#C atoms per F atom
p-SWCNT	0.066	92.84±0.55	7.01±0.56	0.00±0.00	N/A
SWCNT-CF_3	0.11	95.24±1.17	3.43±0.88	1.21±0.11	78±8

c)

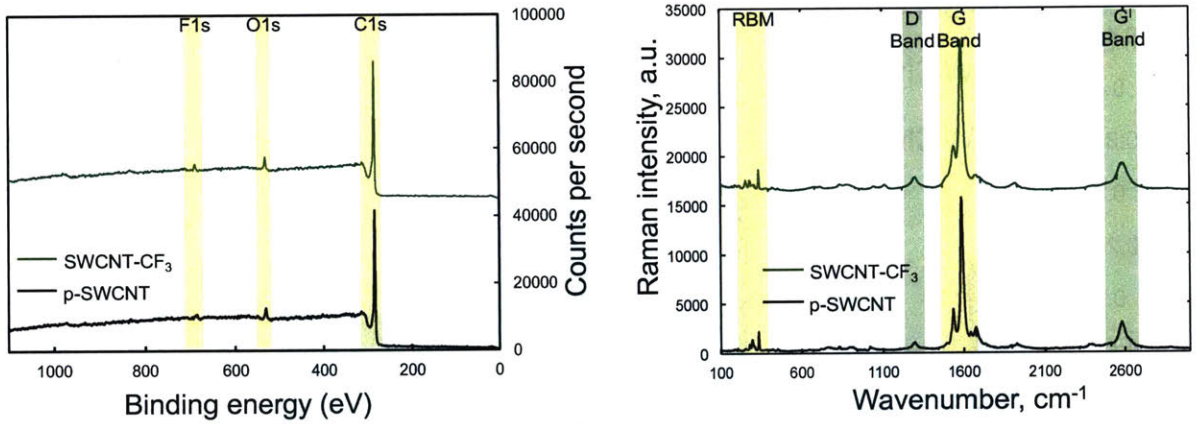

Figure 4.4 (a) Reaction of SWCNT to form SWCNT-CF_3 adduct via Togni's reagent. (b) Table atomic composition (%), and calculated carbon atoms per fluorine atom. (c) XPS survey spectrum of SWCNT-CF_3 an p-SWCNT. (d) Resonance Raman spectrum of SWCNT-CF_3 and p-SWCNT.

4.3.5 SWCNT-CF_2 and SWCNT-CF_3 for chemiresistive ammonia sensing

We sought to investigate the efficacy of our fluorinated SWCNT adducts in detecting NH_3. NH_3, a well-known electron donor, is known to initiate a charge transfer type response to the SWCNTs.[25] The sensory response was investigated by measuring the change in current between two electrodes at a constant bias voltage of 0.10 V. The change in current was converted to a negative change in conductance [$-\Delta G/G_o$ (%) = $((I_o-I)/I_o)$ x 100%], where I_o is the initial

current. This normalized response allows for small differences in the resistivity that can complicate device to device comparisons. **Figure 4.5** shows baseline-corrected responses of three chemiresistive devices that were tested in parallel incorporating p-SWCNT, SWCNT-CF_2 and SWCNT–CF_3 adducts. Interestingly, the response towards NH_3 for this particular batch of Nano-C brand p-SWCNTs was 40 times lower than previously reported under similar conditions by our group.[26] The trifluoromethylated SWCNTs show virtually the same response to NH_3 as the p-SWCNTs. The SWCNT-CF_2 give a reduced sensitivity to NH_3. There is not enough information to determine what the cause of the reduced response could be.

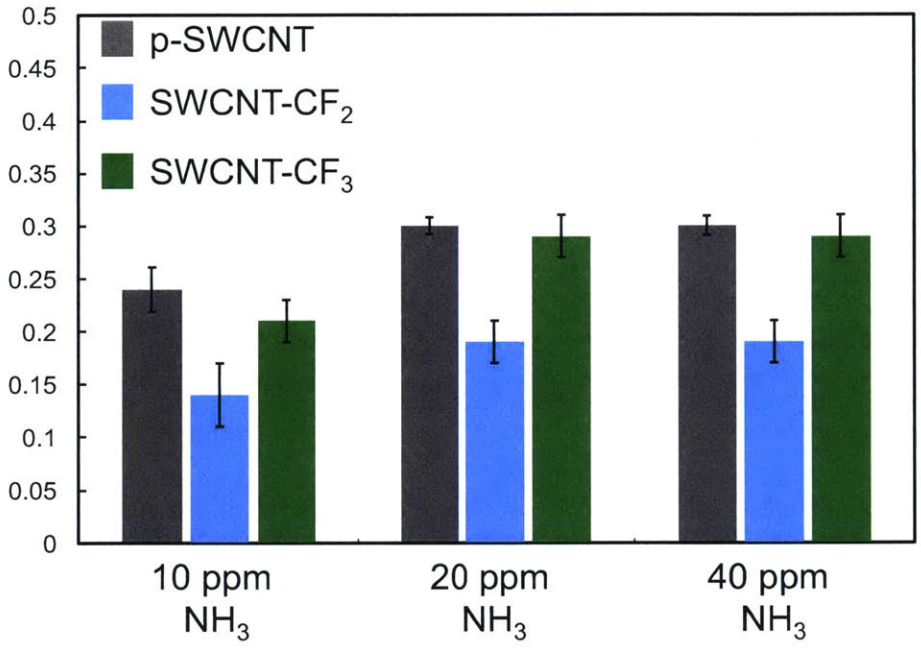

Figure 4.5 Chemiresistive responses averaged across three p-SWCNT/SWCNT-CF_2/SWCNT-CF_3 devices to 60 s exposures of NH_3 at a flow rate of 200 mL/min in dry N_2.

4.4 Conclusions. In summary, five different approaches to the covalent functionalization of SWCNTs have been conducted and characterized via XPS and Resonance Raman spectroscopy. [2+1] cycloadditions of dichlorocarbenes to SWCNTs to form the SWCNT-CCl_2 adduct under

elevated temperatures and extended reaction times gave the best functionalization rates: 2.98% chlorine from XPS and a calculated one $-CCl_2$ group per 48 sidewall carbon atoms. Furthermore, Raman analysis shows an increase in the intensity of the D band relative to the G band to give a I_D/I_G of 0.56, indicating an increase in the number of sidewall defects and the breaking of the conjugation of the SWCNT sp^2 network. Though more work is required to confirm, SWCNT-CBr_2 generated from bromoform, gave promising initial results (3.95 % Br; C_{wall}/CBr_2; I_D/I_G=0.61). Solvent-free preparation using mechanical milling, MM, to synthesize SWCNT-CCl_2 was attempted and modest results were achieved (0.77% Cl; C_{wall}/CCl_2=121; I_D/I_G=0.53). Fluorination of SWCNTs to form both SWCNT-CF_2 and SWCNT-CF_3 adducts were also performed. Both preparations afforded modest results, with the trifluormethylation (1.21% F; C_{wall}/CF_3=78; I_D/I_G=0.11) generating slightly better results than dichlorocarbene cycloaddition (0.96% F; C_{wall}/CF_2=121; I_D/I_G=0.53). For the SWCNT-CF_2 and SWCNT-CF_3 adducts, we tested their response to NH_3 and found the response to be the same or lower than the native p-SWCNT response.

From the above results, it is clear that the solvent-based approach using *o*-DCB as a solvent at elevated temperatures is the most viable path forward to attaining SWCNT-CCl_2 and SWCNT-CBr_2 n-type SWCNTs. The mechanical milling approach is operationally simpler, but suffers from poor functionalization rates. To advance this project, additional methods confirming the functionalization were necessary. UV-vis/NIR spectroscopy and thermogravimetric analysis of the SWCNT adducts can help verify the efficacy of the functionalization. The objective of this work was to synthesize n-type SWCNTs. Electrical characterization of these SWCNT adduct materials in a FET system is required to confirm whether or not n-type characteristics have been achieved as anticipated and designed.[13,27]

4.5 Experimental

4.5.1 Materials

All chemicals and reagents were purchased from Sigma-Aldrich and used without additional purification, except that tetrahydrofuran was distilled from sodium metal and benzophenone. Purified SWCNTs (UPT 200, Batch 1167-24) were acquired from Nano-C, (Westwood, MA) or Sigma Aldrich, Inc. (Saint Louis, MO, USA) (6,5 chirality, carbon (95%), with 93% as SWCNTs).

4.5.2 Instrumentation

Mechanical Milling. Sensing materials were generated by solvent-free ball milling of carbon (e.g., SWCNTs) with commercial small molecule "selectors" using an oscillating mixer mill 3 (MM400, Retsch GmbH, Haan, Germany) within a stainless-steel milling vial (5 mL) equipped with a single stainless steel ball (7 mm diameter). Unless otherwise indicated, a typical experiment involved filling the milling vial with carbon powder (e.g., SWCNTs) and reactant (total mass of powder = 620 mg) and ball milling the mixture for 30 min at 30 Hz.

X-Ray photoelectron spectroscopy (XPS). XPS measurements were performed on a Phi Versaprobe II instrument at the MIT Center for Materials Science and Engineering.

Raman spectroscopy. Raman spectra were collected with excitation at 532 nm (or 633, where noted) laser using a Horiba LabRAM HR800 Raman spectrometer at the MIT Institute of Soldier Nanotechnology.

4.5.3 Synthesis

Synthesis of SWCNT-CCl_2 functionalized via dichlorocarbene generated from chloroform. A typical 10-hour reaction involved immersing 25 mg SWCNT into a well-stirred, highly basic solution of potassium *tert*-butoxide dissolved in 10 mL *o*-DCB at 60 °C in the

presence of phase transfer catalyst, DOWEX (1,2). Dry chloroform was then added drop-wise to the mixture in an inert gas environment. The reaction was quenched with 10 mL of water after the designated reaction time period. The reaction mixture was filtered through a 2.0 μm Millipore membrane filter. The solid filtrate was then scraped off of the membrane and placed in a centrifuge tube with 4.0 mL water, sonicated for 30 seconds and centrifuged for 10 minutes at 8000 rpm. The water was decanted and refilled with an additional 4.0 mL, sonicated and centrifuged. This same sonication/centrifugation procedure was repeated with ethanol and hexanes. Finally, the modified SWCNTs were heated at 100 °C for 5 min on a hot plate to remove chemical residuals before Resonance Raman spectroscopy and X-ray Photoelectron (XPS) measurements. SWCNT-CBr_2 adducts were prepared in the same manner as above.

Synthesis of SWCNT-CCl_2 functionalized via dichlorocarbene generated from $NaCO_2CCl_3$. 600 mg of $NaCO_2CCl_3$ and 20 mg of SWCNT were added to a stainless steel milling vial and mechanically mixed for 30 minutes at 30 Hz. The product powder was placed in 15 mL centrifuge tubes and diluted with 4.0 mL water. The solid filtrate was then scraped off of the membrane and placed in a centrifuge tube with 4.0 mL water, sonicated for 30 seconds and centrifuged for 10 minutes at 8000 rpm. The water was decanted and refilled with an additional 4.0 mL, sonicated and centrifuged. This same sonication/centrifugation procedure was repeated with ethanol and hexanes. Finally, the modified SWCNTs were placed in a vacuum oven at 80 ^{o}C for ten minutes.

Synthesis of SWCNT-CCF_2 functionalized via dichlorocarbene generated $NaCO_2CClF_2$. To 40 mL DMF and 10 mg of SWCNT in a round bottom flask fitted with a magnetic stir bar under an Ar atmosphere, a mixture of 50 mg of $NaCO_2CClF_2$ in 5 mL of diglyme were delivered. The mixture was refluxed overnight. The reaction was quenched with 10 mL water. The crude

reaction mixture was filtered through a 2 μm Millipore membrane filter and then washed three times with diethyl ether. Finally, the modified SWCNTs were placed in a vacuum oven at 80 °C for ten minutes.

Synthesis of SWCNT-CF_3 functionalized via generated Togni's Reagent.

To 40 mL DMF and 10 mg of SWCNT in a round bottom flask fitted with a magnetic stir bar under an Ar atmosphere, 15.3 mL of a 1 mg/mL of $[(MeCN)_4Cu]PF_6$ was delivered. Subsequently, 70 mg of SWCNT were added. After a designated reaction period, the reaction mixture was filtered through a 0.2 μm Millipore membrane filter and washed with DMF. The functionalized SWCNT were then sonicated in DMF, then filtered. Sonication and filtration were repeated in diethyl ether. Finally, the modified SWCNTs were placed in a vacuum oven at 100 °C for 30 minutes.

4.5.4 Chemiresistor fabrication and gas sensing experiments

Preparation of gold electrodes on glass microscope slides. Glass substrates deposited with chromium adhesion layers (10 nm) and gold electrodes (100 nm) were prepared according to a literature procedure [28]. Briefly, glass slides (VWR Microscope Slides) were cleaned by sonication in acetone for 5 min followed by UV-ozone treatment using a UVO cleaner (Jelight Company Inc., Model 42) for 20 min. A 10 nm layer of chromium (99.99%, R.D. Mathis) and a subsequent 100 nm layer of gold (99.99%, R.D. Mathis) were deposited through a custom stainless steel mask using a thermal evaporator (Angstrom Engineering), which resulted in three sets of four channel electrode patterns on a single glass slide, which was cut into three individual devices. Each device contains a gold pattern of four isolated working electrodes with one shared reference-counter electrode on the glass substrate. The gap between one pair of gold electrodes is 1 mm.

Fabrication of SWCNT-adduct chemiresistor platform. p-SWCNT and SWCNT adduct dispersions were prepared with a concentration of 0.25 mg/mL in *o*-DCB. The desired amount of SWCNT adduct dispersion was dropcasted with a 20 μL syringe between four gold electrode pairs on the glass substrate. Typically, between 4-20 μL of the dispersion was required to reach the target electrode resistance of 10-50 kΩ.

Ammonia Gas Detection Measurement. For NH_3 detection measurement, the fabricated array device was placed into a custom-built PTFE enclosure with a small gas inlet and outlet, the gold electrodes of the device were connected to a PalmSens EmStat potentiostat with a MUX16 multiplexer. The inlet port was connected to a gas delivery system (Sierra's Smart-Trak Series 100). Delivery of controlled concentration of gases to devices. To obtain concentrations of NH_3 between 250 ppm – 5000 ppm, pure NH_3 supplied from a gas cylinder (Airgas) was diluted with N_2 using the gas mixing system at total flow rate supplied to devices ranging between 400 – 1000 mL/min. To obtain concentrations of NH_3 between 0.5 ppm – 80 ppm, 1% NH_3 in N_2 supplied from a gas cylinder (Airgas) was diluted with N_2 using the gas mixing system at a total flow rate supplied to devices ranging between 500 – 10000 mL/min. Controlled delivery of gas to devices was accomplished by encasing a device within a custom-built teflon chamber equipped with an inlet and an outlet for gas flow. The potentiostat applied a constant potential of 0.1 V across the electrodes, and the current for each channel of the device was recorded using PS Trace software (v. 4.7) during 60 s of NH_3 vapor exposures. After a linear baseline correction, the change in current resulting from exposure to the analyte was converted to the negative change in conductance ($-\Delta G/G_o$ (%) = $(I_o - I)/I_o) \times 100$), where I_o is initial current), which was taken as the device's response.

4.6 References

(1) Iijima, S.; Ichihashi, T. Single-shell carbon nanotubes of 1-nm diameter. *Nature* **1993**, *363*, 603–605.
(2) Iijima, S. Carbon nanotubes: Past, present, and future. In *Physica B: Condensed Matter*; 2002; Vol. 323, pp 1–5.
(3) Schnorr, J. M.; Swager, T. M. Emerging Applications of Carbon Nanotubes. *Chem. Mater.* **2011**, *23*, 646–657.
(4) Balasubramanian, K.; Burghard, M. Biosensors based on carbon nanotubes. *Anal. Bioanal. Chem.* **2006**, *385*, 452–468.
(5) Lu, W.; Zu, M.; Byun, J.-H.; Kim, B.-S.; Chou, T.-W. State of the art of carbon nanotube fibers: opportunities and challenges. *Adv. Mater.* **2012**, *24*, 1805–1833.
(6) Sun, Y. P.; Fu, K. F.; Lin, Y.; Huang, W. J. Functionalized carbon nanotubes: Properties and applications. *Acc. Chem. Res.* **2002**, *35*, 1096–1104.
(7) Georgakilas, V.; Kordatos, K.; Prato, M.; Guldi, D. M.; Holzinger, M.; Hirsch, A. Organic functionalization of carbon nanotubes. *J. Am. Chem. Soc.* **2002**, *124*, 760–761.
(8) Holzinger, M.; Vostrowsky, O.; Hirsch, A.; Hennrich, F.; Kappes, M.; Weiss, R.; Jellen, F. Sidewall Functionalization of Carbon Nanotubes. *Communications* **2001**, *40*, 4002–4005.
(9) Selvakumar, S.; Somanathan, N.; Reddy, K. A. Chemiresistor Sensors Based on Conducting Polymers for Hypergolic Propellants and Acidic Vapors of Rocket Exhaust Plumes - A Review. *Propellants, Explos. Pyrotech.* **2013**, *38*, 176–189.
(10) Liu, C.; Zhang, Q.; Stellacci, F.; Marzari, N.; Zheng, L. X.; Zhan, Z. Y. Carbene-Functionalized Single-Walled Carbon Nanotubes and Their Electrical Properties. *Small* **2011**, *7*, 1257–1263.
(11) Hu, H.; Zhao, B.; Hamon, M. A.; Kamaras, K.; Itkis, M. E.; Haddon, R. C. Sidewall Functionalization of Single-Walled Carbon Nanotubes by Addition of Dichlorocarbene. *J. Am. Chem. Soc.* **2003**, *125*, 14893–14900.
(12) Bekyarova, E.; Sarkar, S.; Wang, F.; Itkis, M. E.; Kalinina, I.; Tian, X.; Haddon, R. C. Effect of covalent chemistry on the electronic structure and properties of carbon nanotubes and graphene. *Acc. Chem. Res.* **2013**, *46*, 65–76.
(13) Hecht, D. S.; Ramirez, R. J. A.; Briman, M.; Artukovic, E.; Chichak, K. S.; Stoddart, J. F.; Grüner, G. Bioinspired detection of light using a porphyrin-sensitized single-wall nanotube field effect transistor. *Nano Lett.* **2006**, *6*, 2031–2036.
(14) Ha, T.-J.; Chen, K.; Chuang, S.; Yu, K. M.; Kiriya, D.; Javey, A. Highly Uniform and Stable n-Type Carbon Nanotube Transistors by Using Positively Charged Silicon Nitride Thin Films. *Nano Lett.* **2015**, *15*, 392–397.
(15) Lee, Y.-S. S.; Marzari, N. Cycloaddition Functionalizations to Preserve or Control the Conductance of Carbon Nanotubes. *Phys. Rev. Lett.* **2006**, *97*, 116801.
(16) Charpentier, J.; Früh, N.; Togni, A. Electrophilic trifluoromethylation by use of hypervalent iodine reagents. *Chem. Rev.* **2015**, *115*, 650–682.
(17) Kieltsch, I.; Eisenberger, P.; Togni, A. Mild electrophilic trifluoromethylation of carbon- and sulfur-centered nucleophiles by a hypervalent iodine(III)-CF3 reagent. *Angew. Chemie - Int. Ed.* **2007**, *46*, 754–757.
(18) Seyferth, D.; Burlitch, J. M. Concerning the Mechanism of the Reaction of Phenyl(trihalometyl)mercurials with Olefins. *J. Am. Chem. Soc.* **1964**, *86*, 2730–2731.
(19) Gao, X.; Ishimura, K.; Nagase, S.; Chen, Z. Dichlorocarbene Addition to C_{60} from the

Trichloromethyl Anion: Carbene Mechanism or Bingel Mechanism? *J. Phys. Chem. A* **2009**, *113*, 3673–3676.
(20) Zhu, R.; Buchwald, S. L. Copper-catalyzed oxytrifluoromethylation of unactivated alkenes. *J. Am. Chem. Soc.* **2012**, *134*, 12462–12465.
(21) Parsons, A. T.; Buchwald, S. L. Copper-catalyzed trifluoromethylation of unactivated olefins. *Angew. Chemie - Int. Ed.* **2011**, *50*, 9120–9123.
(22) Jorio, A.; Saito, R.; Dresselhaus, G.; Dresselhaus, M. S. *Raman Spectroscopy in Graphene Related Systems*; Wiley-VCH Verlag GmbH & Co. KGaA: Weinheim, Germany, 2011.
(23) Bahr, J. L.; Mickelson, E. T.; Bronikowski, M. J.; Smalley, R. E.; Tour, J. M. Dissolution of small diameter single-wall carbon nanotubes in organic solvents? *Chem. Commun.* **2001**, No. 2, 193–194.
(24) Bouilly, D.; Cabana, J.; Martel, R. Unaltered electrical conductance in single-walled carbon nanotubes functionalized with divalent adducts. *Appl. Phys. Lett.* **2012**, *101*, 53116.
(25) Kong, J. Nanotube Molecular Wires as Chemical Sensors. *Science..* **2000**, *287*, 622–625.
(26) Mirica, K. A.; Weis, J. G.; Schnorr, J. M.; Esser, B.; Swager, T. M. Mechanical Drawing of Gas Sensors on Paper. *Angew. Chemie Int. Ed.* **2012**, *51*, 10740–10745.
(27) Goetz, K. P.; Vermeulen, D.; Payne, M. E.; Kloc, C.; McNeil, L. E.; Jurchescu, O. D.; Eley, D. D.; Pochettino, A.; Gershenson, M. E.; Podzorov, V.; et al. Charge-transfer complexes: new perspectives on an old class of compounds. *J. Mater. Chem. C* **2014**, *2*, 3065–3076.
(28) Frazier, K. M.; Swager, T. M. Robust cyclohexanone selective chemiresistors based on single-walled carbon nanotubes. *Anal. Chem.* **2013**, *85*, 7154–7158.

John F. Fennell Jr.
Major, U.S. Army (Retired)
72 Patterson Road,
Hanscom Air Force Base, MA 01731
(719) 648-9716 | jfennell@mit.edu

Work Experience

Graduate Research Assistant (June 2013 – June 2017)
MIT, Department of Chemistry
Advisor: Professor Timothy M. Swager

Operations and Plans Officer (June 2011 – May 2013)
10th Special Forces Group Support Battalion (Airborne)
United States Army, Fort Carson, CO

Assistant Professor of Chemistry (June 2008 – June 2010)
United States Military Academy (USMA)
United States Army, West Point, NY

Graduate Researcher (June 2006 – May 2008)
National Renewable Energy Lab, Golden, CO
Colorado School of Mines, Department of Chemistry, Golden, CO
M.S. Thesis: "The Preparation of Aminosilane Surfaces for DNA Microarray Applications"
Advisor: Professor Scott M. Cowley

Iraqi Security Forces Liaison Officer (January 2006-May 2006)
Headquarters Troop, 3D Armored Cavalry Regiment
United States Army, Iraq

Company Commander (June 2004 - December 2005)
89th Chemical Company, 3D Armored Cavalry Regiment
United States Army, Fort Carson, CO and Iraq

Training and Operations Officer (January 2003 - May 2004)
43rd Area Support Group
United States Army, Fort Carson, CO and Iraq

Operations and Chemical Officer (January 2002 - December 2002)
Engineer Brigade, 2d Infantry Division
United States Army, Republic of Korea

Support Command Chemical Officer (January 2001 - April 2001)
Division Support Command, 3rd Infantry Division
United States Army, Fort Stewart, GA

Executive Officer (January 2000 - December 2000)
92d Chemical Company, 3rd Infantry Division
United States Army, Fort Stewart, GA

Platoon Leader (August 1999 - December 2000)
92d Chemical Company, 3rd Infantry Division
United States Army, Fort Stewart, GA

Operations and Chemical Officer (October 1997 - August 1999)
3rd Battalion, 7th Infantry Regiment, 3rd Infantry Division
United States Army, Fort Stewart, GA and Kuwait

Education

Massachusetts Institute of Technology (June 2013 – June 2017)
Ph.D., Organic Chemistry
Thesis: "Polymer and Covalent Functionalization Of Single Walled Carbon Nanotubes For Electronic Sensor Applications"
Research Advisor: Professor Timothy M. Swager

Graduate, U.S. Army Command and General Staff College (July 2010-May 2011)
Fort Leavenworth, KS, 2011

Colorado School of Mines (June 2006 to May 2008)
M.S., Chemistry
Thesis: "The Preparation of Aminosilane Surfaces for DNA Microarray Applications"
Research Advisor: Professor Scott M. Cowley

Graduate, **Chemical Officer Advanced Course** (April 2001 – September 2001)
Fort Leonard Wood, MO

Graduate, **Chemical Officer Basic Course** (May 1997 – October 1997)
Fort McClellan AL

Providence College (September 1993 – May 1997)
B.S., Chemistry

Teaching Experience

Kansas City Kansas Community College
Instructor, College Chemistry (Fall 2010)

United States Military Academy
Instructor, Quantitative Chemical Analysis (Fall 2009 - Spring 2010)
Instructor, General Chemistry I-II (Fall 2008 – Summer 2009)

Awards

2015 Best Poster, ACS Polymer Division, 2015 ACS Fall Meeting, Boston MA
2013 Army Commendation Medal (also 2004)
2013 United States Army Advanced Civil Schooling Doctoral Fellowship
2011 Meritorious Service Medal (also 2002 and 2005, 2010)
2009 Defense Threat Reduction Agency Grant Award
2006 United States Army Advanced Civil Schooling Masters Fellowship

2006 Recipient of the Bronze Star Medal (2006)
1997 Joint Forces Expeditionary Medal (1998)
1993 United States Army ROTC Scholarship

Publications

5. Fennell, J. F. Jr.; Hamaguchi, H.; Yoon, B; Swager, T.M. Chemiresistor Devices for Chemical Warfare Agent Detection Based on Polymer Wrapped Single-Walled Carbon Nanotubes. *Sensors*. **2017**, *17 (5), 982*

4. Fennell, J. F.; Liu, S. F.; Azzarelli, J. M.; Weis, J. G.; Rochat, S.; Mirica, K. A.; Ravnsbaek, J. B.; Swager, T. M. Nanowire Chemical/Biological Sensors: Status and a Roadmap for the Future. *Angew. Chemie Int. Ed.* **2016**, *55* (4), 1266–1281.

3. Willis-Fox, N.; Belger, C.; Fennell, J. F.; Evans, R. C.; Swager, T. M. Threading the Needle: Fluorescent Poly- Pseudo -Rotaxanes for Size-Exclusion Sensing. *Chem. Mater.* **2016**, *28* (8), 2685–2691.

2. Shircliff, R. A.; Stradins, P.; Moutinho, H.; Fennell, J.; Ghirardi, M. L.; Cowley, S. W.; Branz, H. M.; Martin, I. T. Angle-Resolved XPS Analysis and Characterization of Monolayer and Multilayer Silane Films for DNA Coupling to Silica. *Langmuir* **2013**, *29* (12), 4057–4067.

1. Shircliff, R. A.; Martin, I. T.; Pankow, J. W.; Fennell, J.; Stradins, P.; Ghirardi, M. L.; Cowley, S. W.; Branz, H. M. High-Resolution X-Ray Photoelectron Spectroscopy of Mixed Silane Monolayers for DNA Attachment. *ACS Appl. Mater. Interfaces* **2011**, *3* (9), 3285–3292.

Presentations

6. Fennell, J., Hamaguchi, H., Swager, T. M. Wrap n'Sense: Single-Walled Carbon Nanotubes Wrapped with Derivatized PEDOT Polymers for Nerve Agent Detection. MIT Polymer Day, Cambridge, MA, USA, April 13, 2016. (poster presentation)

5. Fennell, J., Hamaguchi, H., Swager, T. M. Toward a Lightweight, Low Power CWA Sensor using Derivatized PEDOT-SWCNT Composites. 250th ACS National Meeting & Exhibition, San Diego CA, USA, March 13-17, 2016. (oral presentation)

4. Fennell, J., Hamaguchi, H., Swager, T. M. Wrap n'Sense: Single-Walled Carbon Nanotubes Wrapped with Derivatized PEDOT Polymers for Nerve Agent Detection. MIT Polymer Day, Cambridge, MA, USA, April 13, 2016. (poster presentation)

3. Fennell, J., Hamaguchi, H., Swager, T. M. Wrap n'Sense: Single-Walled Carbon Nanotubes Wrapped with Derivatized PEDOT Polymers for Nerve Agent Detection. 249th ACS National Meeting & Exhibition, Boston, MA, USA, August 16-20. (poster presentation)

2. Beckler, L., Howard, M., James, C., Fennell, J., Bernal-Ostos, J., Stucky, G. Characterization of a Bio-inspired Metal-polymer Matrix Synthesized Through the Bulk Polymerization of Poly(vinyl-imidzole). 2010 Conference of the Institute of Collaborative Biotechnologies, Santa Barbara, CA, March 2010. (poster presentation)

1. Shircliff, R., Fennell, J., Cowley, S., Branz, H., Ghirardi, M. Thin-Film Microelectronics for Gene Expression Analysis. 2007 Laboratory Directed Research and Development Program Meeting. National Renewable Energy Laboratory, Golden, CO, June 2007 (poster presentation)

Leadership and Service

May 2016 – present	MIT Veterans Club Representative
January 2016 - June 2016	Contributor, *Synfacts*
September 2015 – June 2016	Math Coach, Hanscom Primary School
January 2015 – June 2015	Contributor, *Synfacts*
June 2008 – May 2010	American Chemical Society Representative, USMA
May 1997 – January 2015	Commissioned Officer, United States Army

Memberships

American Chemical Society, Polymer Chemistry Division

I would like to thank Professor Tim Swager for "giving a guy a chance" when I happened to be in a tough spot a year into this my studies at MIT. Tim stuck with me and got me up to speed with a lot of effort and time on his part. His optimism, candor and vision are something to be admired. I have met a lot of leaders in my life, but I count Tim as the most insightful and compassionate. I truly owe Tim a debt of gratitude that I hope to pay forward someday.

There are other members of MIT chemistry to whom would like to thank. Jennifer Weismann and Lynn Guthrie for all her work on behalf of graduate students. Rick Danheiser, to whom I am grateful to for cutting me no slack and coining the term "Organic Chemistry Guantanamo". To Steve Buchwald and Jeremiah Johnson, whose courses made organic chemistry more accessible to a knuckle dragger like myself.

I would like to express significant gratitude to Brian Pretti and Kathy Sweeney. Brian's focus on research support and logistics and Kathy's streamlining of administrative procedures made every single researcher's job much easier.

To my lab mates, especially those that served as significant scientific mentors to me. Julia Kalow, Kat Mirica, Jan Schnorr, Joe Walish, Jon Weis, Jan Ravnsbaek, Sebastian Rochat, John Goods and Silvia Rocha, Yanchuan Zhao, Shinsuke Ishihara, Maggie He, Wen Jie Ong, Catagay Dengiz, Bora Yoon, Rong Zhu, Tomo Ikai and Yoshi Inamoto all provided invaluable assistance to me during my time in the lab.

To my office mates over time, thank you for providing me a target at which to direct my frustration and exuberance. Myles Herbert, Vera Schröder, Constantin Voll, Qifan Zhang, Hiro Tsujimoto and Lukas Zeininger have all been there for me through the years.

The Swager lab seems to attract a certain type of person that are just a pleasure to be around for extended periods of time in a basement lab. I count Joe Azzarelli, Lionel Moh, Sophie Liu, Markrete Krikorian, Byungin Koo, Chris Belger, Greg Gutierrez, Grace Han, Kathleen White, Sibo Lin, Nate Romero and Sara Luppino amongst these individuals.

To my beautiful, lovely daughters, Elora and Zara. Thank you for running to the door to greet me every night.

Finally, I must do more than just say thank-you to my wife Caitlin who has endured my choices, both good and bad for over twenty years. Your patience, thoughtfulness and love has provided all the motivation that I have ever needed. I love you.